1-1-2014

A climatology of Central American gyres

Philippe Pierre Papin
University at Albany, State University of New York, pppapin@gmail.com

A CLIMATOLOGY OF CENTRAL AMERICAN GYRES

by

Philippe P. Papin

A Thesis

Submitted to the University at Albany, State University of New York

In Partial Fulfillment of

The Requirements for the Degree of

Master of Science

College of Arts & Sciences

Department of Atmospheric and Environmental Sciences

2014

ABSTRACT

Central American gyres (CAGs) are large, low-level, cyclonic circulations that are observed over Central America during the tropical cyclone (TC) season. CAGs often occur in conjunction with TCs, and can result in torrential rainfall over portions of Central America, the Caribbean Islands, and eastern United States. The lack of prior research on CAGs, their apparent links to TC activity, and their association with high-impact weather motivates this study.

To study CAG occurrence, an algorithm was developed to identify cyclonic circulations possessing similar characteristics to monsoon depressions (MDs) and monsoon gyres (MGs) in other ocean basins. This algorithm also includes a series of tests that distinguishes CAG events from large TCs and non-closed circulations. This algorithm was run between May-November 1980-2010 using the National Centers for Environmental Prediction Climate Forecast System Reanalysis 0.5^{o} gridded dataset to produce the CAG climatology. 42 CAGs were classified (~1.4 per season) with a bimodal distribution of occurrence favoring the early (May-Jun) and late (Sep-Nov) TC season. Stratification of CAG occurrence by the phase of the Madden Julian Oscillation (MJO) shows that over 75% of all CAGs develop in phases 8,1, and 2.

A gyre-relative, time-lagged, CAG composite analysis is performed on CAG cases spanning from three days prior to two days after CAG formation. Positive low-level geopotential height anomalies are present in the east Pacific and Atlantic basins and are associated with anomalous low-level flow before the formation of the CAG. This results in increasing cyclonic vorticity near anomalously high precipitable water over Central America, a pattern that aids the generation of deep convection and the broad closed low-

level cyclonic circulation that defines the CAG. CAGs are also split into two subsets using potential vorticity (PV) on the 350K isentropic surface. *Tropical CAGs* possess upper-tropospheric ridging associated with low PV air, while *trough CAGs* possess upper-tropospheric troughing associated with high PV air. TCs exist in about half of all CAGs, and tend to occur on the eastern side of the CAG circulation. Case studies and conceptual models are presented to illustrate key synoptic features that occur prior to, during, and after CAG formation.

ACKNOWLEDGEMENTS

At the completion of my M.S. thesis, which culminates more than three years of research, I would like to thank my parents, brother, and extended family for giving me the support and inspiration to achieve in my field. Their unwavering love has been the pillar upon which I have been able to forge ahead when it seemed like I was reaching an impasse in my research or thesis writing.

I can't thank my academic co-advisors, Drs. Ryan Torn and Lance Bosart, enough for their constant aid and dedication towards my academic goals. I am constantly provided new perspectives and ideas from Ryan and Lance, from which I have learned and grown further as a scientist. Their mentorship has enabled me to do things I didn't even know were possible, and I am indebted to the opportunities they have provided me during my graduate studies thus far. I also would like to thank the members of the Department of Atmospheric and Environmental Sciences at the University at Albany: especially Barbara Zampella, Sandra George, and Denise Church for their administrative support; Kevin Tyle and David Knight for their technical support; and my fellow grad students (especially Alan Brammer, Alicia Bentley, Ben Moore, Bob Setzenfand, Bill Lamberson, Brian Crandall, Hannah Attard, Kyle Griffin, Kyle MacRitchie, Larry Gloeckler, Matt Janiga, Rosimar Rios-Berrios, and Stephanie Stevenson), not just for their technical assistance and scientific ideas, but for providing a relaxed, friendly atmosphere that made me feel at home in the department.

Finally, I like to thank my undergraduate advisor, Dr. Chris Hennon and my undergraduate professor, Dr. Doug Miller. They gave me the first opportunities to participate in undergraduate research, which ultimately lead to where I am today. By

exposing me to the thrill of launching radiosondes in inclement weather and using data for my own research ideas, they further invigorated my passion for conducting atmospheric science research, and gave me the inspiration to reach my academic goals. Without their guidance, I don't think I would have had the privilege to be where I am today, working towards acquiring knowledge on a subject that brings incredible joy and excitement in my life.

This research was made possible by the gracious support of the National Science Foundation (NSF) grant ATM-0849491.

Albany, New York
October 2014

TABLE OF CONTENTS

LIST OF TABLES

LIST OF FIGURES

Fig. 1.7. Composite structure of MDs occurring in various oceanic basins during local summer. Left panels denote potential temperature anomalies (shading, K) and zonal wind anomalies (black contours with dotted lines indicating negative values, every 2 m s^{-1}). Right panels denote PV (shading, PVU) and meridional wind (contours with dotted lines indicating negative values, every 2 m s^{-1}). Regions are (a,b) north IND, (c,d) WPAC, (e,f) south IND, and (g,h) EPAC. Values shaded or contoured only if t-test is significant at the 5% level [Fig 9, 10, and adapted caption from Hurley and Boos (2014)].

Fig. 1.8. Comparison between the modeling results of Holland (1995) and the August 1991 MG. The top panel (a) depicts 850-hPa streamlines of a MG that developed after 144-hour integration of primitive equations with a Gaussian profile of diabatic heating indicated by the black crosshairs. The red arrow depicts the cyclonic flow of the MG [Fig. 6f and adapted caption from Holland (1995)]. The bottom panel (b) is a synoptic map of a MG on 0000 UTC 11 August 1991 depicting 850-hPa wind (vectors) and outgoing long wave radiation (shading, negative 150-210 W m^{-2}). The crosshair in (b) represents the deepest convection and the red arrow depicts the cyclonic flow of the MG. Labels E and D represent TCs Doug and Ellie respectively [Fig. 8c and adapted caption from Molinari et al. (2007)].

Fig. 1.9. Processes that lead to the development of MG in July 1988. (a)1-25 July 1988 mean 250-hPa wind (vectors, m s^{-1}), 250-hPa isotachs (shading, m s^{-1}), and 250-hPa heights (black contours, m). The dotted line outlines the mean upper-level trough axis. (b) 19 – 25 July 1988 averaged 1000 – 400-hPa layer mean wind (vectors, m s^{-1}). Red arrows represent confluent flow near 150°E. (c) 0000 UTC 24 July 1988 PV the on 350K surface (shaded, PVU), 350K wind (vectors, m s^{-1}), and 850-hPa vorticity (contours, starting and incremented at $2x10^{-5}$ s^{-1}). (d) 0000 UTC 27 July 1988 infrared brightness temperature (shading, K), 850-hPa cyclonic vorticity (hatched shading in black contours, starting at $1x10^{-5}$ s^{-1}), and 850-hPa winds (vectors, m s^{-1}). Upper case letters in all panels represent different vorticity maximums [Fig. 5b, 9d, 10, 11d and caption adapted from Molinari and Vollaro (2012)].

Fig. 1.10. North-south cross-section across MG averaged from 0000 UTC 27 July to 0000 UTC 28 July. Plotted is PV (shaded, blue indicates PV < 0 PVU while yellow indicates PV > 0.5 PVU [Fig. 14b and adapted caption from Molinari and Vollaro (2012)].

Fig. 1.11. Relevant meteorological features associated with a MG at 0000 UTC 29 July 1989. (a) Infrared brightness temperature (shading, K) with surface winds from coastal stations, ships, and buoys (barbs in kt, yellow below gale force and magenta above). (b) Infrared brightness temperature (shading, K), 200-hPa heights (red contours, every 20 m), 200-hPa winds (vectors, m s^{-1}). Yellow L indicates the 200-hPa height minimum. (c) Infrared brightness temperature (shading, K), 850-hPa cyclonic vorticity (purple hatching, shading starting at $5x10^{-5}$ s^{-1}), and 850-hPa winds (vectors, m s^{-1}). Upper case letters refer to individual vorticity maxima. (d) Infrared brightness temperature (shading, K), 500-hPa temperature (green contours, increment is 0.5K), and 500-hPa wind (vectors, m s^{-1}). Letters W and C refer to a temperature maximum and minimum respectively [Fig. 1i, 2c, 3c, 4c, 7a, and caption adapted from Crandall et al. (2014)].

(e) t_0 + 24 h, and (f) t_0 + 48 h. The red circle in each panel denotes the CAG center location at genesis for panels up to genesis (-72 h to 0 h, a – d) and the CAG center location for designated times after genesis (+24 h to +48 h, e – f). Tracks of TCs are also plotted, colorized by the intensity, with the present position plotted as a TC symbol.

Fig 3.8. Relative vorticity averaged over a 5^o box for all time lags of the tropical CAG composite (N = 35). Different colored lines denote curvature relative vorticity (red), shear relative vorticity (blue), and total relative vorticity (black).

Fig. 3.9. Tropical CAG composite (N = 35) Standardized precipitable water anomaly (shaded, sigma), Precipitable water (black contours, mm), and 850 hPa winds (barbs, kts) at (a) t_0 – 72 h, (b) t_0 – 48 h, (c) t_0 – 24 h, (d) t_0, (e) t_0 + 24 h, and (f) t_0 + 48 h. The red circle in each panel denotes the CAG center location at genesis for panels up to genesis (-72 h to 0 h, a – d) and the CAG center location for designated times after genesis (+24 h to +48 h, e – f). Black stippling indicates where the 850-hPa geopotential height is statistically significant to the 95% level using a two tailed student's t-test.

Fig. 3.10. Tropical CAG composite (N = 35) 200-hPa potential vorticity (shaded, PVU), 200-hPa geopotential heights (black contours, dam), and 200 hPa winds (barbs, kts) at (a) t_0 – 72 h, (b) t_0 – 48 h, (c) t_0 – 24 h, (d) t_0, (e) t_0 + 24 h, and (f) t_0 + 48 h. The red circle in each panel denotes the CAG center location at genesis for panels up to genesis (-72 h to 0 h, a – d) and the CAG center location for designated times after genesis (+24 h to +48 h, e – f).

Fig. 3.11. Tropical CAG composite (N = 35) 200 hPa isotachs (rainbow shading, m s^{-1}), Precipitable water (gray to green shading, mm), 200 hPa potential vorticity (warm contours, PVU), 500 hPa omega (blue contours, only negative contoured, hPa s^{-1}), and 200 hPa Irrotational Wind (vectors, m s^{-1}) at (a) t_0 – 72 h, (b) t_0 – 48 h, (c) t_0 – 24 h, (d) t_0, (e) t_0 + 24 h, and (f) t_0 + 48 h. The red circle in each panel denotes the CAG center location at genesis for panels up to genesis (-72 h to 0 h, a – d) and the CAG center location for designated times after genesis (+24 h to +48 h, e – f).

Fig. 3.12. Tropical CAG composite (N = 35) Top: potential vorticity (shaded, PVU), potential temperature (blue contours, K), vertical velocity (purple contours, 10^{-3} hPa s^{-1}) and winds (barbs, knots) Bottom: potential vorticity anomaly (shaded, PVU) potential temperature (blue contours, K) and anomalous winds (barbs, knots) at (a) t_0 – 72 h, (b) t_0 – 48 h. Reference panel for cross-section provided on the bottom left (both a and b).

Fig. 3.13. As in Fig. 3.12 except at (c) t_0 – 24 h, and (d) t_0. Reference panel for cross-sections provided on the bottom left (both c and d).

Fig. 3.14. As in Fig. 3.12 except at (e) t_0 + 24 h, and (f) t_0 + 48 h. Reference panel for cross-sections provided on the bottom left (e) and bottom right (f).

Fig. 3.15. Tropical CAG composite (N = 35) Top: zonal wind (shaded, m s^{-1}), Bottom: temperature anomaly (shaded, ^oC) and relative vorticity (black contours, 10^{-5} s^{-1}) at (a) t_0

Fig. 3.32. 850-hPa standardized geopotential height anomaly (shaded, sigma), 850-hPa geopotential height (black contours, dam), and 850 hPa anomalous winds (barbs, kts) at (a) the earth-relative composite of all CAG events (N = 42) at t_0, (b) earth-relative composite of May-Nov MJO events in RMM phase 8 (N = 818), (c) earth-relative composite of May-Nov MJO events in RMM phase 1 (N = 1142), and (d) earth-relative composite of May-Nov MJO events in RMM phase 2 (N = 1081).

Fig. 3.33. Tropical CAG case study, with 850-hPa standardized geopotential height anomaly (shaded, sigma), 850-hPa geopotential height (black contours, dam), and 850 hPa anomalous winds (barbs, kts) at (a) t_0 – 72 h, (b) t_0 – 48 h, (c) t_0 – 24 h, (d) t_0, (e) t_0 + 24 h, and (f) t_0 + 48 h. The red circle in each panel denotes the CAG center location at genesis for panels up to genesis (-72 h to 0 h, a – d) and the CAG center location for designated times after genesis (+24 h to +48 h, e – f). Tracks of TCs are also plotted, colorized by the intensity, with the present position plotted as a TC symbol.

Fig. 3.34. Tropical CAG case study, with 850-hPa cyclonic vorticity (shaded, > $1x10^{-5}$ s^{-1}), 1000-500 km radial average 850-hPa circulation (black contours, > $1x10^{-5}$ s^{-1}), and 850-hPa winds (vectors, m s^{-1}) at (a) t_0 – 72 h, (b) t_0 – 48 h, (c) t_0 – 24 h, (d) t_0, (e) t_0 + 24 h, and (f) t_0 + 48 h. The red circle in each panel denotes the CAG center location at genesis for panels up to genesis (-72 h to 0 h, a – d) and the CAG center location for designated times after genesis (+24 h to +48 h, e – f). Tracks of TCs are also plotted, colorized by the intensity, with the present position plotted as a TC symbol.

Fig. 3.35. Relative vorticity averaged over a 5^o box for all time periods of the tropical CAG case study. Different colored lines denote curvature relative vorticity (red), shear relative vorticity (blue), and total relative vorticity (black).

Fig. 3.36. Tropical CAG case study (N = 35) Standardized precipitable water anomaly (shaded, sigma), Precipitable water (black contours, mm), and 850 hPa winds (barbs, kts) at (a) t_0 – 72 h, (b) t_0 – 48 h, (c) t_0 – 24 h, (d) t_0, (e) t_0 + 24 h, and (f) t_0 + 48 h. The red circle in each panel denotes the CAG center location at genesis for panels up to genesis (-72 h to 0 h, a – d) and the CAG center location for designated times after genesis (+24 h to +48 h, e – f). Black stippling indicates where the 850-hPa geopotential height is statistically significant to the 95% level using a two tailed student's t-test. Tracks of TCs are also plotted, colorized by the intensity, with the present position plotted as a TC symbol.

Fig. 3.37. Tropical CAG case study (N = 35) 200 hPa potential vorticity (shaded, > 0.75 PVU), 200 hPa geopotential heights (black contours, dam), and 200 hPa winds (barbs, kts) at (a) t_0 – 72 h, (b) t_0 – 48 h, (c) t_0 – 24 h, (d) t_0, (e) t_0 + 24 h, and (f) t_0 + 48 h. The red circle in each panel denotes the CAG center location at genesis for panels up to genesis (-72 h to 0 h, a – d) and the CAG center location for designated times after genesis (+24 h to +48 h, e – f). Tracks of TCs are also plotted, colorized by the intensity, with the present position plotted as a TC symbol.

1. Introduction

1.1 Motivation

Within the tropics, there exist a large variety of low-pressure disturbances that persist on a multitude of spatial scales and intensities. While extensive research has been committed to tropical cyclones (TC), there also exist larger circulations that don't fit the traditional TC criteria, yet possess a closed lower tropospheric cyclonic circulation, deep convection, and the ability to produce heavy rainfall due to the combination of deep convection in a deep moist environment. In other ocean basins, these large circulations are often referred to as monsoon depressions (MDs) or monsoon gyres (MGs). For the purposes of this study, we will refer to these type of circulations occurring in proximity to Central America as Central American Gyres (CAGs).

One such CAG developed over Central America in late September 2010. While this low-level circulation was eventually designated TC Nicole by the National Hurricane Center (NHC; Blake 2011), its structure remained unusually large and uncharacteristic of a traditional TC. Blake (2011) noted that the structure was more reminiscent of a MD, a large-scale cyclonic circulation commonly observed in the Indian (IND) and western Pacific (WPAC) basins. In fitting with the MD classification, the NHC identified a large area of light and variable winds, denoting the center, while the radius of maximum winds of the disturbance was > 300 km from the center. Moreover, the structure of the CAG was asymmetrical, with the majority of deep convection and strongest winds occurring to the east, along the periphery of the circulation. Exceptionally heavy rainfall was observed in association with this CAG, with widespread rainfall totals > 200 mm (7.87 in) across

Mexico, Jamaica, Cuba, and the United States (Brennan 2010; Blake 2011). Jamaica was particularly hard hit, where multiple locations across the island reported rainfall totals > 900 mm (35.43 in) over a five day period. The excessive rainfall associated with the CAG resulted in severe flooding and mudslides, which were blamed for over 90 fatalities across Central America and Jamaica. As a result, the September CAG was one of the deadliest meteorological events that occurred over Central America in 2010.

In addition to the NHC's review of TC Nicole, the unique characteristics of TC Nicole were also discussed and debated by forecasters for the Pre-Depression Investigation of Cloud-systems In the Tropics (PREDICT, Montgomery et al. 2012), a tropical field campaign in 2010. Montgomery et al. (2012) notes that the pregenesis environment of TC Nicole was interesting from a scientific perspective because TC Nicole appeared to originate out of a broad circulation that contained multiple low-level vorticity maxima, primarily located around the eastern periphery of the larger-scale circulation. In addition, the uncertainty related to the track and TC-genesis (TCG) of Nicole was "perhaps the largest of any TC during PREDICT" (Montgomery et al. 2012). In particular, the study cited the desire to understand how TCs can emerge from the "larger gyre complex" associated with multiple low-level vorticity maxima.

Despite the societal impact that CAGs possess with associated rainfall and motivation to better understand TC occurrence within CAGs, little research has been conducted this phenomena over Central America. The primary goal of this research is to formulate a climatology of CAGs in order to identify the synoptic environment associated with these systems before, during, and after their development. This CAG climatology will be used to build conceptual models that document the evolution of different CAG

subsets to educate both operational forecasters and researchers of the different pathways leading to CAG formation.

1.2 Literature Review

1.2.1 Monsoonal Circulations in Other Basins

In the tropical atmosphere, synoptic low-pressure systems play a pivotal role in the meteorology of monsoon climates. While ample literature has documented the existence of MDs in the IND and WPAC oceanic basins (e.g. Beattie and Elsberry 2013, Boos et al. 2014) and MGs in the WPAC basin (e.g. Lander 1994, Crandall et al. 2014), the study of similar monsoonal circulations over Central America has been limited.

1.2.1.1 Monsoon Depressions

MDs are large closed low-level cyclonic circulations, embedded in a larger scale monsoon trough (MT), that feature loosely organized deep convective activity around their center, but do not possess sufficient organization to be classified as a TC. The India Meteorological Department (IMD) defines MDs as a lower tropospheric cyclonic circulation that possesses maximum sustained surface winds between 8.5 m s^{-1} to 13.4 m s^{-1}, while weaker disturbances with lower maximum wind speed are simply referred to as "lows" and stronger systems with higher maximum wind speed are referred to as "deep depressions" (IMD 2003). In comparison, the Joint Typhoon Warning Center (JTWC) defines a MD as a lower tropospheric cyclonic circulation with a 500 km radius, light and variable winds near the circulation center, and loosely organized convection along the periphery of the of the circulation (Aldinger and Stapler 1998). The convection

associated with MDs represents a critical feature, where mesoscale convective systems (MCSs) associated with MDs can contribute to > 50% of the total amount of precipitation during one monsoon season (see Fig. 5f of Romatschke and Houze 2011).

While MD-like systems have been recognized in literature as far back as the late 1800's (Eliot 1890; Piddington 1876), organized research on these disturbances didn't begin until the middle 20th century, (Das 1952, Mulky and Banerji 1960). The majority of this initial research focused on MDs that developed in the north IND basin in response to the Asian monsoonal circulation. Das (1952) identified a MD as a large closed cyclonic circulation in the Bay of Bengal (BoB) between 1 and 5 km above the surface. Mulky and Banerji (1960) used widely spaced rawinsonde observations of 22 MD cases from 1954 – 1958 to diagnosis the basic composite wind structure of MDs. Their analysis identified a cyclonic circulation that extended up to 400-hPa, with an upper-level closed anticyclone present to the northeast of the MD circulation at 200-hPa. Fig. 1.1 shows a comparison of the low-level (950-hPa) and upper-level (200-hPa) flow present with the composite MD in Mulky and Banerji (1960). Note that these early studies of north IND basin MDs were often limited in scope and often hampered by insufficient, unreliable data.

More detailed analysis on MD structure and dynamics became possible as observational datasets and numerical modeling improved. Krishnamurti et al. (1975) was one of several comprehensive published studies on the synoptic structure of MDs, focusing on a case study in the BoB in August 1968. Krishnamurti et al. (1975) identified a closed cyclonic circulation with an initial 500 km radius that extended up to 500-hPa as it tilted eastward with height. The MD moved generally westward into India at a phase

speed of 6 m s^{-1} during its five-day lifecycle, as its outer size radii grew to 1000 km. Thermodynamically, the MD possessed a cold core between 900 – 500-hPa, and a warm core above 500-hPa (Fig 1.2e), with a tropospheric deep column of anomalously high moisture (Fig 1.2d). The strongest convection and precipitation was primarily located west of the MD center, where strong low-level convergence and vertical ascent were observed. Meridional cross sections of zonal wind illustrate the large corridors of westerlies equatorward and easterlies poleward of the MD, where zonal wind maxima are located approximately 5^{o} in latitude from the MD center at 800-hPa (Fig 1.2c). Godbole (1977) composited 5 MDs in the BoB in 1973, and identified a composite MD structure bearing a close resemblance to the synoptic features outlined in Krishnamurti et al. (1975).

Subsequent studies over the next decade used extensive observations from the Summer Monsoon Experiment (SMONEX) in 1979, which identified two MDs that occurred in the BoB and Arabian Sea respectively. The general synoptic characteristics of MDs were confirmed through the more detailed analysis provided by this field campaign (Nitta and Masuda 1981, Sanders 1984, Douglas 1992), although discrepancies remained related to the depth of the cold core of MDs in the low-levels (Douglas 1992). The generality of these MD studies, however, could not be fully assessed given the limited subset of cases provided by only one year's worth of data provided by SMONEX.

Recent studies have primarily use global gridded datasets to enable more detailed climatological investigations of MDs in the north IND basin (Chen and Weng 1999, Yoon and Chen 2005, Chen et al. 2005, Boos et al. 2014). Chen and Weng (1999) created a MD climatology based on visual inspection of streamlines, filtered low-level winds, and

pressure tendency charts from June-August 1979-1994 using the NCEP-National Center for Atmospheric Research (NCAR) 6-hourly reanalysis data (Kalnay et al. 1996). Their analysis found an average of six MDs occurring per summer with an average lifespan of five days, but did not elaborate further on the composite structure of MDs, instead focusing on the role precursor disturbances play in the genesis of MDs in the BoB. Yoon and Chen (2005) adopted a similar classification scheme of MDs, using the European Centre for Medium-Range Weather Forecasts (ECMWF) reanalysis data (Gibson et al. 1997) from 1979-2002. 143 MDs were identified over the 24-year period and were composited in 24 h increments up to five days after MD development (Fig. 1.3). The MD structure depicted a closed low-level circulation on 850-hPa streamlines (Figs. 1.3a-b), with upward vertical velocity (Fig. 1.3a) in conjunction with diabatic heating (Fig. 1.3b) over the 850-hPa circulation, with the max diabatic heating located between 400 – 600-hPa (Fig. 1.3c) during the mature phase of the MD (days 2 – 4). In latter composite time periods (days 4-5), positive vertical velocity and diabatic heating shift to the western side of the MD circulation in response to easterly vertical wind shear. Boos et al. (2014) used the ERA-Interim dataset, a more recently updated ECMWF reanalysis (Dee et al. 2011) and classified MDs by tracking vorticity maximum > 1×10^{-5} s^{-1} that possessed negative sea level pressure perturbations between 4 – 10-hPa relative to the 21-day running mean and surface winds between 8.5 – 13.5 m s^{-1}. The wind speed classification is similar to the IMD (2003) classification of MDs but appears to neglect a size criterion. Using these guidelines, 171 MDs were identified from June-September 1979-2012 in the BoB. Furthermore, Boos et al. (2014) composited 117 of these MDs, using a potential vorticity (PV) framework to describe the structure and evolution of MDs. Fig. 1.4 presents the

composite PV structure associated with these MDs, where a tropospheric PV maximum between 0.8-1.0 PV units (PVU) is observed at 500-hPa, directly over the MD center. Additionally, Boos et al. (2014) looked at a MD case study that formed during the active convective phase of the Madden Julian Oscillation (MJO) centered over the maritime continent. Despite the MD occurring in the latter period (16 Sep 2008) of the traditional Indian monsoon season, the active phase of the MJO helped to enhance low-level westerly flow equatorward of the MD circulation.

In addition to MD structure, extensive research has been preformed to understand the underlining dynamics for MD development, maintenance, and motion. Krishnamurti et al. (1976) investigated the dynamical structure of the MD identified in Krishnamurti et al. (1975), using a full physics numerical model to predict the evolution of the MD. The model depicted a MD that developed where the necessary condition for barotropic instability was satisfied, a reversal in the meridional potential vorticity (PV) gradient in the lower troposphere (700-hPa). This is visualized as horizontal shearing of the zonal wind, a common characteristic of the MT or intertropical convergence zone (ITCZ). To deduce the importance of barotropic instability in MD maintenance, Krishnamurti et al. (1976) examined model energetics, which confirmed that barotropic instability provided a significant contribution to MD maintenance via the conversion of zonal kinetic energy into eddy kinetic energy. Cumulus convection produced by the model was also critical to the maintenance of the MD, since cumulus convection promoted latent heat release (LHR), and LHR was the primary factor in the generation of eddy available potential energy that is later converted to eddy kinetic energy. The LHR of cumulus convection also contributed to the warm core in the upper-troposphere of the MD. Carr (1977)

reinforced this notion that LHR plays a dominant role in the dynamics associated with MDs. The model energetics discussed in Krishnamurti et al. (1976) were also corroborated by Shukla (1978), which also found a small negative conversion of zonal APE to eddy APE, leading to their claim that the impact of baroclinic instability is insignificant compared to the positive impact that barotropic instability and LHR have in the maintenance of MDs. Nitta and Masuda (1981) further emphasized the importance of barotropic instability, which was hypothesized in allowing a July 1979 MD to obtain KE from the mean zonal flow. In contrast, a few studies have argued of the importance of baroclinic processes (Rao and Rajamani 1970, Saha and Chang 1983) in MD development and maintenance. Saha and Chang (1983) in particular provided evidence of a baroclinic unstable structure with a thermal gradient in a MD case study. Despite this assertion, Saha and Chang (1983) do not calculate energetics to assess the importance of baroclinic processes in comparison to the importance of barotropic instability and LHR for MD maintenance. Sanders (1984) noted these contrasting views to MD maintenance, and used quasi-geostrophic (QG) theory in an attempt to reconcile these different maintenance mechanisms. He concluded that QG theory alone could not fully account for the organization of the MD, but could be a useful tool in diagnosing the westward propagation of the MDs via vortex stretching.

The westward propagation of MDs has been the focal point of more recent research of MDs in the north IND basin (Chen et al. 2005, Boos et al. 2014). The westward propagation of MDs is unusual, because the background low to mid tropospheric flow moves from west to east, counter to the upstream propagation of the MD. Chen et al. (2005) conducted a horizontal streamfunction analysis of 143-monsoon

low-pressure system in the north IND basin and made the same conclusion as Sanders (1984), that vortex stretching in the region of ascent west of the MD vortex produces a positive vortex tendency in that direction. Boos et al. (2014) proposed that the motion of MDs is primarily driven by the advection of mid-tropospheric PV via beta gyres. Beta gyres are evident when decomposing the total horizontal streamfunction into its azimuthally symmetric and asymmetric components (Fig 1.5). The asymmetric streamfunction helps to advect the 500-hPa PV maximum associated with MDs (Fig 1.4) northwest at a propagation speed of 2.1 m s^{-1}. A PV budget analysis also confirmed the time tendency of PV in the 600 – 300-hPa layer mean was primarily due to this horizontal advection. Moreover, Boos et al. (2014) states that previous literature, which attributes MDs motion to vortex stretching, is inadequate, since the motion vector of MDs (northwest) is oriented 90^{o} to the right of the greatest vortex stretching southwest of the MD center. In addition, this positive vorticity tendency due to vortex stretching is neutralized by the negative vorticity tendency due to horizontal vorticity advection and dissipation processes in the boundary layer. Boos et al. (2014) finally noted that future work needs to be conduced in understanding how MD genesis occurs, hypothesizing that the development of MDs occurs in a region of enhanced cyclonic vorticity associated with horizontal shear in the low-levels. This hypothesis is similar to the conclusions made in previous literature (Krishnamurti et al. 1976, Shukla 1978, Nitta and Masuda 1981).

The synoptic and dynamical characteristics of MDs described extensively above focuses on disturbances in the north IND basin over the BoB. A smaller subset of literature has also investigated disturbances called MDs that occur in the south IND (Davidson and Holland 1987, Baray et al. 2010), and WPAC basins (Harr et al. 1996,

Aldinger and Stapler 1998, Beattie and Elsberry 2013). Davidson and Holland (1987) conclude that the structure of MDs in the south IND basin was similar to the structure of MDs identified in the north IND basin, with a mid to upper tropospheric warm core and cyclonic vorticity maximum at 850-hPa. Once inland over Australia, the wind field of these MDs resembled the outer structure of a TC without an inner wind core. Similar characteristics were identified by Baray et al. (2010), which identified five MD events in the south IND basin. Harr et al. (1996) documented a similar MD-like disturbance in the WPAC basin, using data obtained from a mini field experiment called Tropical Cyclone Motion (TCM-93). In contrast to the majority of MDs in the BoB region, the MD identified in Harr et al. (1996) eventually became a TC (Robyn) as deep convection (associated with MCSs) developed near the circulation center after a prior period where convection was only organized in bands on the periphery of the MD circulation. The location of this MD over open waters, in combination with the low vertical wind shear, likely contributed to its subsequent organization from a MD to a TC. Beattie and Elsberry (2013) identified 44 MD cases in the summer of 2009 in the WPAC basin using ECMWF analysis, QuikSCAT satellite surface winds, infrared satellite imagery, and TRMM 3-hourly precipitation. Their MD assessment also highlighted the role of cross equatorial flow aiding in the increase of horizontal shear and cyclonic vorticity of the MT in the WPAC, which aided the formation of cyclonic vorticity lobes that comprise the MD circulation. In a companion study, Beattie and Elsberry (2013) conduced a more detailed analysis of the structure of these WPAC MDs, and found that 17 of the 44 MDs went on to become TCs, supporting the theory that a significant percentage of WPAC MDs go on to generate TCs. Beattie and Elsberry (2013) also found that the wind field of WPAC

MDs was frequently more elliptical rather than circular in shape (mean diameters: 812 km latitude, 1098 km longitude), and possessed relatively large standard deviations in either direction (288 km latitude, 387 km longitude). A meridional cross-section of a representative MD showed an upper tropospheric warm core structure, where a cyclonic relative vorticity maximum is observed in the low to middle troposphere and an anticyclonic relative vorticity maximum is found in the upper-troposphere (Fig. 1.6). This profile is consistent the strongest cyclonic flow located at 850-hPa decreasing with height and becoming anticyclonic around 200-hPa over the MD center. The vertical structure of WPAC MDs is consistent with previous research of MDs in the north and south IND basins (e.g. Krishnamurti et al. 1975, Davidson and Holland 1987).

Finally, Hurley and Boos (2014) preformed a global climatology of monsoon low-pressure systems similar to MDs, using ERA-Interim reanalysis (Dee et al. 2011). Hurley and Boos (2014)'s MD identification method is identical to the method used in Boos et al. (2014) and also allows for the comparison of composite MD-like disturbances occurring in multiple basins (e.g. north IND, south IND, WPAC, and east Pacific [EPAC], Fig. 1.5). In general, MD-like disturbances in these four basins possess a similar vertical composite structure, with a well-defined warm core in the mid to upper troposphere and tropospheric PV > 0.5 PVU maximized in the 600 – 400-hPa layer (note PV is negative in the southern hemisphere, Fig. 1.5h). Zonal and meridional winds are maximized in the lower troposphere approximately 5 degrees away from the center of the MD circulation. There are subtle differences in the thermal structure in the lower troposphere, where the north IND composite MD structure reveals a distinct cold core between 1000 – 800-hPa (Fig. 1.5a), while the WPAC composite MD structure does not (Fig 1.5c). The EPAC

composite MD structure shows a more complicated structure of warm temperature anomalies from 1000 – 900-hPa and cold temperature anomalies from 900 – 800-hPa primarily poleward of the MD (Fig 1.5c), while the south IND composite MD depicts mainly negative temperature anomalies from 1000 – 800-hPa poleward of the MD center (Fig 1.5 g). These subtle differences in the thermal structure of the lower troposphere, however, do not appear to modify the wind structure that characterizes MD circulations.

1.2.1.2 Monsoon Gyres

Monsoon gyres (MGs) as defined by the JTWC are large closed low-level cyclonic circulations that have a radius more than double (1250 km) that of a MD and have an asymmetrical convective distribution, primarily on the southern and eastern periphery of the broad circulation (Aldinger and Stapler 1998). In long-lived events this convection can axis-symmetrize and evolve into a MD or TC. The pioneering research on MGs was conducted by Lander (1994), which documented the evolution of a MG that lasted two weeks in the WPAC basin in August 1991 (Fig. 1.7). Using this case study, Lander (1994) crafted an initial set of MG criteria, which closely mirror the JTWC's definition above.

One feature that is common during the development of a MG, which also separates its classification from that of a MD, is the presence of mid-latitude forcing, primarily by an upper-tropospheric trough in proximity to the developing MG. Lander (1994) investigated the evolution of the August 1991 MG, documenting an upper tropospheric trough that interacted with a reverse-oriented MT (where the trough axis is oriented SW-NE in its instantaneous position). In response to this trough interaction,

convection developed at lower latitudes to the southeast, associated with a weak surface low. It is this surface feature that tracked slowly westward in the following days that L94 classified as a MG. Holland (1995) elaborated further on the mid-latitude interaction that lead to the formation of the August 1991 MG. He stated that the MG formed as a result of a frontal passage in the mid-latitudes that invigorated convection in the deep tropics, as previously mentioned by Lander (1994). Moreover, Holland (1995) hypothesized several possible mechanisms that could lead to MG development. After ruling out spontaneous vortex rollups (Guinn and Schubert 1993) from trailing vorticity of a frontal zone and PV from upper-tropospheric troughs as direct mechanisms for MG development, Holland (1995) gave credence to LHR that results from enhanced convection driven by the intrusion of a mid-latitude system into the tropics. Holland (1995) tested this argument by using a non-linear baroclinic model, as described by Wang et al. (1993), in which heating is fixed to a Gaussian profile centered at 20^{o}N. The resulting low-level circulation that formed in the model is consistent with the observed MG in the August 1991 case, where the circulation is very large and extends westward of the heated region associated with the convection. This result is also similar to the response expected per Gill (1980) given diabatic heating occurring off the equator in the tropics. Fig. 1.8 represents a favorable comparison between the modeling results presented in Holland (1995) compared to a synoptic map of the August 1991 gyre. Here, Molinari et al. (2007) provide qualitative support (Fig 1.8b) that the genesis of the August 1991 MG can be attributed to diabatic heating caused by active convection. The comparison shows that when developing, MG circulations are centered northwest of the deepest heating and convection, with agrees with the ideas presented in Holland (1995).

Molinari and Vollaro (2012) argue that the genesis of MGs can also be tied to mid-latitude jet dynamics. In this study, a MG in July 1988 was analyzed prior and during its evolution. Fig. 1.9 depicts a series of paneled images that illustrate the processes that result in the formation of the July 1988 MG. Initially, a quasi-stationary ridge developed over the Asian continent with a corresponding trough near 150^{o}W during July 1988 (Fig. 1.9a). This configuration allowed for a jet exit region to emerge at 145^{o}E, which provided a favorable region for anticyclonic wavebreaking (Thorncroft et al. 1993, Moore et al. 2010). This anticyclonic wavebreaking pattern allowed for low-level confluent flow to occur (red arrows near 20^{o}N, 150^{o}E, Fig. 1.9b), with the mean flow guiding a series of mid-latitude disturbances with low-level vorticity southward, west of this area of confluence (systems B, C, and D, Fig. 1.9c). The confluent flow in the lower troposphere permitted convective development to occur along a MT (Fig 1.9d), which led to additional extension to the westerly winds due to diabatic heating, similar to the results shown in previous modeling studies (Gill 1980, Holland 1995). Finally, low-level vorticity associated with a southward moving mid-latitude low (D, Fig 1.9d) merged with vorticity associated with the tropical convection (E, Fig 1.9d). These series of events resulted in the formation of a MG with a 2000 km radius.

The evolution described in Molinari and Vollaro (2012) suggests that direct forcing (where mid-latitude troughs provide low-level vorticity in-situ) and indirect forcing (confluence created by anticyclonic wavebreaking leading to tropical convection) from the mid-latitudes are responsible for MG formation. This is in contrast to Holland (1995) where mid-latitude troughs are believed to have no direct contribution to MG development, other than modifying the tropospheric flow pattern to favor confluence that

results in the generation of deep convection. However, Molinari and Vollaro (2012) point out that the initial size of the July 1988 MG results from a broad region of cyclonic vorticity after the merger of vorticity pieces associated with the deep convection and the mid-latitude trough. The convective asymmetry of the MG is related to strong subsidence upstream of the upper-tropospheric trough. The presence of the upper-tropospheric trough to the MG circulation also modifies the vertical PV profile of the MG. Molinari and Vollaro (2012) identified a tropospheric PV maxima around 300-hPa over the July 1988 MG and PV > 0.5 PVU that extends to the top of the troposphere (Fig 1.10). The PV maximum at 300-hPa implies cyclonic flow and the presence of an upper-tropospheric trough in proximity to the MG. It is important to emphasize this difference in the vertical PV structure in comparison to a MD (Fig. 1.4, 1.6), where PV is maximized in the mid-troposphere with a distinct decrease in PV in the upper-troposphere, which separates higher PV values above the tropopause (Fig 1.4). In MDs, the low PV air in the upper-troposphere is due the existence of anticyclonic flow at this level over the low-level cyclonic flow that characterizes the MD (Fig 1.6). Thus, one fundamental difference that separates the classification of MGs versus the smaller but similar lower-tropospheric MDs is the presence of an upper-tropospheric trough, which provides high PV air in the upper-troposphere in MG cases.

Crandall (2012) and Crandall et al. (2014) investigated a MG that occurs in July 1989. Similar to the MGs investigated in Lander (1994), Holland (1995), and Molinari and Vollaro (2012), the lower tropospheric circulation of the July 1989 MG appears to form after a series of upper-tropospheric troughs drop into the tropics via anticyclonic wavebreaking. These troughs feature a deep vertical penetration, which provides lower

tropospheric cyclonic vorticity and modifies the lower tropospheric flow. This flow modification results in confluence in a moist environment, enabling convection that generates additional lower tropospheric cyclonic vorticity. In addition to Crandall (2012)'s analysis, he introduced an objective method for the tracking and identification of MGs, primarily based on azimuthally averaged circulation at 850-hPa at large radii. MG tracking was enabled by using the maximum circulation value to objective identify the MG center of circulation. This identification technique is superior to tracking the sea level pressure minimum (as done in Lander [1994]), because TCs that occur in relation to MGs can obtain a minimum sea level pressure that is lower than the MG itself, and therefore track the TC rather than the MG. When investigating the July 1989 MG, Crandall et al. (2014) focused on this mutual interaction between the MG and TC Ken-Lola. In their analysis, TC Ken-Lola forms from a mesovortex within the circulation on the southeastern flank of the July 1989 MG and proceeds to track cyclonically around the larger circulation of the MG, rotating into the northern quadrant of the circulation (Fig. 1.11a). During this evolution, the cloud structure of the MG takes on a "fish-hook" pattern reminiscent of other MGs identified (e.g. Lander 1994). The spatial pattern of the cloudiness appears to be a result of an upper-tropospheric low interacting with the convection associated with the MG (Fig 1.11b). Crandall et al. (2014) argue that mid and upper tropospheric temperature advection is directly associated with regions of cloudy and clear air (Fig 1.11d). In particular, the subsidence in the region of cold air advection on the northwestern flank of the MG appears to give the MG its characteristic asymmetrical convective structure. This result backs up the findings of Molinari and

Vollaro (2012) in that the upper-tropospheric trough is important to the asymmetrical convective distribution of the MG, which distinguishes MGs from MDs.

In addition to MG case studies, there have been several studies that have conducted a climatological investigation of MGs (Chen et al. 2004, Wu et al. 2013). Chen et al. (2004) used the NCEP-NCAR reanalysis data (Kalnay et al. 1996) to identify MG circulations from 1979-2002, identifying ~12.5 MGs seasonally (July-October). However, it is questionable if the disturbances identified in Chen et al. (2004) are MGs, because of a criterion that requires the presence of a weak anticyclone above the cyclonic vortex associated with the MG. This criterion appears to be in contrast to the findings of Lander (1994), Molinari and Vollaro (2012), Crandall (2012) and Crandall et al. (2014), which documented the presence of upper-tropospheric troughing in proximity to the MG circulation, especially during formation. In a follow up study, Chen et al. (2008) noted that only 13% of all MGs identified in the 1979-2002 period were associated with mid-latitude troughs, casting doubt into whether the remainder of the MGs identified in the study bear the same characteristics as those identified in prior literature (e.g. Lander 1994, Molinari and Vollaro 2012). It is also possible that some disturbances identified in Chen et al. (2004) could be large TCs. While an additional criterion requires the closed vortex to have an east-west horizontal scale > 2500 km (1250 km radius), the large size of the outer circulation alone does not preclude the possibility that a TC could expand its outer wind radii to the same spatial scale as a MD or MG. When providing the initial classifying characteristics of MGs, Lander (1994) notes that the MG circulation he describes is not the result of an expanding wind circulation of a preexisting TC. Thus, large TCs should be omitted when attempting a climatological investigation of MGs.

Wu et al. (2013) uses a filtering process to remove TCs when constructing their MG climatology. Their methodology uses a low-pass filter of 850-hPa winds that includes a step where TC circulations are removed from the wind field, preventing large TCs from being counted in the climatology. Using this method combined with additional size criteria, an average of 3.4 MGs were identified annually from 2000-2010. However, similar to Chen et al. (2004) it is unclear that the systems identified in Wu et al. (2013) are MGs due to the lack of an identification feature, other than size, that distinguishes MGs from MDs. Thus, it is possible that the cases identified in Wu et al. (2013) contain large MDs in addition to MGs. An investigation of the composite 200-hPa flow associated with the identified MG cases in Wu et al. (2013) reveals broad anticyclonic flow (Fig 1.12a), while a meridional cross section similarly shows this anticyclonic zonal flow associated with anticyclonic vorticity near the tropopause (Fig 1.12b-c). Such features are consistent with a MD-like structure, rather than a MG-like structure, which exhibits upper tropospheric cyclonic flow associated with a PV maximum (Molinari and Vollaro 2012, Crandall 2012, Crandall et al. 2014). Given these possible inconsistencies in the identifying characteristics of MGs, caution should be used when discussing the composite characteristics of MGs in Chen et al. (2004) and Wu et al. (2013).

1.2.2 Monsoonal Circulations over Central America

As mentioned in section 1.1, there has been a relative lack of research investigating similar type large-scale cyclonic circulations over Central America. The

purpose of this section is to summarize relevant research that will be built upon when conducting a climatology of similar type disturbances to those outlined in section 1.2.

The rainy season over Central America, typically from May – October, garners a significant amount of research in this region (Mosino and Garcia 1966, Hastenrath 1967, Coen 1973, Magana et al. 1999). One important feature that is unique to the Central America rainy season is the existence of a distinct minimum in precipitation during the mid-summer (July-August) called the mid-summer drought, which is most notable along the EPAC coastline of Central America (Magana et al. 1999, Small et al. 2007). Magana et al. (1999) investigated the physical mechanisms that drive these rainfall oscillations, and found that during active rainfall periods (June and September – October) a mean low-level cyclonic wind circulation is present over Central America and the Gulf of Mexico (GoM) where enhanced westerly flow in the EPAC is observed (Fig. 1.3 a). Magana et al. (1999) propose this circulation is generated in response to stationary convective heating occurring off the equator as discussed in Gill (1980). During the mid-summer drought, when less rainfall occurs, a low-level anticyclone occurs in conjunction with enhanced easterly flow at 925-hPa and less convective activity over the EPAC (Fig 1.3b). Small et al. (2007) elaborated further on the climatological aspects of the mid-summer drought, but also suggested that the manifestation of the mid-summer drought could be related to the suppression of transient rain-bearing synoptic systems that impact Central America.

One such Central American synoptic-scale phenomenon is known as a *temporal* (Lessmann 1964, Fernandez and Barrantes 1996, Pena and Douglas 2002), identified as a cyclonic tropical disturbance that produces nearly continuous rainfall for a period of 2 – 4 days over a large portion of Central America. These systems are frequently associated

with convection that is embedded within the disturbance and occasionally associated with strong low-level winds. TCs are sometimes indirectly associated with temporales, but they are not a necessary requirement. While a detailed climatology of temporales has not been performed, they are generally said to occur between May through November, with peaks in activity in June and September – October in association with the latitudinal migration of the EPAC ITCZ. Fernandez and Barrantes (1996) highlight one case study of a Pacific temporal that occurs in May 1982 (Fig 1.14). The low-level wind structure looks similar to a MD and MG in other basins, with a large closed cyclonic circulation located over Central America (Fig 1.14a). Visible satellite imagery depicts active deep convection occurring over the cyclonic circulation (Fig. 1.14b), while a vertical time series of temperature anomalies plotted during the May 1982 temporal depicts negative temperature anomalies between 900 – 600-hPa, but generally positive temperature anomalies above 600-hPa (Fig. 1.14c). These meteorological features are suggestive that the synoptic characteristics of the May 1982 temporal are similar to that of a MD or MG, but over Central America. While not explicitly discussed in the rest of this study, the May 1982 temporal was objectively identified as a CAG case in the climatology that will be presented in chapter 3.

Aiyyer and Molinari (2008) indirectly looked at large gyre circulations though the context of the MJO, where the MJO was investigated in its role of modulating the frequency and location of TC genesis (TCG) in the EPAC and GoM in August – September 1998. During the convectively inactive phase of the MJO over Central America, convective activity was suppressed into the EPAC primarily associated with the ITCZ around 10^{o}N (Fig. 1.15a). However, during the convectively active phase

of the MJO, deep convection with characteristic low brightness temperature migrated northward over Central America and the adjacent ocean basins in association with the generation of a time-mean large-scale cyclonic circulation in the Gulf of Mexico (Fig. 1.15b). Aiyyer and Molinari (2008) refer to this entity as a cyclonic gyre that forms in response to the convectively active MJO. This broad cyclonic circulation was not only present in the time-mean, but also instantaneously, as the NHC noted the cyclonic gyre possessed characteristics similar to a MD prior to its development into TC Frances (Lawrence 1998, Pasch et al. 2001). Boos et al. 2014 also identified a convectively active MJO event occurring in conjunction with the development of a MD in the north IND basin, where the MJO enhanced low-level westerly flow equatorward of the MD. Aiyyer and Molinari (2008) also show that the convectively active MJO in Sep 1998 resulted in barotropic kinetic energy conversion from the base state to eddies over Central America. The evolution of the synoptic wind pattern over Central America in Sep 1998 from one that is zonal to one that depicts a large cyclonic gyre similar in definition to a MD is consistent with studies that showed the importance of barotropic instability in MD formation in the north IND basin (Krishnamurti et al. 1976, Shukla 1978, Nitta and Masuda 1981). While not explicitly discussed in the rest of this study, the Sep 1998 gyre identified in Aiyyer and Molinari (2008) was objectively identified as a CAG case in the climatology that will be presented in chapter 3.

1.3 Research Goals and Thesis Structure

This research expands upon work conducted on MDs and MGs in other oceanic basins by applying their identification characteristics to similar circulations over Central

America using a global gridded reanalysis dataset. In particular, an algorithm will be created based upon the prior classifications of MDs and MGs in order to produce an objective 1980-2010 climatology of CAGs. Noting the importance of upper tropospheric features that discriminate between MD and MG-like structures, individual CAG cases will be tested by the algorithm for the presence of upper-tropospheric troughs near the CAG center. Thereafter, a gyre-relative composite analysis will be preformed on the two CAG subsets identified in the 1980-2010 climatology in order to document the structure, motion, and evolution of CAG events prior to and after their development. The author hypothesizes that the 1980-2010 CAG climatology will reveal significant differences between the two CAG subsets, with CAGs associated with upper tropospheric troughs resembling a MG-like structure, while CAGs without upper tropospheric troughs resembling a MD-like structure. The author also hypothesizes that the composite CAG structure will depict formation processes similar to that of a MD, where there is a breakdown of the zonal mean flow into a large cyclonic circulation, and that convective processes such as LHR are important to the maintenance of the CAG. Moreover, CAGs are hypothesized to occasionally occur in conjunction with TCs, and CAGs are also hypothesized to occur more frequently in occurrences of a convectively active MJO over Central America, as seen in Aiyyer and Molinari (2008).

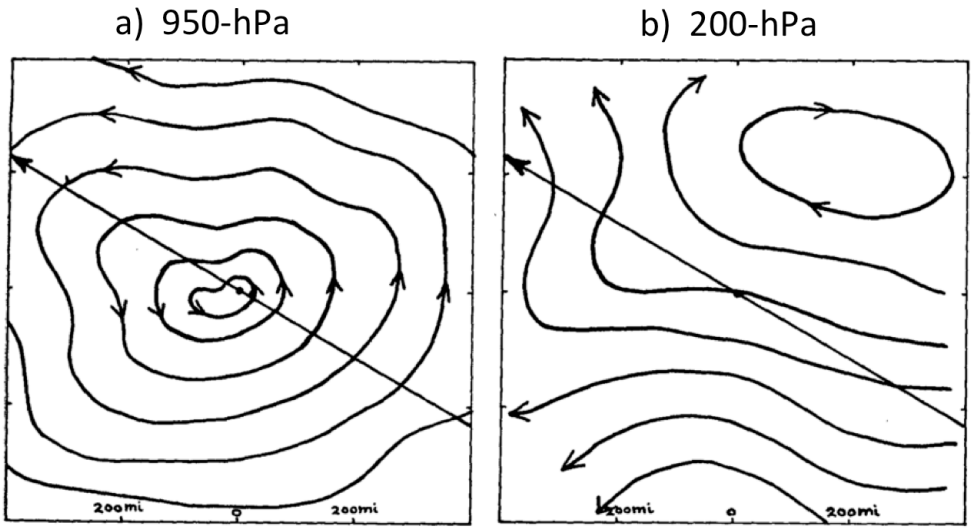

Fig. 1.1. Streamlines of flow associated with 22 MD cases identified at (a) 950-hPa and (b) 200-hPa. The large vector arrow in both plots represents the direction of motion of the MD (300 degrees) [Fig. 3, 10, and caption adapted from Mulky and Banerji (1960)].

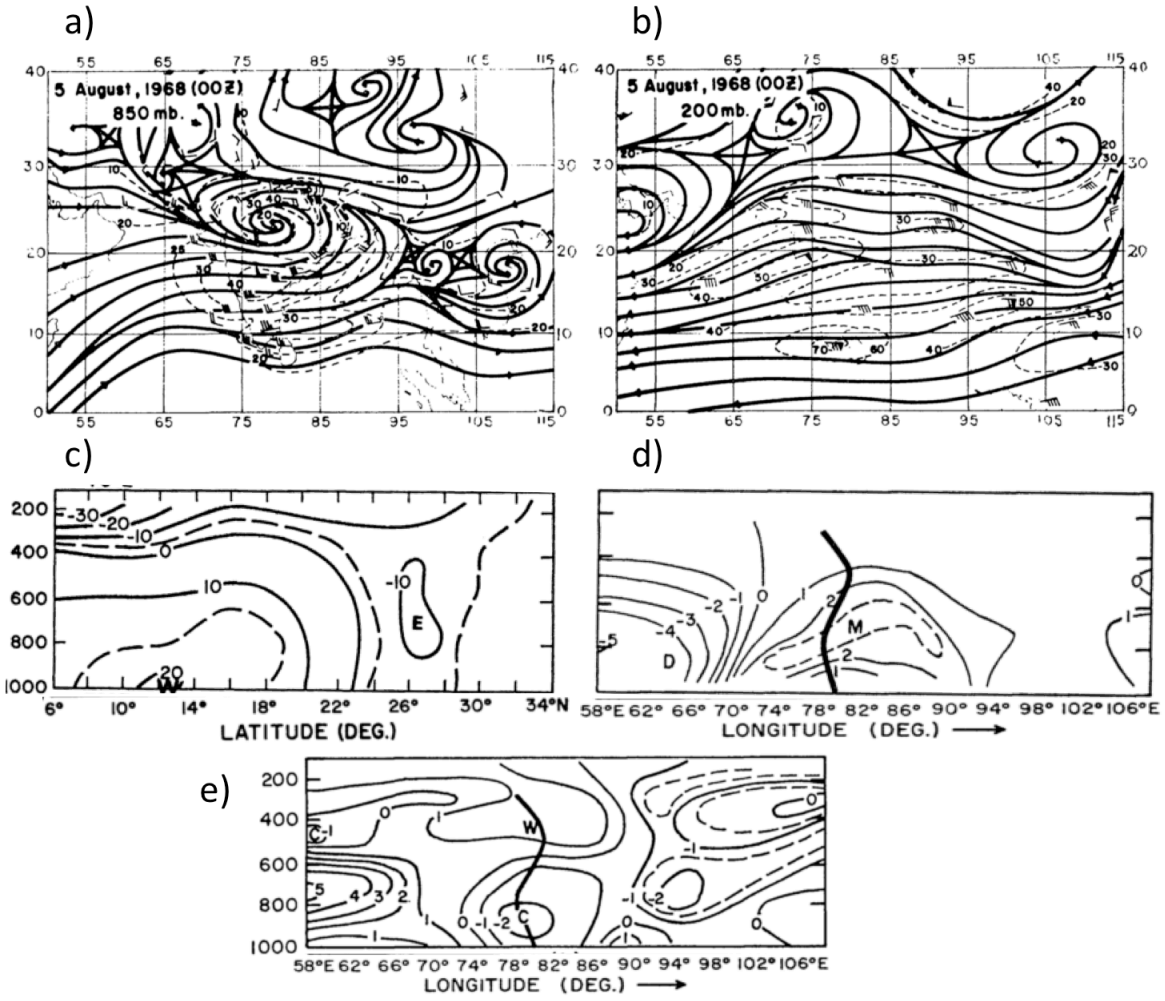

Fig. 1.2. Paneled depiction of synoptic scale features associated with a MD identified at 0000 UTC 5 August 1968. Panel (a) shows 850-hPa streamlines (black contours) with 850-hPa isotachs (black dotted lines, m s^{-1}). Panel (b) shows 200-hPa streamlines (black contours) with 200-hPa isotachs (black dotted lines, m s^{-1}). Panel (c) is a vertical cross-section depicting zonal winds (alternating dotted and solid black lines, m s^{-1}). The uppercase W and E represent westerly and easterly zonal wind maxima. Panel (d) is a vertical cross-section of specific humidity anomaly (black contours, g kg^{-1}). The uppercase M and D represent specific humidity maxima and minima. Panel (e) is a vertical cross-section of temperature anomaly (black contours, ^{o}C). The uppercase W and C represent temperature maxima and minima respectively. The thick black line is panels (d) and (e) represents the vertical tilt of the cyclonic circulation of the MD [Fig. 2b,3b,6b,7b,9b and adapted caption from Krishnamurti et al. (1975)]

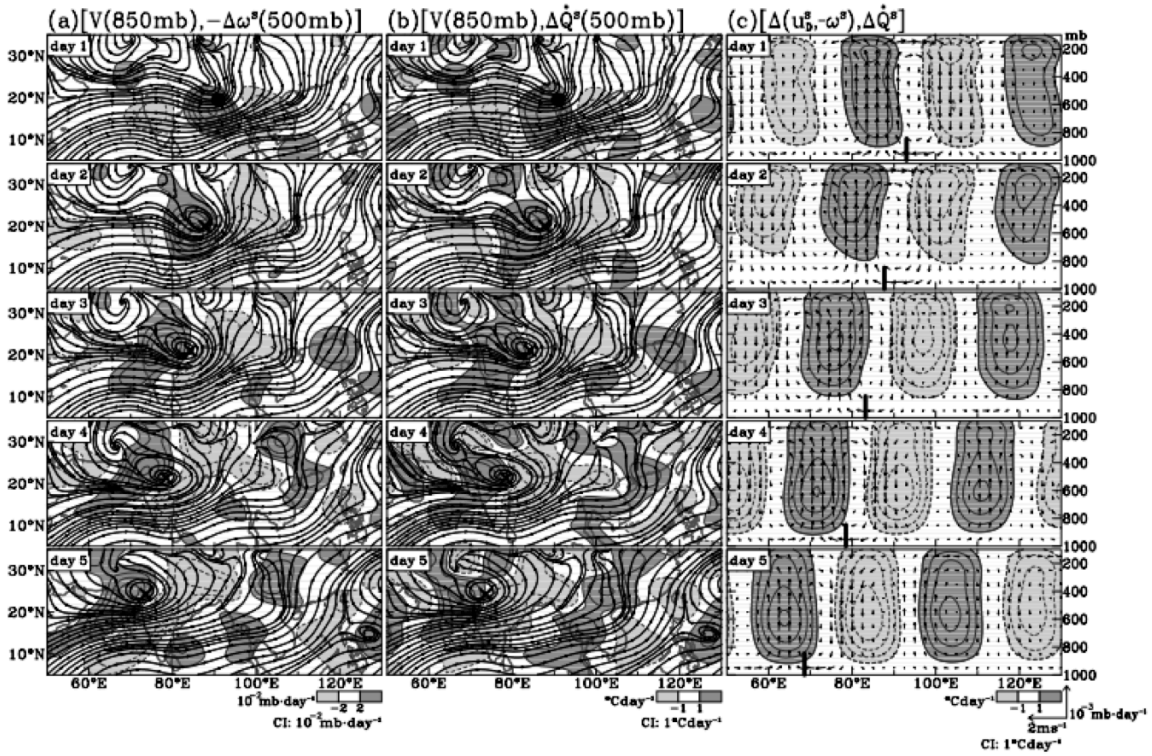

Fig. 1.3. Composite MD depicted by the (a) 850-hPa streamlines (black contours) and vertical velocity (shaded, 10^{-2} mb day^{-1}), (b) 850-hPa streamlines (black contours) and diabatic heating (shaded, ^{o}C day^{-1}), and (c) east-west vertical cross-section of diabatic heating (shaded, ^{o}C day^{-1}) and the vertical circulation (vectors as noted) [Fig. 4 adapted citation from Chen et al. (2005)].

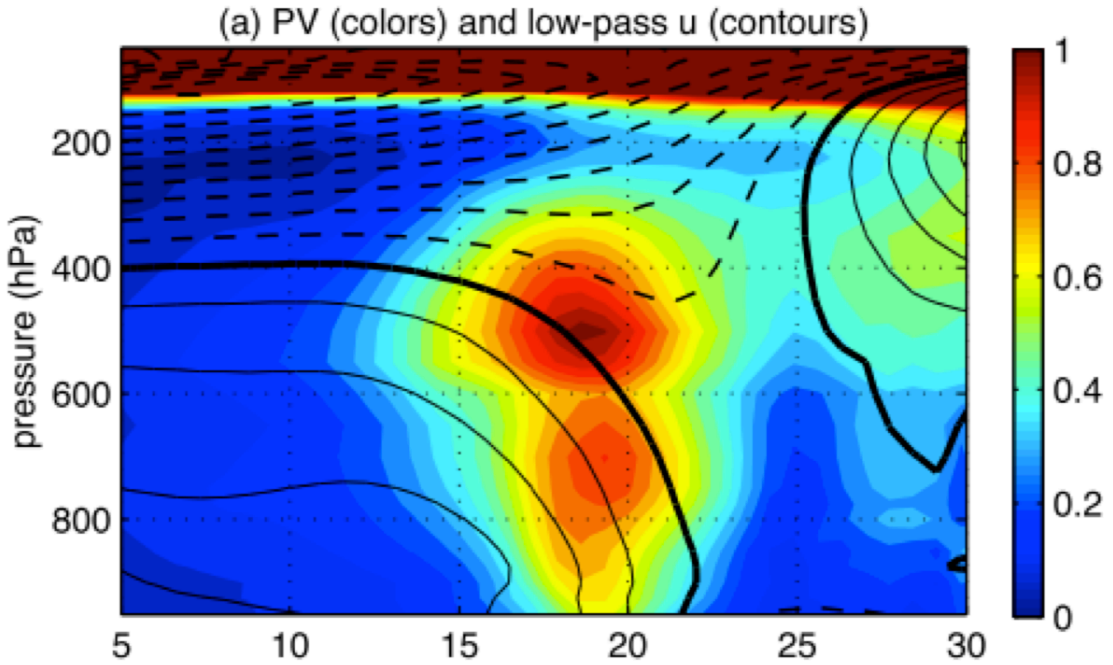

Fig. 1.4. Composite vertical cross-section of 117 MDs in the BoB. Plotted is potential vorticity (shaded, PVU) and 21-day smoothed zonal wind (black contours where negative values are dashed, 3 m s^{-1} interval) [Fig. 8a and adapted caption from Boos et al. (2014)].

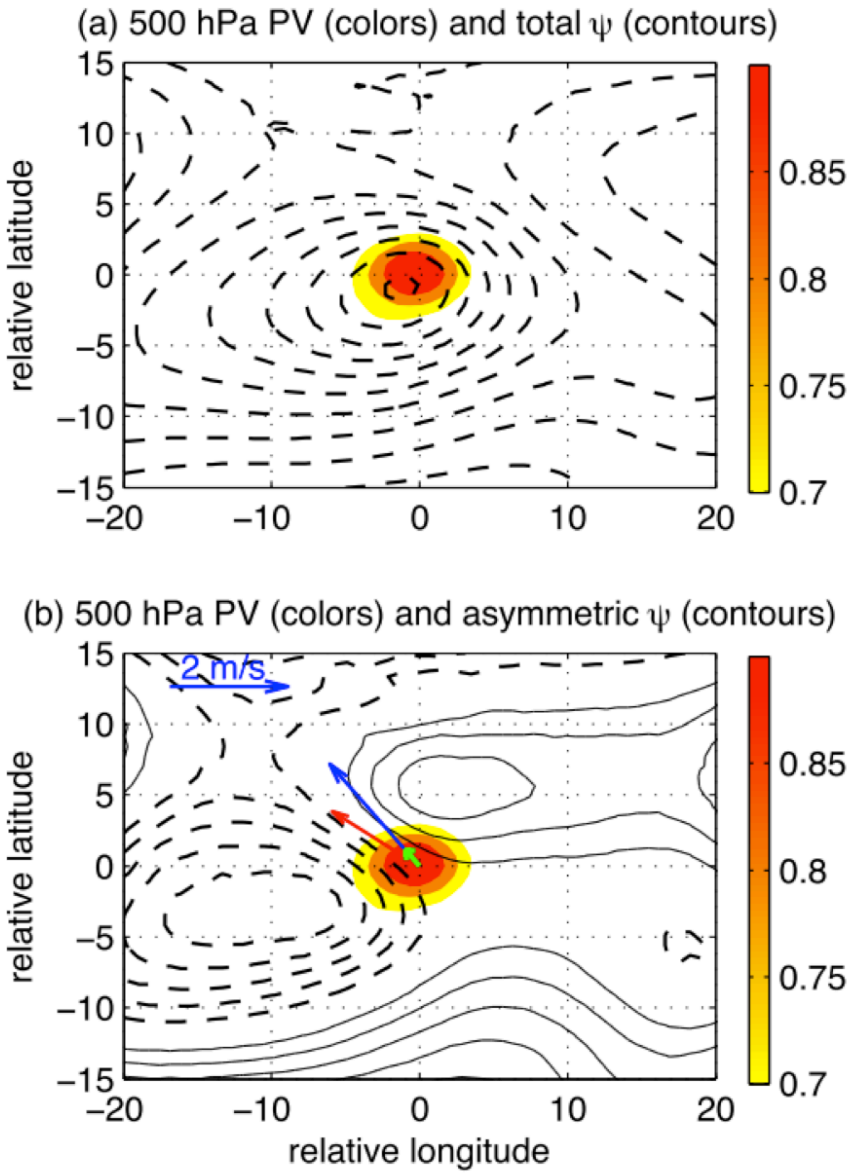

Fig. 1.5. Decomposition of streamfunction associated with 117 MDs in the BoB in system-relative coordinates. (a) Depicts 500-hPa PV (shaded, interval 0.1 PVU starting at 0.7 PVU) and 500-hPa total horizontal streamfunction (black contours with dashed representing counterclockwise flow, interval of 10^6 m^2 s^{-1}). (b) As in (a), except with the azimuthally asymmetric portion of the streamfunction (black contours with dashed representing counterclockwise flow, interval of $5x10^5$ m^2 s^{-1}). The blue arrow in (b) is the total horizontal wind vector averaged in a $2x2^o$ box around the PV maximum, the green arrow is the climatological mean horizontal wind vector averaged over the same area, and the red arrow is the storm propagation velocity [Fig. 11 and adapted caption from Boos et al. (2014)].

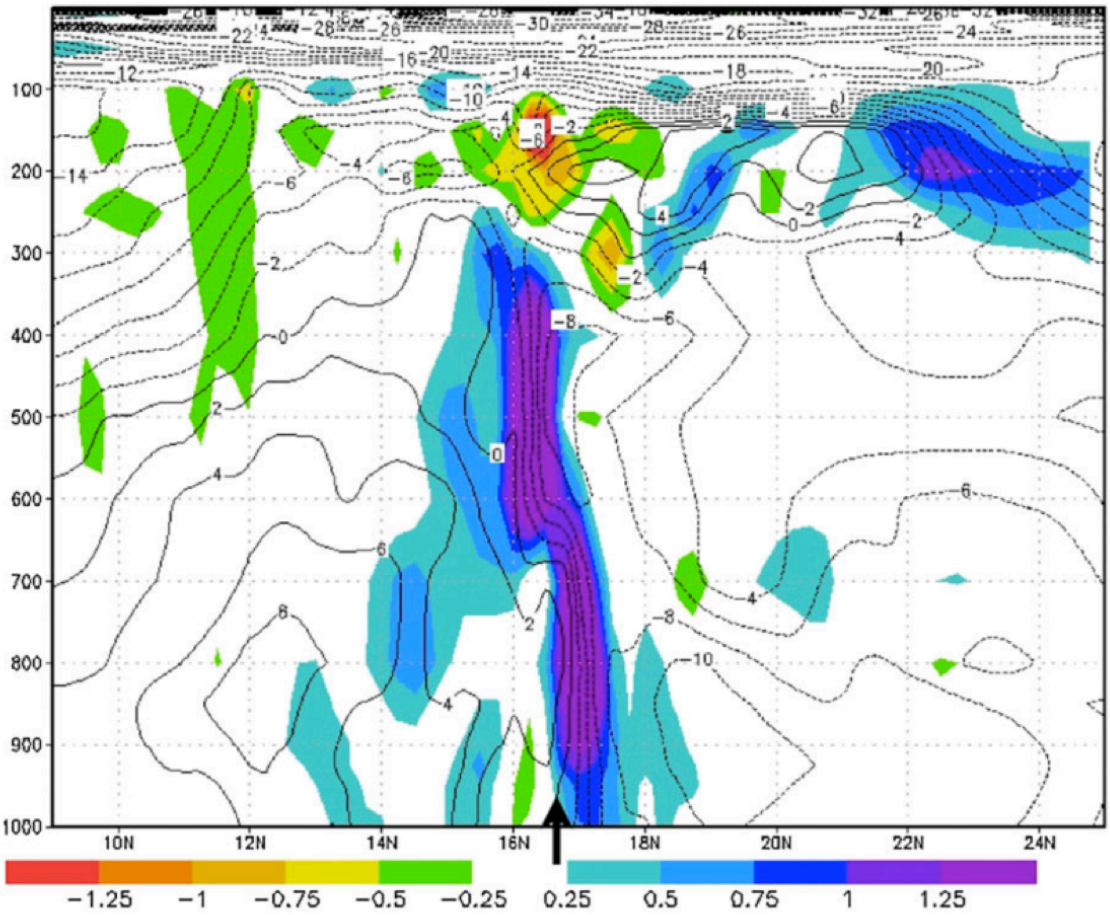

Fig. 1.6. North-south vertical cross-section at 141°E of a MD depression occurring on 1800 UTC 22 August 2009. Fields plotted are relative vorticity (shaded, 10^{-4} s^{-1}) and zonal winds (black contours with dotted lines indicating negative values, m s^{-1}). Arrow points to the center of the MD [Fig. 3b and adapted caption from Beattie and Elsberry (2013)].

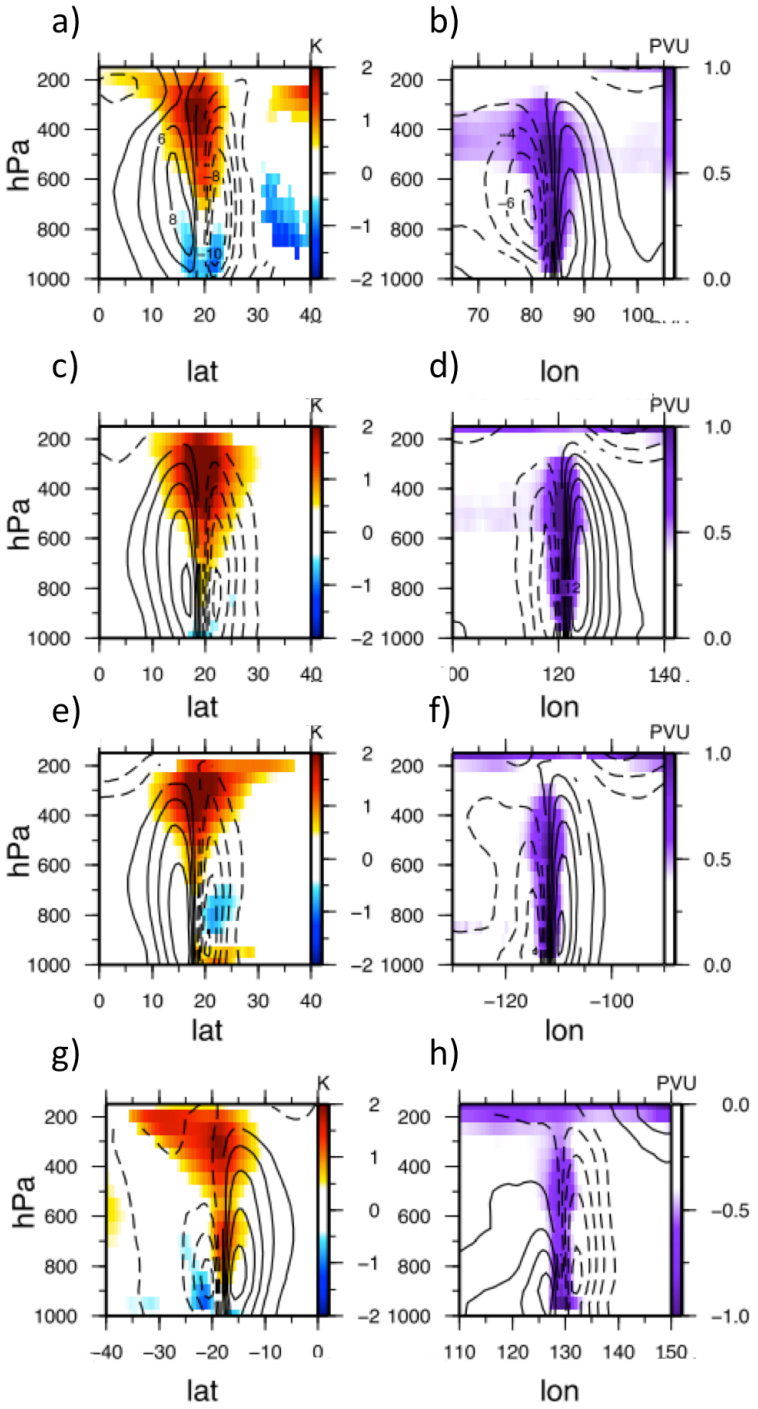

Fig. 1.7. Composite structure of MDs occurring in various oceanic basins during local summer. Left panels denote potential temperature anomalies (shading, K) and zonal wind anomalies (black contours with dotted lines indicating negative values, every 2 m s^{-1}). Right panels denote PV (shading, PVU) and meridional wind (contours with dotted lines indicating negative values, every 2 m s^{-1}). Regions are (a,b) north IND, (c,d) WPAC, (e,f) south IND, and (g,h) EPAC. Values shaded or contoured only if t-test is significant at the 5% level [Fig 9, 10, and adapted caption from Hurley and Boos (2014)].

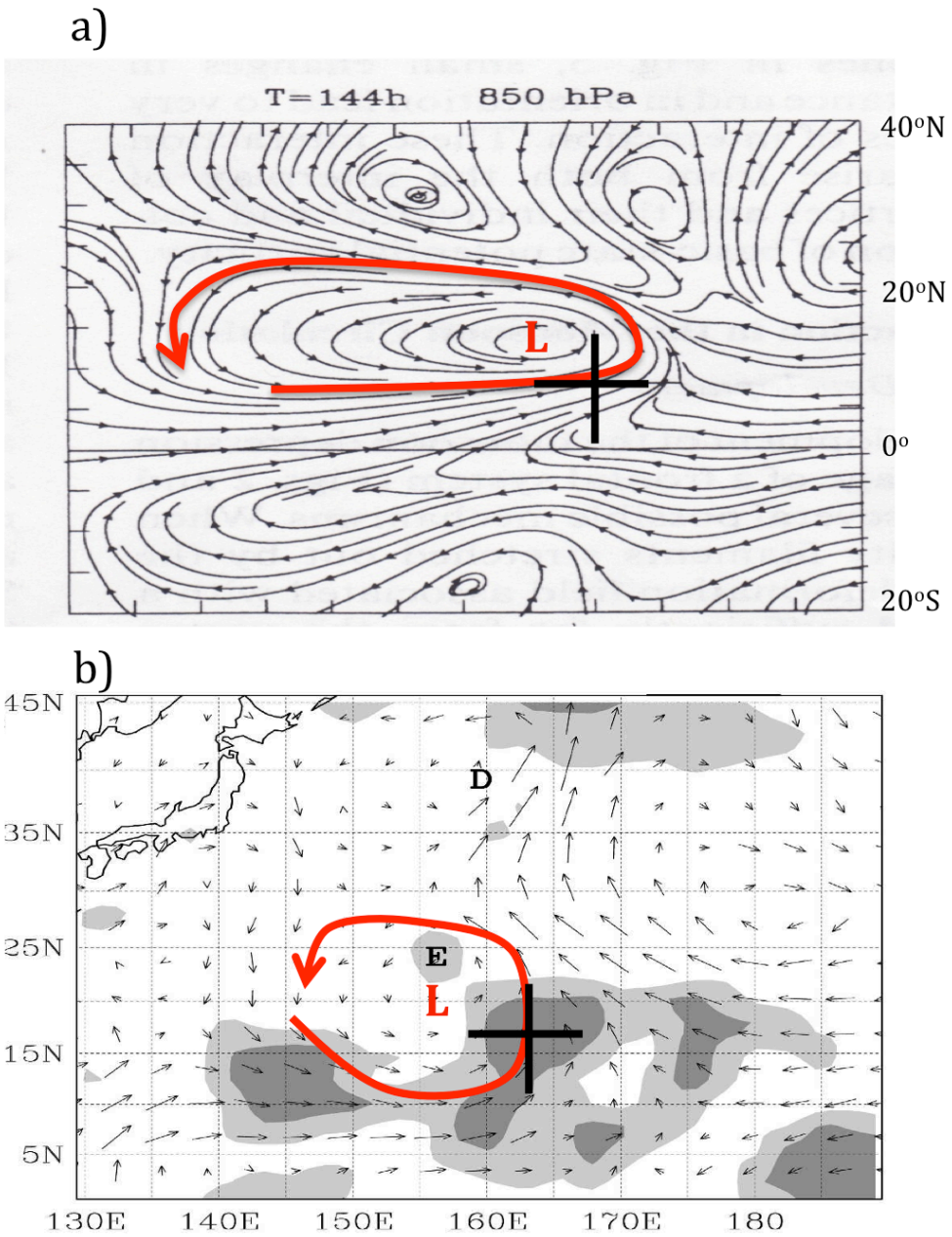

Fig. 1.8. Comparison between the modeling results of Holland (1995) and the August 1991 MG. The top panel (a) depicts 850-hPa streamlines of a MG that developed after 144-hour integration of primitive equations with a Gaussian profile of diabatic heating indicated by the black crosshairs. The red arrow depicts the cyclonic flow of the MG [Fig. 6f and adapted caption from Holland (1995)]. The bottom panel (b) is a synoptic map of a MG on 0000 UTC 11 August 1991 depicting 850-hPa wind (vectors) and outgoing long wave radiation (shading, negative 150-210 W m^{-2}). The crosshair in (b) represents the deepest convection and the red arrow depicts the cyclonic flow of the MG. Labels E and D represent TCs Doug and Ellie respectively [Fig. 8c and adapted caption from Molinari et al. (2007)].

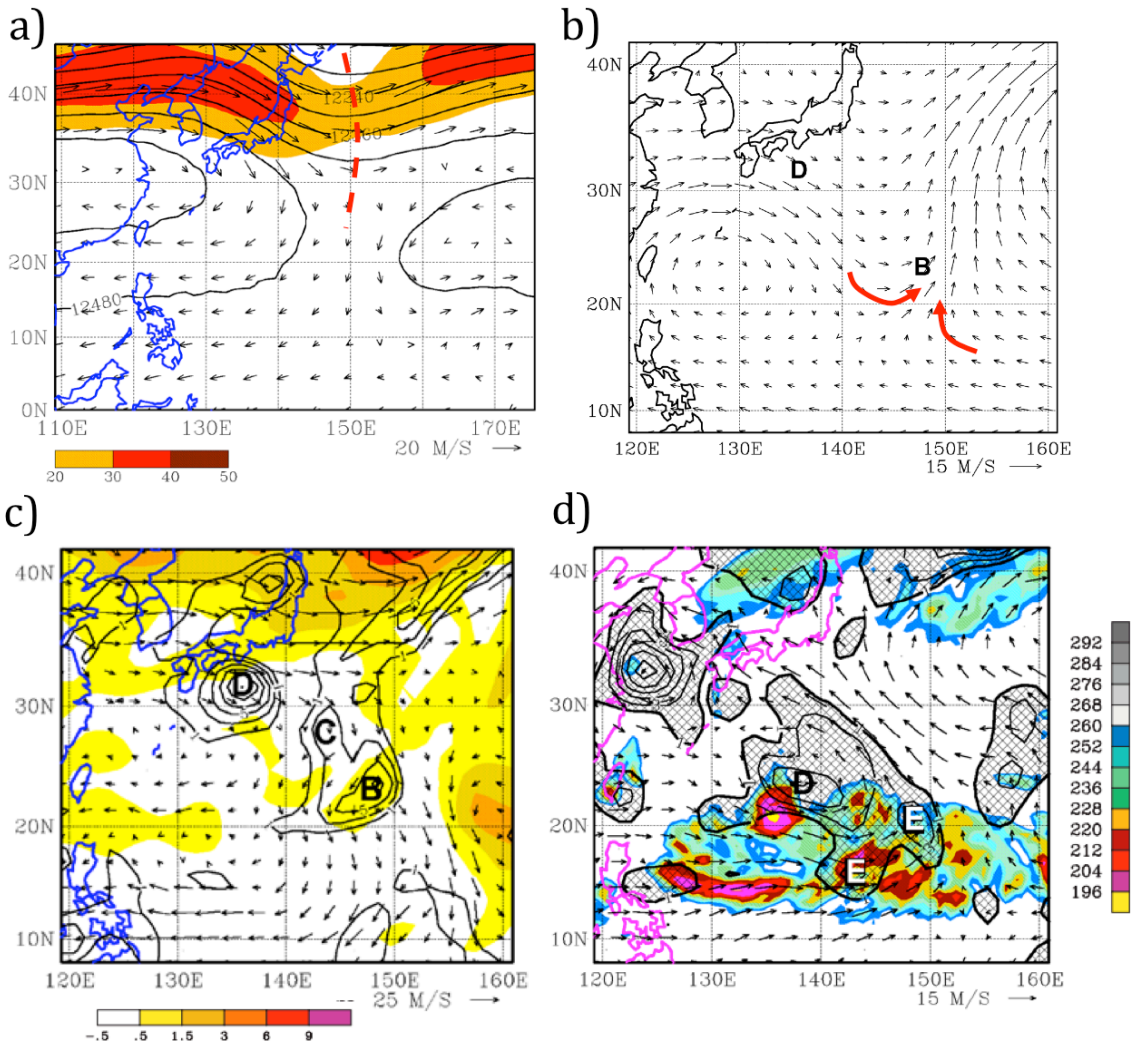

Fig. 1.9. Processes that lead to the development of MG in July 1988. (a)1-25 July 1988 mean 250-hPa wind (vectors, m s^{-1}), 250-hPa isotachs (shading, m s^{-1}), and 250-hPa heights (black contours, m). The dotted line outlines the mean upper-level trough axis. (b) 19 – 25 July 1988 averaged 1000 – 400-hPa layer mean wind (vectors, m s^{-1}). Red arrows represent confluent flow near 150°E. (c) 0000 UTC 24 July 1988 PV the on 350K surface (shaded, PVU), 350K wind (vectors, m s^{-1}), and 850-hPa vorticity (contours, starting and incremented at $2x10^{-5}$ s^{-1}). (d) 0000 UTC 27 July 1988 infrared brightness temperature (shading, K), 850-hPa cyclonic vorticity (hatched shading in black contours, starting at $1x10^{-5}$ s^{-1}), and 850-hPa winds (vectors, m s^{-1}). Upper case letters in all panels represent different vorticity maximums [Fig. 5b, 9d, 10, 11d and caption adapted from Molinari and Vollaro (2012)].

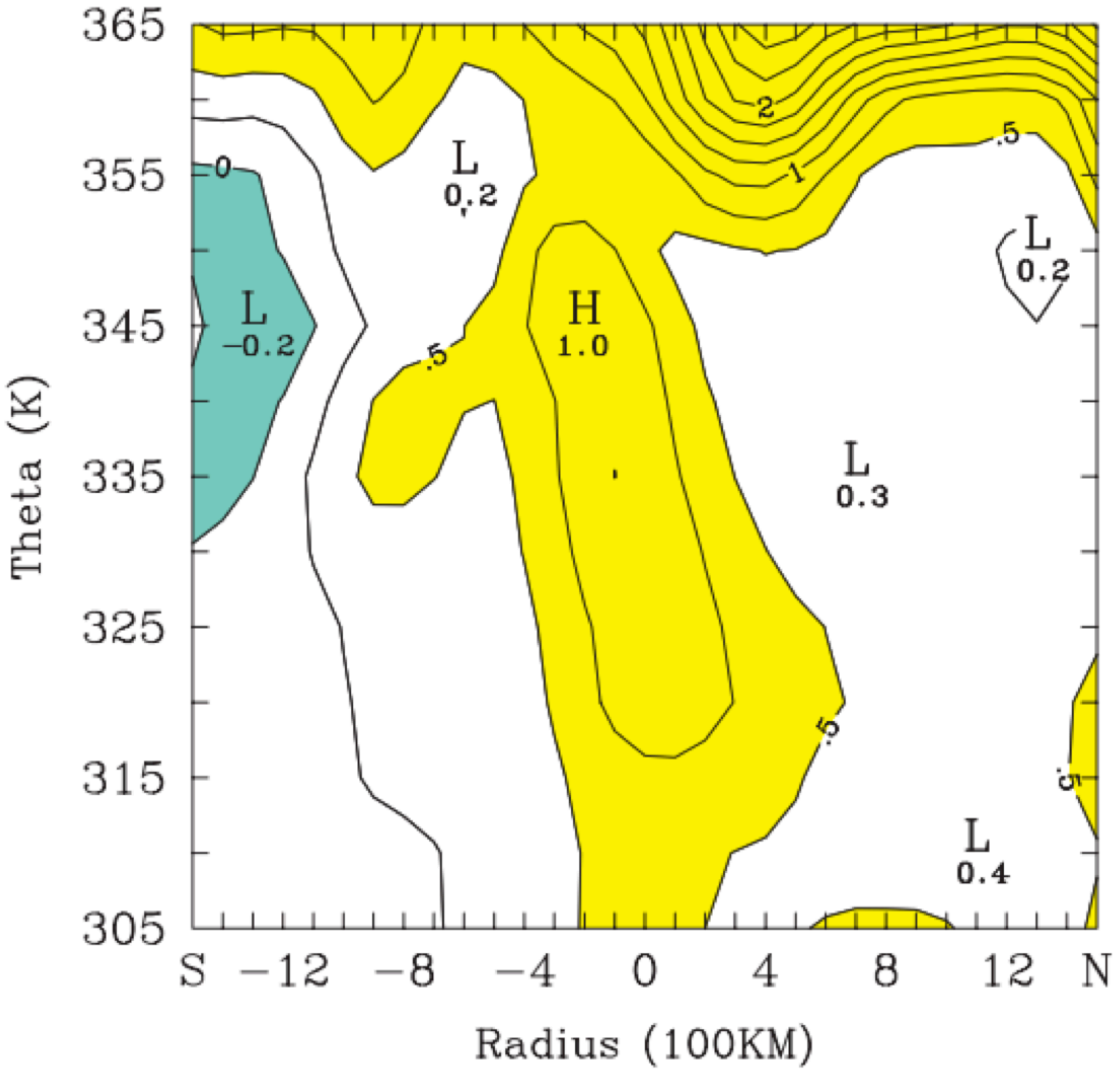

Fig. 1.10. North-south cross-section across MG averaged from 0000 UTC 27 July to 0000 UTC 28 July. Plotted is PV (shaded, blue indicates PV < 0 PVU while yellow indicates PV > 0.5 PVU [Fig. 14b and adapted caption from Molinari and Vollaro (2012)].

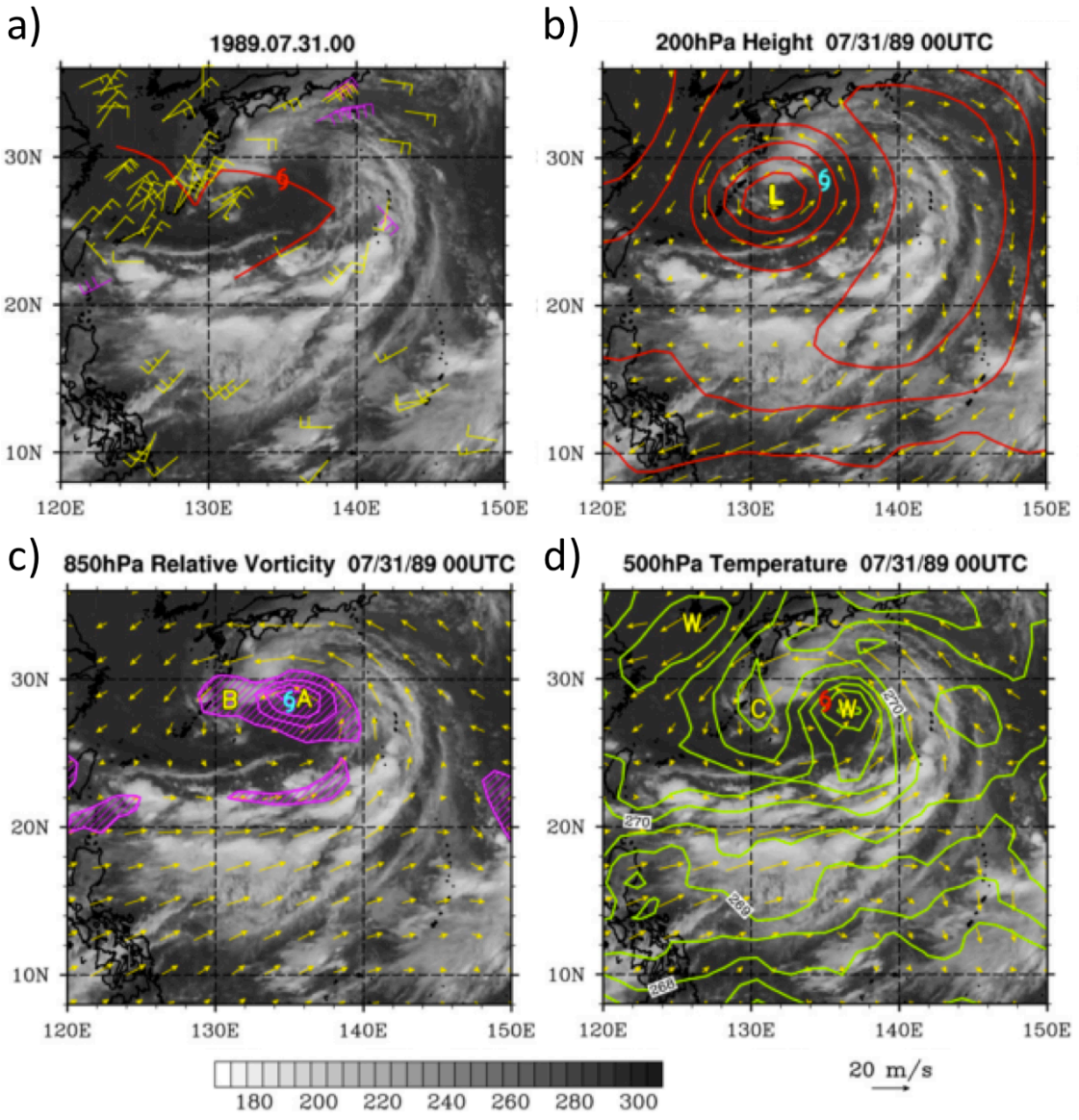

Fig. 1.11. Relevant meteorological features associated with a MG at 0000 UTC 29 July 1989. (a) Infrared brightness temperature (shading, K) with surface winds from coastal stations, ships, and buoys (barbs in kt, yellow below gale force and magenta above). (b) Infrared brightness temperature (shading, K), 200-hPa heights (red contours, every 20 m), 200-hPa winds (vectors, m s^{-1}). Yellow L indicates the 200-hPa height minimum. (c) Infrared brightness temperature (shading, K), 850-hPa cyclonic vorticity (purple hatching, shading starting at $5x10^{-5}$ s^{-1}), and 850-hPa winds (vectors, m s^{-1}). Upper case letters refer to individual vorticity maxima. (d) Infrared brightness temperature (shading, K), 500-hPa temperature (green contours, increment is 0.5K), and 500-hPa wind (vectors, m s^{-1}). Letters W and C refer to a temperature maximum and minimum respectively [Fig. 1i, 2c, 3c, 4c, 7a, and caption adapted from Crandall et al. (2014)].

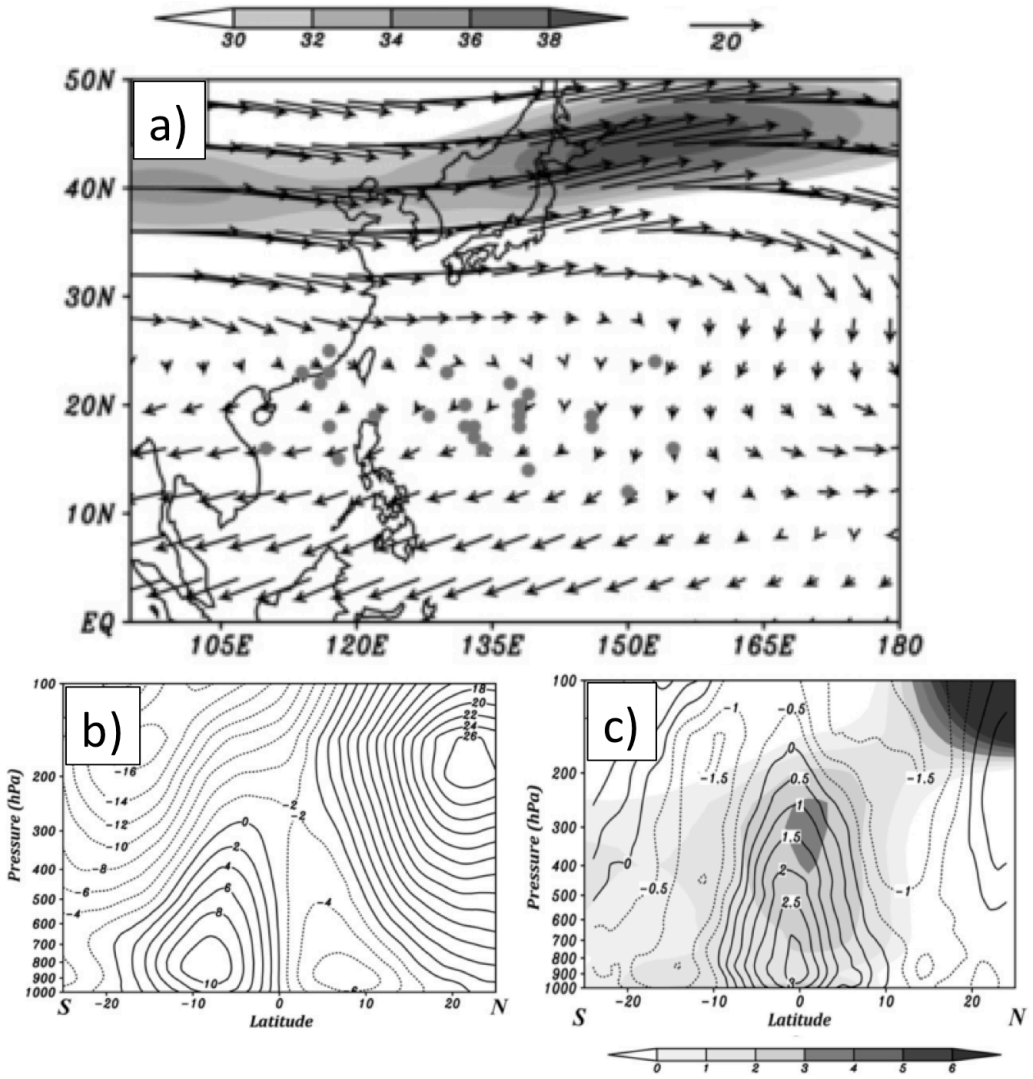

Fig. 1.12. Composite figures of 37 MGs identified from 2000-2010. (a) August-October 10-day low-pass filtered 200-hPa wind (vectors, m s^{-1}) and isotachs (shading top color bar, m s^{-1}). MG centers are depicted as gray dots. (b) North-south vertical cross-section of 10-day low-pass filtered zonal wind (contours with dotted lines indicating negative values, m s^{-1}) at the time of max MG intensity. (c) North-south vertical cross-section of 10-day low-pass filtered temperature anomalies (shading bottom color bar, ^{o}C) and vorticity (black contours with dotted lines indicating negative values, 10^{-5} s^{-1}). The composite MG center is both vertical cross-sections is at zero degrees [Fig. 4b,6a,7a and caption adapted from Wu et al. (2013)].

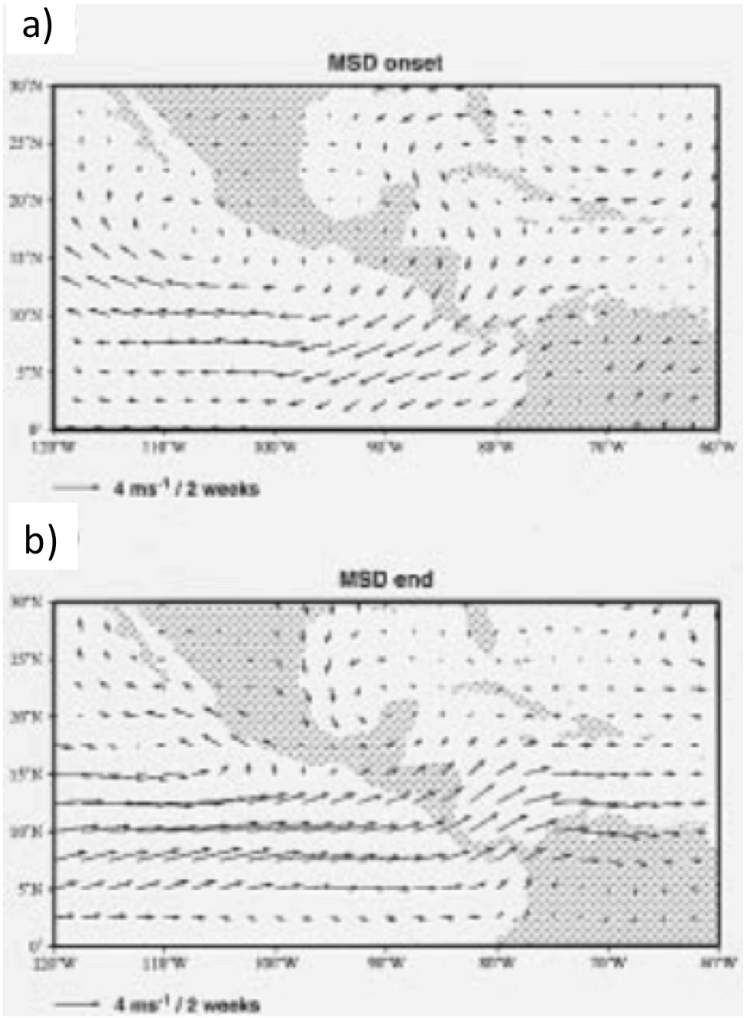

Fig. 1.13. Biweekly composite 925-hPa winds (vectors, m s^{-1}) between two biweekly periods during (a) the onset of MSD, and (b) the end of the MSD [Fig. 8 and caption adapted from Magana et al. (1999)].

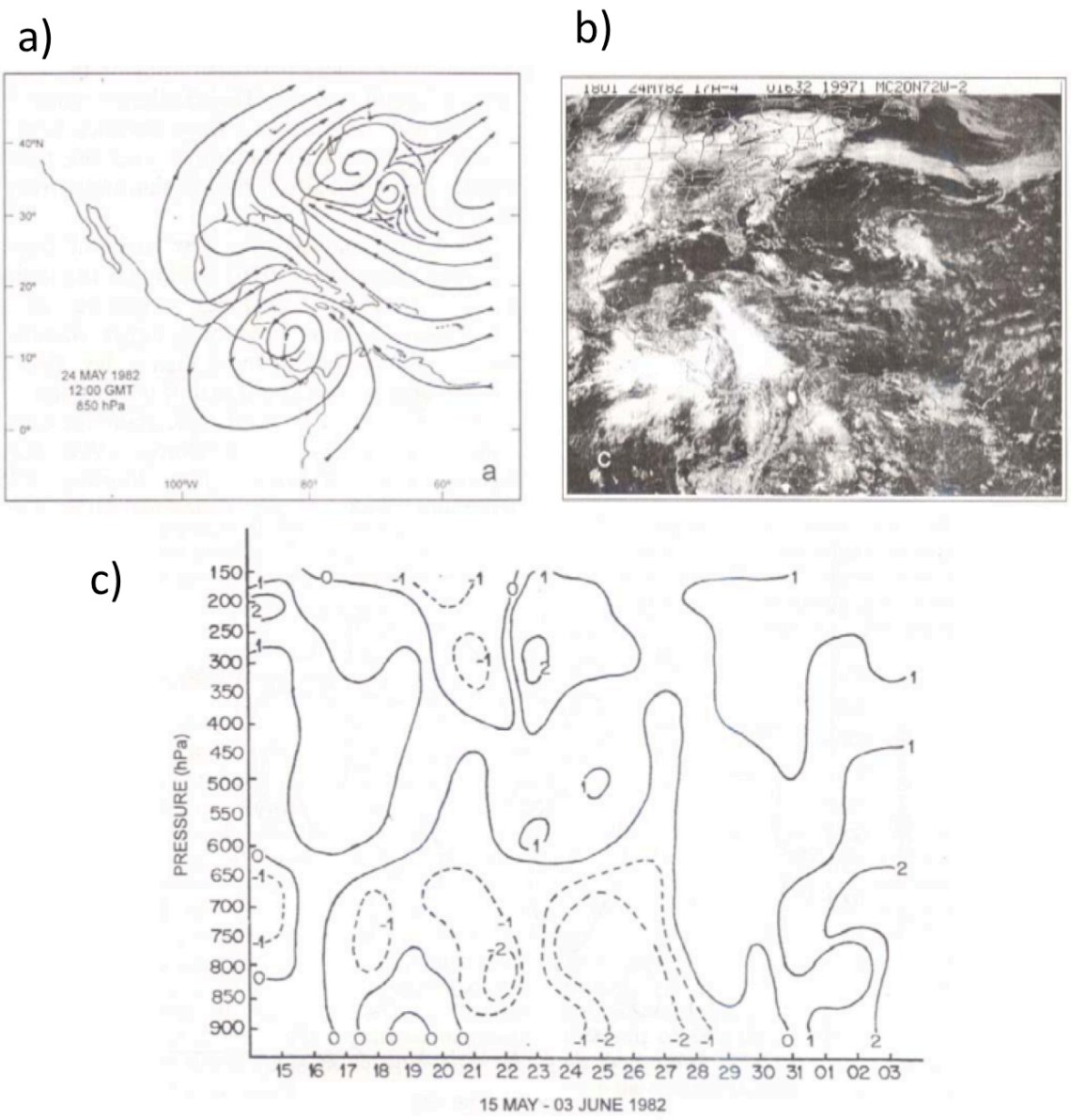

Fig. 1.14. Case study of a temporal in May 1982. (a) 850-hPa streamlines at 1200 UTC 24 May 1982. (b) Visible satellite imagery at 1801 UTC 24 May 1982. (c) Vertical cross-section time-series of temperature anomalies (black contours with dotted lines indicating negative values, ^{o}C) from 15 May – 3 June 1982 [Fig 2c, 3a, 5, and caption adapted from Fernandez and Barrantes (1996)].

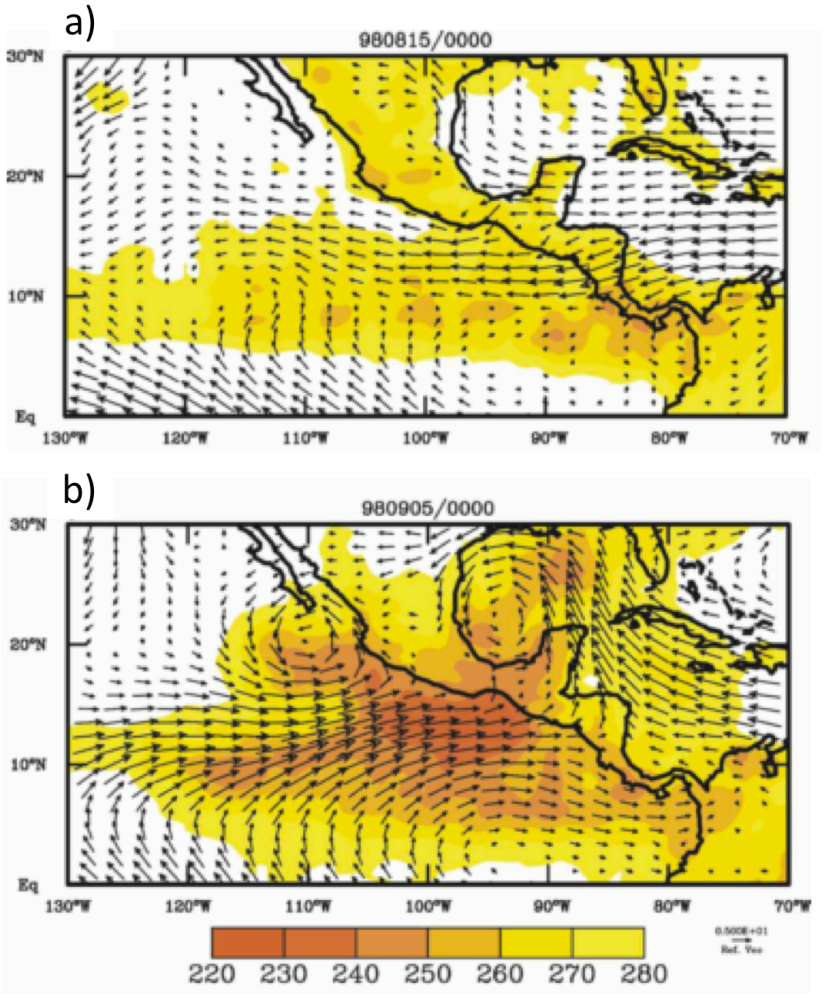

Fig. 1.15. Formation of a large cyclonic gyre in the GoM during a convectively active MJO. Depicted are 20-day low-pass filtered brightness temperature (shaded, K) and 850-hPa winds (vectors, m s^{-1}) for (a) 0000 UTC 15 August 1998 during a convectively inactive MJO period and (b) 0000 UTC 05 September 1998 during a convectively active MJO period [Fig. 4b, 4d, and caption adapted from Aiyyer and Molinari (2008)].

2. Data and Methodology

2.1. Data Sources

A climatology was developed for CAG cases during the ATL and EPAC hurricane season. To conduct this climatology, this study uses gridded data from the National Centers for Environmental Prediction (NCEP) Climate Forecast System Reanalysis (CFSR; Saha and Coauthors 2010) at $0.5^{o} \times 0.5^{o}$ resolution for four times daily synoptic times (0000, 0600, 1200, and 1800 UTC). This dataset provided a homogeneous 31-year (1980-2010) period to study the climatology of CAG disturbances. National Climatic Data Center's (NCDCs) Gridded geostationary Satellite archive (GridSat) (Knapp and Coauthors 2011) was attained for Infrared (IR) satellite imagery over the same time interval. NCDC's International Best Track Archive for Climate Stewardship (IBTrACS; Knapp et al. 2010) provided TC positions and tracks related to CAG. The real time multivariate Madden Julian Oscillation (RMM) Index was used to identify the MJO for this particular study (Wheeler and Hendon 2004). Text files containing the RMM index at daily intervals since 1974 were obtained from the Center for Australian Weather and Climate Research (http://cawcr.gov.au/staff/mwheeler/maproom/RMM/).

Beyond these primary datasets, a series of derived variables were calculated in order to classify CAG occurrences. One important variable used in the identification of CAGs is circulation, which is defined by using the circulation theorem, which mathematically states:

$$C = \oint \vec{\zeta} \cdot d\vec{l} = \iint A\,\zeta\,dxdy \qquad (1)$$

Where ζ represents relative vorticity, and the integration symbols represent integration of this variable over a given circular area, A. Positive values of circulation, C, are given by integrating counterclockwise around a radial. Such a process can be conducted using a gridded dataset by centering a circle on a given grid point, then averaging the total relative vorticity of all grid points extending radially outward from the center. ζ results when C is divided by a circular area in the limit that the area shrinks to zero. Thus, circulation in this sense is analogous to area average relative vorticity, $\bar{\zeta}$, at a given radius for a given grid point. Circulation is a convenient variable because it is a conserved quantity within the integrated circuit selected. It also allows for the objective identification of a center point using the maximum C of the circuit of rotating flow, a useful tool that will be later used to identify CAG center of circulation.

Tangential wind (V_t) can also be defined given an areal measure of circulation. When calculating azimuthal average V_t around a gyre, a variation of the circulation theorem is used:

$$V_t = \frac{\iint (\nabla \times \vec{v}) dA}{2\pi r} = \frac{C}{2\pi r} \quad (2)$$

Where C is the area average vorticity, and r is the distance between the center of the gyre and the distance the azimuthal average is being calculated for. Here, positive (negative) values of V_t denote cyclonic (anticyclonic) or counter clockwise (clockwise) flow in then northern hemisphere. Azimuthally averaged V_t was calculated at 50 km intervals from the center of the gyre outwards to 1500 km in order to capture the radial tangential wind profile of the gyre circulation.

2.2. Methodology

2.2.1. Gyre Definition

Previous literature has provided a variety of different criteria when classifying large-scale low-level cyclonic circulations in the tropics. The vast majority of literature focuses on identifying characteristics of both MDs and MGs in the WPAC and IND ocean basins. The initial set of criteria of MGs devised by Lander (1994) is primarily a subjective set of qualifications (e.g. visually estimate outer closed isobar with radius of 1250 km or greater). Without an objective set of criteria, it is difficult to replicate the results of this study. Lander (1994) also acknowledges that there is a spectra of atmospheric configurations between a traditional monsoon trough in the WPAC versus a fully closed wind circulation associated with a MG. Furthermore, recent studies have differed on the specific guidelines that characterize a MG (e.g. Chen et al. 2004, Chen et al. 2008, Molinari and Vollaro 2012, Crandall 2012, Wu et al. 2013, Crandall et al. 2014). These different terminologies have often resulted in widely varying numbers of MG events as well as related TCG events within the gyre envelope. For the purposes of this study, we will adopt several identification criteria similar to that used by Crandall (2012), who calculated circulation at different radial means when identifying a MG circulation in July 1988.

Differences also exist in establishing a MD definition. While generally occurring at smaller radii than MGs, literature has noted sizes ranging from 500 km in radius (Aldinger and Stapler 1998, Beattie and Elsberry 2013) up to 1250 km (Saha and Chang 1983, Douglas 1992). The lifespan of MDs are also typically shorter, due to the majority

of MD events transforming into TC like vortices (with a decreasing radius of maximum winds) after a 2-3 day period (Lander 2004, Beattie and Elsberry 2013). Additional differences in MD characteristics can also be attributed to the variation of genesis locations between the IND and WPAC basins.

2.2.2. Objective Algorithm

Given the wide-ranging differences in definition between MDs and MGs in other basins, this study focused on creating new, objective criteria used to identify similar type disturbances over Central America. The criteria devised were used to develop an algorithm that could distinguish CAG occurrences versus non-events. The following tests below contain these criteria that were used to analyze possible CAG events:

2.2.2.1. Domain and Longevity

1) Latitude Range: (5-30^{o}N)
2) Longitude Range: (100-70^{o}W)
3) Lifespan (greater than or equal to 48 h)

The domain and longevity test focuses on restricting the domain size and limiting the time period required for classification. The domain size was chosen to focus on large-scale low-level cyclonic circulations that develop in close proximity to Central America. The lifespan requirement is used to eliminate transient events that would not have

fulfilled the lifespan definitions referred to in previous literature of MGs and MDs. The 48-hour threshold is a more relaxed lifespan definition in comparison to Lander (1994) and Ritchie and Holland (1999), but closer to a recent study on MGs (Wu et al. 2013), which identified MGs lifespans ranging from 4-17 days. A similar lifespan threshold was also used to identify MDs in Hurley and Boos (2014).

2.2.2.2 Circulation Magnitude

1) 500-1000 km radial average C at 850 hPa must exceed 1×10^{-5} s^{-1} for each given time period.
2) The maximum C value is designated as the CA gyre center

The circulation magnitude test is used as a first pass to filter out non-gyre occurrences. The 1×10^{-5} s^{-1} minimum threshold was chosen to remove circulations that were too weak to be considered a CAG. This was verified by testing the threshold value on WPAC MDs and MGs identified in previous studies (Lander 1994, Harr et al. 1996, Molinari and Vollaro 2012, Wu et al. 2013). When MDs and MGs were first classified in these previous studies, the circulation threshold given above was always exceeded in each event, providing support that this value could discriminate gyre events from null cases. This C magnitude threshold has also been used in the identification of MDs in recent literature (Boos et al. 2014, Hurley and Boos 2014). The C magnitude provides a "first cut" at filtering out non-gyre periods that will be further restricted in additional tests.

As noted in section 2.1, the circulation maximum of a particular area value can objectively identify the center of a rotating system of that radius. This circulation maximum also indicates the location that maximizes the component of wind following a circular curve. Thus, the gridpoint containing the maximum circulation value is used as the center of the CA gyre, which is important for calculating V_t in subsequent tests. For identifying large systems on the same horizontal magnitude as MDs and MGs observed in the WPAC and IND basins, this study chose a 500-1000 km radial average of circulation that spans the size spectrum of these disturbances. This is similar, but broader than the 666 km circulation radius chosen by Wu et al. (2013) for the identification of MGs events in the WPAC, but smaller than the 900-1200 km radial average circulation chosen by Crandall (2012). The lower radial average is used because we want to identify both MD and MG-like circulations and MDs are often smaller in spatial scale compared to MGs.

2.2.2.3 Azimuthally Averaged Tangential Wind

1) The maximum azimuthally averaged V_t must exceed 5 m s^{-1}
2) The maximum azimuthally averaged V_t must exist at a distance greater than 500 km from the objectively identified gyre center.

The azimuthally averaged tangential wind test helps to filter out large circulations that may occur due to the existence of large TCs, while still ensuring the identified circulation is large and robust in nature. This is completed by noting that TC scale

circulations often have their maximum azimuthally averaged V_t close to the circulation center, and almost always within 500 km from the center of circulation. Fig. 2.1 illustrates the differences in azimuthally averaged V_t associated with (a) a large TC circulation (Hurricane Ivan, Sep 2004) versus (b) a gyre circulation (Sep 2010). Even using the relatively course resolution of CFSR (~55 km), the radius of maximum azimuthally averaged V_t associated with Hurricane Ivan is 100 km, well below the 500 km threshold necessary for gyre classification. Compare this with the broad maximum azimuthally averaged V_t of the gyre at 750 km, which exceeds the threshold distance. The minimum magnitude threshold of V_t was chosen to eliminate systems that were too weak to be classified as CAGs, using the same logic discussed for the circulation magnitude test by testing this threshold value on previously identified cases of MDs and MGs in other basins. This value is roughly consistent with the previous circulation magnitude threshold, but more restrictive in that it limits the max azimuthally averaged tangential wind to occur at radii greater than 500 km. The magnitude threshold of azimuthally averaged V_t is less restrictive than Crandall (2012), which required a MG case study to reach an azimuthally averaged V_t of 8 m s^{-1} within the MG circulation. Hurley and Boos required MDs identified in their climatology to possess maximum total wind between 8.5 – 13.5 m s^{-1} although this value is without any azimuthal averaging, which would likely lower the raw maximum wind.

2.2.2.4 *Arc Averaged Tangential Wind*

1) Average V_t is calculated in an arbitrary 60^o arc between 500-1000 km away from the CA gyre center.
2) Arc averaged V_t must exceed 1 m s^{-1}
3) Next arc is rotated 10^o clockwise around the gyre center until completing one loop. Each arc must satisfy condition 2).

This test aids in filtering out non-closed circulations that otherwise might qualify as CAGs. Since positive V_t in the northern hemisphere indicates cyclonic flow, by observing positive average V_t in all arcs around the CA gyre candidate, you can conclude a given circulation is closed rather than merely a wind axis. This provides an effective way to discriminate a strong monsoon trough versus a closed gyre, which was cited in Lander (1994) as being a difficult determination factor in classification. The minimum threshold arc averaged V_t value (1 m s^{-1}) was chosen to diagnosis cyclonic flow at every arc length from the center, yet still allow for asymmetries in the flow that are present in some CAG candidates. While the minimum threshold value may seem lenient, this value must be exceeded in all arc lengths around the gyre candidate (36 arcs in total). Fig. 2.2 depicts an example of using the arc averaged V_t test on two different disturbances, (a) a trough axis in Aug 1995, and (b) the Sep 2010 objectively defined CAG. While the trough axis contains sufficient cyclonic arc averaged V_t in the northern quadrant, the lack of significant cyclonic wind in the southern quadrant causes the arc averaged V_t value to fall below the 1 m s^{-1} threshold. In contrast, the CAG case, while not perfectly

symmetrical, is sufficiently closed in all quadrants with arc averaged V_t safely remaining above the threshold at all arcs.

Using these tests collectively allows for a largely objective way to classify CAG events that possess similar characteristics to MDs and MGs in other basins. For the purposes of this study, the algorithm was run from May-Nov from 1980-2010 in order to conduct a climatological study of CAG occurrence during the traditional TC season in the EPAC and ATL basins. Fig. 2.3 visually details each step outlined in flowchart form. Note that all tests must be satisfied consecutively in each 6 h synoptic time up to the 48 h lifespan threshold. Beyond this period, the algorithm will continue to extend the lifespan of the CAG event as long as all tests remain satisfied. The threshold values selected in each test were fine-tuned to capture a subset (19) of CAG candidates identified prior to the creation of the algorithm, using graphics that allowed for the subjective identification of characteristics associated with MDs and MGs in previous literature. The objective algorithm reclassified all but two of these visually identified CAG cases, and classified many more CA gyre instances that went unnoticed by visual inspection. Both cases not reclassified failed the 48-hour consecutive lifespan requirement, with at least one 6-hour time period failing one of the tests noted above.

After objectivity identifying CA gyre candidates, GridSat imagery during the CAG lifespan was analyzed to confirm that identified cases were convectively active. While the vast majority of algorithm identified CAG cases that were convectively active broad low-level cyclonic circulations consistent with the CAG criteria established, a few cases were removed from the climatology for being extratropical circulations. This most often occurred at the beginning and ends of the season (May and Nov) on the northern

edge of the domain, and were easily identified by the lack of deep convection (< -40^{o}C) within 1000 km of the gyre center. In rare cases, some CAG events contain two or more discrete 48 h or greater periods of gyre classification. In these cases, the first time period of identified CAG characteristics is chosen as the genesis period, and all discrete gyre classification periods beyond the initial development are considered the same event.

In rare instances (3 occurrences in a 31 year period), the CAG algorithm will attempt to classify a large TC located in the western Caribbean as a CAG. These TC-induced CAG candidates are not filtered out by the algorithm because of the asymmetrical nature of the large-scale circulation in comparison to the inner wind maxima associated with the TC. In these cases, the large-scale (500-1000 km) 850-hPa circulation maxima is shifted far enough from the TC center to allow the max azimuthally averaged V_t to fall outside of the minimum 500 km radius threshold of the objectively defined CAG center. While these events can, like traditional CAGs, produce heavy rainfall across Central America, these CAG candidates are not distinct from the circulation comprised of the TC itself. *Temporals*, as discussed in the section 1.2.2 (Fernandez and Barrantes 1996, Pena and Douglas 2002), can sometimes be classified as these types of large-scale low-level wind protrusions from TC circulations. For the purposes of this climatology, however, these events will be omitted from the dataset.

2.2.3 Composite analysis

After all CAG cases were finalized, specialized fields documenting the composite structure of CAG cases were created. These fields employ a gyre-relative perspective,

where grid points for each CAG event are centered on the average point of all cases. It is important to note that this compositing method possesses a few drawbacks, because the longitudinal distance of grid points in the CFSR dataset varies with latitude, and the shifting of grid points to a gyre center point also shifts the orography of Central America, which could dilute the value of meteorological fields near the surface. Despite these shortcomings, the gyre-relative framework is effective at capturing synoptic scale features that are important to the evolution of CAGs, and were deemed superior to the use of an earth-relative framework when compositing CAG occurrences.

One aspect that motivates this study is documenting the synoptic flow that occurs in the days leading up to CAG genesis. Time lagged composites were produced to capture these details, centering on the time of CAG genesis (t_0), the first period where all criteria necessary for CAG classification are satisfied. Time lags were created starting three days before genesis (t_0 - 72 h) evolving forward to two days after genesis (t_0 + 48 h).

Composite anomalies were used to distinguish gyre relevant features from the mean. In order to properly assess the usefulness of these anomalies, standardization was preformed on a variety of variables using the formula below:

$$z = \frac{x - \bar{x}}{\sigma} \tag{3}$$

Where x represents an atmospheric variable, $\bar{x}$ is the climatological mean, and σ is the climatological standard deviation. The climatological mean and standard deviation is defined as the 31-year average and standard deviation (1980-2010) from the CFSR dataset, where mean variables are a daily climatology created for each synoptic hour using the first 4 harmonics of the CFSR dataset. Standardizing anomalies allow for direct

comparison of like atmospheric variables regardless of location or time of year. Statistical significance using a two-tailed student t-test at the 95% confidence interval was calculated on these variables to confirm significance of these standardized anomalies given a sample size of gyre events.

2.2.4 Gyre classification and case studies

To examine the presence of upper-level PV in close proximity to the low-level circulation of CAG at t_0, a test used in the CAG identification algorithm was modified to investigate upper level PV occurrence. Ertel's PV on the 350 K isentropic surface was averaged in an arbitrary 60^o arc between 500-1000 km from the CAG center (Fig. 2.4). Similar to the arc-averaged V_t test, this PV test is repeated by rotating the arc at 10^o increments until completing a full revolution around the CAG center. If this value exceeds 2 PVU in any arc averaged bin, then it is assumed that an upper-level trough exists within 1000 km of the CAG low-level circulation. This assumption was independently verified by checking 350 K PV plots to visually determine the position of upper-level troughs relative to a CAG circulation. CAGs that feature an upper-level trough in close proximity to the circulation at t_0, are referred to as trough CAGs. Otherwise, the CAG is categorized as a tropical CAG, in the absence of an upper tropospheric trough at t_0. PV was chosen on the 350 K isentropic surface, because this represents a theta surface typically located near the tropopause at tropical latitudes. This also maintains consistency with several recent studies on MGs in the WPAC (Molinari and Vollaro 2012, Crandall 2012). One case study on each category of CAG was

preformed, using 24 Sep – 01 Oct 2010 as the tropical CAG case, while 21-24 May 1991 was chosen as the trough CAG case.

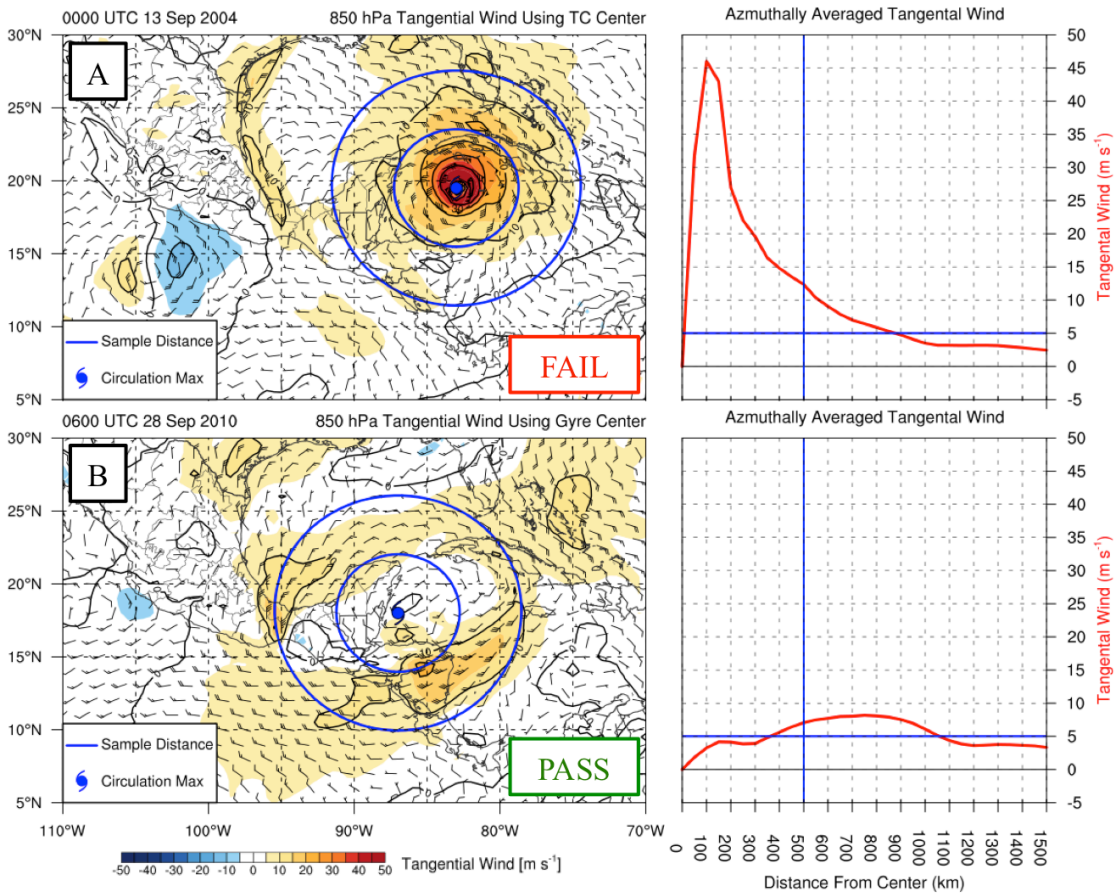

Fig. 2.1. Visual illustrating the azimuthally averaged tangential wind test investigating (a) Hurricane Ivan on 0000 UTC 13 Sep 2004 and (b) objectively identified CA gyre on 0600 UTC 28 Sep 2010. Left panels contain tangential wind (color shading and light black contours, interval 5 m s^{-1}), and total wind (barbs, knots). Inner (outer) blue circles represent 500 km (1000km) distance radially from center. Right panels display azimuthally averaged tangential wind (red line). Horizontal (vertical) blue lines represent the magnitude (distance) threshold of azimuthally averaged tangential wind maximum.

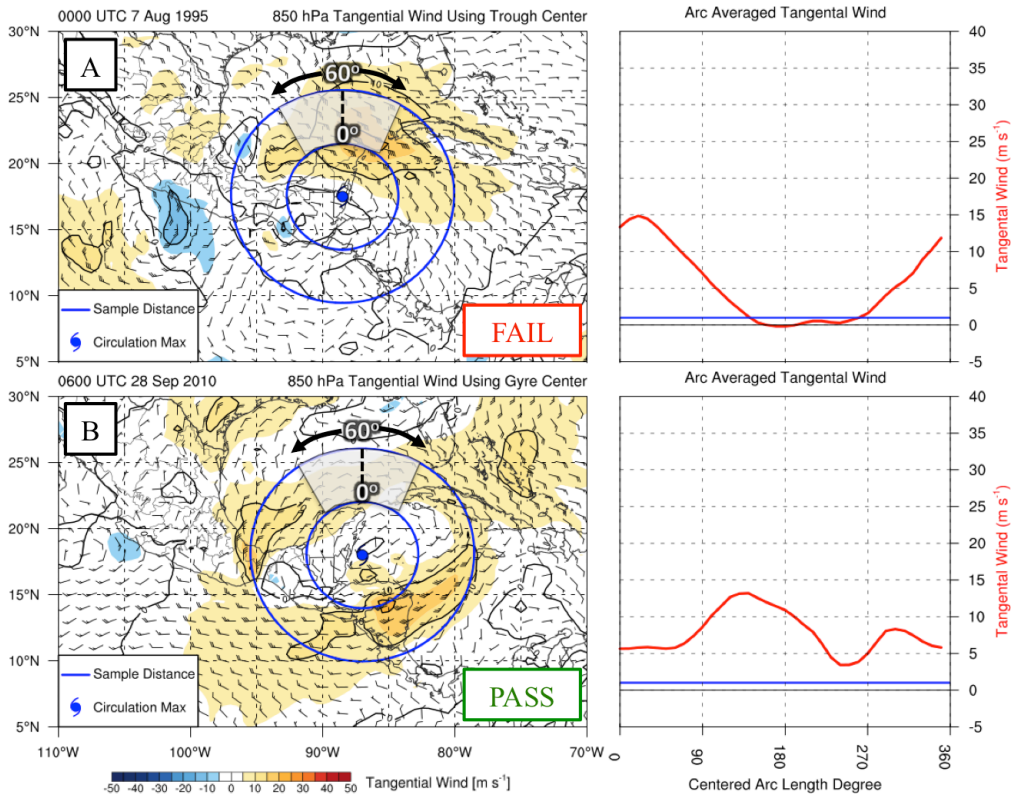

Fig. 2.2. Visual illustrating the arc averaged tangential wind test investigating (a) trough axis on 0000 UTC 7 Aug 1995 and (b) objectively identified CA gyre on 0600 UTC 28 Sep 2010. Left panels contain tangential wind (color shading and light black contours, interval 5 m s^{-1}), and total wind (barbs, knots). Inner (outer) blue circles represent 500 km (1000km) distance radially from center. Transparent white area represents a 60^{o} arc centered on true north (0^{o}). Right panels contain arc averaged tangential wind (red line) starting at arcs centered at true north (0^{o}). Horizontal blue lines represent the magnitude threshold of arc averaged tangential wind minimum.

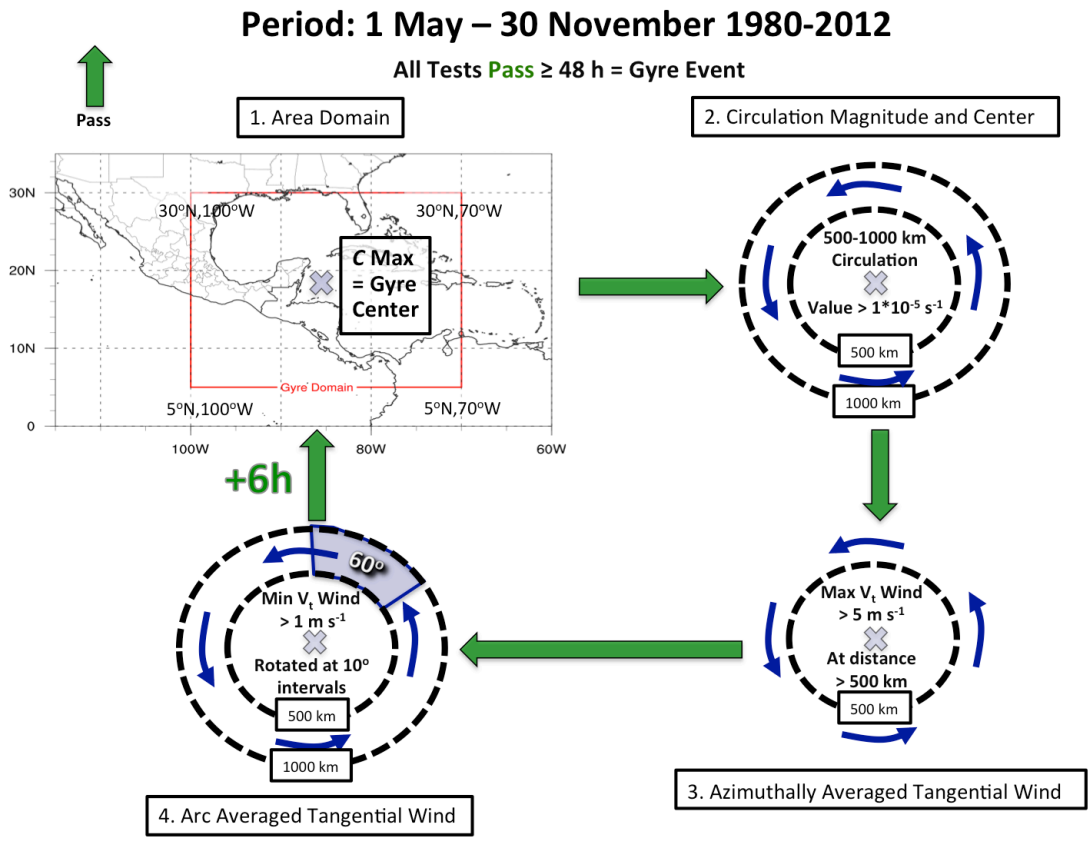

Fig. 2.3. Schematic flow chart illustrating how the CA gyre algorithm tests for gyre occurrences at each time interval. The light blue X represents the gyre center as defined by the max circulation. The blue arrows represent flow around the gyre between 500-1000 km. Green arrows represent the algorithm moving through each sequential step to complete one time integration of the algorithm.

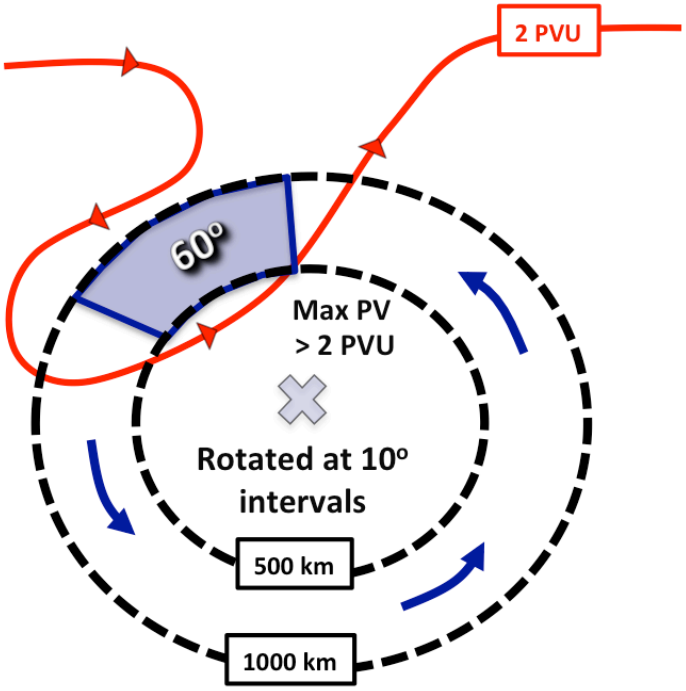

Fig. 2.4. Schematic illustrating how an adapted test from the CA gyre algorithm was used to identify trough CAG cases. The light blue X represents the gyre center. The red line with arrows represents the flow along the 2 PVU contour at the 350 K surface. Blue arrows represent the low-level flow associated with the CA gyre.

3. Results

3.1. Central American Gyre Climatology

The objective technique used for identifying CAG occurrence, as documented in section 2.2.2, was applied at 6 h synoptic times from May 01 – Nov 30 between 1980 – 2010. During this 31-year period, 42 CAGs were identified, corresponding to roughly 1.4 gyres per year.

Table 3.1 presents a general set of statistics providing the min, max, and mean values of genesis latitude and longitude, lifespan, max azimuthal averaged wind, and radius of max winds for all CAG events. The mean position of CAG cases at genesis was located inland over Honduras (14.3^{o}N, 85.4^{o}W). The lifespan of CAGs range from 2 – 7 days but on average roughly last three days (71 h). The max azimuthally averaged wind associated with CAGs ranges between 5.2 to 15.5 m s^{-1} while the radius of these maximum winds range from the minimum threshold of 500 km up to 1050 km.

The location variability of the genesis of CAGs does not appear to have a strong relationship with the date of genesis, as illustrated in Fig. 3.1. In general most CAGs develop over or near Central America (18), although there are a significant number of CAGs that develop in the Caribbean (13) with fewer cases in the Gulf of Mexico (4) and EPAC (4) over the climatological period. There is one significant CAG genesis outlier located on the edge of the domain just north of Hispaniola. This CAG is unique for playing a role as a precursor disturbance for the strongest Atlantic TC in recorded history (Wilma 2005). Despite no obvious development tendency with time, there is a weak tendency for CAGs to develop southeast of the mean development location in the southwest Caribbean during the latter part of the traditional TC season (Oct – Nov).

When looking at genesis variability by time of year (Fig 3.2), there exists a distinct bimodal distribution in genesis occurrence, with peaks in CAG activity in the early (May – June; 10 CAGs) and latter (September – November; 31 CAGs) portions of the traditional TC season. Interestingly, these seasonal periods of enhanced CAG activity appear in conjunction with seasonal increases of TC activity in the western Caribbean (Inoue et al. 2002). This apparent positive relationship between CAG and TC activity will be investigated further in section 3.4.

CAG occurrence is nearly nonexistent in the middle of boreal summer (July – August, 1 CAG). One idea proposed to explain this lack of CAG activity is related to the hypothesized importance of meridional gradient reversals of zonal wind being important for CAG development. To provide qualitative support for this hypothesis, Fig. 3.3 plots climatological 850-hPa zonal winds from May 1 – Nov 30 averaged over the CAG domain longitude (100 – 70^{o}W), where CAG cases are plotted by their genesis data and latitude. During active periods of CAG formation (May – Jun, Sep – Nov), a meridional gradient reversal of the zonal wind is evident equatorward of Central America in the EPAC at ~5^{o}N, where the climatological zonal winds are the most positive. However, between Jul – Aug, there is a distinct weakening of the meridional gradient reversal of zonal wind equatorward of Central America. This period coincides with an acceleration of the low-level Caribbean jet, which strengthens easterly flow between 10 – 15^{o}N. Further work is needed to confirm that this zonal wind structure aids in the generation of CAGs on an individual case basis, but these preliminary findings suggest that climatological flow plays a role in modulating CAG frequency. This period of the summer that also corresponds to the mid-summer drought, a documented climatological

feature in literature over Central America discussed in section 1.2.2 (Magana et al. 1999, Small et al. 2007). Chapter 4 will further discuss this lack of CAG activity in the middle of boreal summer and its relation to the mid-summer drought.

3.2. Central American Gyre Types

As discussed in section 2.2.4, gyre cases were divided into two categories using an objective test identifying the presence of an upper-tropospheric trough at CAG genesis. The motivation for dividing the total number of CAGs into two distinct categories was driven by characteristic differences in the development of larger-scale circulations documented in the WPAC basin. MGs are believed to be induced by mid-latitude forcing, often in the form of upper-level mid-latitude trough that descends into the tropical latitudes an interacts with a monsoon trough, the interaction of the lower and upper-level features resulting in a large, low-level, closed cyclonic circulation (Lander 1994). MDs in contrast are primarily absent of upper-level mid-latitude troughs and tend to form in-situ of a monsoon trough underneath upper-level anticyclonic flow (Douglas 1992, Harr et al. 1996).

CAGs forming *without* an upper tropospheric trough (defined as a region where PV > 2 PVU on the 350 K surface) within 1000 km of the CAG center were classified as *tropical* CAGs. Tropical CAGs represent the majority (N=35; ~83%) of CAGs identified in the climatology and are primarily associated with upper-level ridging, where westerly upper-level mid-latitude flow remains poleward of the CAG at genesis. A simple schematic illustrating the 350 K isentropic flow, PV, and low-level flow associated with the CAG is provided in Fig. 3.4a. Tropical CAGs most closely resemble MDs as

identified in the WPAC and IND basins (Douglas 1992, Harr et al. 1996) where a broad upper-level anticyclone, associated with low PV air, dominates the upper-troposphere in proximity to the low-level circulation associated with the tropical CAG.

CAGs forming *in association* with an upper-tropospheric trough within 1000 km of the gyre center are classified as *trough* CAGs. A schematic of a trough CAGs is provided in Fig. 3.4b. Trough CAGs are associated with higher PV air on the 350K surface, which is advected equatorward along a southwest – northeast oriented trough, often referred to as a *PV streamer*. This stream of higher PV air is deposited equatorward, downstream of an amplified midlatitude ridge. Trough CAGs represent only a small portion (N = 7, ~17%) of all CAGs cases, and their different upper-tropospheric characteristics bare closer similarities to MGs as observed in the WPAC basin (Lander 1994, Molinari and Vollaro 2012), which undergo significant upper-tropospheric trough interaction in their early lifecycle.

Differences between tropical and trough CAGs also appear in their genesis location. Fig. 3.5 illustrates these spatial differences in genesis location in terms of CAG type. While most tropical CAGs are located over Central America, the mean location of trough CAGs is significantly further northeast into the northwestern Caribbean. Five out of seven trough CAGs identified were poleward of *all* identified tropical CAGs in the 1980-2010 climatology. This result is not unexpected since strong upper-tropospheric troughs become less common south of 20^{o}N during the traditional TC season (Waugh and Polvani 2000).

3.3. Composite Analysis

3.3.1. Tropical CAG Composite

In order to identify the structure of environmental features related to CAGs before, during, and after genesis, a gyre-relative composite analysis was preformed on objectively identified trough and tropical CAGs in the 1980-2010 climatology. As discussed in section 3.2, CAGs, forming without an upper-tropospheric trough in their proximity (< 1000 km) were included in the tropical CAG composite (N=35). To deduce the significance of the results compared to climatology in the standardized composite fields, statistical significance using a two-tailed student t's test was calculated for the 95% confidence interval.

Time-lagged gyre-relative composites of 850-hPa geopotential height reveal the development of a large low-level cyclonic circulation. A distinct geopotential height pattern is evident by t_0 – 48 h and remains up to gyre genesis, t_0, where negative standardized height anomalies between -0.25 to -0.75 σ develop over Central America and are located between positive standardized height anomalies between + 0.25 to + 0.50 σ in the EPAC and ATL basins respectively (Figs. 3.6b-d). While these positive height anomalies in the EPAC remain quasi-stationary, the positive height anomalies in the ATL basin migrate westward with time as an extension of the subtropical ridging anchored near Bermuda. Beyond t_0, negative standardized 850-hPa geopotential height anomalies (< -1.50 σ) associated with the tropical CAG are also associated with low composite 850-hPa geopotential heights (< 148 dam) (Figs. 3.6d-f). These 850-hPa geopotential height anomalies are also statistically significant to the 95% confidence interval relative to the climatological 850-hPa heights at the composite time. Anomalous 850-hPa westerly flow

between 5 – 10 knots in the EPAC exist at t_0 – 72 h equatorward of Central America, while anomalous 850-hPa easterly flow between 5 – 10 knots are present poleward of Central America by t_0 – 48 h. These wind anomalies appear in association with meridional gradients in anomalous heights occurring poleward and equatorward of Central America. These wind anomalies also remain prevalent through the remainder time periods (Figs. 3.6b-f). Because these wind anomaly corridors also precede tropical CAG development (t_0), it is hypothesized they aid in the development of a tropical CAG, by generating low-level cyclonic (shear) vorticity over Central America.

In support of this hypothesis, the increase of cyclonic relative vorticity near Central America prior to the development of the tropical CAG appears to be an important characteristic of the tropical CAG composite. In the days prior to tropical CAG formation, there is an extensive area of relatively weak ($< 2.5 \times 10^{-5}$ s^{-1}) 850-hPa cyclonic relative vorticity across the southwestern Caribbean near Central America (Figs. 3.7a-c). This region of cyclonic relative vorticity appears to be the result of a zonal wind gradient between the relatively light and viable 850-hPa wind near Panama (< 2.5 m s^{-1}) and much stronger easterly wind (> 10 m s^{-1}) in the northwestern Caribbean. Additionally, there is relatively little curvature in this total wind between t_0 – 72 h to t_0 – 48 h across this region, suggesting that cyclonic *shear* vorticity is a significant contribution towards the total relative vorticity over this region (Figs. 3.7a-b). At and beyond t_0, strips of cyclonic relative vorticity ($> 2.5 \times 10^{-5}$ s^{-1}) have organized in a symmetric circle around the tropical CAG center, roughly parallel to the strongest winds (Fig 3.7d-f). In addition, there is a prominent maximum of 1000-500 km radial average 850-hPa circulation ($> 1 \times 10^{-5}$ s^{-1}) centered at the tropical CAG center. This circulation maximum, a

macroscopic measure of rotation, is maximized where there is a relative minimum in cyclonic relative vorticity, a microscopic measure of rotation. This is a common characteristic of CAGs, where the largest cyclonic relative vorticity is organized in strips well away from the circulation center, often over the lower terrain of Central America and ocean basins. This vorticity pattern is also a consequence of the broad wind maxima that exist within CAGs. The flow around the tropical CAG has also attained more curvature, a result not surprising given that CAGs are objectively defined to be closed cyclonic circulations and need sufficient curvature in the wind field to pass this criteria.

The relative roles of shear and curvature vorticity were tested by partitioning the total 850-hPa relative vorticity into its shear and curvature components, averaging the vorticity in a 5^{o} box around the tropical CAG genesis point (Fig. 3.8). From t_0 – 72h to t_0 – 48 h, shear relative vorticity accounts for the majority of the total relative vorticity over the composite location of the tropical CAGs. As the circulation associated with the tropical CAG composite increases in magnitude, it attains a larger portion of its total relative vorticity from the curvature of the flow. By t_0 + 48 h, the average curvature relative vorticity (1.8×10^{-5} s^{-1}) accounts for the majority of the total relative vorticity (2.8×10^{-5} s^{-1}) associated with the tropical CAG.

The resulting 850-hPa flow near the tropical CAG composite also occurs in association with statistically significant anomalously high precipitable water (PWAT). This anomalously high PWAT is evident as far back at t_0 – 72 h over the Caribbean (Fig. 3.9a) and slowly shifts westward with time over or just east of the tropical CAG composite center, while gradually increasing in magnitude to > +1.25 σ (Fig. 3.9b-d). In contrast to the abundance of high PWAT (> 55 mm) over Central America, negative

standardized PWAT anomalies between -0.25 to -0.75 σ become evident from over the EPAC after tropical CAG genesis (Figs. 3.9d-f). These negative PWAT anomalies in the EPAC occur after the highest PWAT (> 50 mm) shifts northward over Central America and the western Caribbean. The abundance of high PWAT near the tropical CAG center is a critical ingredient to the generation of substantial precipitation over Central America in association with tropical CAG events.

The presence of upper-level ridging over the tropical CAG is evident at the 200-hPa level, centered near 15°N, 80°W from t_0 – 72 to t_0 – 24 h in the tropical CAG composite (Figs. 3.10a-c). Upper tropospheric ridging is associated with low-PV air, which is clearly evident (< 0.75 PVU) near the ridge axis. Anticyclonic flow is also evident, with light and variable flow near the tropical CAG center, with stronger easterly flow between 20-30 knots equatorward and 30-50 knot westerly flow poleward over North America. This strong westerly flow is associated with a strong meridional positive PV gradient. Over time, the position of the 200-hPa ridging strengthens as it shifts northeastward, centered just northeast of the composite tropical CAG center (Figs. 3.10d-f). Upper-level ridging associated with the tropical CAG is a common characteristic associated with warm-core cyclonic disturbances.

The enhancement of the 200-hPa ridge is likely the consequence of enhanced irrotational outflow, resulting from convection occurring in the tropical CAG. Initially, the majority of 200-hPa irrotational outflow is equatorward of 10°N from 80-120°W, in association with moist convection in the EPAC ITCZ, where high PWAT > 50 mm and scattered 500-hPa ascent (< -1×10^{-3} hPa s^{-1}) is present (Figs. 3.11a-c). As convection develops with the tropical CAG, in association with vertical ascent (< -1.5×10^{-3} hPa s^{-1})

and high precipitable water (> 55 mm) over Central America, a significant expansion of irrotational wind > 5 m s^{-1} occurs in all directions, emanating from the enhanced ascent from t_0 to t_0 + 48 h (Figs. 3.11d-f). This divergent wind at 200-hPa is likely aiding additional upper-tropospheric ridging centered over and just east of the tropical CAG (Figs. 3.10d-f), where the irrotational flow is advecting lower PV values poleward. The 200-hPa irrotational wind also crosses a positive meridional 200-hPa PV gradient over Florida at t_0 + 48 h, where the advection of lower PV tightens the PV gradient resulting in stronger westerly 200-hPa flow > 15 m s^{-1} over Florida (Fig. 3.11f).

To assess changes in the vertical structure associated with tropical CAG genesis, a variety of meridional cross sections through the tropical CAG center were plotted for the same composite times. From t_0 – 72 to t_0 – 48 h there are few substantial PV anomalies through the low and middle troposphere, although there is a hint of a weak -PV anomaly (-0.10 to -0.50 PVU) developing near the top of the troposphere between 200 – 100-hPa (Figs. 3.12 a-b, bottom panels). The composite flow over and equatorward of the tropical CAG genesis point from 850 – 700-hPa is easterly between 5 – 10 knots (Figs. 3.12a-b, top panels). This composite easterly flow is weaker than the climatological easterly flow, and thus the anomalous flow is depicted as weak westerly (~5 knots) equatorward of the tropical CAG genesis point (Figs. 3.12a-b, bottom panels). Low to mid tropospheric ascent (< -1×10^{-3} hPa s^{-1}) is also present equatorward of the tropical CAG genesis point. By t_0 – 24 h, this ascent has strengthened (< -2×10^{-3} hPa s^{-1}), while also expanding in size, both horizontally and vertically, now centered closer to the tropical CAG genesis point (Fig. 3.13c). The larger area of ascent is possibly redistributing the PV profile of the atmosphere, with initial development of a weak +PV

anomaly between +0.10 to +0.25 PVU centered above the tropical CAG genesis point between 700 – 400-hPa, while a –PV anomaly between -0.25 to -1.00 PVU is becoming established between 200 – 100-hPa. We hypothesize that PV redistribution is driven by warming in the middle to upper troposphere from latent heat release (LHR) associated with deep convection, where isentropes bow downward below 200-hPa and bow upward above 200-hPa. The PV redistribution in the low-levels has also resulted in a weak poleward PV gradient reversal, which is critical in satisfying barotropic instability. This general pattern becomes more pronounced from t_0 to t_0 + 48 h (Figs. 3.13d and 3.14e-f), where vertical ascent < -2.5×10^{-3} hPa s^{-1} has now become organized in symmetric corridors poleward and equatorward of the tropical CAG center. This ascent is likely associated with convection that has continued to modify the PV profile, where a growing +PV anomaly tower between +0.10 to +0.50 PVU developing in the troposphere from 1000 – 300-hPa is complemented by a corresponding –PV anomaly between -0.25 to -1.00 PVU from 200 – 100-hPa. These PV anomalies are associated with adjusted flow, where cyclonic flow associated with the +PV anomaly related to the low-level cyclone of the tropical CAG center is predominantly observed between 1000 – 500-hPa, while anticyclonic flow associated with the –PV anomaly and upper-level ridge is observed above 500-hPa. The above vertical diagnosis of the atmosphere suggests that tropical CAGs possess warm core characteristics since cyclonic flow decreases with height and becomes anticyclonic in the upper-troposphere.

The warm-core characteristics of the composite tropical CAG can also be diagnosed by looking at temperature anomalies (Figs. 3.15-3.17, bottom panels). As time evolves from t_0 – 72 to t_0 + 48 h, there is the slow but steady increase of positive

temperature anomalies in the mid to upper troposphere, reaching a maximum of > 1.5°C by t_0 + 48 h (Fig 3.17f) above the tropical CAG center. The development of the low-level cyclonic circulation associated with the tropical CAG can also be observed by investigating meridional cross sections of zonal wind from t_0 – 72 h to t_0 (Figs. 3.15-3.16, top panels). There initially exists a poleward reversal in zonal winds from westerly to easterly in the lower troposphere (Fig. 3.15a). While the equatorward zonal westerly flow is confined to the low-levels primarily below 850-hPa, the poleward zonal easterly flow > 2 m s^{-1} north of Central America extends vertically up to 500-hPa. Over time, these zonal winds increase in magnitude and grow vertically with both zonal easterlies and zonal westerlies poleward and equatorward of the tropical CAG center, respectively, extending vertically to near 400-hPa by t_0 (Fig. 3.16d). With the presence of a large anticyclone in the upper-troposphere, these zonal winds reverse above 400-hPa, with zonal westerlies poleward of the tropical CAG center, and zonal easterlies equatorward of the tropical CAG center. The anticyclonic easterly flow, maximized near 200-hPa, also increases in magnitude equatorward of the tropical CAG center, from around -10 m s^{-1} at t_0 – 72 h (Fig. 3.15a) to -14 m s^{-1} at t_0 + 48 h (Fig. 3.17f). This increase in magnitude is possibly related to enhanced outflow, where northerly 200-hPa irrotational wind between 5 – 10 m s^{-1} represents roughly half of the > 15 m s^{-1} 200-hPa flow equatorward of 10°N (Figs. 3.11d-f).

The relative vorticity structure representative of tropical CAGs is illustrated in Figs. 3.15-3.17 (bottom panel). Over time, cyclonic relative vorticity organizes and intensifies between 1000 – 500 hPa over the tropical CAG center (Figs. 3.15-3.17a-f). However, as the tropical CAG matures, the cyclonic relative vorticity associated with the

gyre is not maximized at the composite 850-hPa tropical CAG center, but rather in corridors just poleward and equatorward of the CAG center in the low-levels (Figs. 3.17e-f). This is an expected result, because CAGs possess a large radius of maximum winds and vorticity maxima tend to be focused in corridors on the outer edges of the larger gyre circulation, along where similar columns of vertical ascent exist (Figs. 3.13-3.14d-f, top panels). These corridors of cyclonic vorticity, with maximum near 4×10^{-5} s^{-1} and 2×10^{-5} s^{-1} respectively at 850-hPa, merge over the tropical CAG center and gradually decrease in magnitude with increasing height (Figs. 3.17e-f). Anticyclonic relative vorticity with a minimum of -2×10^{-5} s^{-1} is observed in the upper-troposphere over the tropical CAG, associated with upper-tropospheric ridging at 200-hPa (Figs. 3.10e-f). The decrease of cyclone relative vorticity at increasing height is consistent with the flow illustrated in Figs. 3.13-3.14d-f, and is also indicative of a warm-core circulation.

3.3.2. Trough CAG Composite

As discussed in section 3.2, CAGs forming in proximity to an upper-tropospheric trough (< 1000 km) were included in the trough CAG composite (N=7). It is important to note the relatively low sample size for this subset of CAG cases, which does increase uncertainty in the generalization of these composite results. To mitigate some of these concerns, the primary results of the trough CAG composites will focus on the regions of the composite that are statistically significant at the 95% confidence level relative to climatology. Regions that are not statistically significant are discussed, but are deemphasized relative to the regions that are statistically significant.

Time-lagged composites of low-level (850-hPa) geopotential height reveal the development of a low-level cyclonic circulation associated with trough CAGs (Fig. 3.18). Similar to the tropical CAG composite, negative standardized height anomalies between -0.75 to -1.00 σ over Central America are located between two positive height anomalies between +0.75 to +1.00 σ in the EPAC and North America. One difference between the tropical and trough CAG composite fields is related to the origin of the standardized positive height anomalies. Trough CAG lagged composites depict that the poleward positive standardized height anomalies originate over the Great Lakes at $t_0 - 72$ h, migrating southeastward and intensifying by t_0 (Figs. 3.18a-d). This enhanced 850-hPa geopotential ridging is statistically significant, despite the low trough CAG sample size, and represents a critical difference from tropical CAGs, where enhanced 850-hPa ridging results from an extension of the Bermuda ridge. While positive standardized height anomalies also exist in the EPAC along 10^{o}N, similar to the tropical CAG composite, these height anomalies are not statistically significant. From t_0 to $t_0 + 48$ h, a large area of statistically significant negative standardized height anomalies < -1.50 σ develops in association with a composite 850-hPa height minimum < 148 dam over the low-level trough CAG circulation (Figs. 3.18d-f). Also associated with these 850-hPa height anomalies are anomalous 850-hPa winds, with prevalent easterlies between 5 to 10 knots in the ATL basin poleward of Central America, while 5 to 10 knot westerlies are prevalent across the EPAC basin equatorward of Central America (Figs. 3.18c-f). These wind anomalies likely manifest due to the anomalous height gradient created by the geopotential height pattern, similar to the tropical CAG composite field.

The position of these 850-hPa wind anomalies in the EPAC and ATL basins, respectively, also favors the existence of 850-hPa cyclonic relative vorticity across Central America and the Caribbean (Fig 3.19). Similar to the tropical CAG composite, there is a gradient in the wind magnitude from the light and variable flow (< 2.5 m s^{-1}) over Central America in comparison to the stronger southeasterly flow (5 – 10 m s^{-1}) in the western Caribbean at t_0 – 72 h (Fig. 3.19a). Unlike the tropical CAG composite, this gradient is oriented southwest to northeast, similar in orientation to the scattered regions of cyclonic vorticity (~ 1.5×10^{-5} s^{-1}) primarily over the western Caribbean. The initial lack of curvature in the flow over the Caribbean suggests that shear vorticity provides a significant contribution of the total cyclonic relative vorticity over the region near the trough CAG genesis point. By t_0, the composite wind pattern obtains more cyclonic curvature, coinciding with trough CAG genesis (Fig. 3.19d). The 1000-500 km radial mean 850-hPa circulation is maximized (> 1×10^{-5} s^{-1}) over the trough CAG center, while strips of cyclonic relative vorticity maxima (> 2.5×10^{-5} s^{-1}) are oriented along the periphery of the circulation maximum. By t_0 + 48 h these cyclonic vorticity maxima are asymmetrical around the circulation maximum, with stronger cyclonic vorticity maxima (> 5×10^{-5} s^{-1}) in a northeastern semicircle around the trough composite CAG center (Fig. 3.19f).

As hypothesized, shear vorticity represents the majority of the total 850-hPa relative vorticity early on in the trough composite CAG evolution (t_0 – 72 h, Fig. 3.20). However, the ratio between shear and curvature vorticity becomes roughly equal by t_0, likely owing to the additional curvature of the wind as a closed cyclonic circulation develops. While curvature vorticity does composite the majority of the total relative

vorticity by t_0 + 48 h, its magnitude (1.7×10^{-5} s^{-1}) is not significantly greater than the shear vorticity (1.3×10^{-5} s^{-1}). The remaining shear vorticity near the trough composite CAG suggest that large-scale 850-hPa height gradients continue to play an important role in enhancing the 850-hPa winds, especially northeast of the trough CAG center.

In connection with the enhanced 850-hPa across the western Caribbean, there is a similar enhancement noted in the composite PWAT field (Fig. 3.21). Between t_0 – 72 h to t_0 there is a build up of enhanced PWAT (final maximum > 1.50 σ and > 55 mm) primarily located over the Caribbean (Figs. 3.21a-d). Moreover, this region of enhanced precipitable water is statistically significant at the 95% confidence interval starting on t_0 – 48 h (Fig. 3.21b). Unlike the tropical CAG composite, enhanced PWAT is primarily east of the trough CAG center at t_0 and remains that way through the end of the composite (Figs. 3.21d-f). This results in an asymmetrical moisture distribution zonally across the trough CAG circulation. By t_0 + 48 h there is a increasingly large region of negative standardized PWAT anomalies between -0.50 to -1.00 σ located over the Gulf of Mexico and portions of Central America (Figs. 3.21f), although these values are not statistically significant. In this occurrence, the base of the upper-tropospheric trough (as depicted in Figs. 3.22d-f) is likely depositing drier air equatorward as it interacts with the trough CAG. Extensive northerly 850-hPa flow between 10 to 15 knots over the western Gulf of Mexico in association with lower standardized PWAT anomalies may also result in a equatorward propagating cool surge into Central America (e.g. Schultz et al. 1998).

The aforementioned upper-tropospheric trough associated with trough CAGs can be seen in the 200-hPa composite. From t_0 – 72 h to t_0 + 24 h, PV originating from higher latitudes drops equatorward in the Gulf of Mexico, resulting in the formation of a

southwest to northeast oriented PV streamer (Figs. 3.22a-e). This advection of higher PV equatorward is co-located with a corridor of anticyclonic wavebreaking occurring downstream of a 200-hPa jet exit region over the southwestern US. AWB helps draw higher PV from higher latitudes into the Gulf of Mexico, resulting in a PV streamer with PV > 1 PVU along the trough axis from t_0 + 24 h to t_0 + 48 h (Figs. 3.22e-f). This resulting PV streamer provides the foundation from which trough CAGs are differentiated from tropical CAGs. Instead of light anticyclonic flow dominating the upper-level structure, 25-35 knot southwesterly 200-hPa flow is cutting through the composite trough CAG center, southeast of the 200-hPa trough axis. Anticyclonic flow is observed downstream of the trough CAG, centered over the Greater Antilles between Cuba and Hispaniola.

This upper-level structure also alters the convective structure associated with trough CAGs, represented by the vertical ascent at 500 hPa ($< -1 \times 10^{-3}$ hPa s^{-1}) displaced east of the trough CAG center (Figs. 3.23e-f). The vertical ascent is co-located with the region of highest PWAT > 55 mm located over the northwest Caribbean and Cuba. Much of the ascent located downstream of the trough CAG is also located in a region where there is mid-latitude forcing for ascent, where cyclonic vorticity advection by the thermal wind (vertical wind shear) is aiding in lift in this high PWAT region. This is one possible explanation for the prevalence of downshear convection.

This downshear convection also aids the development of a 200-hPa jet streak downstream of the trough CAG. Irrotational flow (> 5 m s^{-1}) over the Bahamas, linked with deep moist convection, impinges upon the 200-hPa PV gradient draped across the trough CAG center. From t_0 to t_0 + 24 h, the PV gradient tightens to the northeast of the

trough CAG center. This tightened PV gradient results from a combination of irrotational outflow advecting negative PV air downstream of the trough CAG center with the advection of higher PV air west of the trough CAG center resulting form AWB (Figs. 3.23d-e). This tightened PV gradient results in the development of a new 200-hPa jet streak > 25 m s^{-1}, downstream of the trough CAG, offshore of the eastern US coastline (Figs. 3.23d-f). The right entrance region associated with an upper-level jet streak is a favorable region for upward vertical motion, and it is not surprising this is coincident with the largest vertical ascent (< -2×10^{-3} hPa s^{-1}) in the trough CAG composite.

While vertical ascent, associated with deep convection, plays a pivotal role in the development of an upper-level jet streak downstream of the trough CAG, it does not appear to play as important of a role in the generation of the trough CAG cyclonic circulation. A meridional cross-section through the trough CAG composite reveals the presence of a deep upper-tropospheric +PV anomaly (maximum ~ +3.00 PVU) that extends from the tropopause down to 500-hPa as far back at t_0 – 72 h (Fig. 3.24a). Tropospheric-deep ascent is only occasionally observed in the meridional composite, most notably at t_0, which, similar to the tropical CAG composite, may aid in PV redistribution via LHR (Fig. 3.25d). This PV redistribution primarily occurs equatorward of the trough CAG with weak +PV anomalies between +0.10 to +0.25 PVU around 850-hPa and –PV anomalies between -0.25 and -1.00 PVU between 200 – 100-hPa. More importantly, however, appears to be the progression of +PV anomalies equatorward towards the genesis point of the trough CAG. By t_0, a +PV anomaly between +0.25 to +1.00 PVU is primarily observed from the tropopause (near 150-hPa) down to the 850-hPa level, just poleward of the trough CAG genesis point (Fig. 3.25d). The +PV anomaly

also appears to be tilted poleward while increasing in raw PV with height. Beyond t_0, the equatorward migration of this tropospheric deep +PV anomaly continues, and by t_0 + 48 h the +PV anomaly has become more vertically upright, consistent with the alignment of the 850-hPa cyclone (Fig. 3.18f). We hypothesize that the upper-tropospheric trough, with associated +PV anomaly, has moved in proximity to the trough CAG circulation, where the deep vertical penetration of the upper-tropospheric +PV anomaly is enhancing the weak +PV anomaly, initially spawned by convection in the lower troposphere. A tropospheric deep cyclonic circulation results, increasing in magnitude with height while possessing vertical tilt.

This tropospheric deep cyclonic circulation is confirmed by investigating the vertical cyclonic relative vorticity structure (Figs. 3.27 – 3.29, bottom panels). Initially the strongest cyclonic relative vorticity (maximum > 4×10^{-5} s^{-1}) is primarily located in the middle to upper troposphere (500 – 150-hPa) in association with the upper-level trough, poleward of the trough CAG genesis point (Figs. 3.27a-b, bottom panels). However, as this cyclonic relative vorticity maximum moves equatorward with time, it merges with developing cyclonic relative vorticity in the low-levels, associated with the developing trough CAG at t_0 (Fig. 3.28d, bottom panels). By t_0 + 48 h cyclonic relative vorticity is prominent throughout the troposphere at the trough CAG center (Fig. 3.29f, bottom panel).

The southwesterly vertical wind shear over the trough CAG, implied by the 200-hPa flow in Fig. 3.22, can be shown by looking at the vertical structure of zonal winds in the trough CAG (Fig. 3.29e-f, top panels). Unlike the tropical CAG composite, the trough CAG composite does not possess a strong upper-level anticyclone overhead but rather

shifted equatorward of the trough CAG center, with predominantly westerly zonal winds (between 4-12 m s^{-1}) above 400-hPa over the trough CAG center. This is consistent with the > 20 knot southwesterly 200-hPa observed in Figs. 3.22e-f, indicative of moderate westerly vertical wind shear present after genesis of the trough CAG. The development of the trough CAG in the lower troposphere is also evident, where at t_0 – 72 h there is a poleward reversal in the zonal winds at the lowest levels (1000 – 850-hPa) where weak zonal westerlies between 2 to 4 m s^{-1} occur equatorward of the trough CAG composite center and zonal easterlies near -4 m s^{-1} occur poleward of the trough CAG center (Fig. 3.27a). Similar to the tropical CAG composite, this coupled westerly and easterly zonal wind grows vertically with time (Figs. 3.27 – 3.29), despite the unfavorable vertical wind shear.

The cold core nature of the upper-level cyclone can be observed from t_0 – 72 h to t_0 (Figs. 3.27-3.28, bottom panels) poleward of the trough CAG genesis point. Here there is a distinct couplet of negative temperature anomalies between -1.0 to -1.5^{o}C at the 850 – 400-hPa level with positive temperature anomalies +1.0 to +1.5^{o}C in the upper levels (250 – 150-hPa) along a depressed tropopause (defined as the 2 PVU surface on Fig. 3.23a). As this upper-level cold core cyclone migrates equatorward with time, the negative temperature anomalies erode away in the middle to upper troposphere, as the disturbance appears to be embedded in larger-scale positive temperature anomalies. This temperature distribution is not an unusual occurrence when an upper-level trough becomes cutoff from the mid-latitude flow, becoming trapped underneath a poleward ridge, as observed in the 200 hPa horizontal field (Figs. 3.22d-f). This results in positive temperature anomalies with maximum > 1.5^{o}C in the mid to upper troposphere over the

trough CAG by t_0 + 48 h, indicating the trough CAG possesses warm core characteristics. Further away from the trough CAG center, larger positive temperature anomalies (> +2.5^{o}C) exist poleward of the trough CAG (Fig. 3.29f). This is in contrast to the tropical CAG composite, which only exhibits positive temperature anomalies directly over the center. In addition, there appears to be a low-level (1000 – 850-hPa) thermal gradient present over the trough CAG at t_0, where climatological temperatures near the center are compared with a large region of -1.5 to -2.5^{o}C temperature anomalies poleward of the trough CAG at t_0 + 24 h (Fig. 2.29e, bottom panel). The apparent temperature gradient over the trough CAG center is not suggestive of a purely tropical low-level circulation.

3.4. CAGs and Tropical Cyclones

One of the motivating factors behind studying large-scale low-level circulations is related to how CAGs result in the development and interaction of TCs. Given that CAGs have been rarely researched, little is known about the general qualities and characteristics of TC vortices that exist within a CAG. Table 2 provides a general set of statistics on TCs within gyre circulations. Among the values presented are total number of TCs associated with CAGs (occurring within 1000 km of the CAG circulation center) including TCs that originate outside of the CAG before or after the CAG develops and then moves within 1000 km of the CAG center. Included within the table are also the total number of TCs that *develop* within 1000 km of CAGs after CAG formation, the number of CAGs associated with at least one TC, and finally information on the mean intensity and distance of TCs within CAGs. These different categories provide context to the proximity, intensity, and frequency of TCs when they are coincident with CAGs, and will aid in the

comparison of TC events that occur within other large-scale circulations in other basins (e.g. MGs, Wu et al. 2013).

TCs within CAGs do occur with some frequency, where approximately 50% of all CAGs (21) being associated with at least one TC. However, it is unusual to have more than one TC present within a CAG circulation. The relatively smaller size of CAGs (~ 600 km radius) in comparison to MGs (> 1000 km radius) likely limits the maximum number of TCs that can be observed within one circulation. There are a handful of cases where multiple TCs are involved in a single CAG circulation (e.g. May – June 2008 [TCs Barbara and Arthur], June 2010 [TCs Alex and Darby], and September 2010 [TCs Matthew and Nicole]). One observation made from these multiple TC CAG events is that most multiple TC CAG occurrences occur with TCs occurring in both the EPAC and ATL basins, with the CAG often present over Central America.

The organization of TCs associated with CAGs varies from case to case. In some CAG cases, the TC associated with the CAG circulation is the dominant vorticity maximum within the CAG, ultimately leading to the transition of the CAG into a smaller TC-like vortex in the latter stages of the CAG lifecycle. Moreover, TCs are witnessed far more frequently with tropical CAGs than trough CAGs, and developing TCs have only been identified within tropical CAGs. The lack of developing TCs in trough CAGs could possibly be explained by the implied increase in vertical wind shear that results from a mid-latitude upper-level trough bisecting the circulation of the composite trough CAG (Figs. 3.22d-f). Tropical CAGs have lighter upper-tropospheric flow that is more conducive for TCG (Figs. 3.10d-f).

When TCs exist within 1000 km of the CAG center, they tend to be relatively weak, with a mean intensity just over tropical storm threshold (18.3 m s^{-1}). There are some notable exceptions, such as TCs Florence (1988), Ida (2009), and Stan (2005), which all became category 1 hurricanes on the Saffir-Simpson wind scale at their maximum intensity while embedded in a CAG circulation. In these rare occurrences, the inner core TC circulation tends to be rather small with a radius of maximum winds (RMW) generally < 100 km in comparison to that of the CAG in which the RMW is objective identified as > 500 km. The TC circulation in this occurrence is more akin to a mesovortex of the CAG that rotates cyclonically around the larger CAG circulation. This cyclonic motion is a general characteristic among most TCs that become embedded in a CAG circulation. Since both the TC and the CAG are primarily lower-tropospheric circulations that decrease in intensity with height, its appropriate to think of this interaction in the context of two barotropic cyclones imparting cyclonic flow on one another via binary interaction, similar to the results presented in Carr and Elsberry (1995). In this barotropic interaction, the CAG is the larger and more dominant circulation, and the smaller TC circulation will tend to rotate cyclonically around the CAG. This general evolution can be captured by looking at TC positions at lagged composite times of all CAGs, with the mean TC position shifting from southeast of the CAG center to nearly due north of the CAG composite center from t_0 – 24 h to t_0 + 48 h (Figs. 3.30c-f). There is also a tendency for TCs to be located in the eastern quadrant of the CAG circulation, at the mean distance 460.6 km away from the CAG center. This observation is similar to the assessment made in Wu et al. (2013), which identified that TCs primarily formed in the eastern quadrants of MGs where vertical wind shear was lower.

3.5. CAGs and the Madden Julian Oscillation

Another motivating factor identified in this study was to identify large-scale precursor conditions that might lead to increase frequency of CAG events in the climatology. One such large-scale intraseasonal oscillation in the tropics is the MJO, which modulates both convection and tropospheric flow along the low-latitudes near the equator. The MJO therefore could result in a more favorable large-scale environment for CAG formation. To illustrate the MJO's relationship with CAGs, Fig. 3.31 presents an MJO RMM phase space diagram that identifies the phase of each CAG event at t_0. CAG events preferentially occur in phases 8, 1, and 2, with more than three fourths (76.2 %) of all CAGs occurring these phases. These favored MJO phases occur in both trough and tropical CAGs cases at genesis. When looking only at occurrences in which the MJO is active ($\sigma > 1$), the percentage of CAG events occurring in RMM phases 8, 1, and 2 remains roughly consistent (75.9%).

To capture the modification of the large-scale low-level flow provided by the MJO, phases 8, 1, and 2 were composited for all events occurring from 1 May – 30 Nov over the CAG climatological period (1980-2010). These MJO composites were then compared to the earth-relative CAG composite at t_0 (Fig. 3.32a). At genesis, the CAG composite has a unique hemispheric signal at 850-hPa equatorward of 10^{o}N, where positive standardized height anomalies occur over the Pacific basin, and negative standardized height anomalies occur over South America and the ATL basin. This pattern is consistent with the May-Nov MJO composites for phases 8, 1, and 2, which is not

unexpected given the concentration of CAG genesis events occurring in these phases (Figs. 3.32b-d).

One important observation taken from comparing the CAG composite to the MJO composites is a similar corridor of anomalous westerly 850-hPa flow in the EPAC that extends away from the immediate flow associated with the CAG circulation (Fig. 3.32). This suggests that the MJO may be modulating the large-scale anomalous 850-hPa flow in the EPAC, which is an important characteristic associated with CAG development. In contrast, the MJO composites do not possess similar positive standardized height anomalies in the northern ATL basin near Bermuda as seen in the CAG composite. As a result, the MJO composites show little evidence of enhanced easterly flow across the ATL basin in the absence of an anomalous height gradient. Thus, the MJO composite structure does not fully explain the anomalous low-level geopotential height or wind pattern that is present at CAG genesis, especially in the ATL basin. While there is a strong tendency for CAGs to occur phases 8, 1, and 2 of the MJO, its important to realize the MJO itself is not a necessary or sufficient factor in CAG genesis, because a small minority of CAG cases do occur outside of the active MJO phases.

3.6. Case Studies

3.6.1. Tropical CAG Case Study

The tropical CAG case used for this study is represented by a CAG that developed on 0000 UTC 24 September 2010, the same CAG that was first observed during the PREDICT field campaign (Montgomery and Coauthors 2012). As discussed in section 3.2, tropical CAGs are identified at genesis as large low-level cyclonic circulations

associated with low PV air (< 2.00 PVU) at the 350K isentropic surface, indicative of upper-tropospheric ridging. Interestingly, this CAG was the longest lasting event in the climatology, satisfying the CAG criteria for 7 consecutive days (168 h). For brevity, the case studies presented in section 3.6 will only cover the same time lagged composite periods presented for the CAG composites (t_0 – 72 h to t_0 + 48 h).

As discussed in the tropical CAG composite in section 3.3.1, large-scale 850-hPa anomalous standardized height gradients aid in the generation of anomalous wind corridors in the EPAC and ATL basins prior to tropical CAG genesis at t_0. Prior to the development of the tropical CAG in the case study (Figs. 3.33a-c), there are positive standardized height anomalies (+0.25 – +1.00 σ) equatorward of 10°N. Between 10-20°N there is a region of negative standardized height anomalies (-0.25 – -1.00 σ) that extend eastward over Central America and into the Caribbean. Poleward of 20°N in the ATL basin, there is a large, enhanced subtropical ridge (+1.00 – +2.00 σ) that replaces the negative height anomalies originally associated with recurving TC Igor (Figs. 3.33a-c). This overall 850-hPa anomalous height spatial pattern in the composite results in anomalous height gradients that produce anomalous westerly and easterly 850-hPa winds between 5 – 10 kt in the EPAC and ATL basins respectively. After CAG development (Fig 3.33d-f), the strongest negative standardized geopotential height anomalies become associated with the CAG (< -3.00 σ), although it remains embedded in a larger corridor of negative geopotential height (between -0.25 – -1.00 σ) over Central America.

The anomalous 850-hPa wind corridors in the EPAC and ATL basins also contribute the formation of scattered weak cyclonic vorticity (> 1×10^{-5} s^{-1}) along 15°N in the EPAC, across Central America, and the Caribbean (Figs. 3.34a-c). Despite the

large corridor of 850-hPa cyclonic vorticity, the vorticity is initially poorly organized, with little curvature in the low-level flow near the future genesis location of the tropical CAG. As a result, the 1000-500 km radial average 850-hPa circulation is $< 1 \times 10^{-5}$ s^{-1}, one of the thresholds necessary for CAG classification. When partitioning the total 850-hPa relative vorticity into its shear and curvature components, the majority of the cyclonic relative vorticity near the future location of the tropical CAG results from shear vorticity (Fig. 3.35). It is hypothesized that this shear vorticity is generated from the anomalous low-level flow present in the EPAC and ATL basins prior to the development of the tropical CAG (Figs. 3.33a-c). A maximum in circulation ($> 1 \times 10^{-5}$ s^{-1}) develops at t_0, which is in association with a closed circulation in the southern Caribbean (Fig. 3.34 d). The resulting CAG development also includes the recent development of TC Matthew, which is identified as an intense cyclonic vorticity maxima ($> 21 \times 10^{-5}$ s^{-1}) located to the northeast of the tropical CAG center at t_0. TC Matthew only represents one of the multiple spokes of cyclonic vorticity that are organizing along the periphery of the CAG circulation. As the tropical CAG moves inland and intensifies as the large-scale circulation increases (Fig. 3.34e), TC Matthew remains a discrete entity as it rotates cyclonically around the northern quadrant of the tropical CAG. By t_0 + 48 h, TC Matthew is dissipating over the higher terrain of Mexico, but the tropical CAG is intensifying, with multiple cyclonic vorticity maxima ($> 5 \times 10^{-5}$ s^{-1}) rotating around the outer periphery of the large cyclonic circulation over Central America (Fig. 3.34f). The intensification of the tropical CAG coincides with a significant increase in curvature vorticity, which by t_0 + 48 h represents the majority of the total relative vorticity averaged over the CAG (Fig. 3.35). Beyond this period, the CAG stalls and then moves northeast back over the Caribbean,

where one of the easternmost vorticity maxima would further organize and contribute to the formation of TC Nicole (not shown).

As the tropical CAG organizes and develops, its surrounding environment is blanketed by ample moisture. Enhanced PWAT (> +1.00 σ) first appears over the Caribbean, migrating from the eastern Caribbean to the western Caribbean and Central America by t_0 (Figs. 3.36a-d). By t_0 + 48 h the highest PWAT has enveloped the tropical CAG center (between +1.00 – +2.00 σ), while a large region of enhanced PWAT (> 0.50 σ) exists outside of the circulation over Mexico, the Gulf of Mexico, and Caribbean.

Another important feature that characterizes tropical CAGs is their association with upper-tropospheric low-PV air in conjunction with upper-level ridging at the time of genesis. While there is an initial southwest-northeast oriented PV streamer over the western Caribbean at t_0 - 72 h, it's quickly replaced by an upper-level anticyclone with characteristic low-PV air (< 0.75 PVU) overhead of the CAG by t_0 (Figs. 3.37a-d). As the tropical CAG tracks west-northwest with time, this low-PV air remains prevalent around its circulation, with high-PV air (> 2.00 PVU) remaining poleward of 30^{o}N (Figs. 3.37e-f). The high-PV air is also associated with the strongest westerly winds at 200-hPa (> 40 m s-1) in association with the polar jet located across North America (Figs. 3.38d-f). Interestingly, the strongest upper-level flow in the tropics near the tropical CAG is located equatorward of 10^{o}N over the EPAC. In this region, southeasterly flow from 25 – 35 m s^{-1} appears to be connected with a region of equatorward irrotational outflow originating from 500-hPa vertical ascent associated with the tropical CAG (Figs. 3.38e-f). This ascent, occurring in a moisture rich environment (> 50 mm) near the tropical CAG center is likely the indicator of convective activity in association with the CAG. This

suggests that convective activity associated with the tropical CAG is helping to modify its upper-tropospheric environment.

A meridional cross section through the center of the tropical CAG further illustrates the tropospheric changes occurring in proximity to the tropical CAG. The initial PV streamer in the western Caribbean at t_0 – 72 h and t_0 – 48 h (Figs. 3.39a-b), associated with +PV anomalies (> +2 PVU) from 300 – 150-hPa, quickly moves out of the Caribbean, with the resulting tropospheric pattern depicting -PV anomalies (between -0.25 – -2.00 PVU) above 300-hPa by t_0 – 24 h (Fig. 3.40c). Some tropospheric deep ascent (< -2×10^{-3} hPa s^{-1}) begins to develop overhead of the tropical CAG genesis point at t_0, although this has only resulted in a small region of +PV in the low to mid troposphere (between +0.10 – +0.25 PVU) (Fig. 3.40d). The development of a more established +PV tower doesn't occur until t_0 + 24 h and beyond (Figs. 3.41e-f), where ascent north and south of the tropical CAG center help redistribute the PV field, developing –PV anomalies (between -0.50 – -2.00 PVU) in the upper-troposphere above the level of max LHR, while +PV anomalies (between +0.50 – +2.00 PVU) develop below the level of max LHR. The sharp bowing down of 350 K isentropes over the tropical CAG center identifies this LHR maximum, where condensing water vapor is releasing heat over the tropical CAG center.

The development of a tropospheric warm core associated with the tropical CAG occurs gradually. After the upper-level cold core PV anomaly moves out of the cross section in t_0 – 72 h and t_0 – 48 h, there is the gradual development of positive temperature anomalies (between +1 to +2^{o}C) over the tropical CAG center by t_0 + 24 h to t_0 + 48 h (Figs. 3.42 – 3.44a-f, bottom panels). Note the gradual intensification of the low-level

zonal flow where strengthening westerlies occur equatorward of the tropical CAG center, while strengthening easterlies occur poleward of the tropical CAG center (Figs. 3.42 – 3.44a-f, top panels). This also corresponds to an increase in the cyclonic relative vorticity below 500-hPa in corridors poleward and equatorward of the tropical CAG center (Figs. 3.42 – 3.44a-f, bottom panels). The strengthening low-level zonal flow and cyclonic relative vorticity is consistent with the intensification of the large-scale CAG circulation at 850-hPa (Fig. 3.34). Above 300-hPa this pattern reverses as the upper-level anticyclonic flow intensifies, represented by strengthening westerly flow poleward of the tropical CAG and strengthening easterly flow equatorward of the tropical CAG (Figs. 3.42 – 3.44 a-f, top panels). The case study characteristics presented here are similar in nature to the composite structure of a tropical CAG.

3.6.2. Trough CAG Case Study

The trough CAG used in this study developed on 0000 UTC 21 May 1991 in the extreme southeastern corner of the Gulf of Mexico. As discussed in section 3.2, trough CAGs are identified at genesis as large low-level cyclonic circulations associated with high PV air (> 2.00 PVU) at the 350K isentropic surface, indicative of upper-tropospheric troughing. This trough CAG had a lifespan of 3 days (72 h) as it moved slowly to the northwest while interacting with upper-tropospheric high-PV air.

As discussed in the trough CAG composite in section 3.3.2, large-scale 850-hPa anomalous standardized height gradients aid in the generation of anomalous wind corridors in the EPAC and ATL basins prior to tropical CAG genesis at t_0. As one increases in latitude from the equator in the EPAC, there is a shift from positive

standardized geopotential height (between +1.00 – +2.00 σ) to negative standardized geopotential heights centered over Central America (between -0.50 – -1.00 σ) This anomalous height gradient drives anomalous westerly winds (> 10 kt) across the EPAC between the equator to 15°N. In the ATL basin, we see a similar anomalous height gradient, but in reverse, where standardized negative geopotential height anomalies (between -0.50 – -1.00 σ) become positive standardized geopotential height anomalies (between +1.00 – +2.00 σ) as one moves poleward into the subtropical Atlantic. This anomalous height gradient results in a corridor of enhanced easterly flow (> 10 kt) across the Caribbean and tropical ATL basin. After CAG development (Figs. 3.45d-f), the strongest negative standardized geopotential height anomalies become associated with the CAG (< -3.00 σ), although it remains embedded in a larger corridor of negative geopotential height (between -0.25 – -1.00 σ) over Central America. Similar to the trough CAG composite, the source region of the enhanced 850-hPa subtropical ridging over the ATL basin appears to originate over eastern North America and move southeastward in the ATL basin, rather than as an extension of subtropical ridging from the ATL basin that extends westward towards North America.

The majority of 850-hPa vorticity and large-scale circulation is initially focused over Central America (Figs. 3.46a-b), where the aforementioned corridors of anomalous 850-hPa flow aid in generating cyclonic vorticity (> 1×10^{-5} s^{-1}). However, these low-level jet corridors do not denote a closed circulation, a requirement for CAG classification. At t_0 – 24 h a new source region of cyclonic vorticity and large-scale circulation develops over the Gulf of Mexico, related to an upper-level trough that has cutoff from the mid-latitude flow (Fig. 3.46c). This region of vorticity and circulation

interacts and merges with the original vorticity over Central America, culminating in the development of a trough CAG over the southeastern Gulf of Mexico at t_0 (Fig. 3.46d). While initially elongated, this circulation intensifies and becomes more cyclonic in nature by t_0 + 48 h (Fig. 3.46f). The cyclonic vorticity embedded in the trough CAG rotates cyclonically around the mean center, with the strongest cyclonic vorticity maxima (> 15 $\times 10^{-5}$ s^{-1}) primarily oriented in a strip north and east of the trough CAG center. While less coherent than the evolution of the tropical CAG case study, there is a gradual shift in the partitioning of total relative vorticity from shear vorticity prior to trough CAG formation t_0 – 24 h to curvature vorticity by t_0 + 48 h (Fig. 3.47).

As noted in the trough CAG composite, PWAT tends to be asymmetrical around the trough CAG center. This similarity is also noted in the PWAT case study. Initially there is a large region of anomalously high standardized PWAT anomalies (> 1.00 σ) located over portions of Central America, the Caribbean, and Gulf of Mexico (Figs. 3.48a-b). As the trough CAG begins to organize at t_0 (Fig. 3.48d), however, much of the highest PWAT anomalies (> 1.00 σ) shift towards the eastern side of the CAG center, while negative standardized PWAT anomalies (< -1.00 σ) become more prevalent across Mexico and the EPAC on the west side of the CAG center. This PWAT asymmetry across the trough CAG center remains through t_0 + 48 h (Fig. 3.48f), although the anomalies shift somewhat, where the largest positive PWAT anomalies (> 2.00 σ) become situated northeast of the CAG center ,while negative PWAT anomalies (< -1.00 σ) are located primarily southwest of the CAG center. The rotation of the enhanced PWAT anomalies is possibly due to advection of the cyclonic flow around the trough CAG.

A key component in the classification of a trough CAG is related to the presence of an upper tropospheric trough in proximity to the low-level circulation center. At $t_0 - 72$ h a 200-hPa trough located over Texas breaks off from the mid-latitude flow and drops southeastward into the GoM by $t_0 - 24$ h (Figs. 3.49a-c). This fracture of this upper-level high-PV air into the GoM is similar to a cyclonic wavebreaking event (Thorncroft et al. 1993), where high-PV air (> 2.00 PVU) breaks underneath an upper-tropospheric ridge of low-PV air (< 1.00 PVU) Given a sufficient Rossby penetration depth, this 200-hPa cyclone can penetrate deep into the lower troposphere (e.g. Fig. 3.46c-f) and interact with the low-level circulation associated with the formative trough CAG. By t_0 (Fig. 3.49d), this high-PV air is within 1000 km of the center of the trough CAG and by $t_0 + 48$ h (Fig 3.49f), this 200-hPa cyclone is nearly superimposed over the trough CAG center at 850-hPa.

This 200-hPa low is also associated with strong upper-level flow along its periphery, and the resulting jet structure is important for the development of cloudiness and convection along the outer periphery of the trough CAG. The largest 500-hPa vertical ascent is maximized ($< -2 \times 10^{-3}$ hPa s^{-1}) northeast of the trough CAG center from t_0 to $t_0 + 48$ h (Figs. 3.50d-f), where high PWAT (> 50 mm), low 200-hPa PV (< 0.50 PVU) and irrotational outflow (> 10 m s^{-1}) emanating from the 500-hPa ascent are also present. Some of this ascent is aided by being positioned in the right jet entrance region of a 200-hPa jet streak (> 40 m s^{-1}) offshore of the eastern US coastline. Meanwhile, there is little vertical ascent over the trough CAG center, with the trough CAG center primarily under a region of high 200-hPa PV (> 2.00 PVU) while bisected by a 15 – 25 m s^{-1} 200-hPa southerly jet. The strong southerly winds associated with the 200-hPa jet provides an

unfavorable environment for TCG. No TCs developed or occurred within this trough CAG case study.

An investigation of the meridional PV through the trough CAG reveals the interaction of low-level and upper-level PV anomalies. Prior to trough CAG formation, there are scattered regions of tropospheric deep vertical ascent ($> 2 \times 10^{-3}$ hPa s^{-1}) occurring along the meridional cross section near the trough CAG genesis point. In general, low-PV is observed in the upper troposphere with an extensive area of -PV anomalies (between -0.25 – -2.00 PVU) above 300-hPa at t_0 – 48 h (Fig. 3.51b, bottom panel). As the upper tropospheric cyclone begins to move into the same longitude as the trough CAG genesis point, a corridor of high PV air (> 2.00 PVU) above 300-hPa is observed overhead of the trough CAG center during trough CAG genesis (Fig. 3.52d, top panel) in association with +PV anomalies > 2.00 PVU between 400 – 150-hPa (Fig. 3.52d, bottom panel). This high PV air is also in contact with weaker lower tropospheric +PV anomalies (between +0.10 – +2.00 PVU) below 500-hPa. By t_0 + 48 h, an established tropospheric deep +PV anomaly with maximum > +2.00 PVU has become established over the trough CAG center, with increasing PV with height (Fig. 3.53f). Isentropes are bowing upward from 400 – 200-hPa at and just equatorward of the trough CAG center in association with the +PV anomaly, with a PV profile increasing with height indicative of a hybrid tropical disturbance that possesses upper-level troughing overhead.

The hybrid or subtropical nature of this trough CAG is also evident when investigating the zonal winds and temperature anomalies along the meridional cross section. Focusing primarily after the trough CAG has developed (t_0 + 48 h, Fig. 3.56f)

there is a distinct temperature anomaly gradient near the trough CAG center (Fig. 3.56f, bottom panel). Positive temperature anomalies between +3 to +5^{o}C are observed throughout the troposphere, primarily poleward of the trough CAG center, in association with upper tropospheric ridging located over eastern North America (Fig. 3.38f). Equatorward of the trough CAG center, negative temperature anomalies between -1 to -2^{o}C are observed in association with the upper tropospheric trough present over the trough CAG. The implied temperature anomaly gradient over the trough CAG is not unusual for a subtropical entity, and similar mid-level thermal gradients have been observed in case studies of MGs in the WPAC basin (Crandall et al. 2014). When investigating the zonal wind profile of the trough CAG, there is a tropospheric deep corridor of easterly flow (between 5 – 10 m s^{-1}) poleward of the CAG center, and westerly flow (between 5 – 15 m s^{-1}) equatorward of the CAG center. This roughly corresponds to the time when the upper-tropospheric cyclone has become superimposed upon the low-level circulation of the trough CAG (Fig. 3.56f, top panel). While these zonal wind corridors are maximized outside of the trough CAG center, similar to the tropical CAG, these winds do not decrease with height, and relative vorticity actually increases with height (max > 10 × 10^{-5} s^{-1} between 250 – 200-hPa) over the trough CAG center (Fig 3.56f, bottom panel).

Table 1. Climatological statistics associated with Central American Gyres (N = 42) from 1980-2010.

Parameter	Mean	Max	Min
Latitude at Genesis (^{o}N)	14.3	25.5	8.0
Longitude at Genesis (^{o}W)	85.4	94.0	70.0
Lifespan (h)	71	168	48
Max Azimuthal Avg. Wind ($m\ s^{-1}$)	8.4	15.5	5.2
Radius of Max Winds (km)	595	1050	500

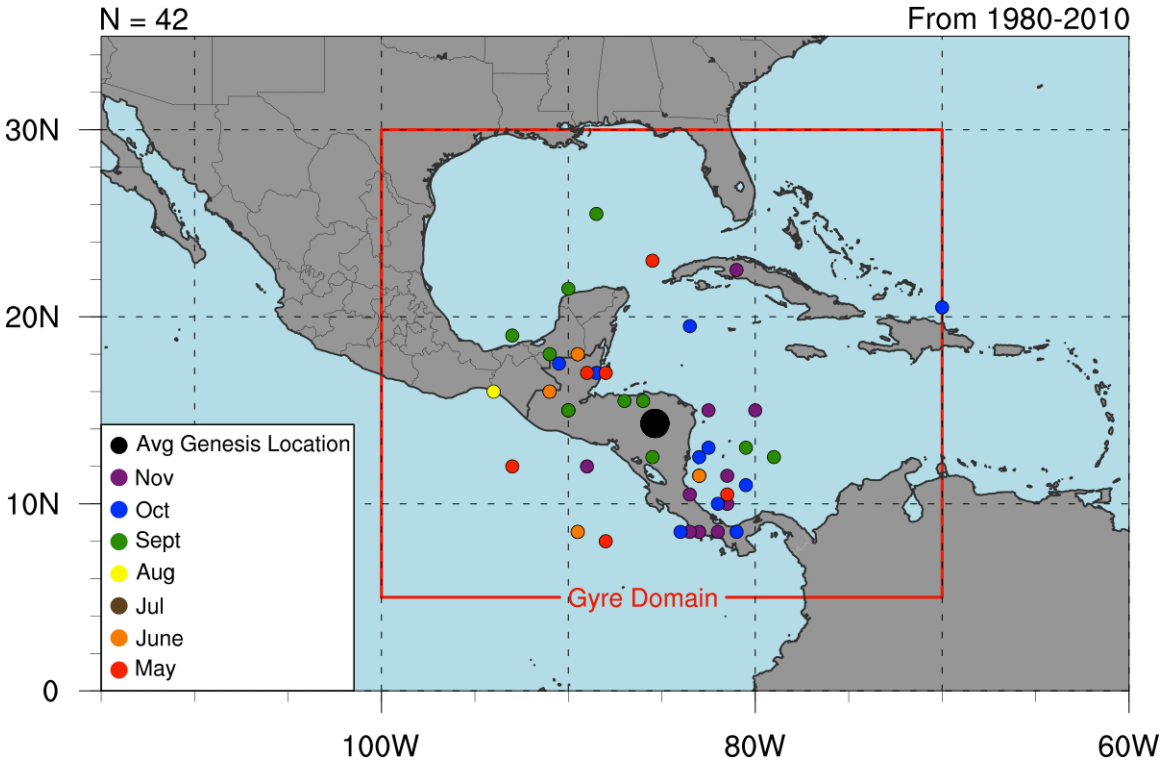

Fig. 3.1. Locations of CAG formation across the algorithm domain (1980-2010). The color of each dot represents the month CAG formation occurred, according to the legend, with the larger black dot presenting the average location.

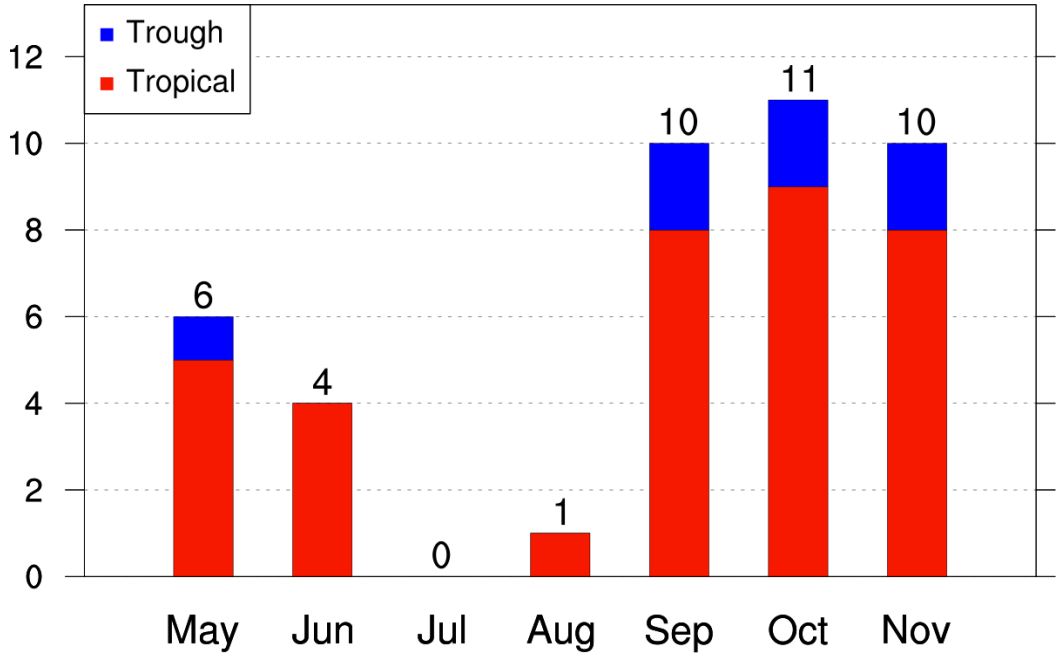

Fig. 3.2. Frequency of CAG formation (1980-2010) separated by month (May-November). Red and blue regions represent the number of CAGs classified as tropical events versus trough influenced events (as documented in chapter 2).

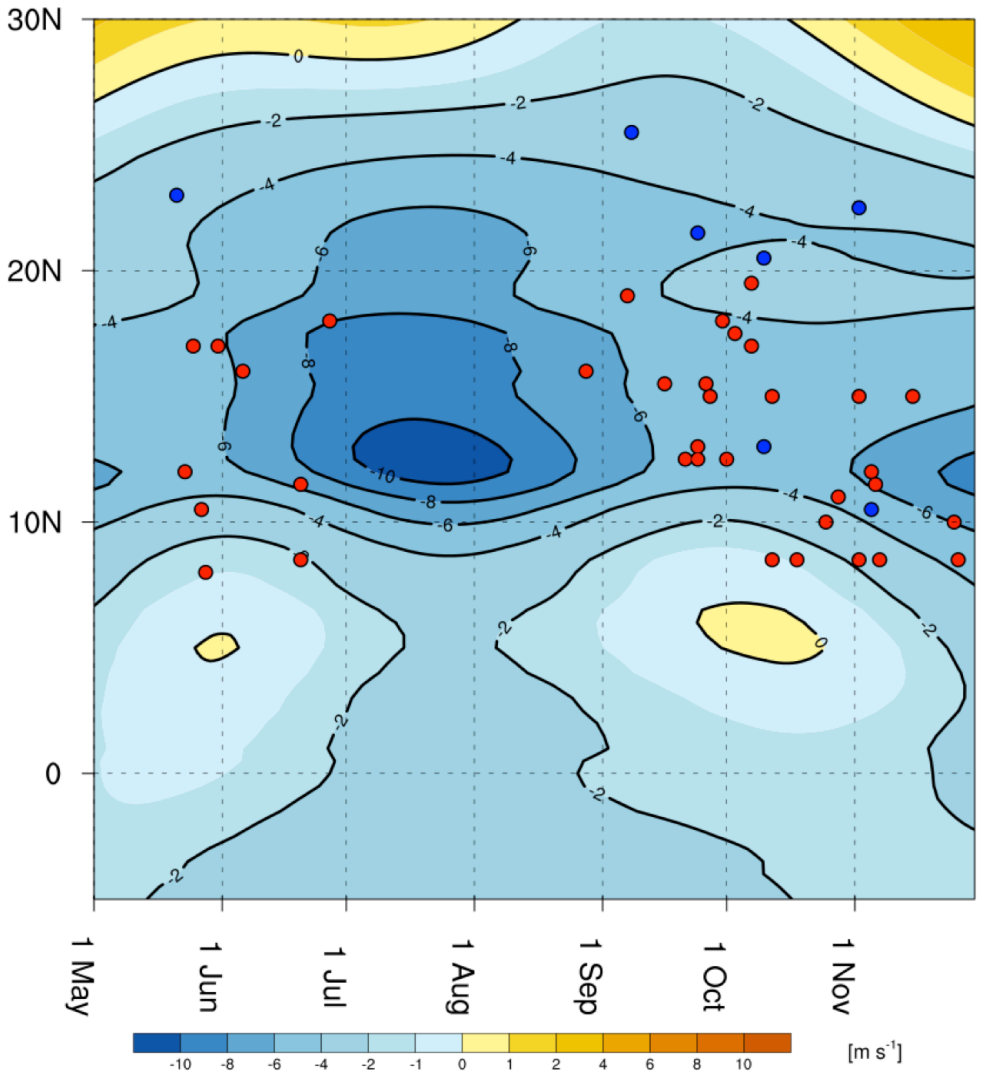

Fig. 3.3. Latitude distribution of climatological 850-hPa zonal winds (shaded, m s^{-1}) averaged between 100-70°W from 1 May – 30 Nov. Red (blue) dots correspond to the genesis of tropical (trough) CAGs.

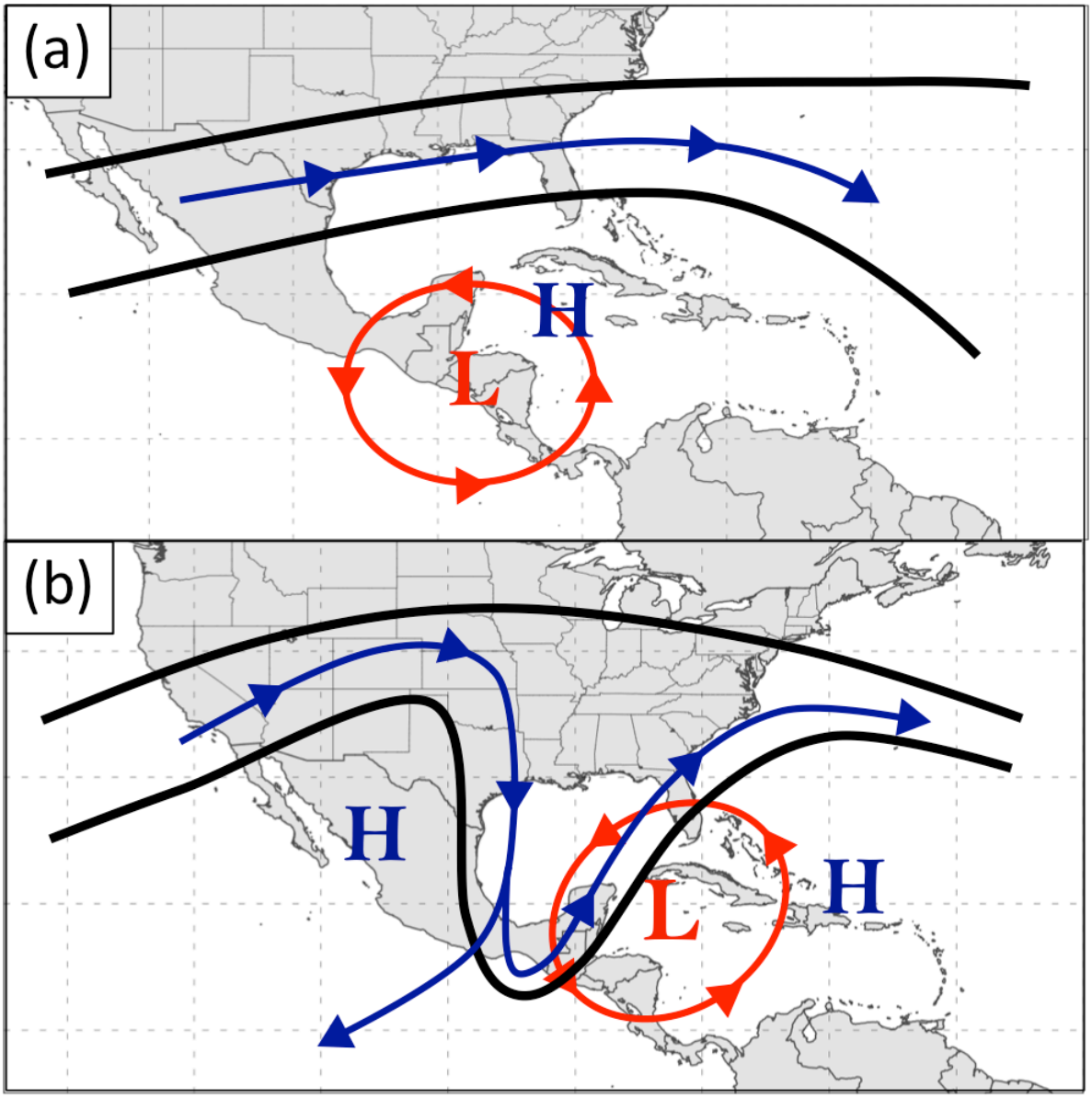

Fig. 3.4. Schematic representation of the different CAG formation characteristics: (a) a CAG that forms without an upper-tropospheric trough (tropical CAG) and (b) a CAG that forms in conjunction with an upper-tropospheric trough (trough CAG). Black lines represent the 1 and 2 PVU surfaces on an idealized 350 K isentropic surface. Blue arrows indicate the motion of the flow on the idealized 350 K isentropic surface, while red arrows indicate the motion of the flow at the 850-hPa level. A blue "H" denotes the location of upper-tropospheric anticyclones, while a red "L" denotes the center of the CAG at genesis.

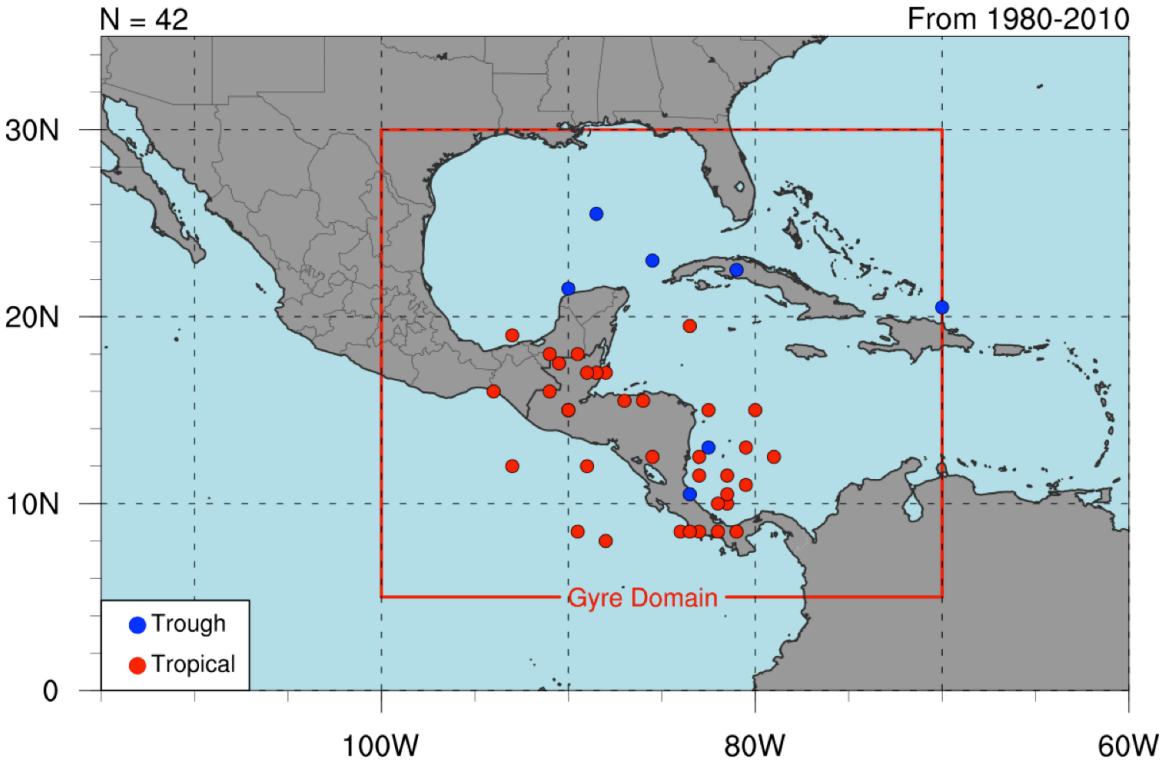

Fig. 3.5. As in Fig 3.1 except the color of each dot represents the type of CAG at genesis, with tropical CAGs (N=35) depicted as red dots, while trough CAGs (N=7) depicted as blue dots.

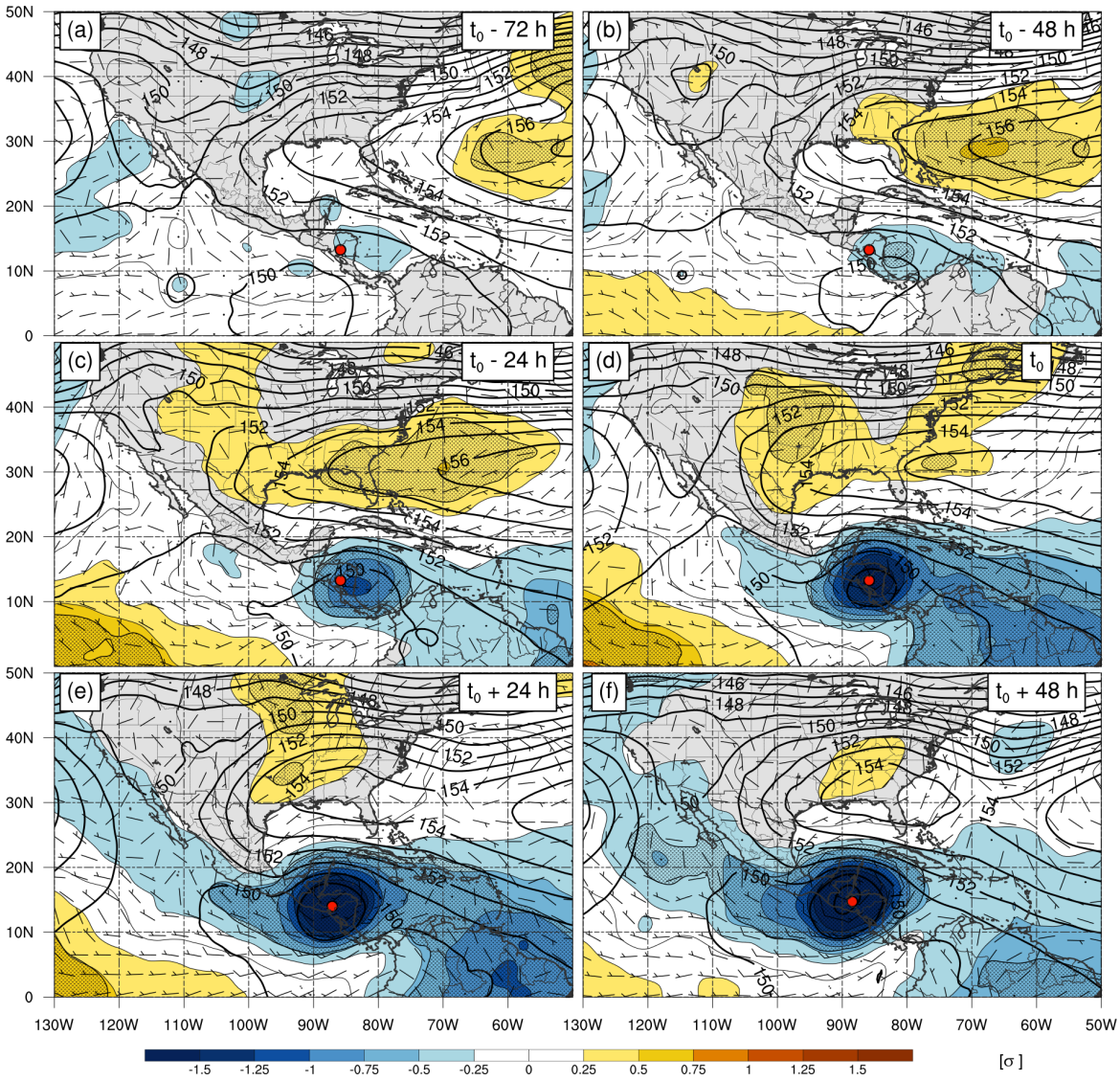

Fig. 3.6. Tropical CAG composite (N = 35) 850-hPa standardized geopotential height anomaly (shaded, sigma), 850-hPa geopotential height (black contours, dam), and 850 hPa anomalous winds (barbs, kts) at (a) t_0 – 72 h, (b) t_0 – 48 h, (c) t_0 – 24 h, (d) t_0, (e) t_0 + 24 h, and (f) t_0 + 48 h. The red circle in each panel denotes the CAG center location at genesis for panels up to genesis (-72 h to 0 h, a – d) and the CAG center location for designated times after genesis (+24 h to +48 h, e – f). Black stippling indicates where the 850-hPa geopotential height is statistically significant to the 95% level using a two tailed student's t-test.

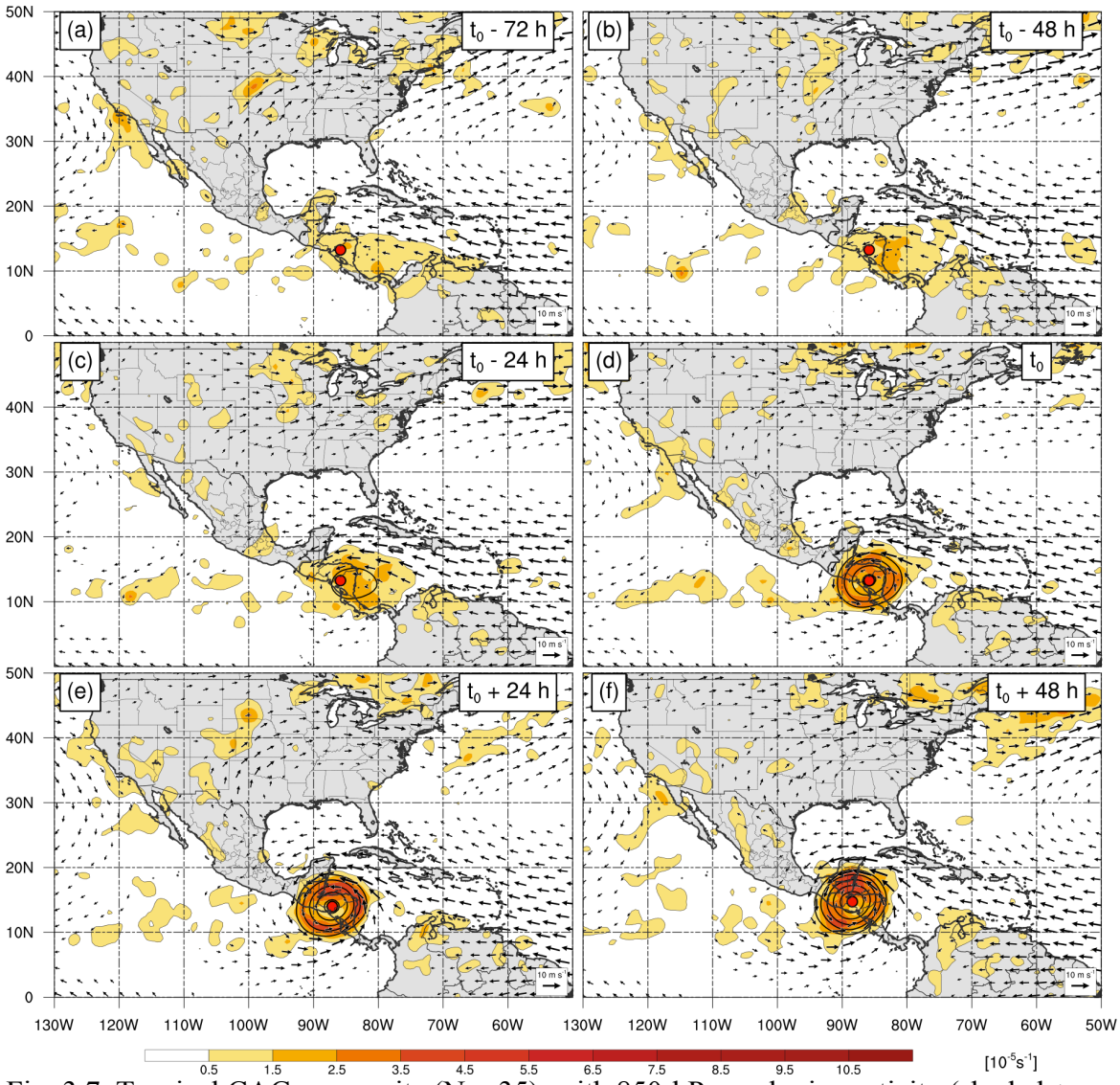

Fig. 3.7. Tropical CAG composite (N = 35), with 850-hPa cyclonic vorticity (shaded, > $0.5x10^{-5}$ s^{-1}), 1000-500 km radial average 850-hPa circulation (black contours, > $1x10^{-5}$ s^{-1}), and 850-hPa winds (vectors, m s^{-1}) at (a) t_0 – 72 h, (b) t_0 – 48 h, (c) t_0 – 24 h, (d) t_0, (e) t_0 + 24 h, and (f) t_0 + 48 h. The red circle in each panel denotes the CAG center location at genesis for panels up to genesis (-72 h to 0 h, a – d) and the CAG center location for designated times after genesis (+24 h to +48 h, e – f). Tracks of TCs are also plotted, colorized by the intensity, with the present position plotted as a TC symbol.

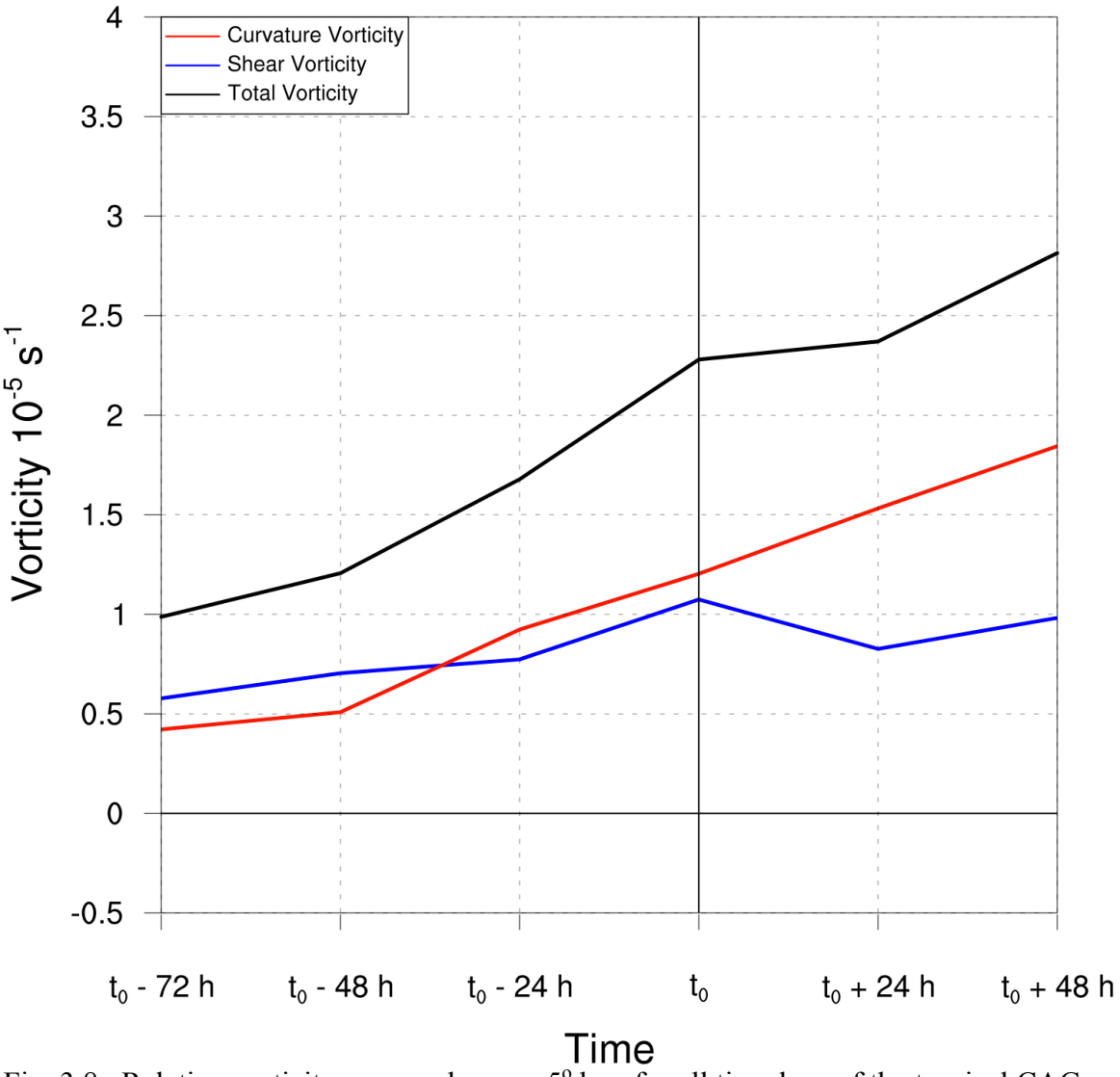

Fig. 3.8. Relative vorticity averaged over a 5° box for all time lags of the tropical CAG composite (N = 35). Different colored lines denote curvature relative vorticity (red), shear relative vorticity (blue), and total relative vorticity (black).

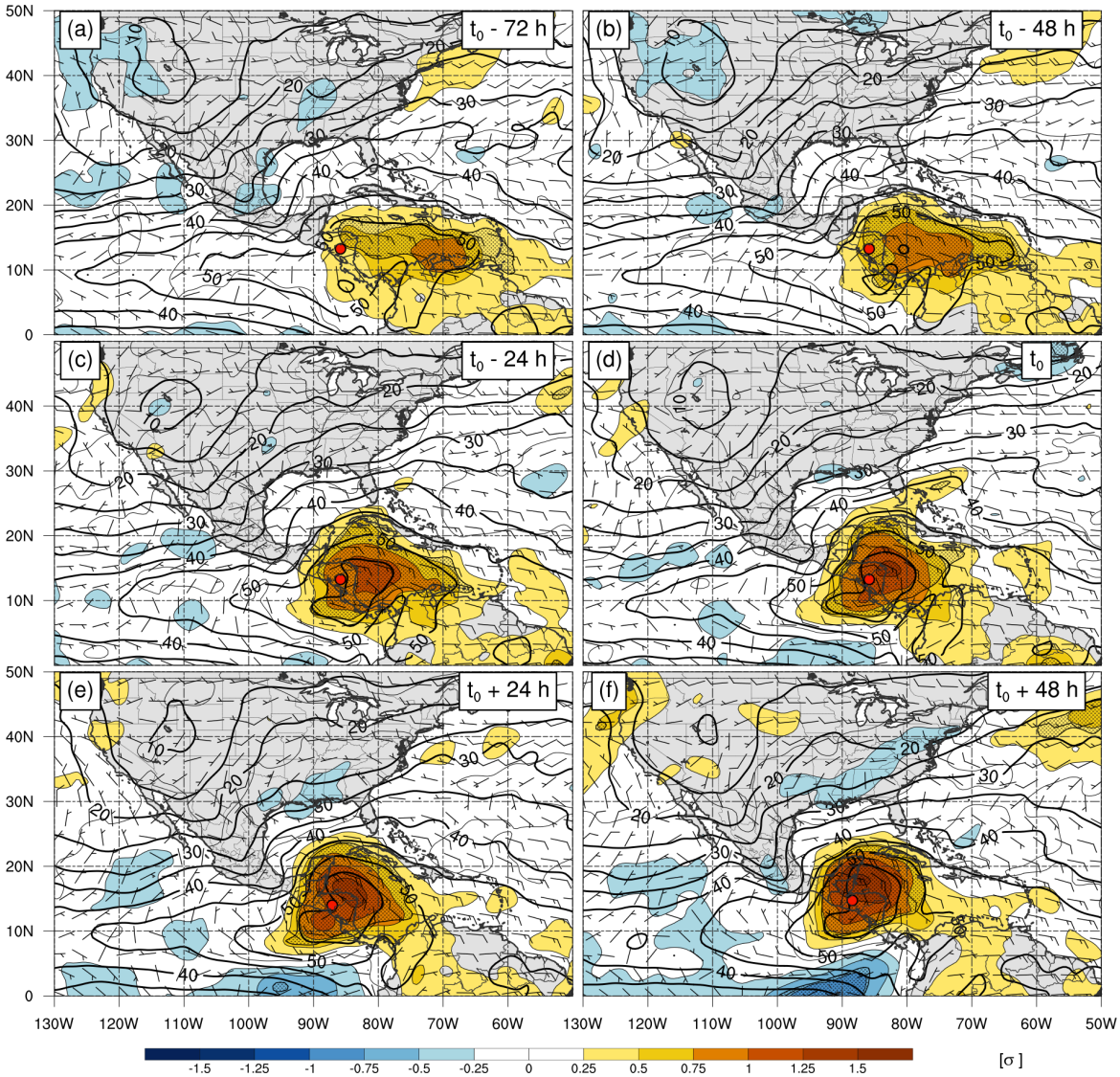

Fig. 3.9. Tropical CAG composite (N = 35) Standardized precipitable water anomaly (shaded, sigma), Precipitable water (black contours, mm), and 850 hPa winds (barbs, kts) at (a) t_0 – 72 h, (b) t_0 – 48 h, (c) t_0 – 24 h, (d) t_0, (e) t_0 + 24 h, and (f) t_0 + 48 h. The red circle in each panel denotes the CAG center location at genesis for panels up to genesis (-72 h to 0 h, a – d) and the CAG center location for designated times after genesis (+24 h to +48 h, e – f). Black stippling indicates where the 850-hPa geopotential height is statistically significant to the 95% level using a two tailed student's t-test.

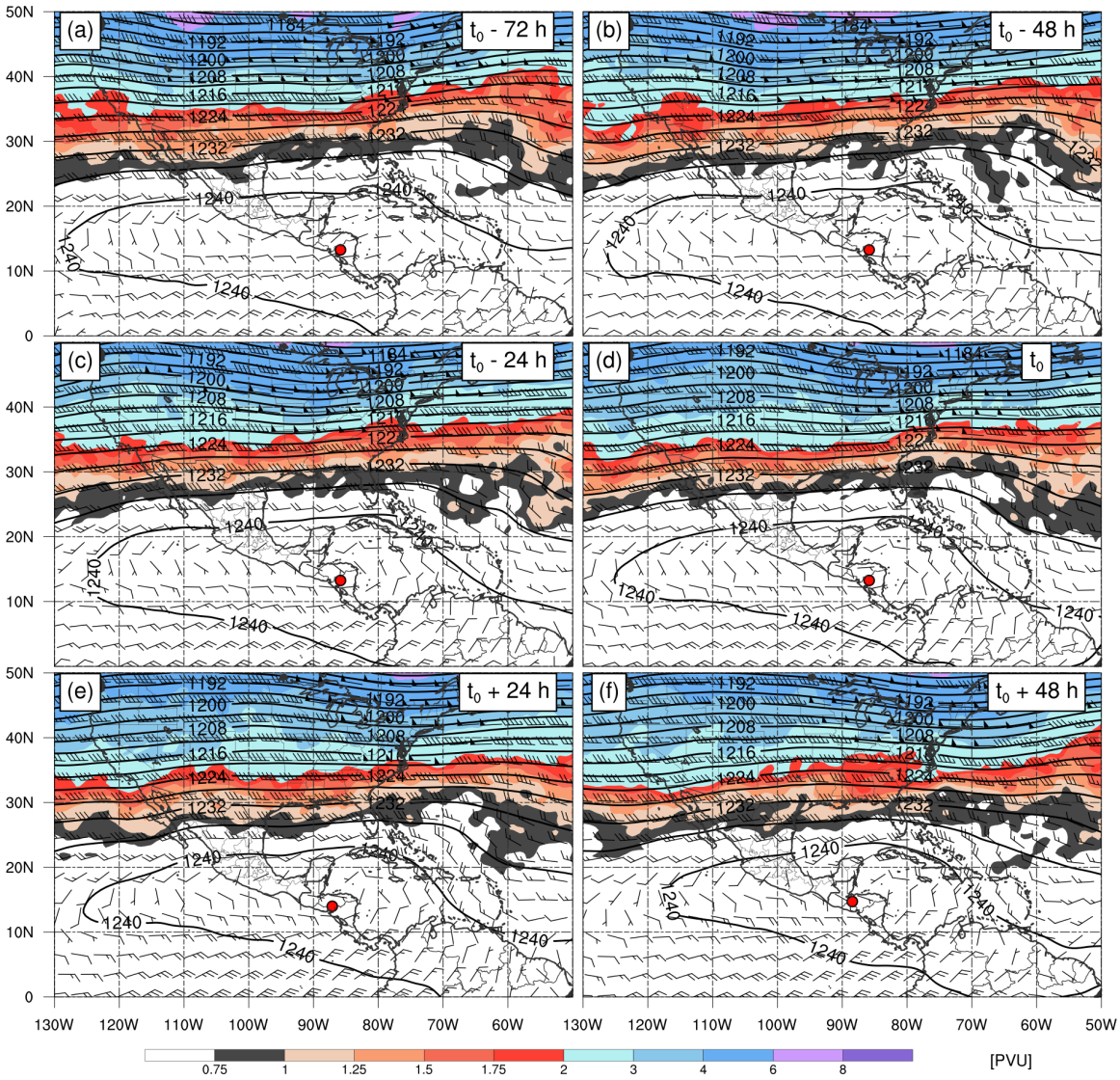

Fig. 3.10. Tropical CAG composite (N = 35) 200-hPa potential vorticity (shaded, PVU), 200-hPa geopotential heights (black contours, dam), and 200 hPa winds (barbs, kts) at (a) t_0 – 72 h, (b) t_0 – 48 h, (c) t_0 – 24 h, (d) t_0, (e) t_0 + 24 h, and (f) t_0 + 48 h. The red circle in each panel denotes the CAG center location at genesis for panels up to genesis (-72 h to 0 h, a – d) and the CAG center location for designated times after genesis (+24 h to +48 h, e – f).

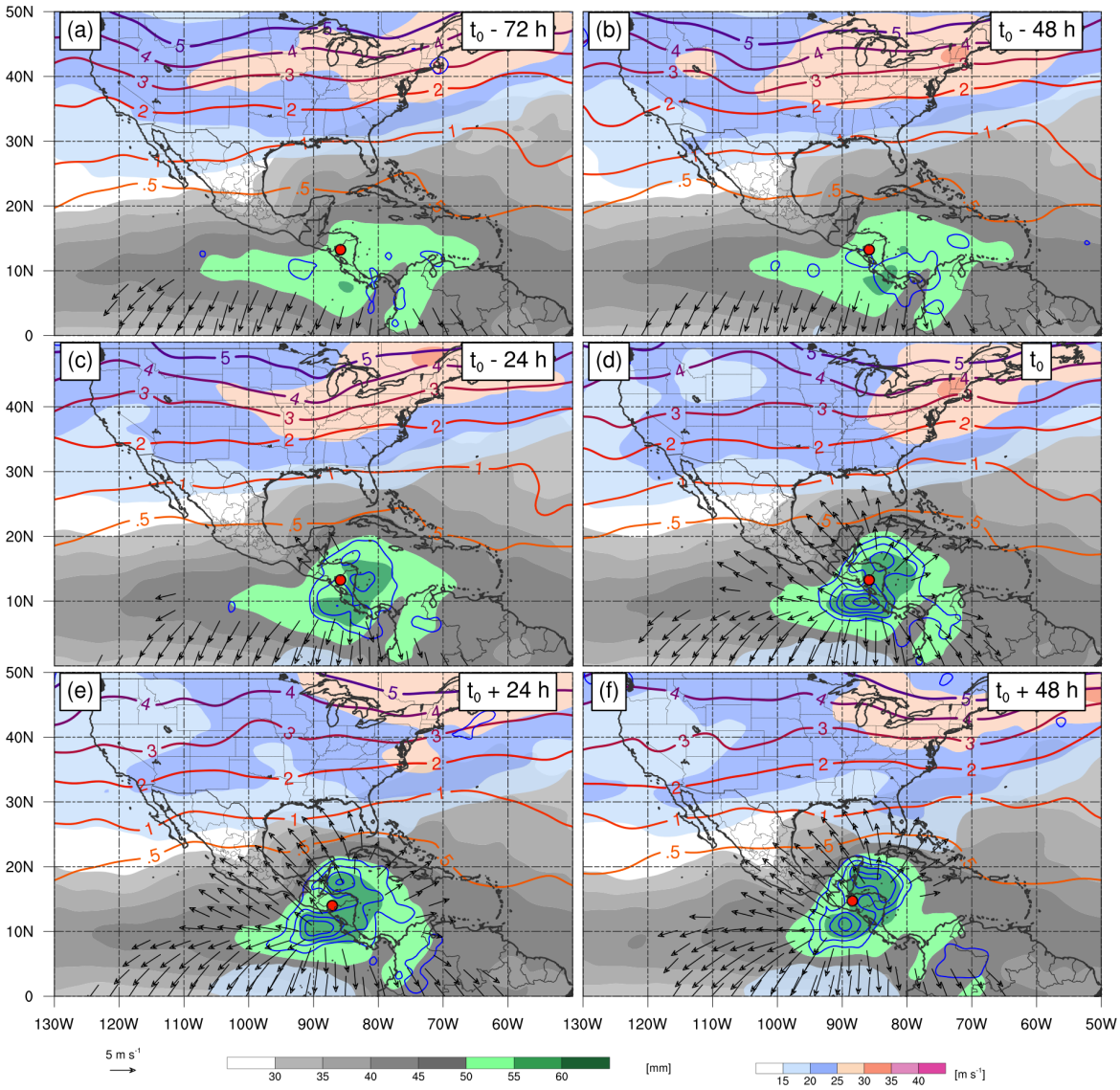

Fig. 3.11. Tropical CAG composite (N = 35) 200 hPa isotachs (rainbow shading, m s^{-1}), Precipitable water (gray to green shading, mm), 200 hPa potential vorticity (warm contours, PVU), 500 hPa omega (blue contours, only negative contoured, hPa s^{-1}), and 200 hPa Irrotational Wind (vectors, m s^{-1}) at (a) t_0 – 72 h, (b) t_0 – 48 h, (c) t_0 – 24 h, (d) t_0, (e) t_0 + 24 h, and (f) t_0 + 48 h. The red circle in each panel denotes the CAG center location at genesis for panels up to genesis (-72 h to 0 h, a – d) and the CAG center location for designated times after genesis (+24 h to +48 h, e – f).

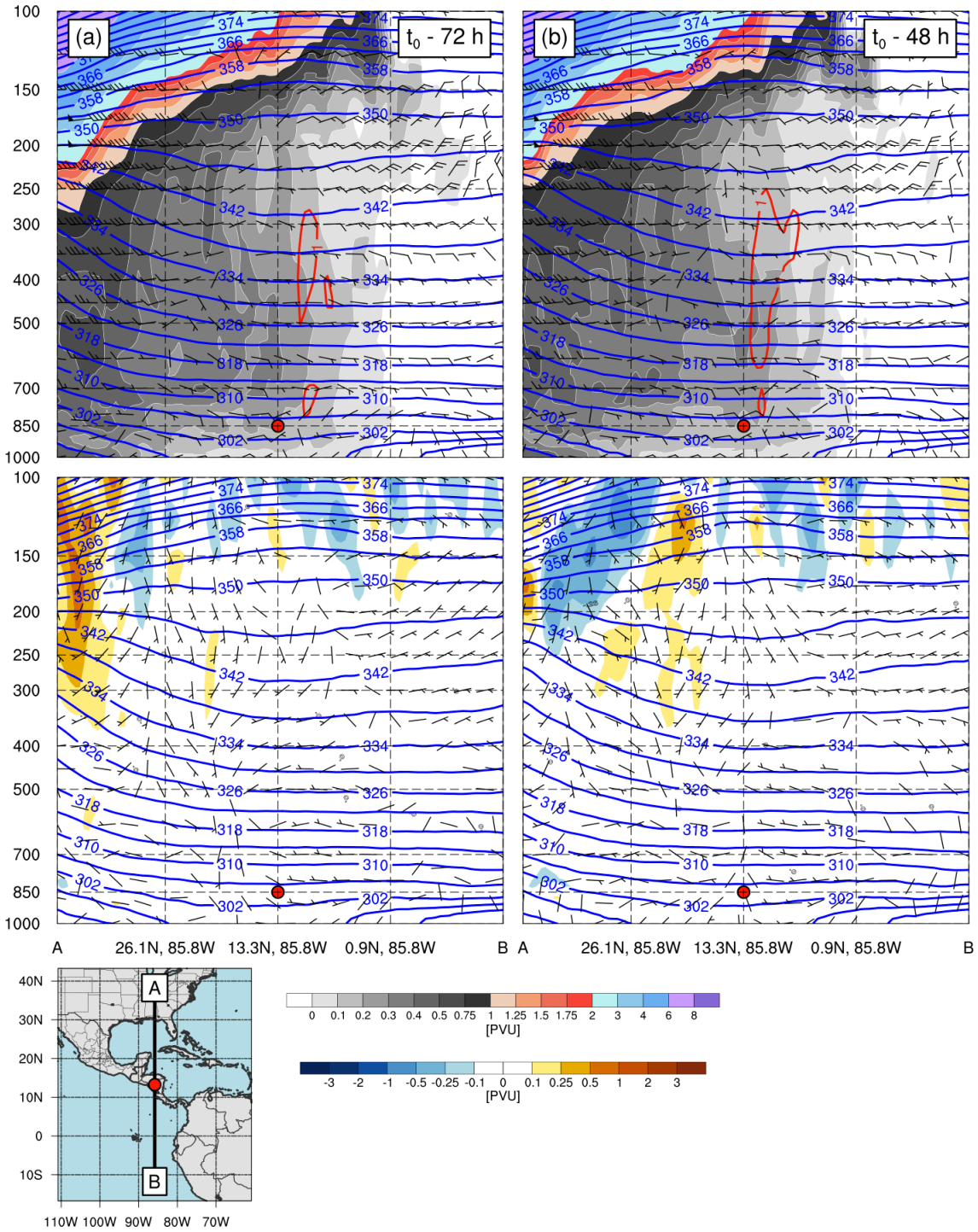

Fig. 3.12. Tropical CAG composite (N = 35) Top: potential vorticity (shaded, PVU), potential temperature (blue contours, K), vertical velocity (purple contours, 10^{-3} hPa s^{-1}) and winds (barbs, knots) Bottom: potential vorticity anomaly (shaded, PVU) potential temperature (blue contours, K) and anomalous winds (barbs, knots) at (a) t_0 – 72 h, (b) t_0 – 48 h. Reference panel for cross-section provided on the bottom left (both a and b).

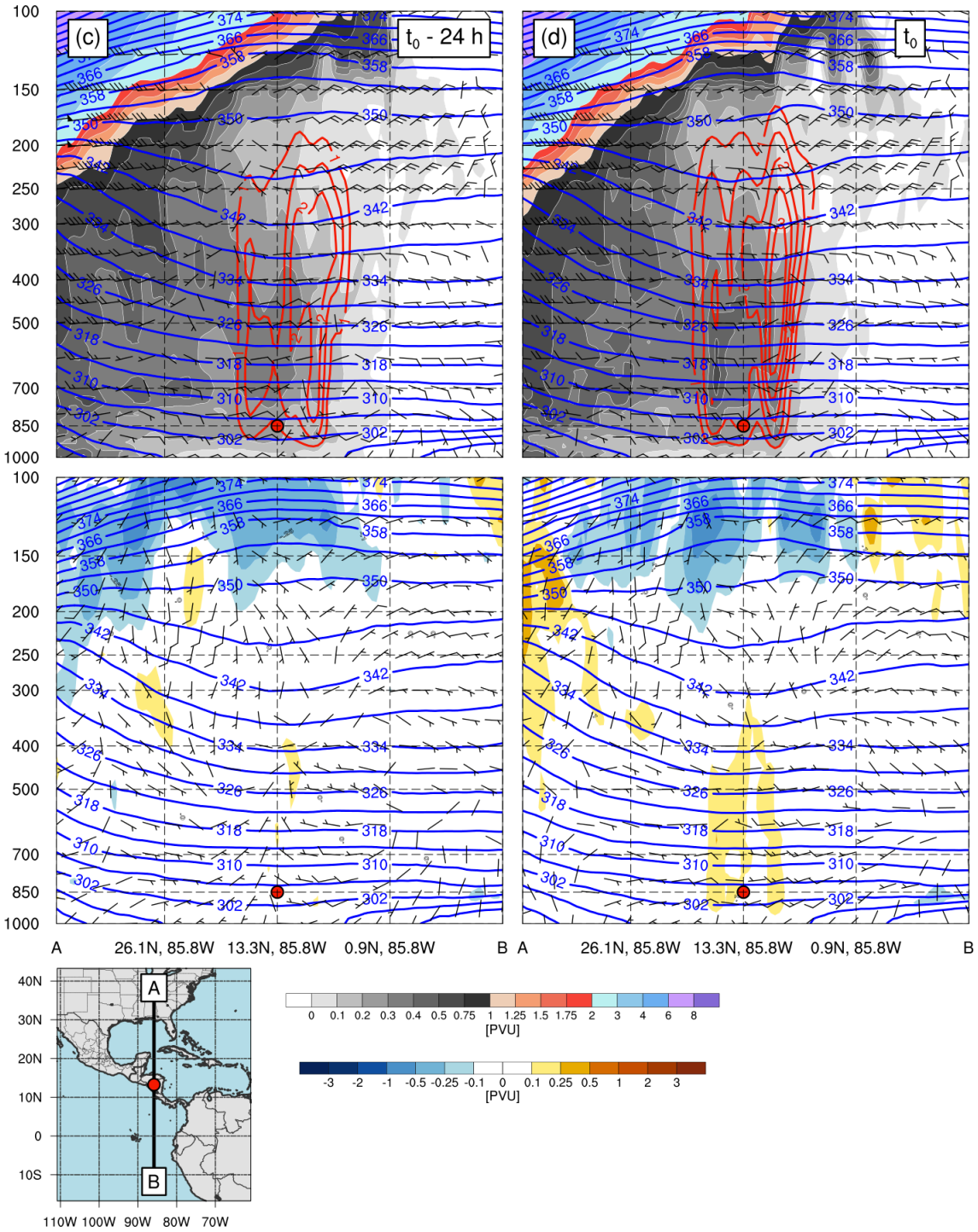

Fig. 3.13. As in Fig. 3.12 except at (c) t_0 – 24 h, and (d) t_0. Reference panel for cross-sections provided on the bottom left (both c and d).

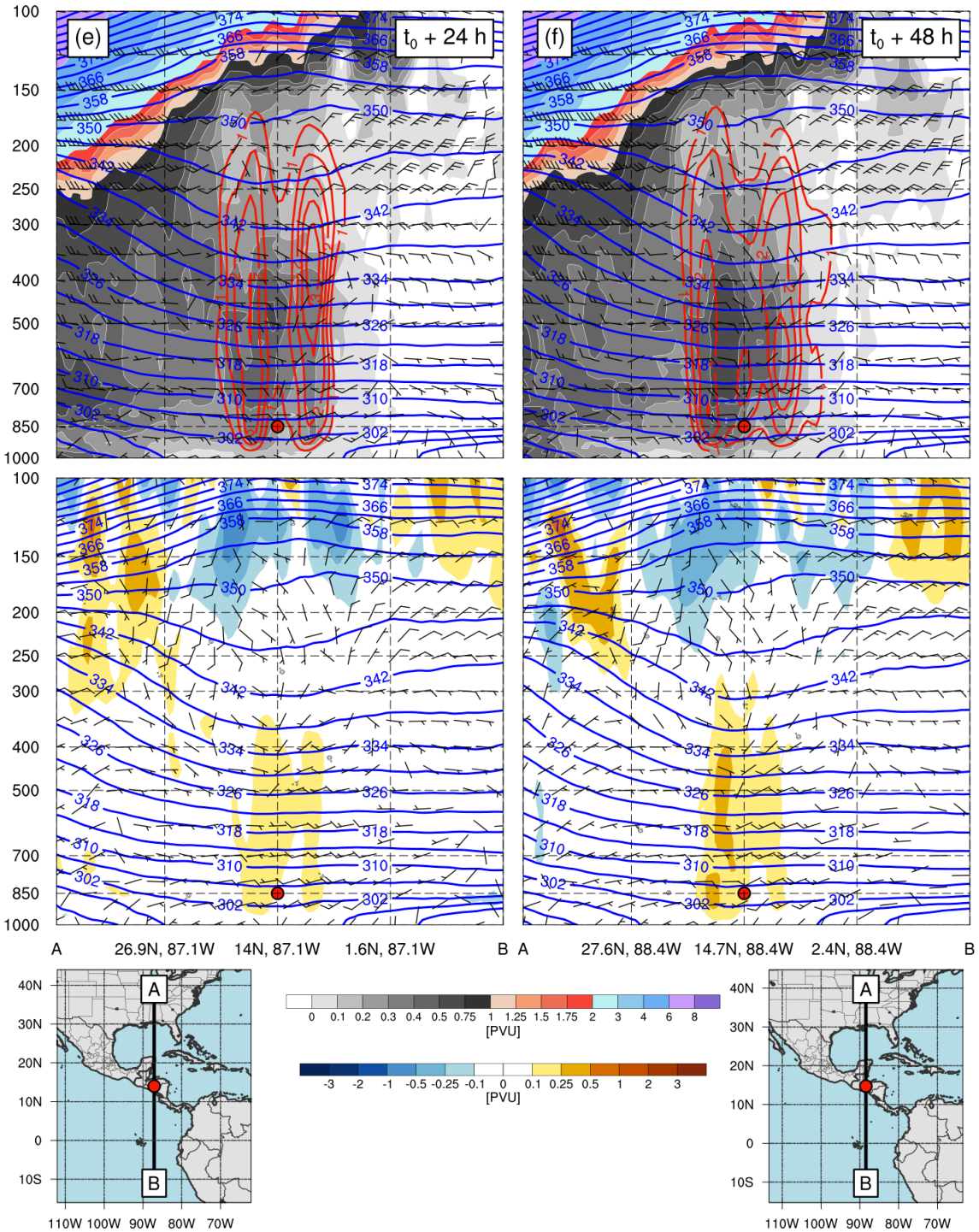

Fig. 3.14. As in Fig. 3.12 except at (e) t_0 + 24 h, and (f) t_0 + 48 h. Reference panel for cross-sections provided on the bottom left (e) and bottom right (f).

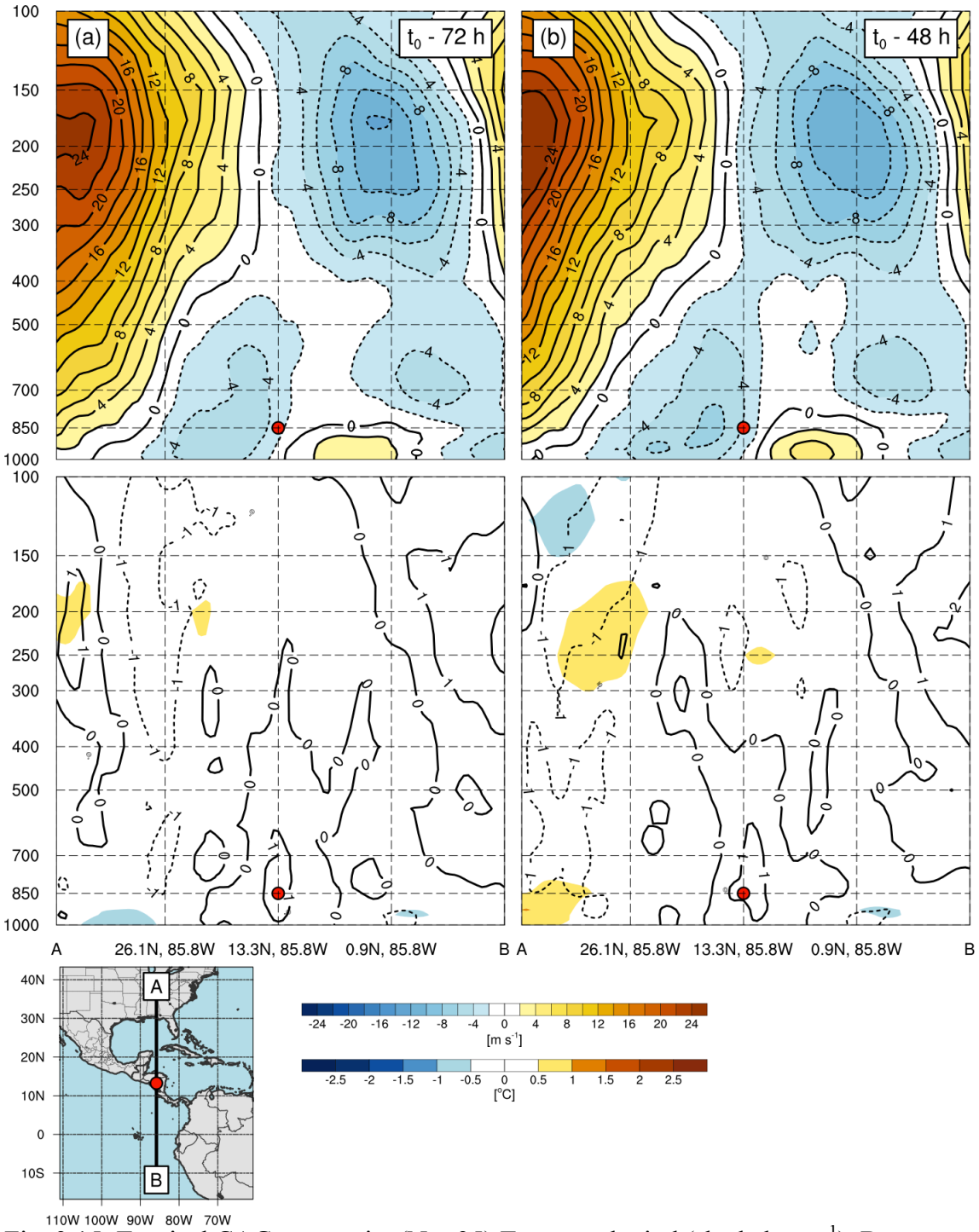

Fig. 3.15. Tropical CAG composite (N = 35) Top: zonal wind (shaded, m s^{-1}), Bottom: temperature anomaly (shaded, °C) and relative vorticity (black contours, 10^{-5} s^{-1}) at (a) t_0 – 72 h, (b) t_0 – 48 h. Reference panel for cross-section provided on the bottom left (both a and b).

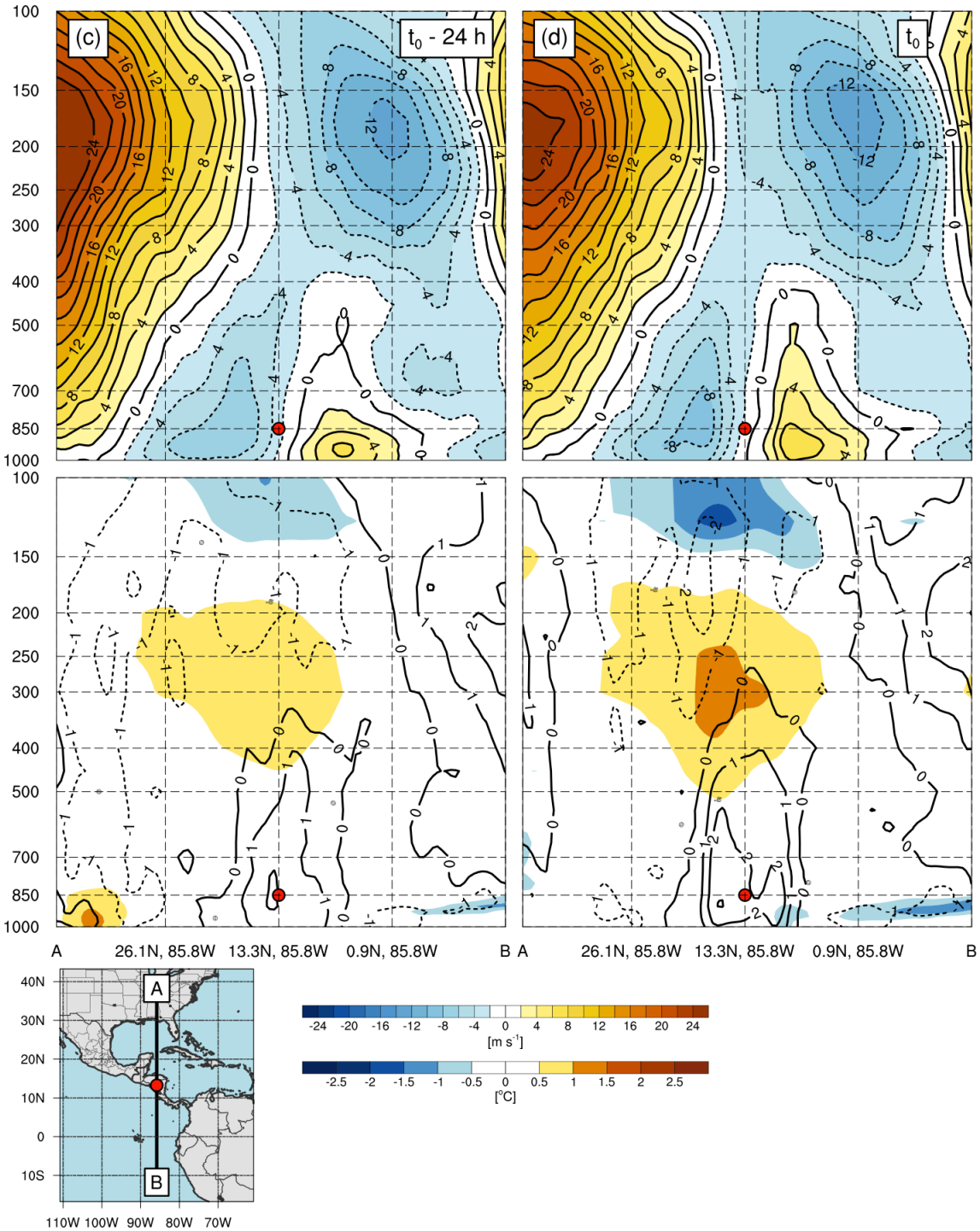

Fig. 3.16. As in Fig. 3.15 except at (c) t_0 – 24 h, and (d) t_0. Reference panel for cross-sections provided on the bottom left (both c and d).

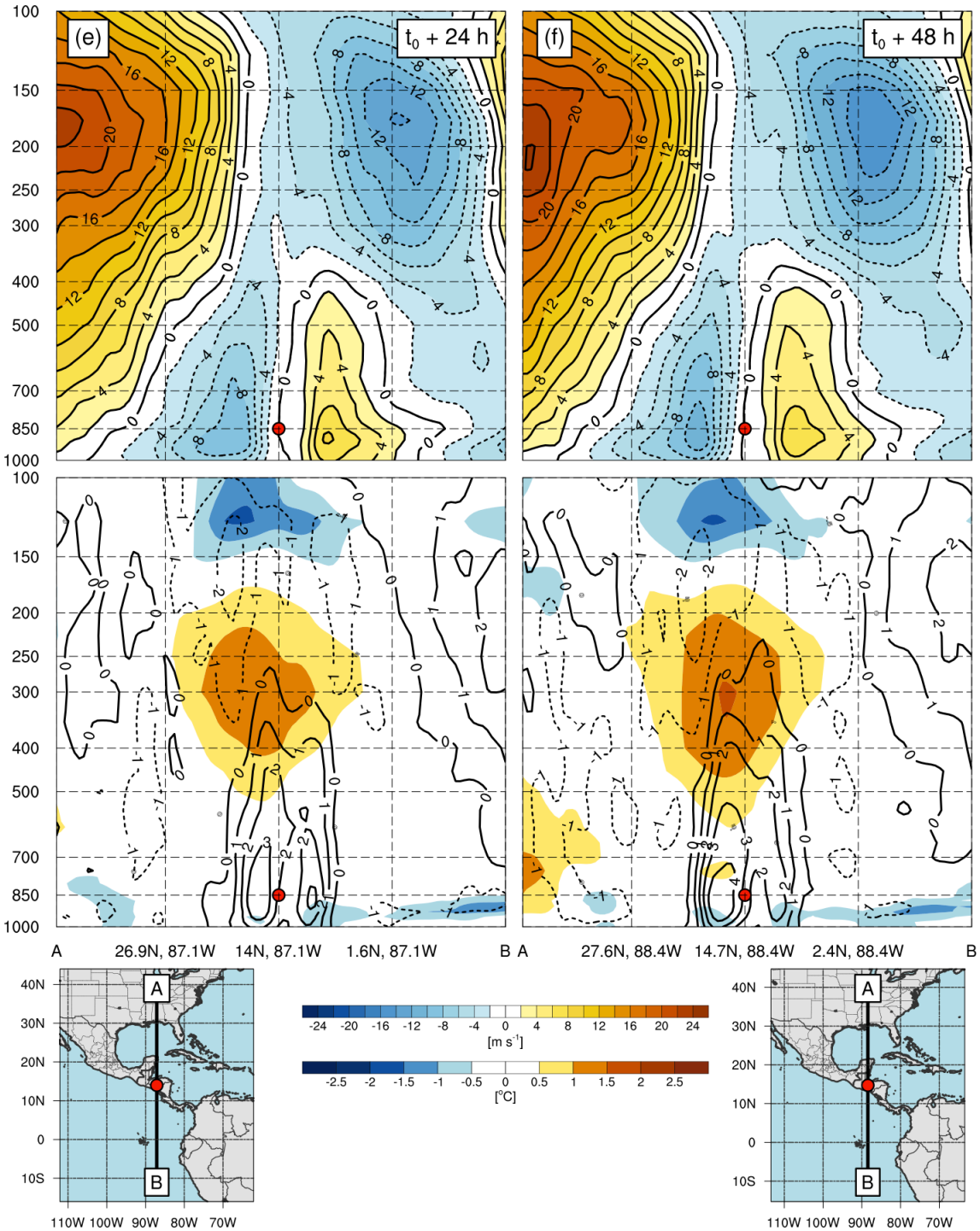

Fig. 3.17. As in Fig. 3.15 except at (e) t_0 + 24 h, (f) t_0 + 48 h. Reference panel for cross-sections provided on the bottom left (e) and bottom right (f).

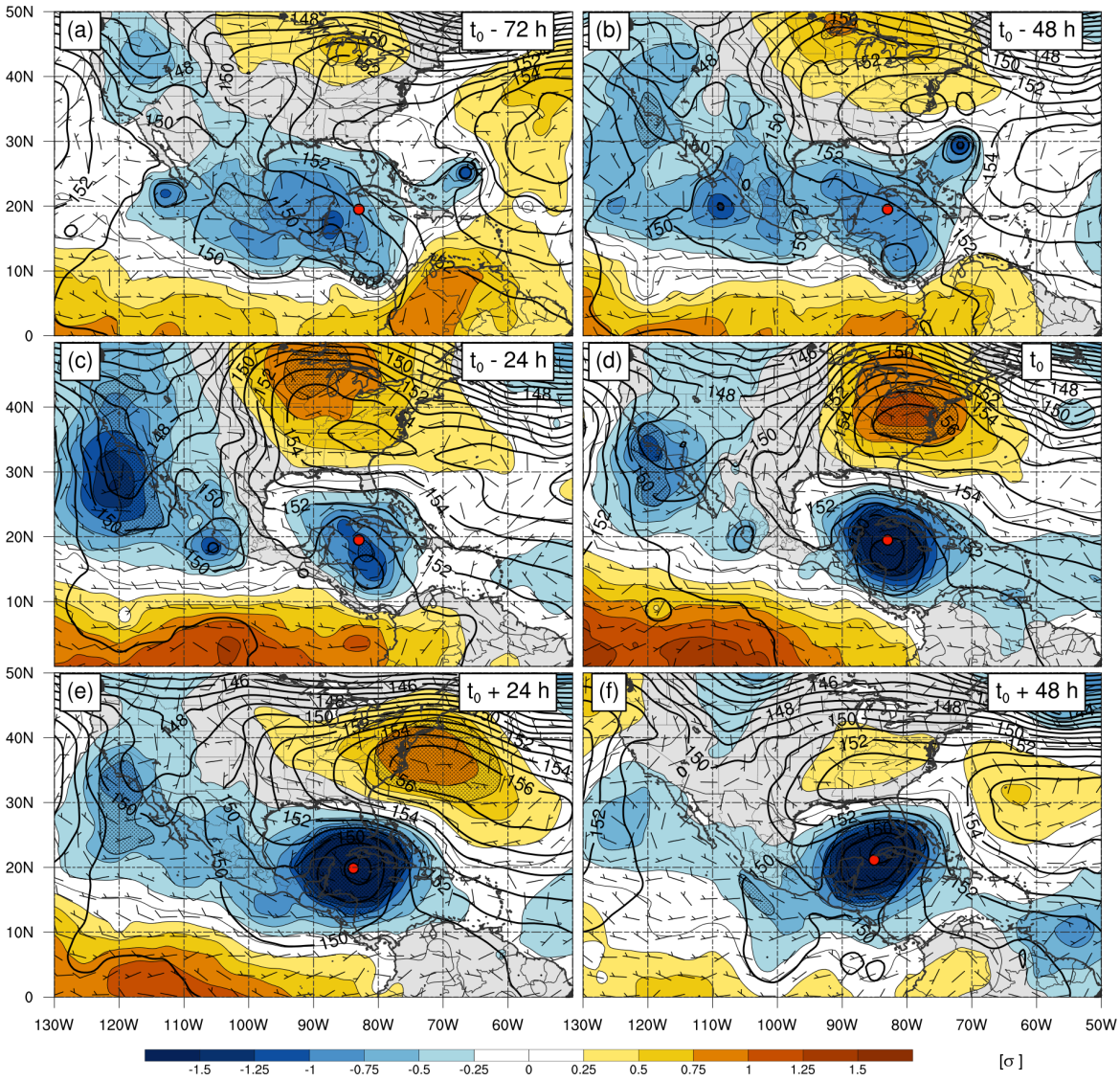

Fig. 3.18. As in Fig 3.6 except for trough CAG composite (N = 7).

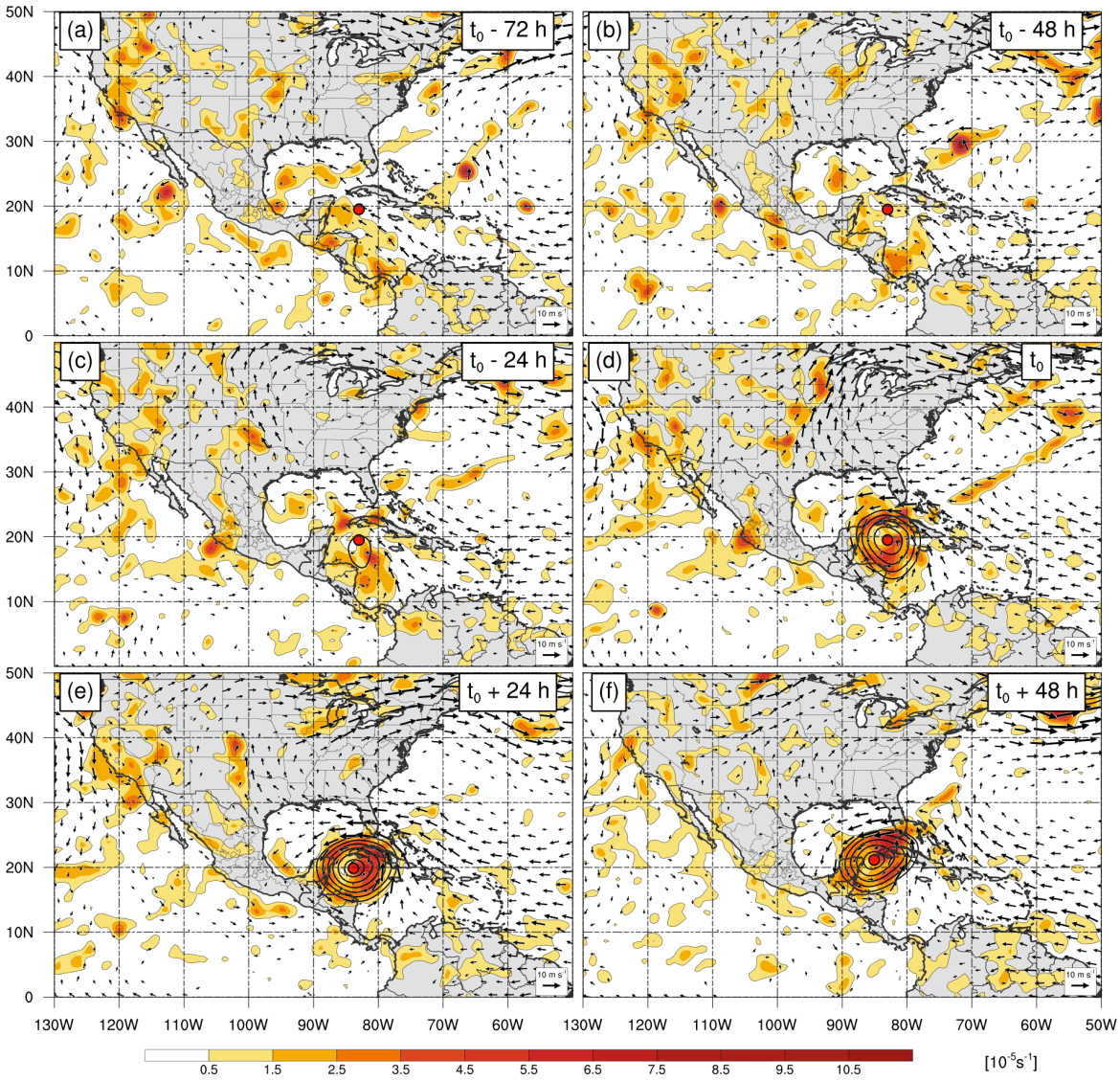

Fig. 3.19. As in Fig 3.7 except for trough CAG composite (N = 7).

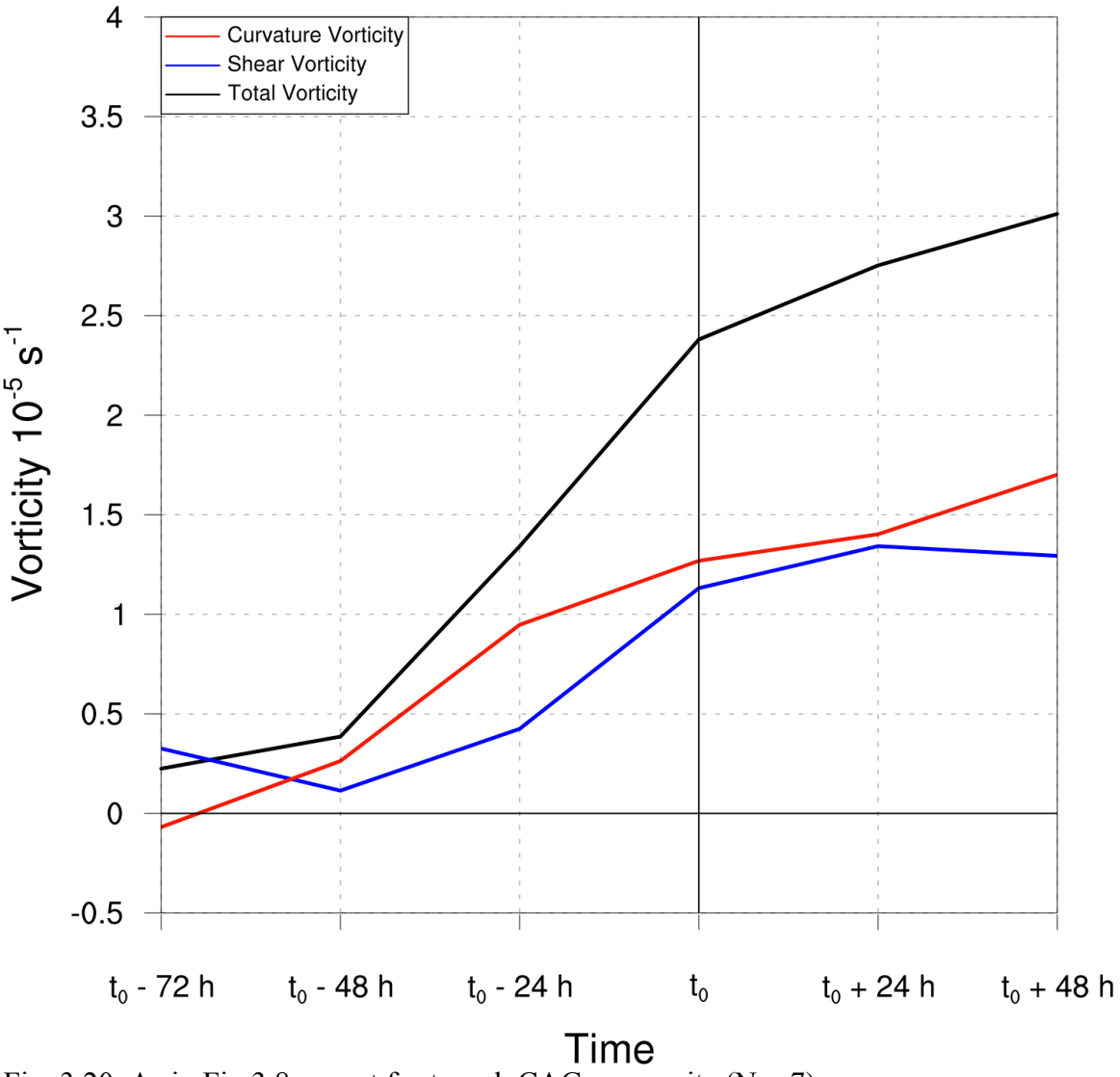

Fig. 3.20. As in Fig 3.8 except for trough CAG composite (N = 7).

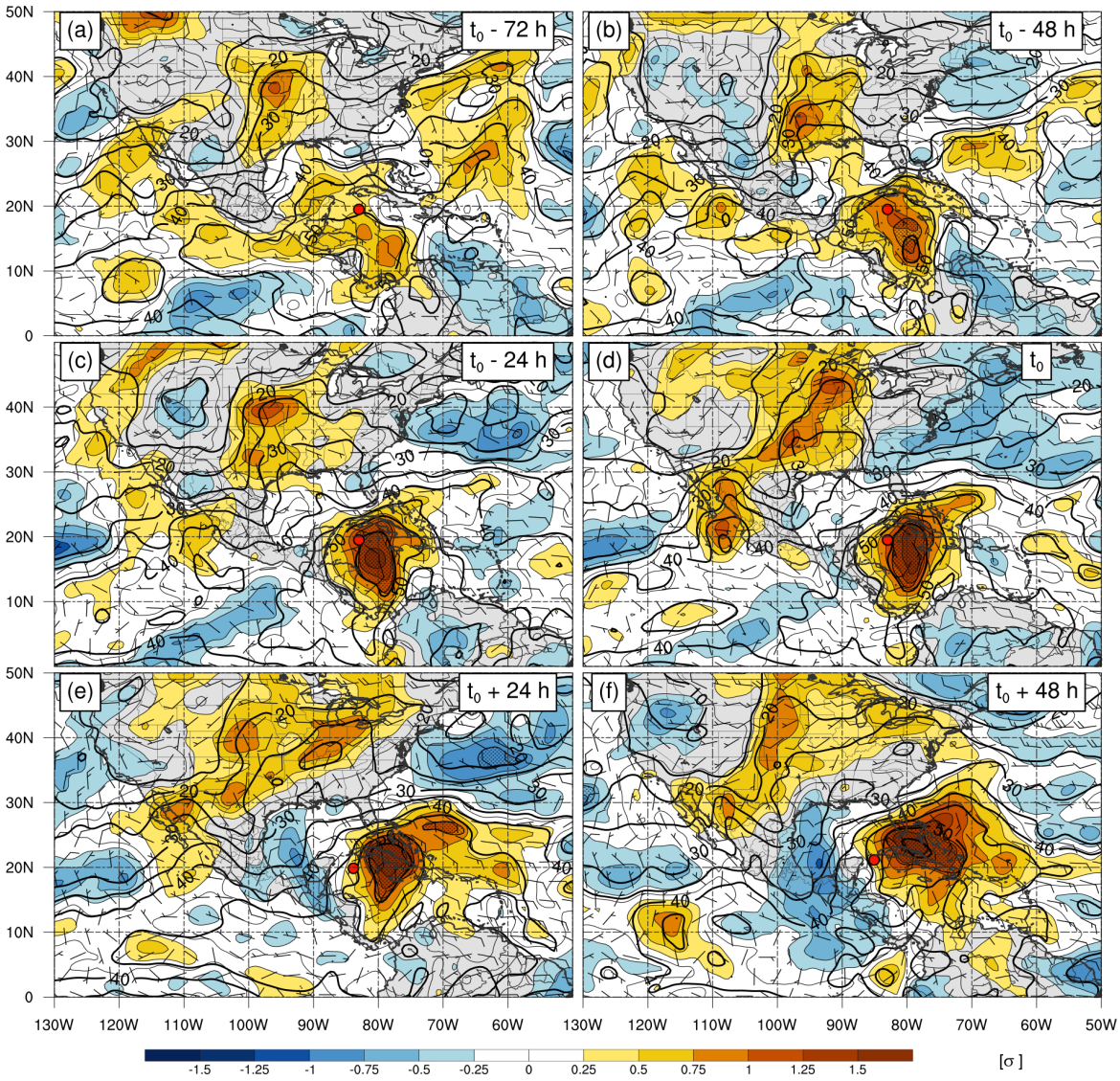

Fig. 3.21. As in Fig 3.9 except for trough CAG composite (N = 7).

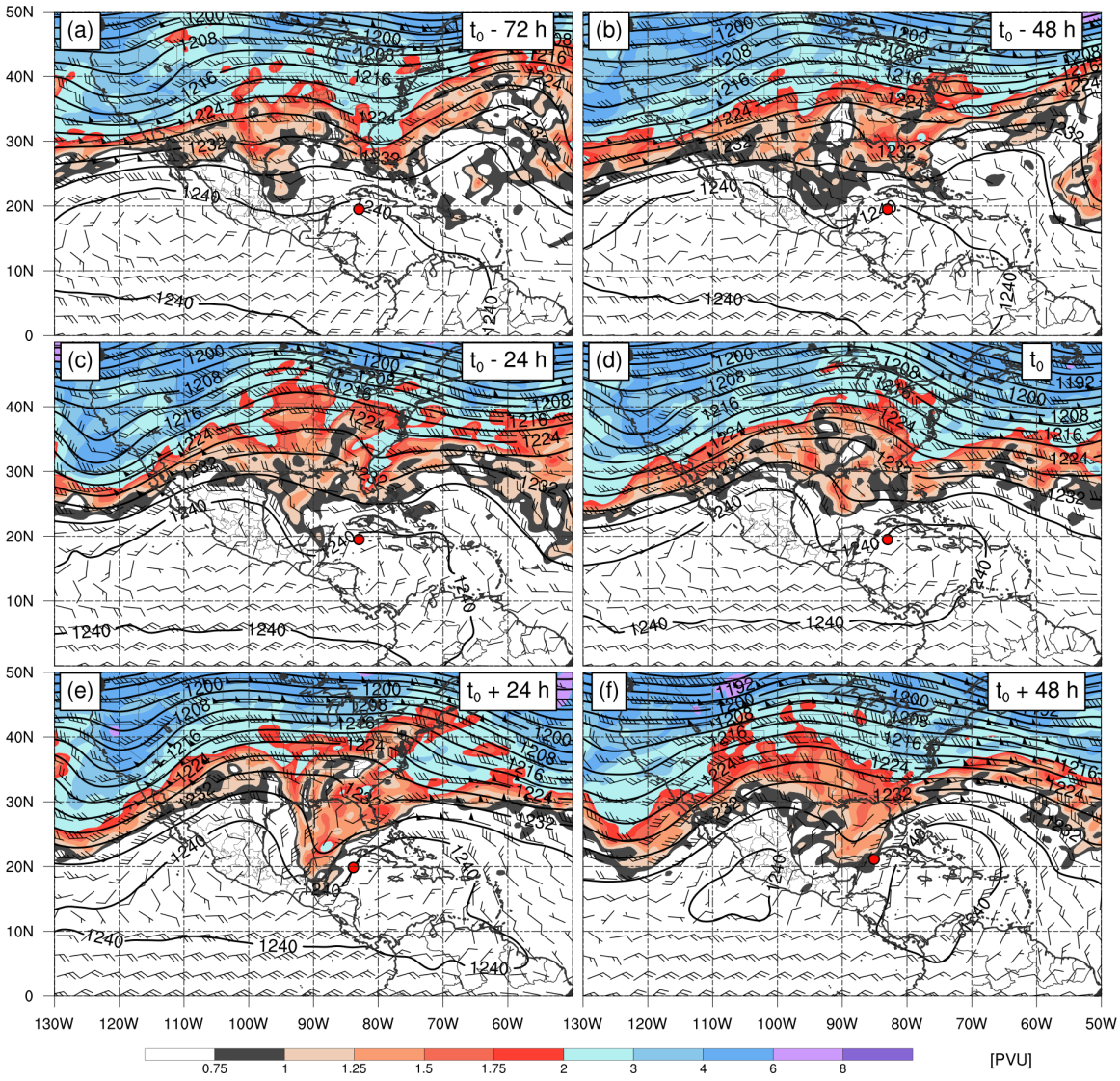

Fig. 3.22. As in Fig 3.10 except for trough CAG composite (N = 7).

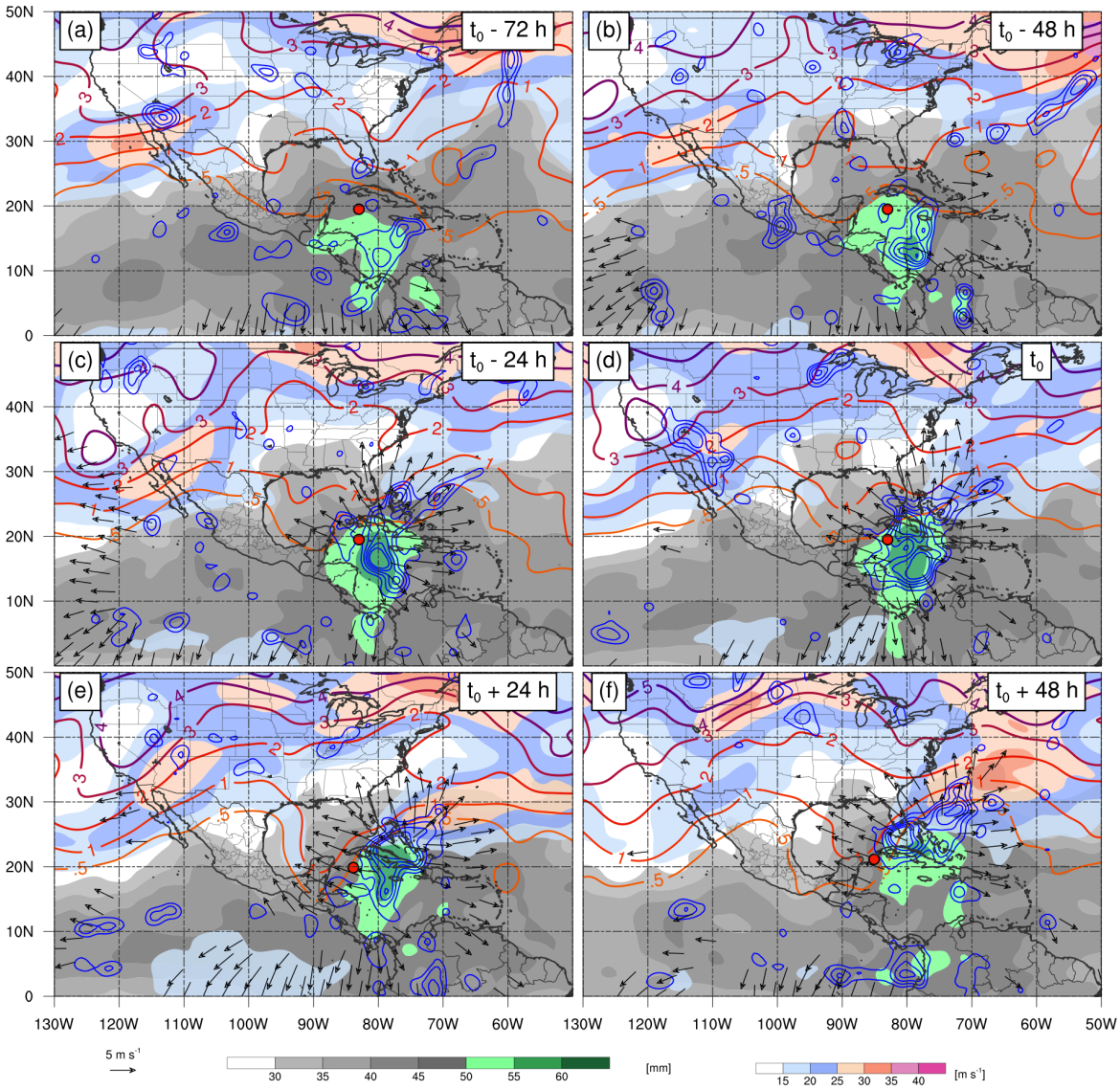

Fig. 3.23. As in Fig 3.11 except for trough CAG composite (N = 7).

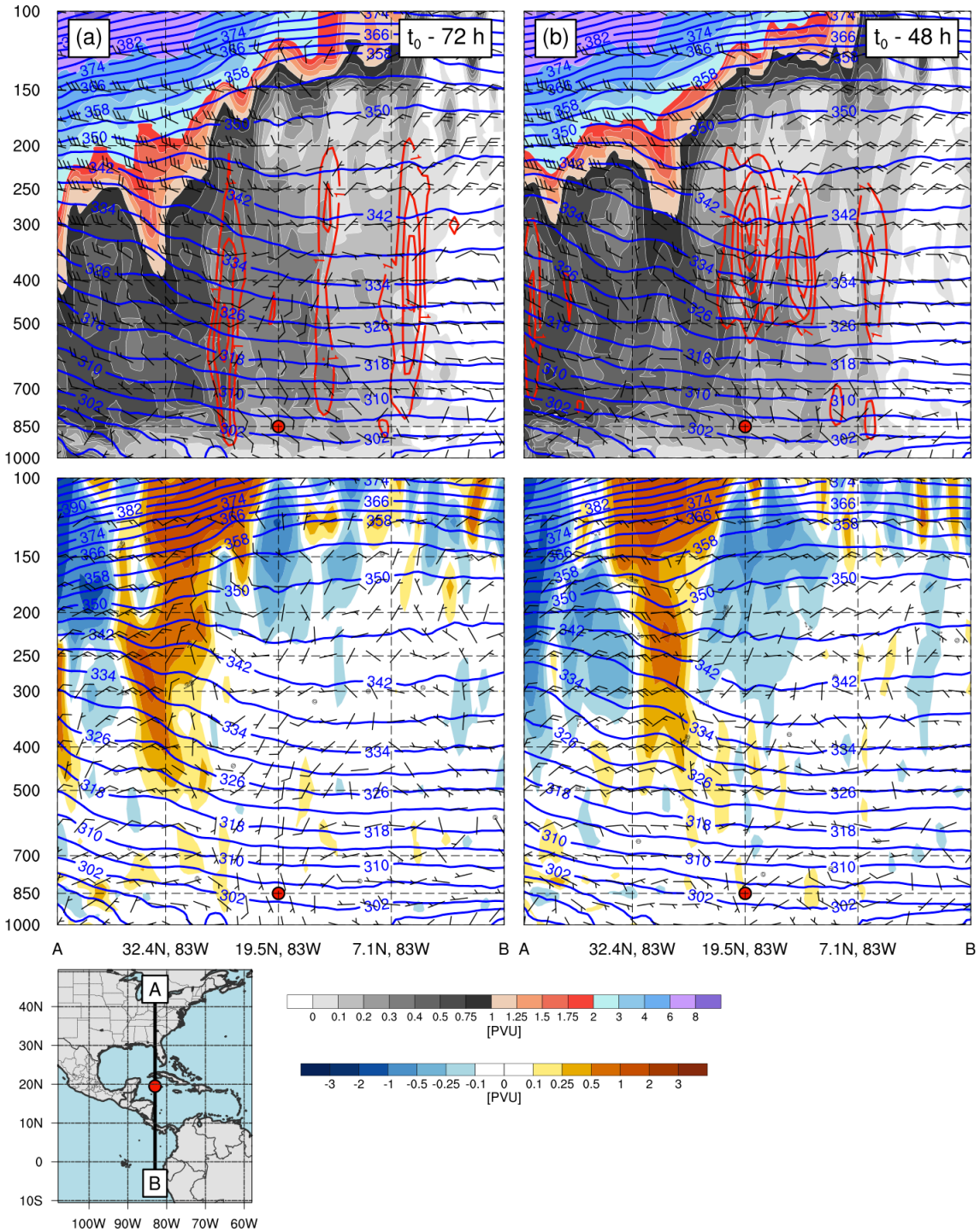

Fig. 3.24. As in Fig 3.12 except for trough CAG composite (N = 7).

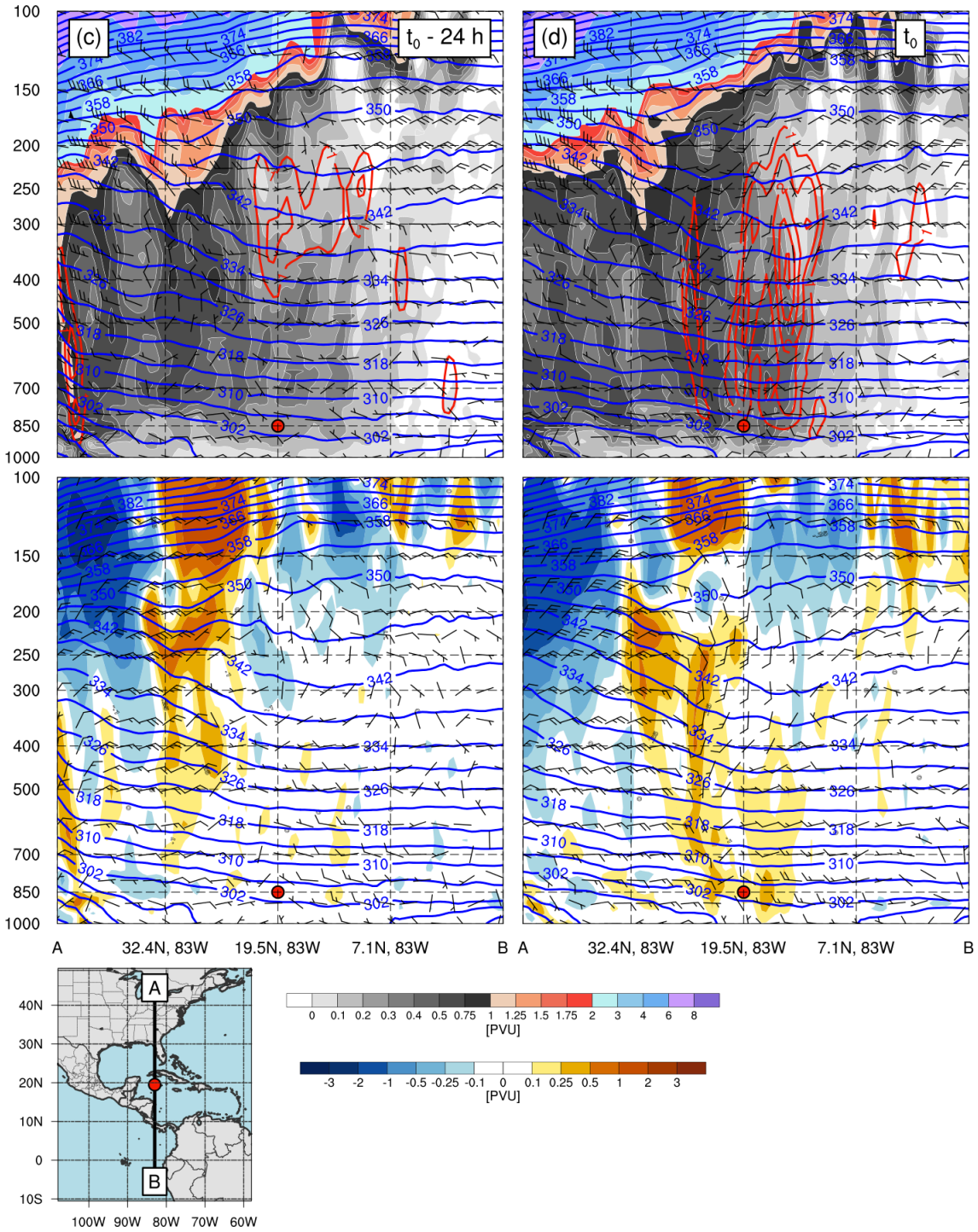

Fig. 3.25. As in Fig 3.13 except for trough CAG composite (N = 7).

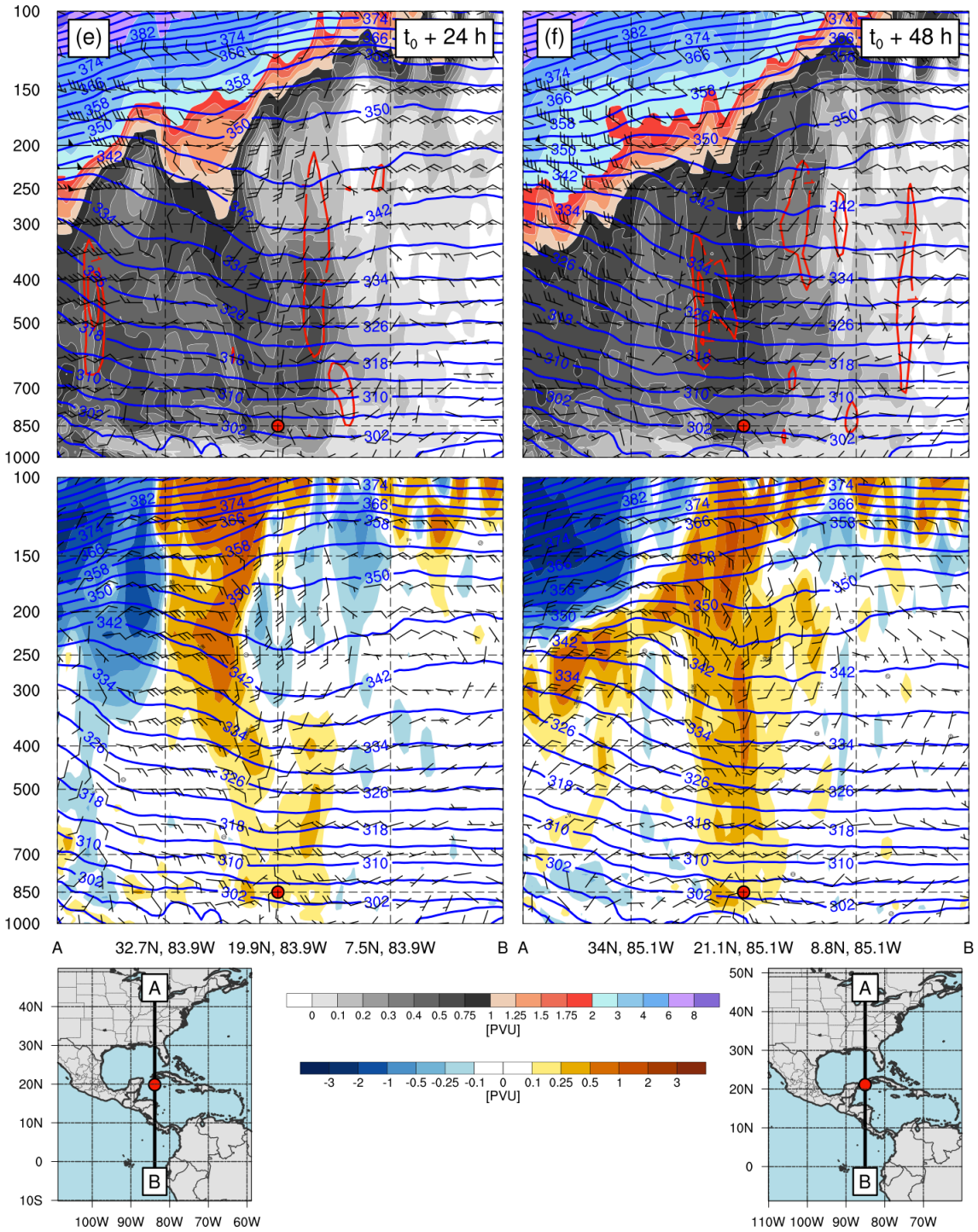

Fig. 3.26. As in Fig 3.14 except for trough CAG composite (N = 7).

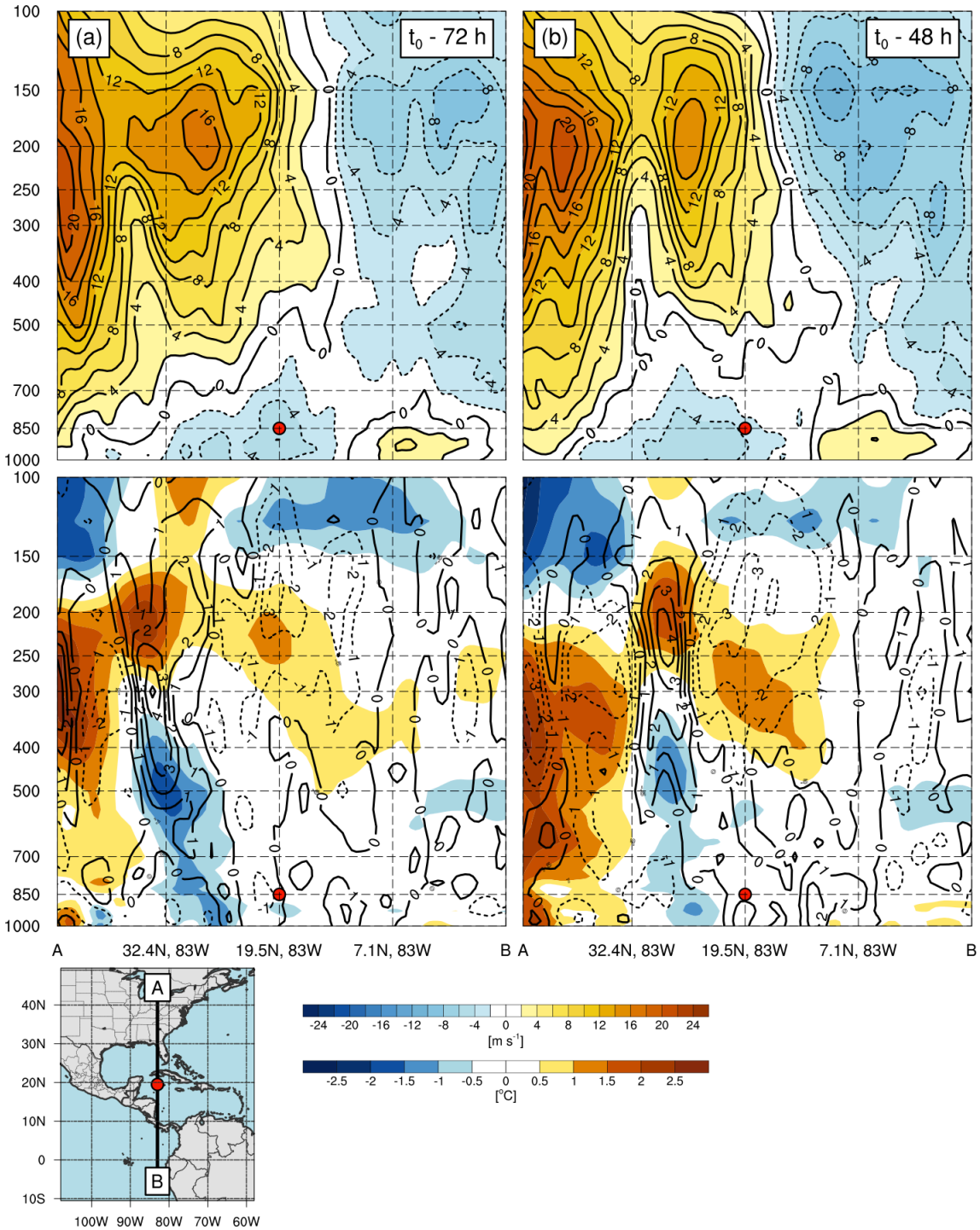

Fig. 3.27. As in Fig 3.15 except for trough CAG composite (N = 7).

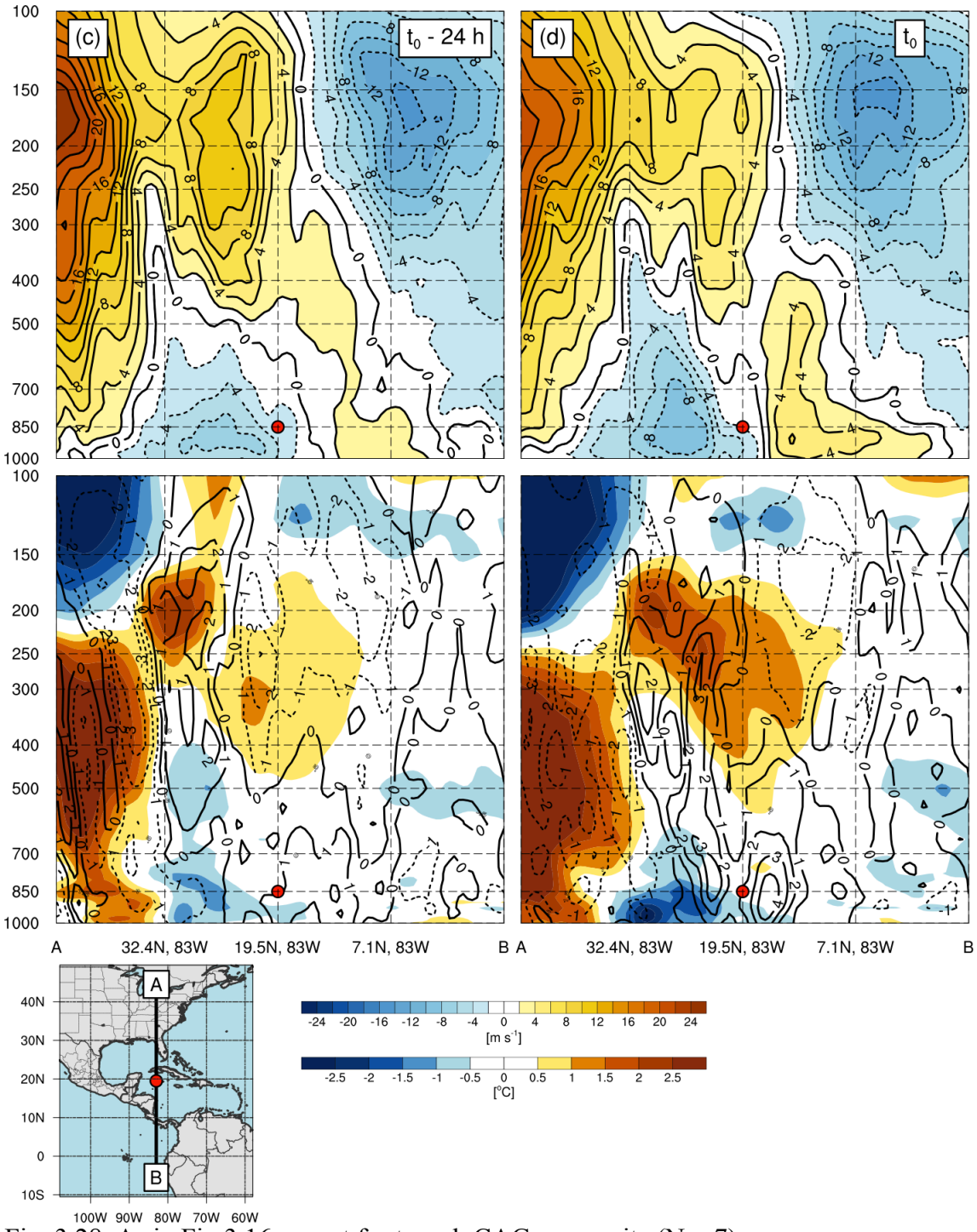

Fig. 3.28. As in Fig 3.16 except for trough CAG composite (N = 7).

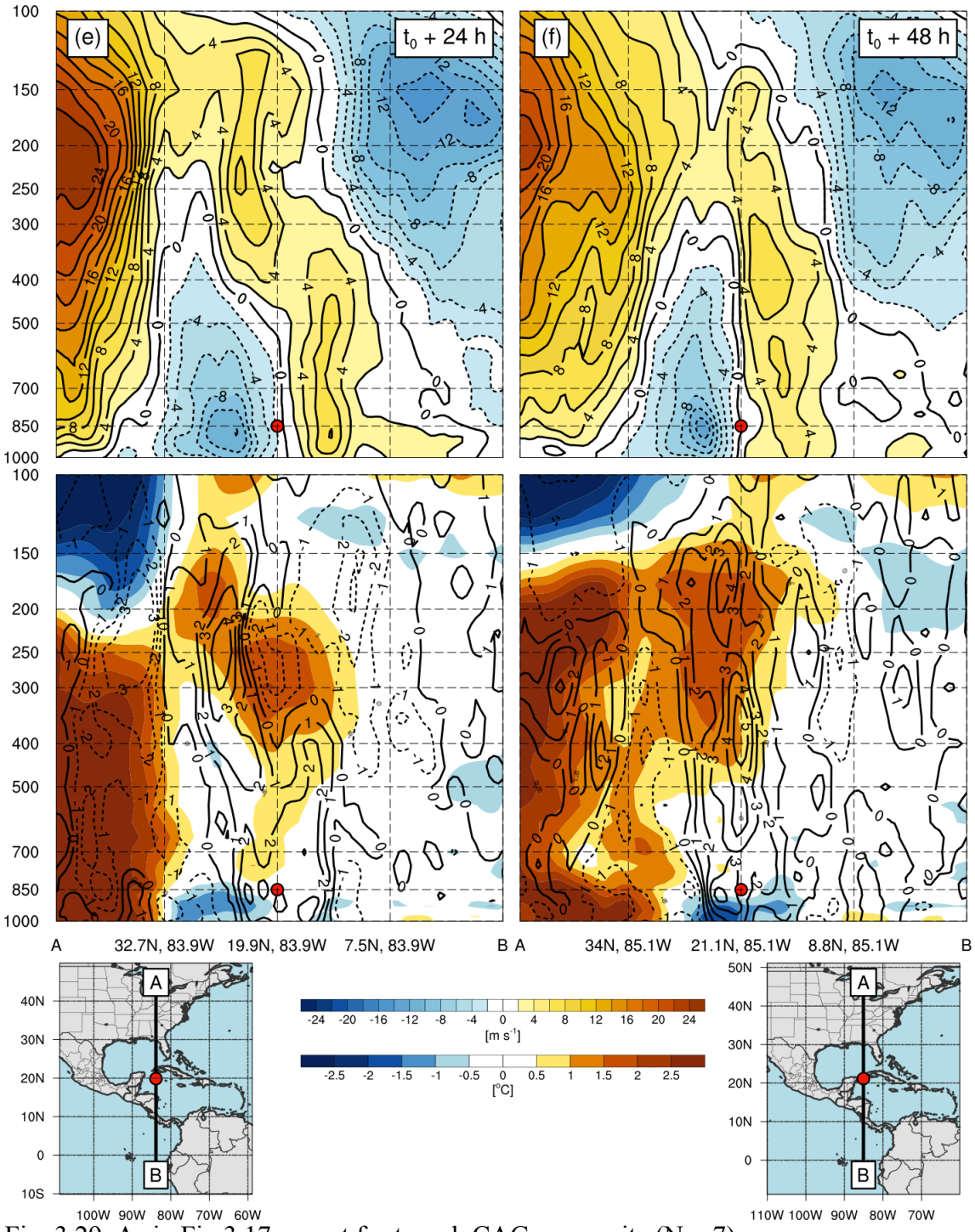

Fig. 3.29. As in Fig 3.17 except for trough CAG composite (N = 7).

Table 2. Climatological statistics of TCs associated with all CAGs (N = 42), tropical CAGs (N = 35), and trough CAGs (N = 7) within 1000 km of the CAG center.

Parameter	All CAGs	Tropical CAGs	Trough CAGs
Total Number of TCs	26	24	2
Total Number of developing TCs	14	14	0
Total Number of CAGs with at least 1 TC	22	20	2
Mean TC Intensity (m s^{-1})	18.3	18.2	19.1
Mean TC distance from CAG center (km)	460.6	478.9	301.7

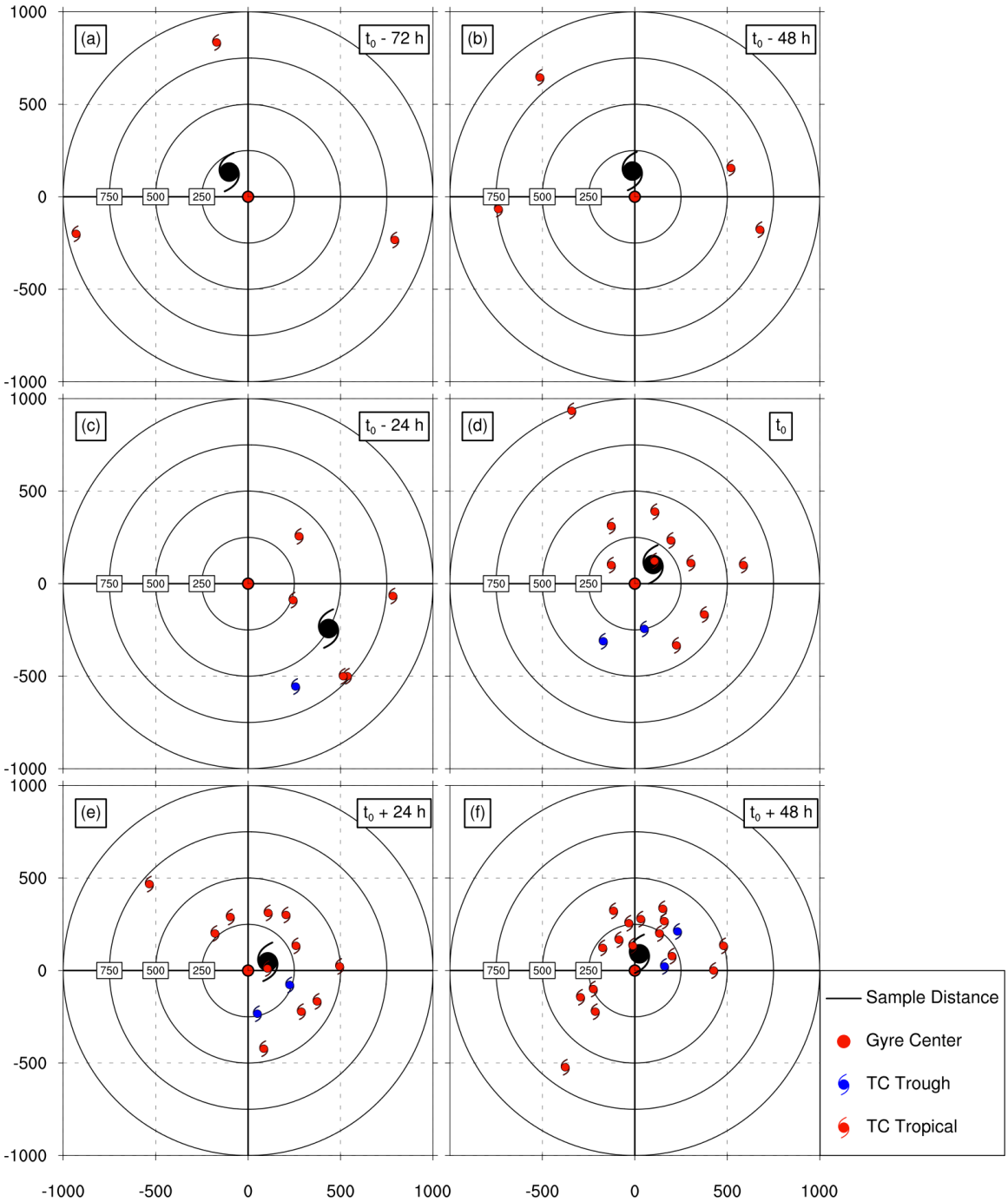

Fig. 3.30. Composite gyre-relative locations of TCs associated with all CAG events (N = 42) at (a) t_0 – 72 h, (b) t_0 – 48 h, (c) t_0 – 24 h, (d) t_0, (e) t_0 + 24 h, and (f) t_0 + 48 h. The CAG center is denoted by a red circle in the middle at each composite plot, while TCs associated with tropical (trough) CAGs are signified by red (blue) TC symbols, with the mean position of all TCs denoted as a larger black TC symbol. Distance range rings (in km) are provided from the CAG center as a reference.

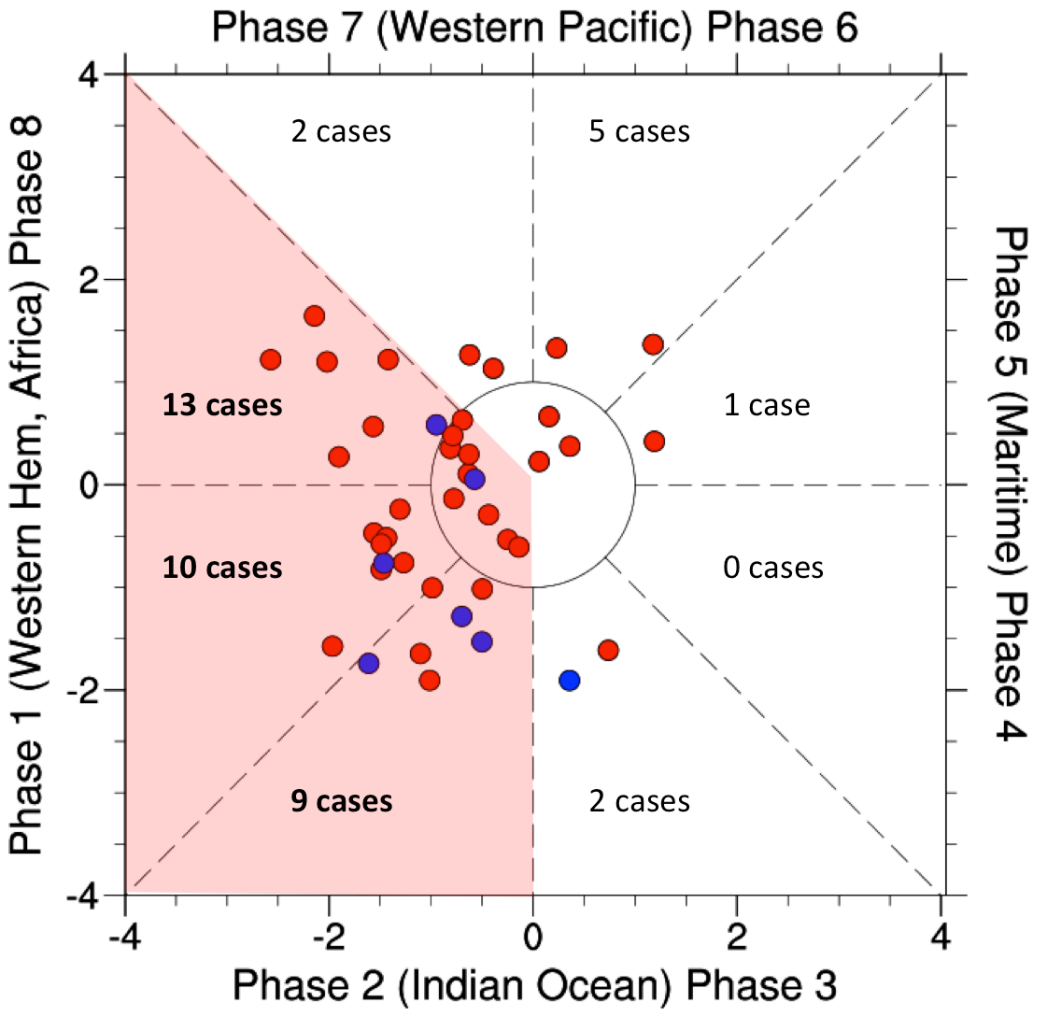

Fig. 3.31. MJO RMM Phase diagram with all CAG positions identified at t_0 (gyre genesis). Red (blue) dots represent the given RMM phase position of tropical (trough) CAGs. Total CAG cases in each phase are provided with phases 8, 1, and 2 highlighted in red.

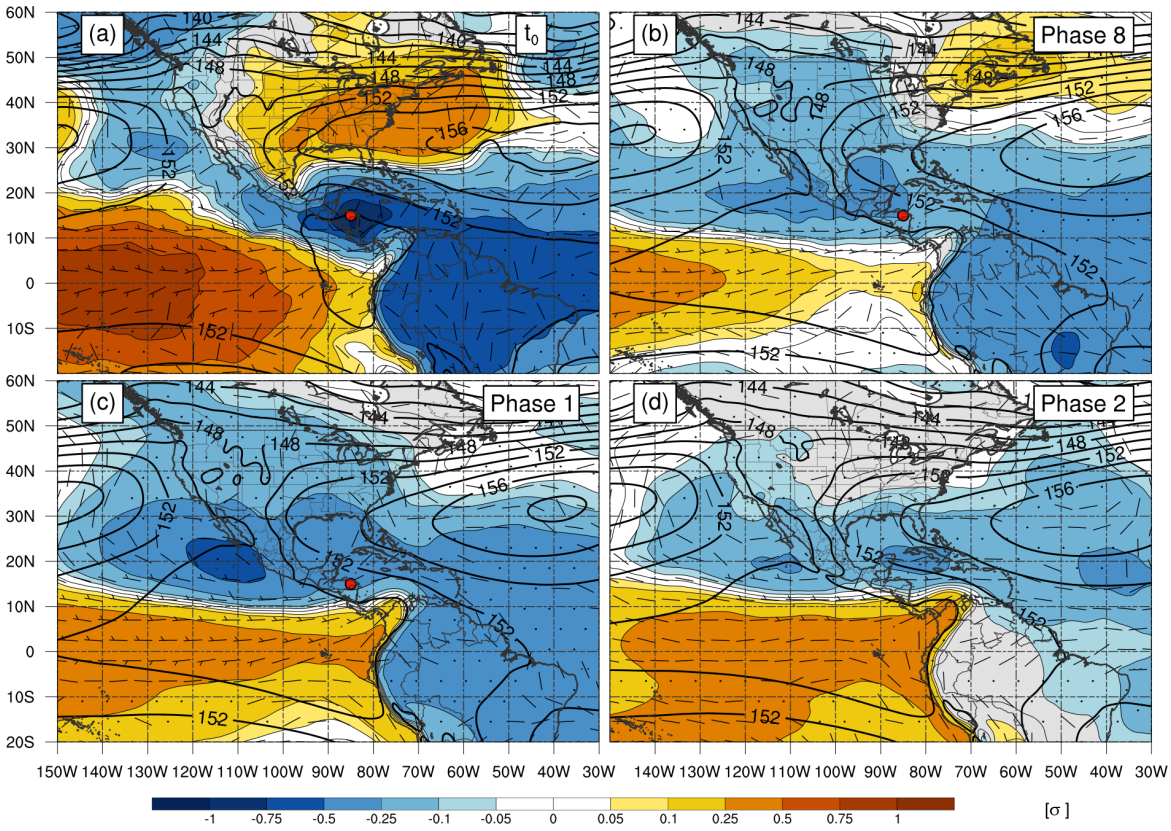

Fig. 3.32. 850-hPa standardized geopotential height anomaly (shaded, sigma), 850-hPa geopotential height (black contours, dam), and 850 hPa anomalous winds (barbs, kts) at (a) the earth-relative composite of all CAG events (N = 42) at t_0, (b) earth-relative composite of May-Nov MJO events in RMM phase 8 (N = 818), (c) earth-relative composite of May-Nov MJO events in RMM phase 1 (N = 1142), and (d) earth-relative composite of May-Nov MJO events in RMM phase 2 (N = 1081).

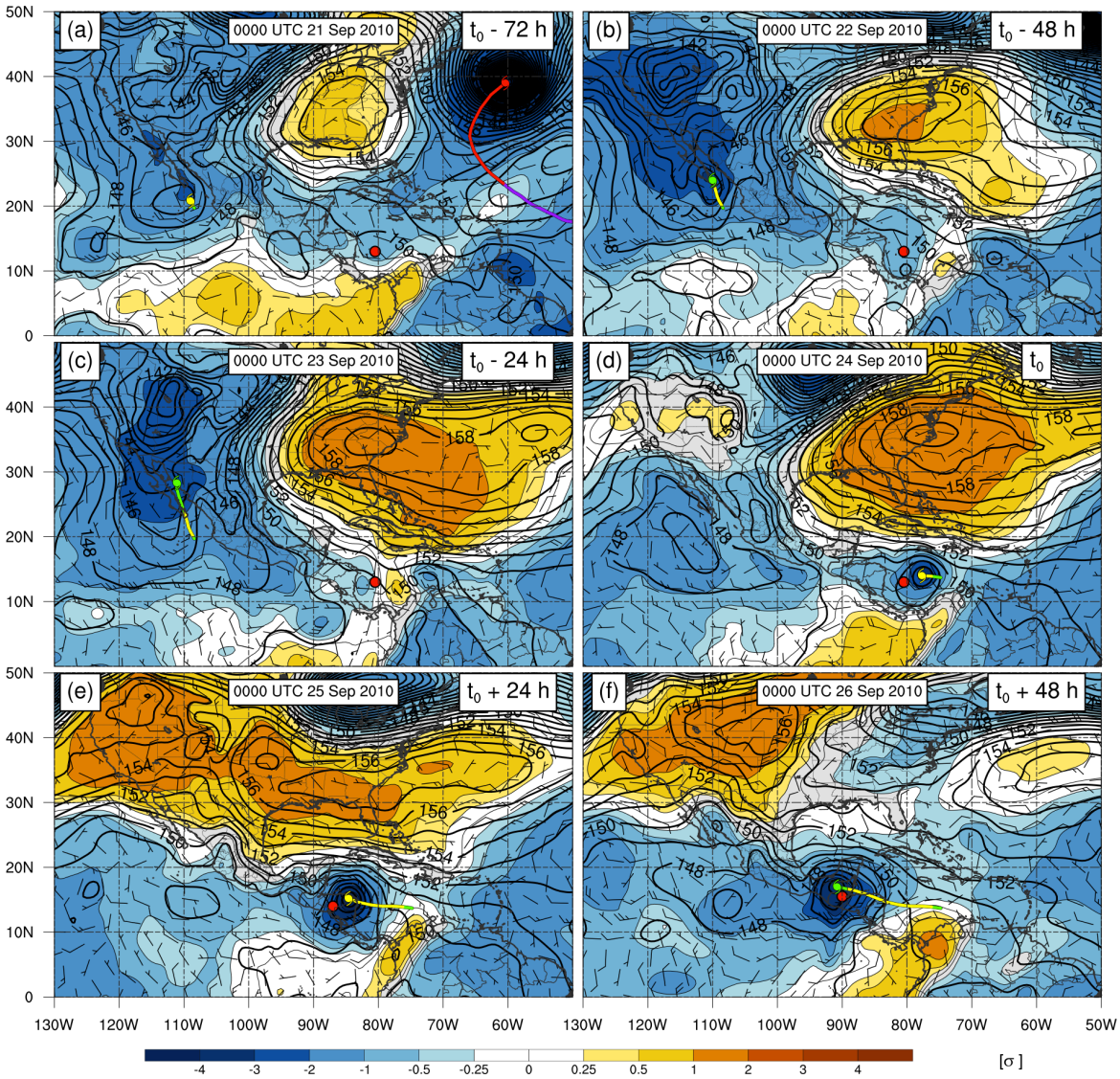

Fig. 3.33. Tropical CAG case study, with 850-hPa standardized geopotential height anomaly (shaded, sigma), 850-hPa geopotential height (black contours, dam), and 850 hPa anomalous winds (barbs, kts) at (a) t_0 – 72 h, (b) t_0 – 48 h, (c) t_0 – 24 h, (d) t_0, (e) t_0 + 24 h, and (f) t_0 + 48 h. The red circle in each panel denotes the CAG center location at genesis for panels up to genesis (-72 h to 0 h, a – d) and the CAG center location for designated times after genesis (+24 h to +48 h, e – f). Tracks of TCs are also plotted, colorized by the intensity, with the present position plotted as a TC symbol.

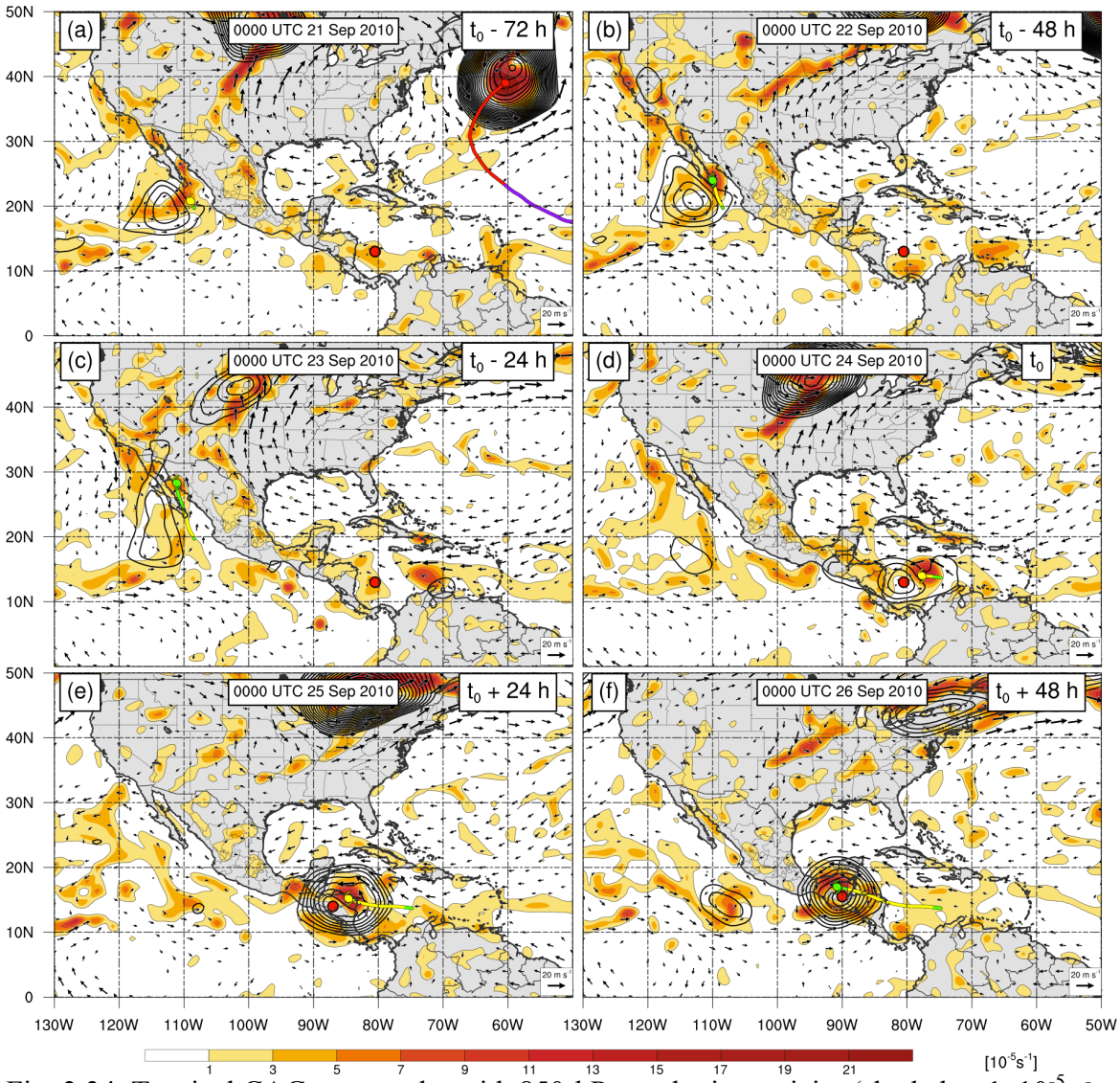

Fig. 3.34. Tropical CAG case study, with 850-hPa cyclonic vorticity (shaded, > $1x10^{-5}$ s^{-1}), 1000-500 km radial average 850-hPa circulation (black contours, > $1x10^{-5}$ s^{-1}), and 850-hPa winds (vectors, m s^{-1}) at (a) t_0 – 72 h, (b) t_0 – 48 h, (c) t_0 – 24 h, (d) t_0, (e) t_0 + 24 h, and (f) t_0 + 48 h. The red circle in each panel denotes the CAG center location at genesis for panels up to genesis (-72 h to 0 h, a – d) and the CAG center location for designated times after genesis (+24 h to +48 h, e – f). Tracks of TCs are also plotted, colorized by the intensity, with the present position plotted as a TC symbol.

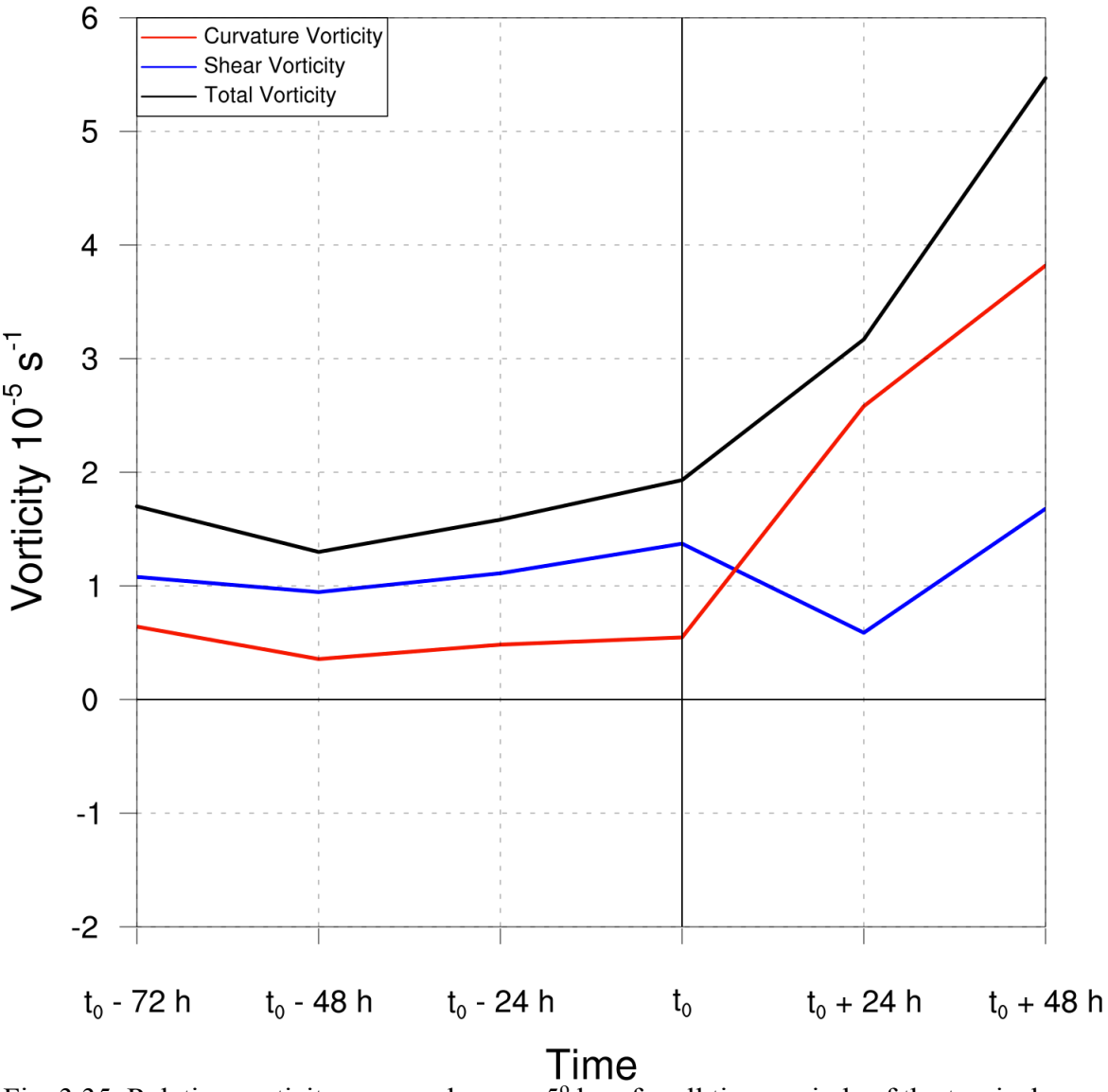

Fig. 3.35. Relative vorticity averaged over a 5° box for all time periods of the tropical CAG case study. Different colored lines denote curvature relative vorticity (red), shear relative vorticity (blue), and total relative vorticity (black).

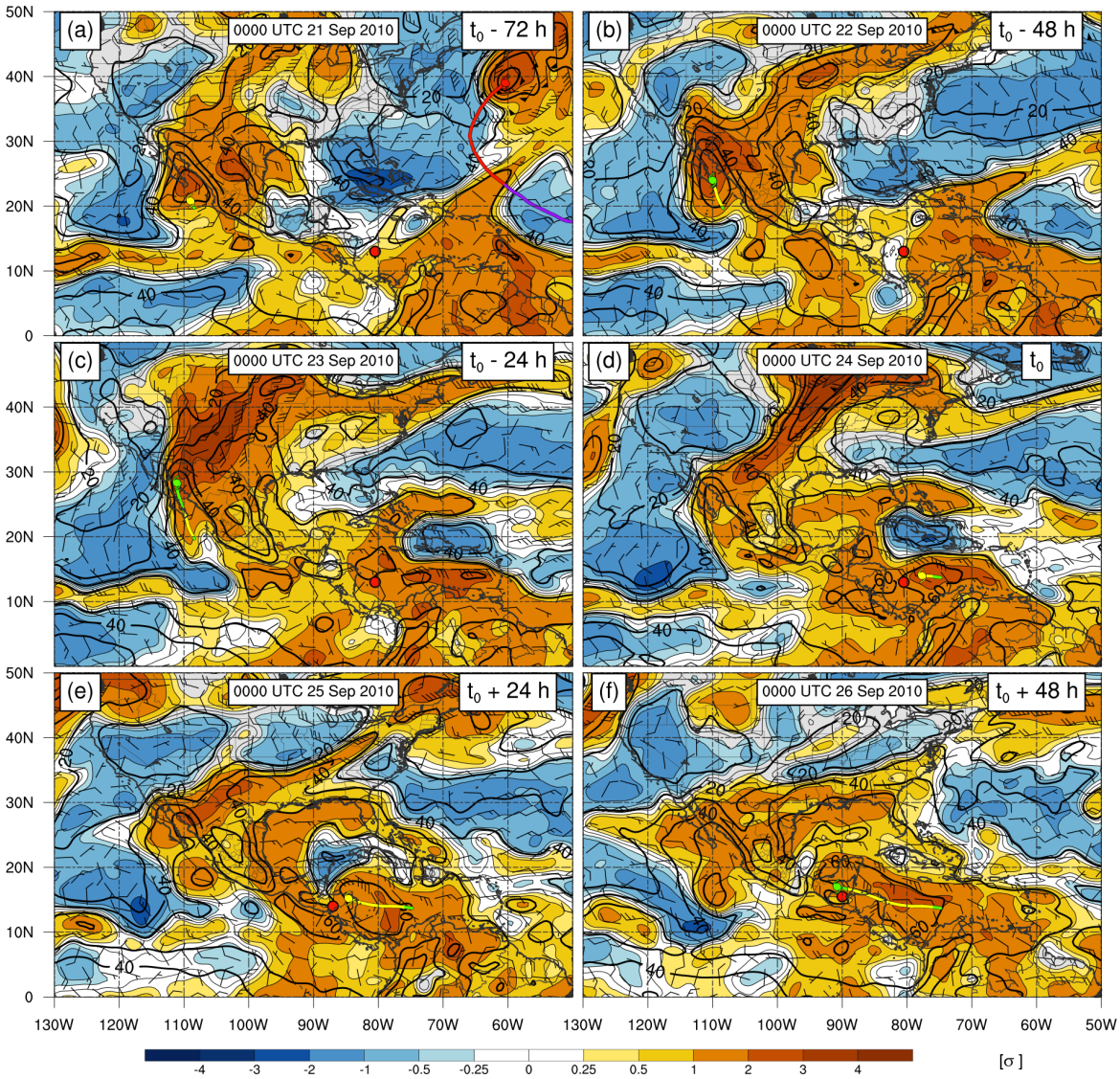

Fig. 3.36. Tropical CAG case study (N = 35) Standardized precipitable water anomaly (shaded, sigma), Precipitable water (black contours, mm), and 850 hPa winds (barbs, kts) at (a) t_0 – 72 h, (b) t_0 – 48 h, (c) t_0 – 24 h, (d) t_0, (e) t_0 + 24 h, and (f) t_0 + 48 h. The red circle in each panel denotes the CAG center location at genesis for panels up to genesis (-72 h to 0 h, a – d) and the CAG center location for designated times after genesis (+24 h to +48 h, e – f). Black stippling indicates where the 850-hPa geopotential height is statistically significant to the 95% level using a two tailed student's t-test. Tracks of TCs are also plotted, colorized by the intensity, with the present position plotted as a TC symbol.

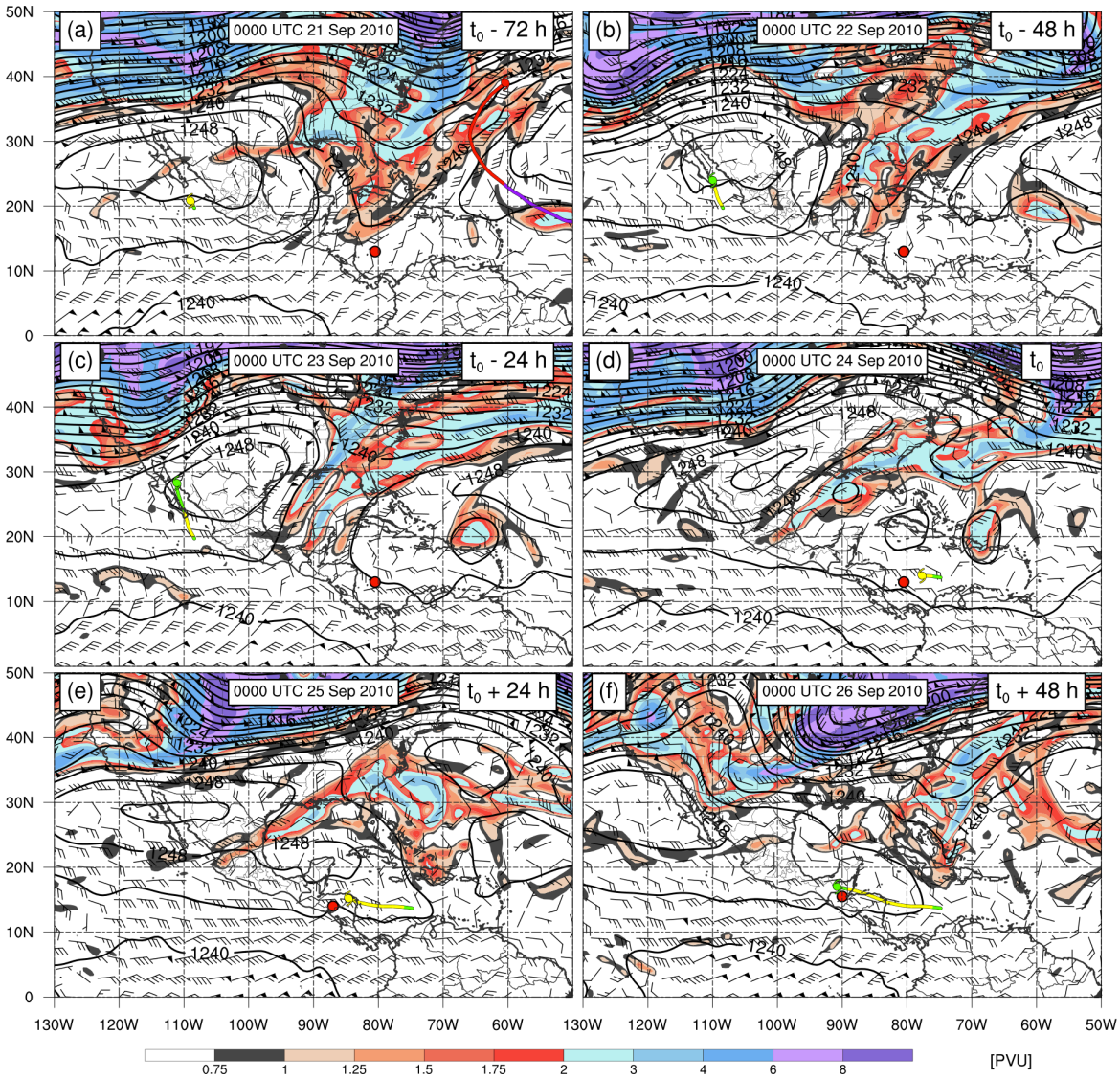

Fig. 3.37. Tropical CAG case study (N = 35) 200 hPa potential vorticity (shaded, > 0.75 PVU), 200 hPa geopotential heights (black contours, dam), and 200 hPa winds (barbs, kts) at (a) t_0 – 72 h, (b) t_0 – 48 h, (c) t_0 – 24 h, (d) t_0, (e) t_0 + 24 h, and (f) t_0 + 48 h. The red circle in each panel denotes the CAG center location at genesis for panels up to genesis (-72 h to 0 h, a – d) and the CAG center location for designated times after genesis (+24 h to +48 h, e – f). Tracks of TCs are also plotted, colorized by the intensity, with the present position plotted as a TC symbol.

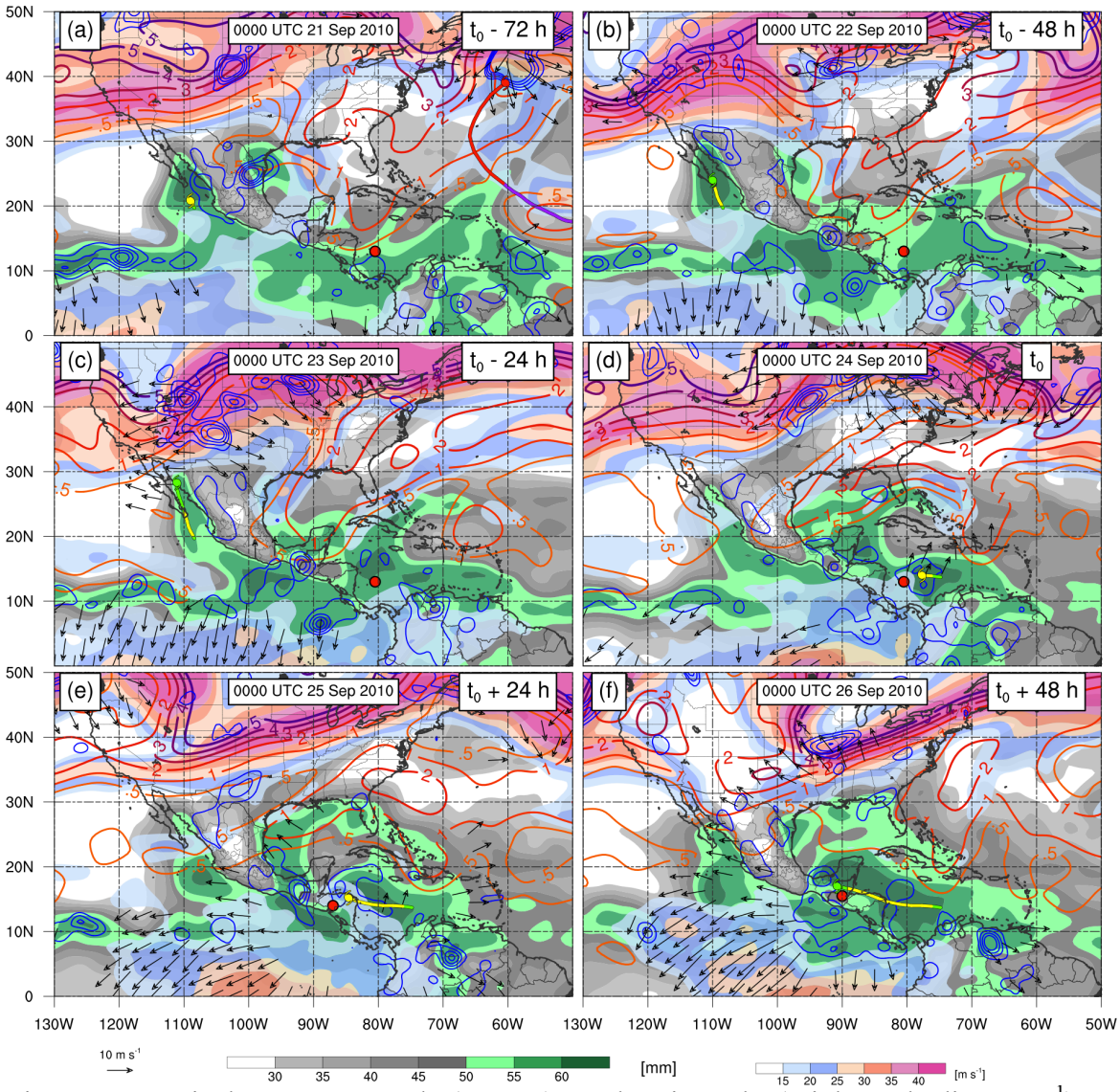

Fig. 3.38. Tropical CAG case study (N = 35) 200 hPa isotachs (rainbow shading, m s^{-1}), Precipitable water (gray to green shading, mm), 200 hPa potential vorticity (warm contours, PVU), 500 hPa omega (blue contours, only negative contoured, hPa s^{-1}), and 200 hPa Irrotational Wind (vectors, m s^{-1}) at (a) t_0 – 72 h, (b) t_0 – 48 h, (c) t_0 – 24 h, (d) t_0, (e) t_0 + 24 h, and (f) t_0 + 48 h. The red circle in each panel denotes the CAG center location at genesis for panels up to genesis (-72 h to 0 h, a – d) and the CAG center location for designated times after genesis (+24 h to +48 h, e – f). Tracks of TCs are also plotted, colorized by the intensity, with the present position plotted as a TC symbol.

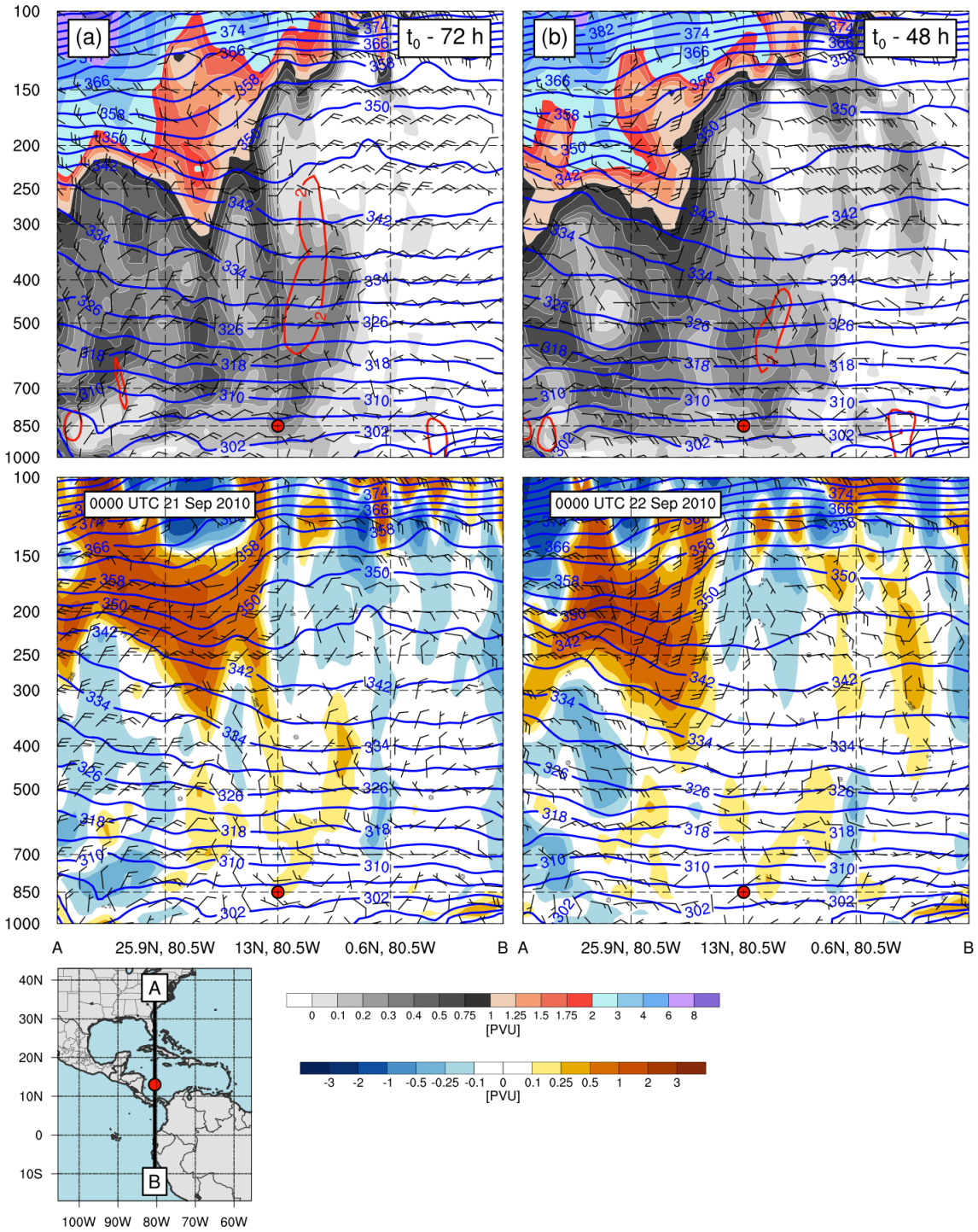

Fig. 3.39. Tropical CAG case study (N = 35) Top: potential vorticity (shaded, PVU), potential temperature (blue contours, K), vertical velocity (purple contours, 10^{-3} hPa s^{-1}) and winds (barbs, knots) Bottom: potential vorticity anomaly (shaded, PVU) potential temperature (blue contours, K) and anomalous winds (barbs, knots) at (a) t_0 – 72 h, (b) t_0 – 48 h. Reference panel for cross-section provided on the bottom left (both a and b).

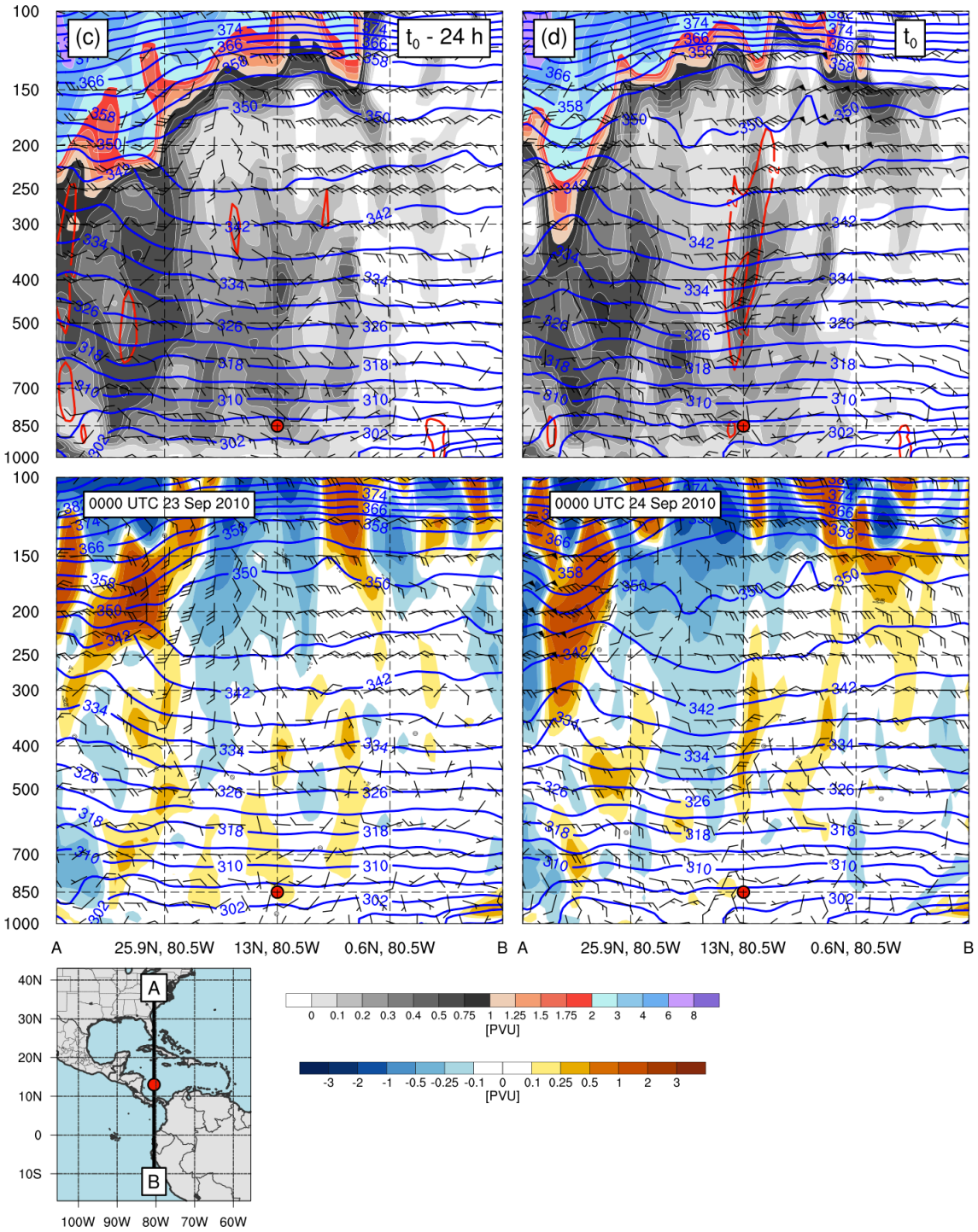

Fig. 3.40. As in Fig. 3.39 except at (c) t_0 – 24 h, and (d) t_0. Reference panel for cross-sections provided on the bottom left (both c and d).

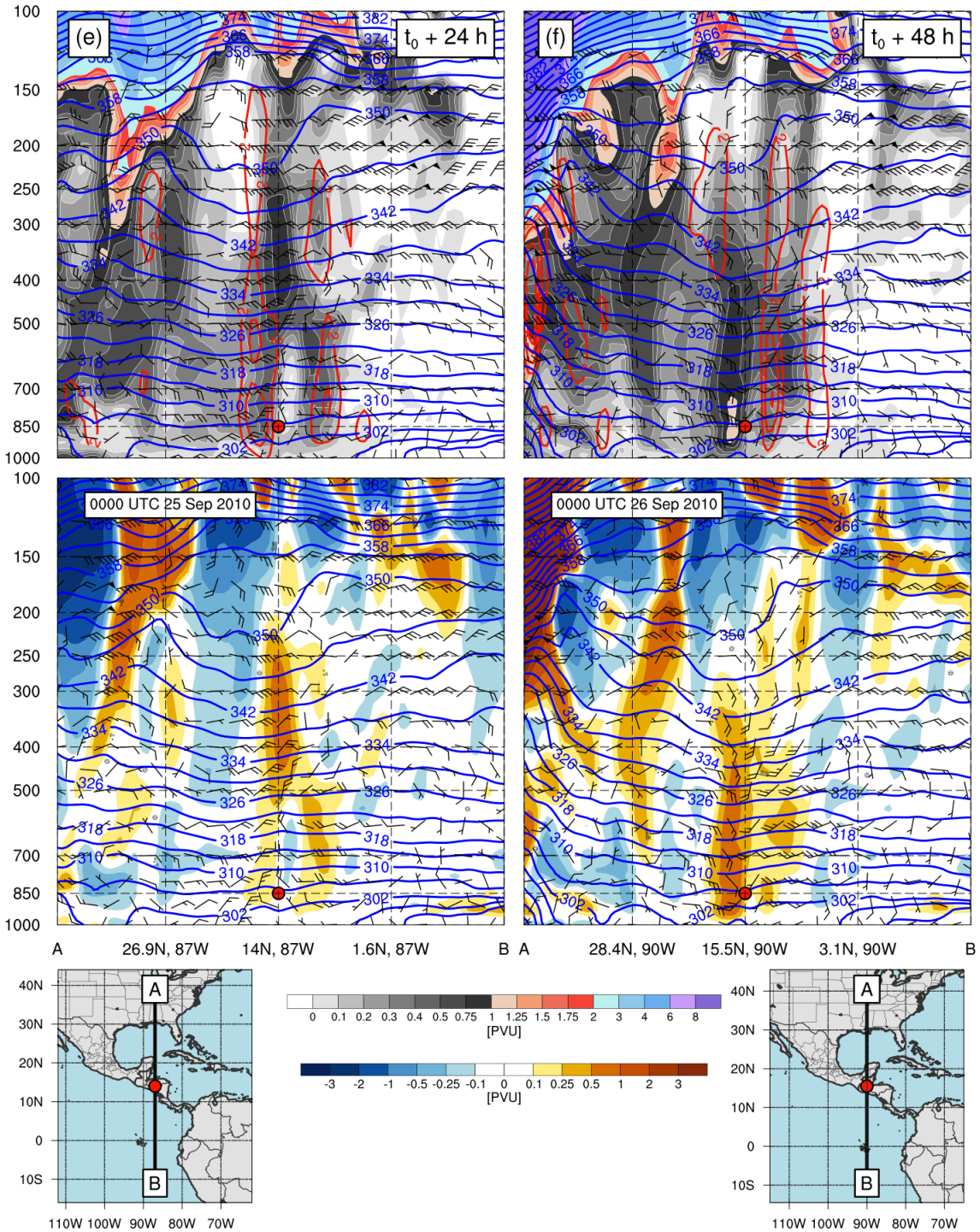

Fig. 3.41. As in Fig. 3.39 except at (e) t_0 + 24 h, and (f) t_0 + 48 h. Reference panel for cross-sections provided on the bottom left (e) and bottom right (f).

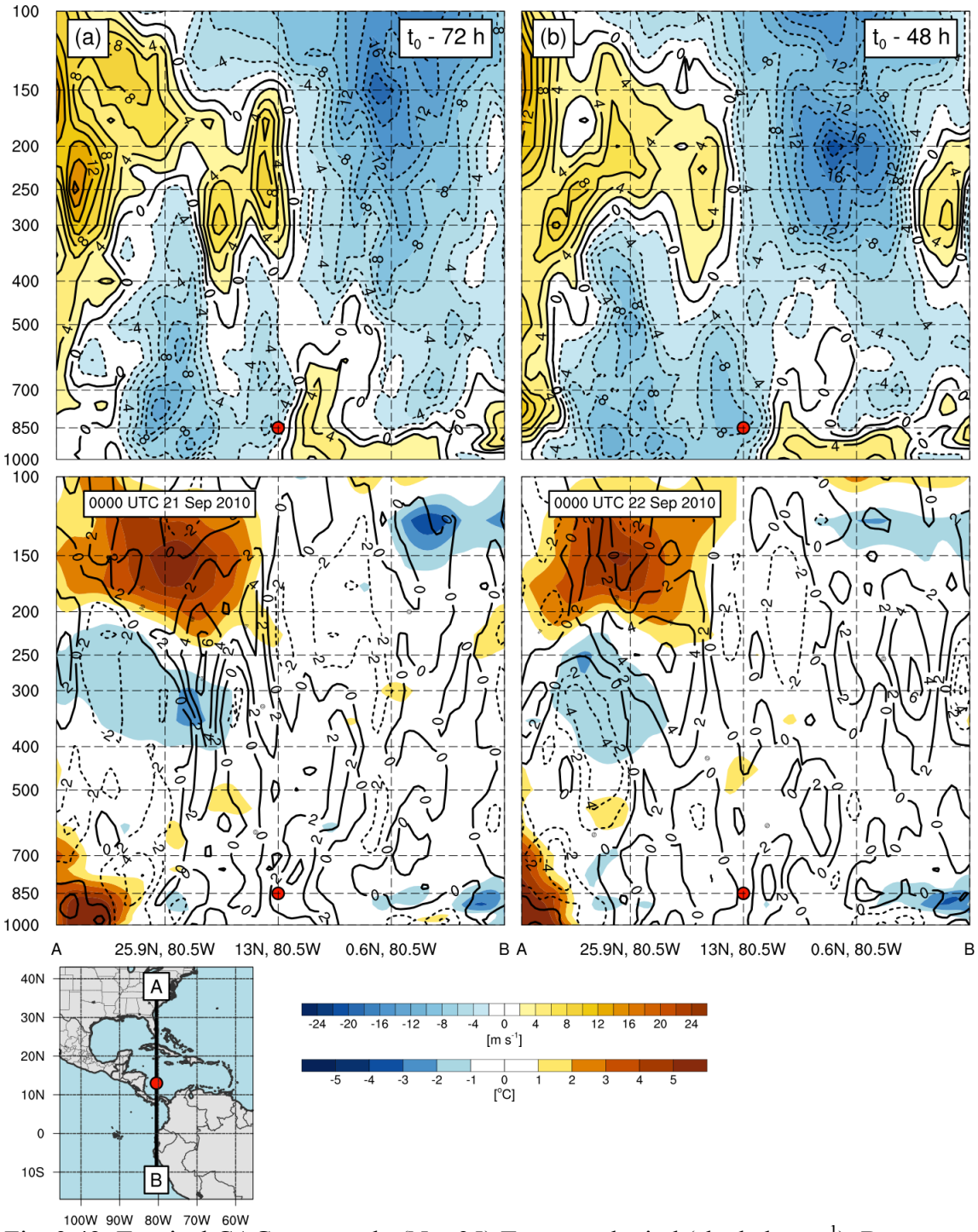

Fig. 3.42. Tropical CAG case study (N = 35) Top: zonal wind (shaded, m s^{-1}), Bottom: temperature anomaly (shaded, °C) and relative vorticity (black contours, 10^{-5} s^{-1}) at (a) t_0 – 72 h, (b) t_0 – 48 h. Reference panel for cross-section provided on the bottom left (both a and b).

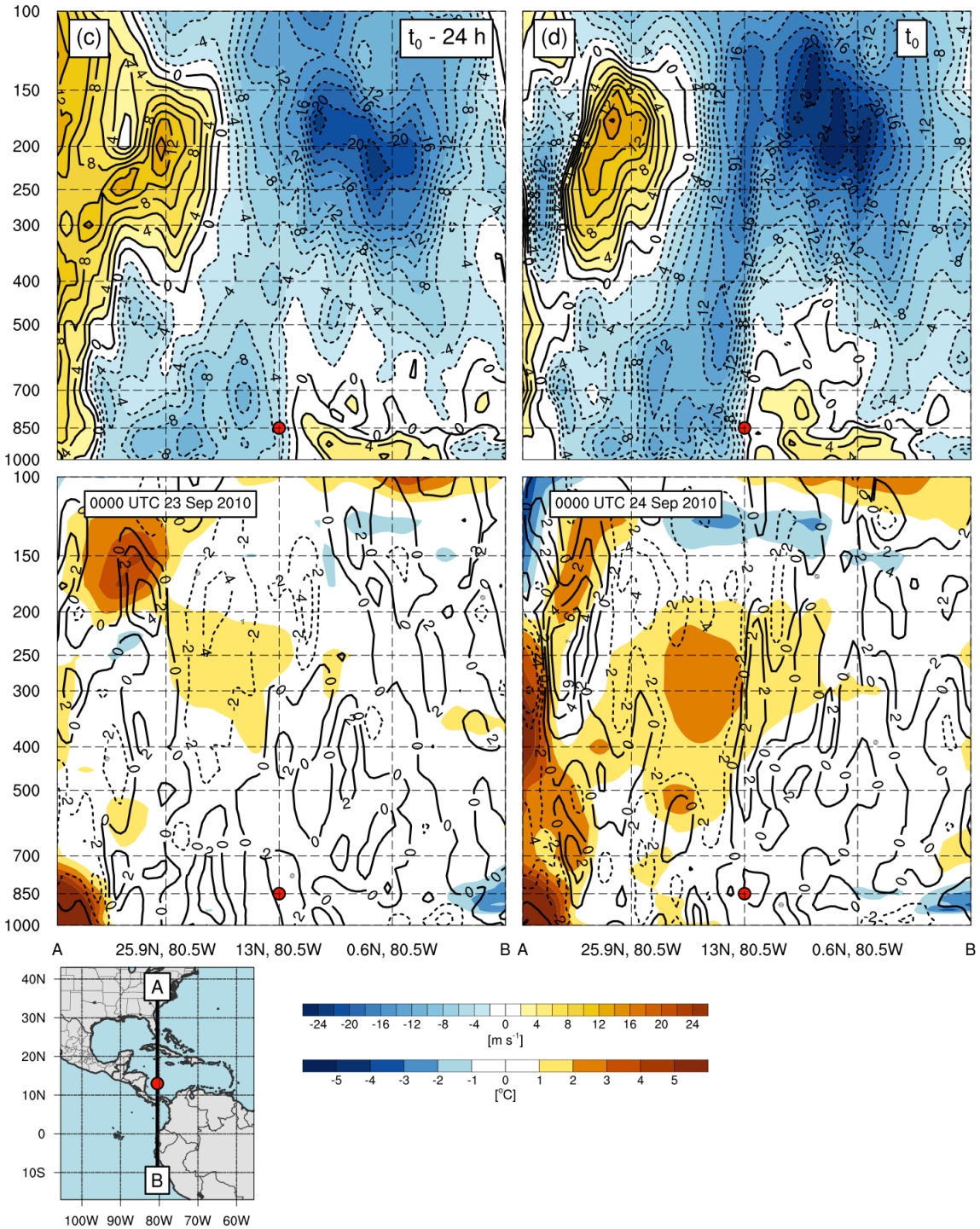

Fig. 3.43. As in Fig. 3.42 except at (c) t_0 – 24 h, and (d) t_0. Reference panel for cross-sections provided on the bottom left (both c and d).

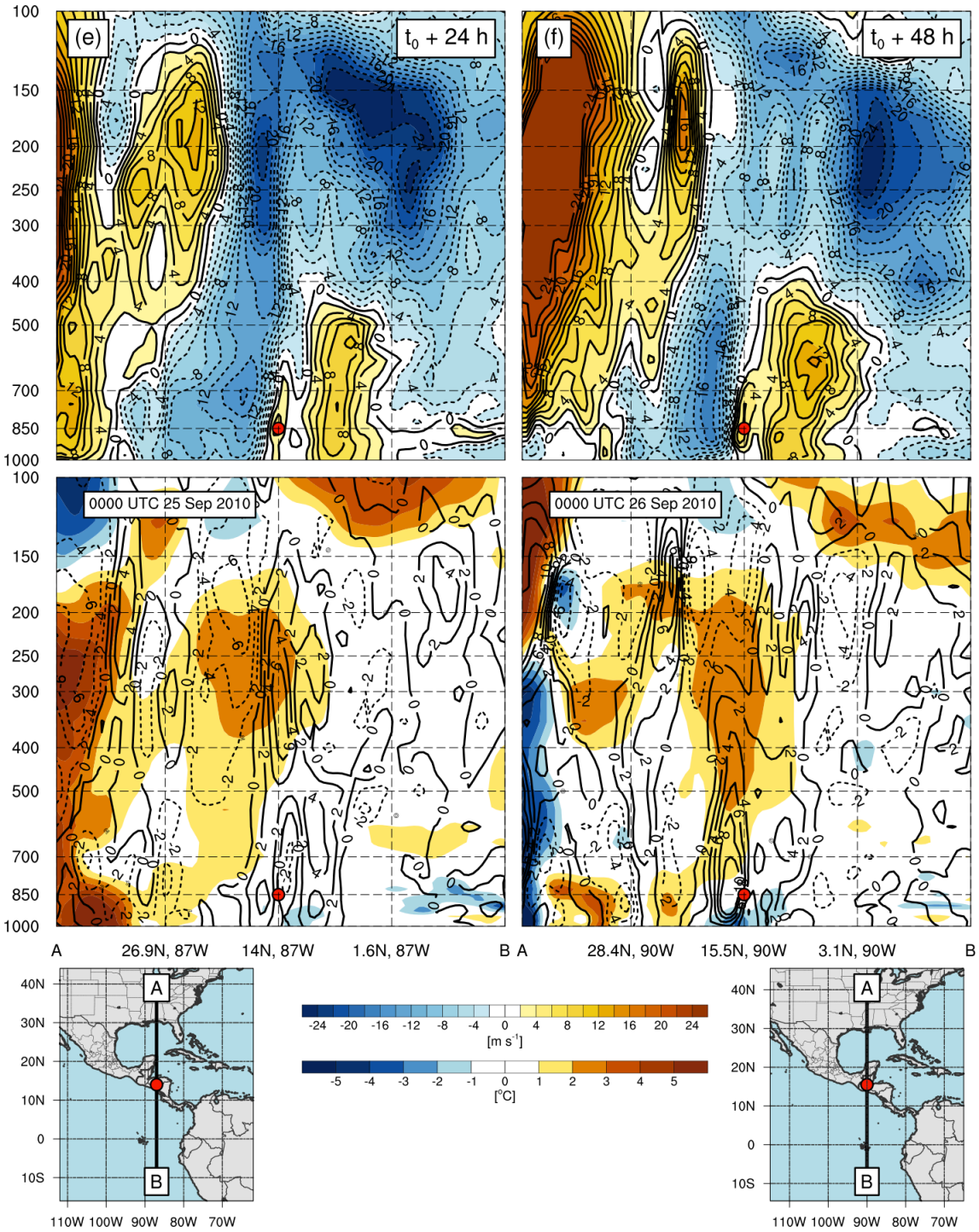

Fig. 3.44. As in Fig. 3.42 except at (e) t_0 + 24 h, (f) t_0 + 48 h. Reference panel for cross-sections provided on the bottom left (e) and bottom right (f).

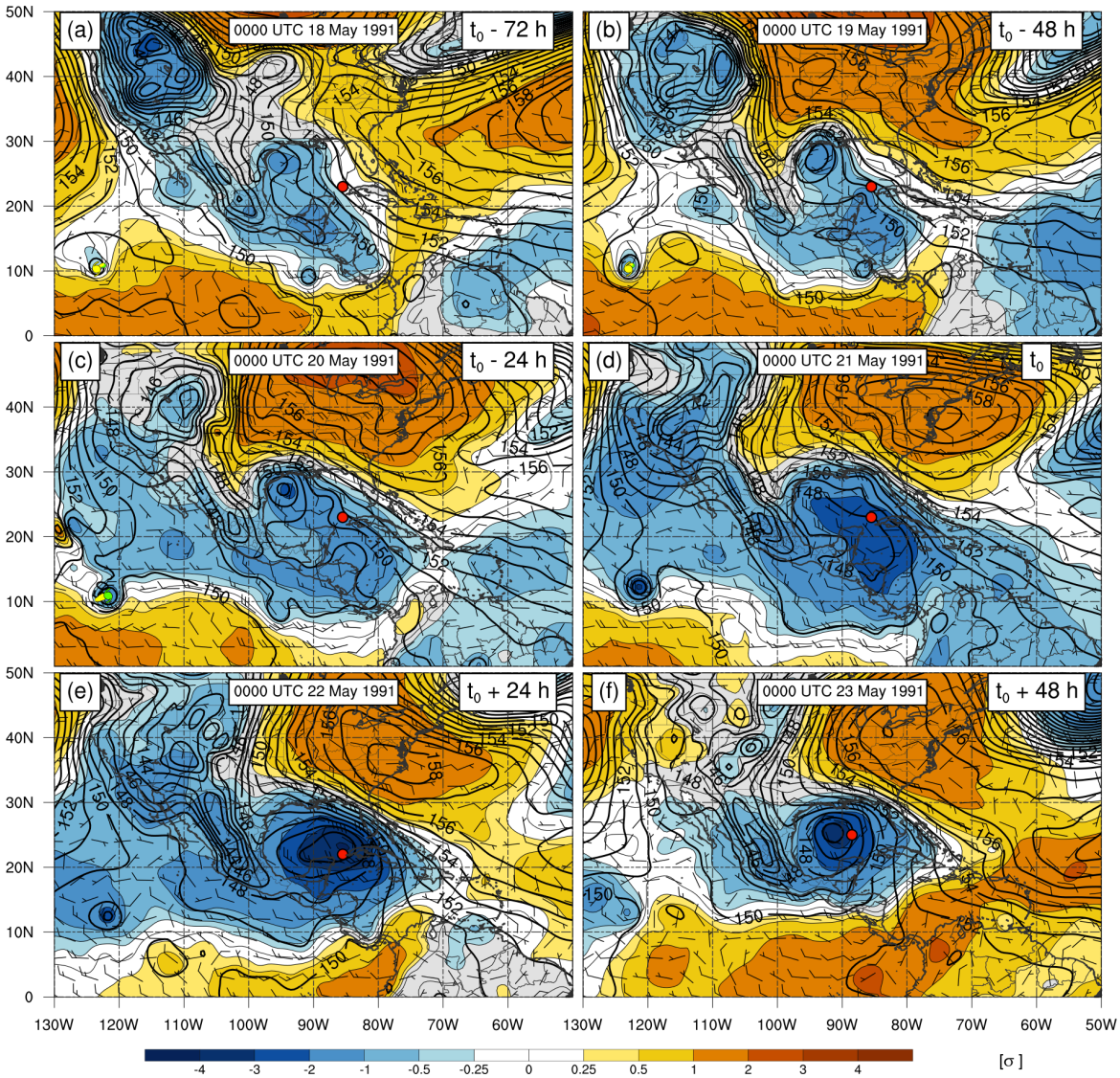

Fig. 3.45. As in Fig 3.33 except for trough CAG case study.

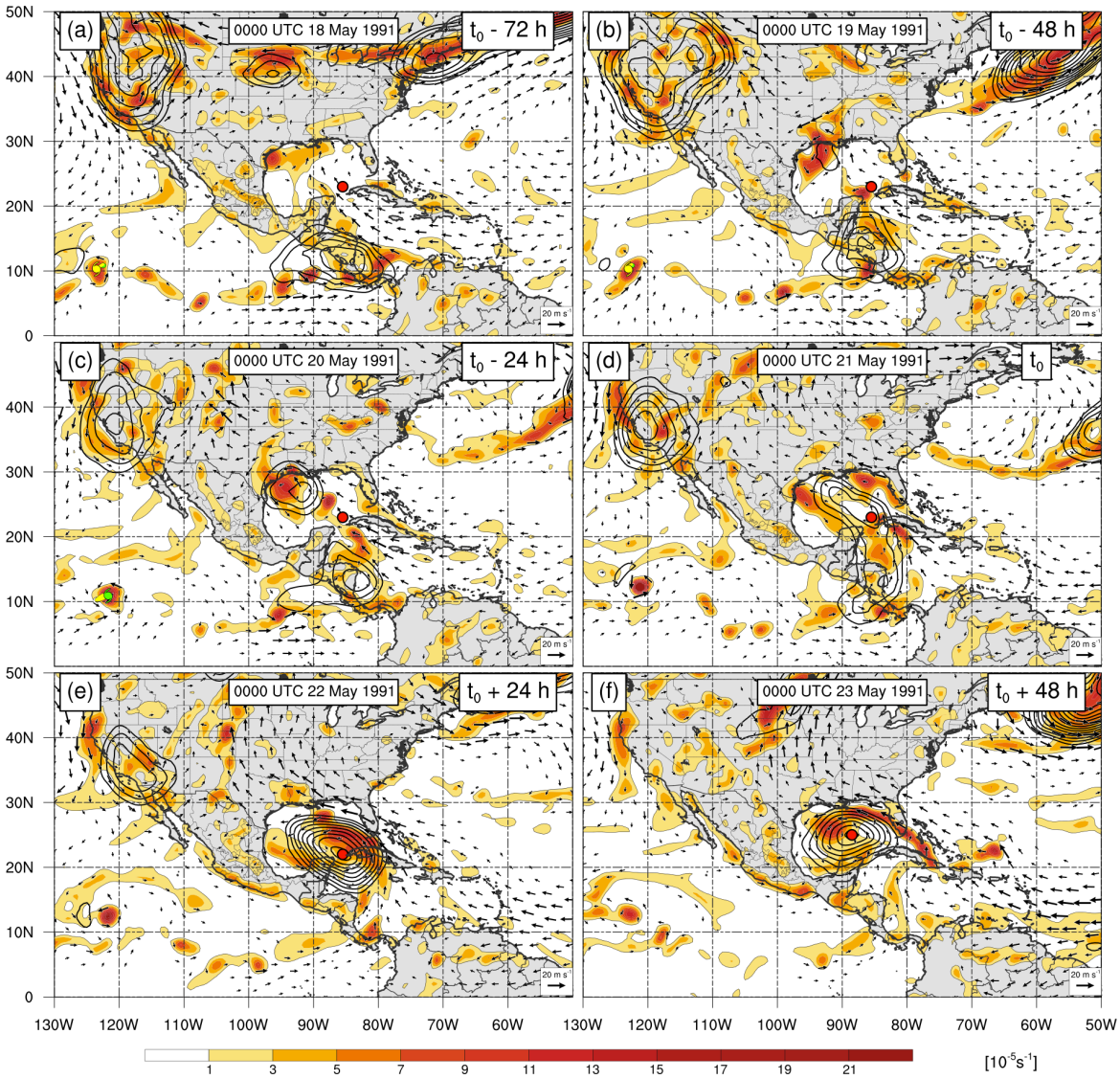

Fig. 3.46. As in Fig 3.34 except for trough CAG case study.

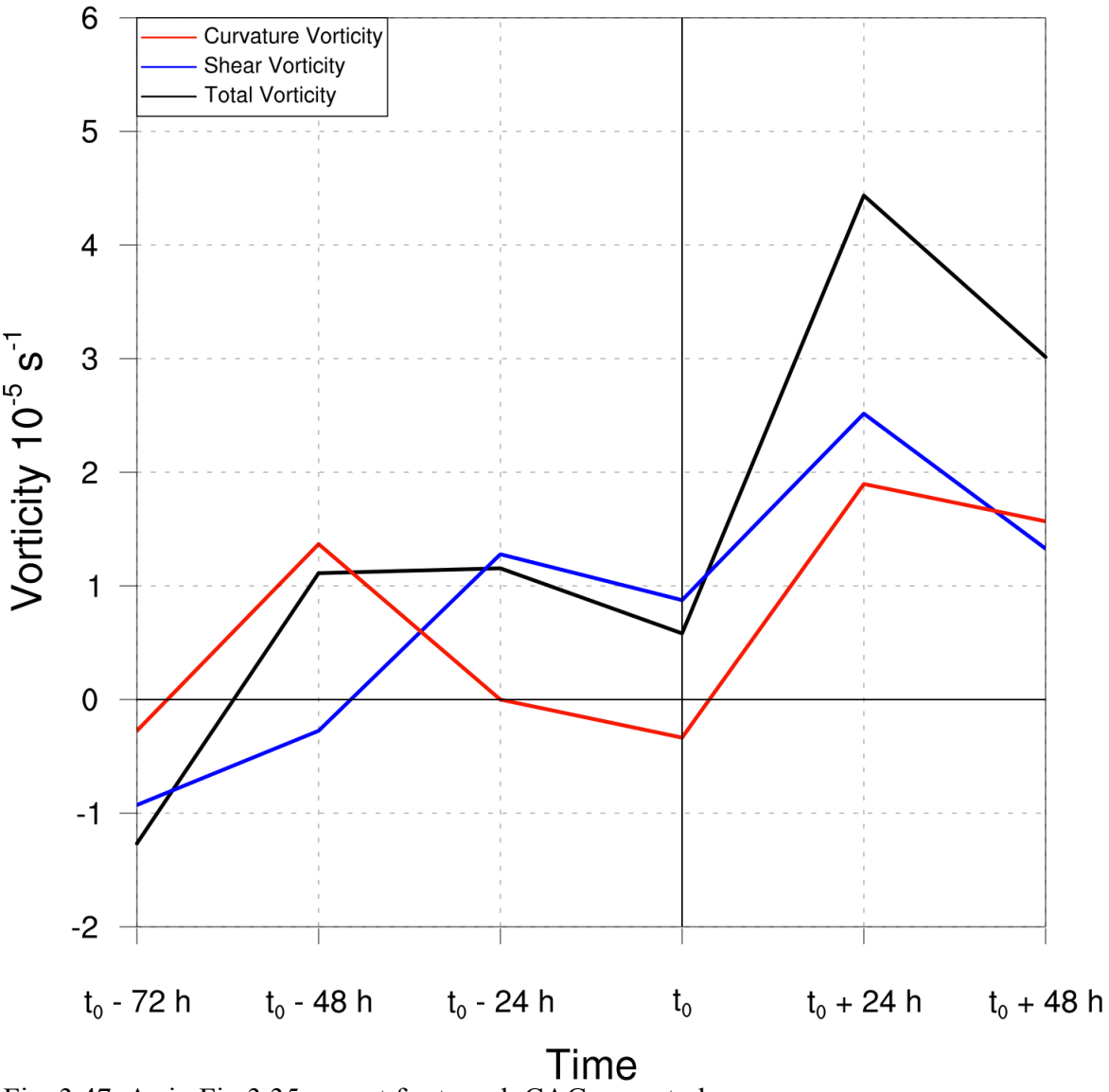

Fig. 3.47. As in Fig 3.35 except for trough CAG case study.

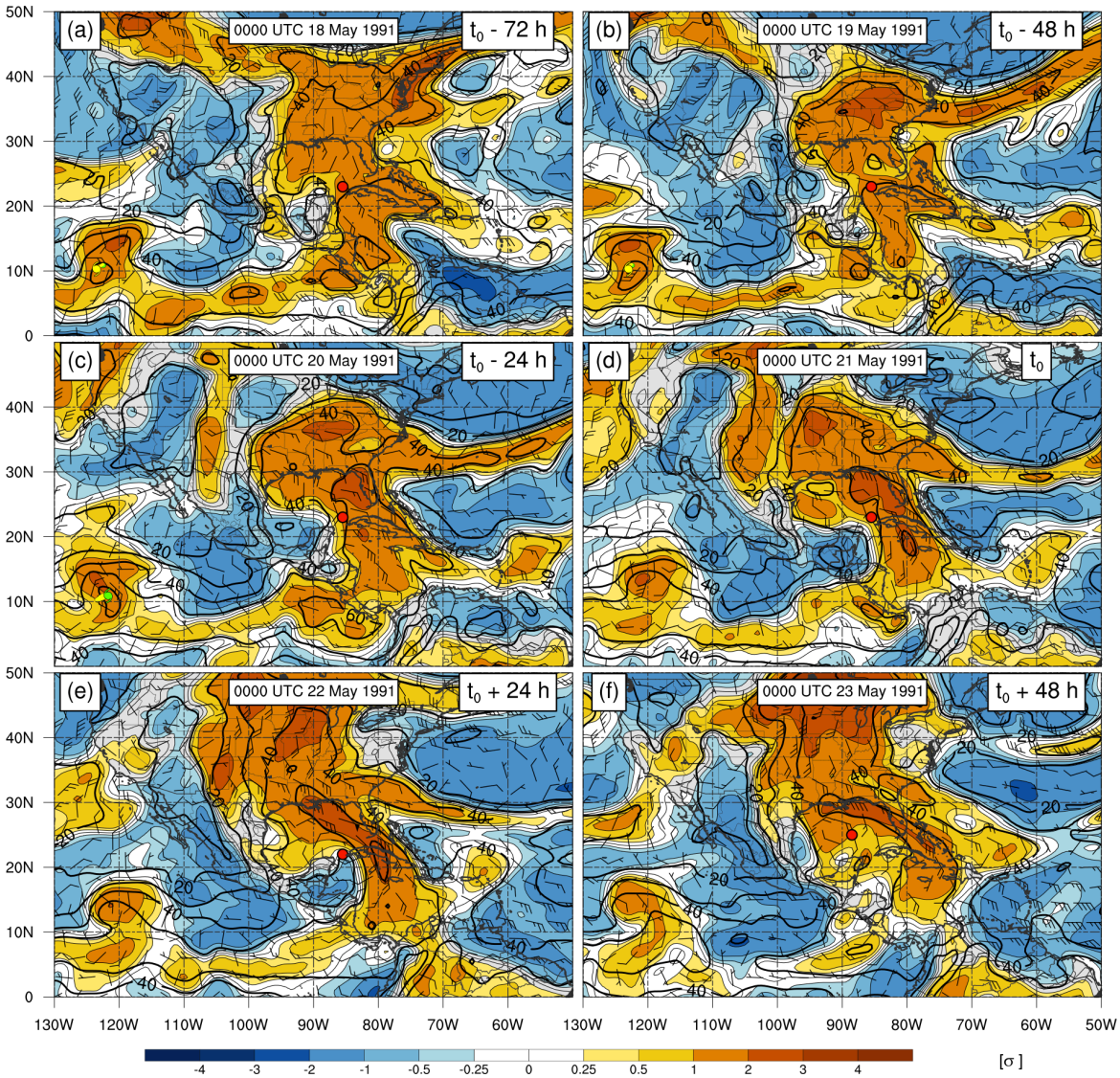

Fig. 3.48. As in Fig 3.36 except for trough CAG case study.

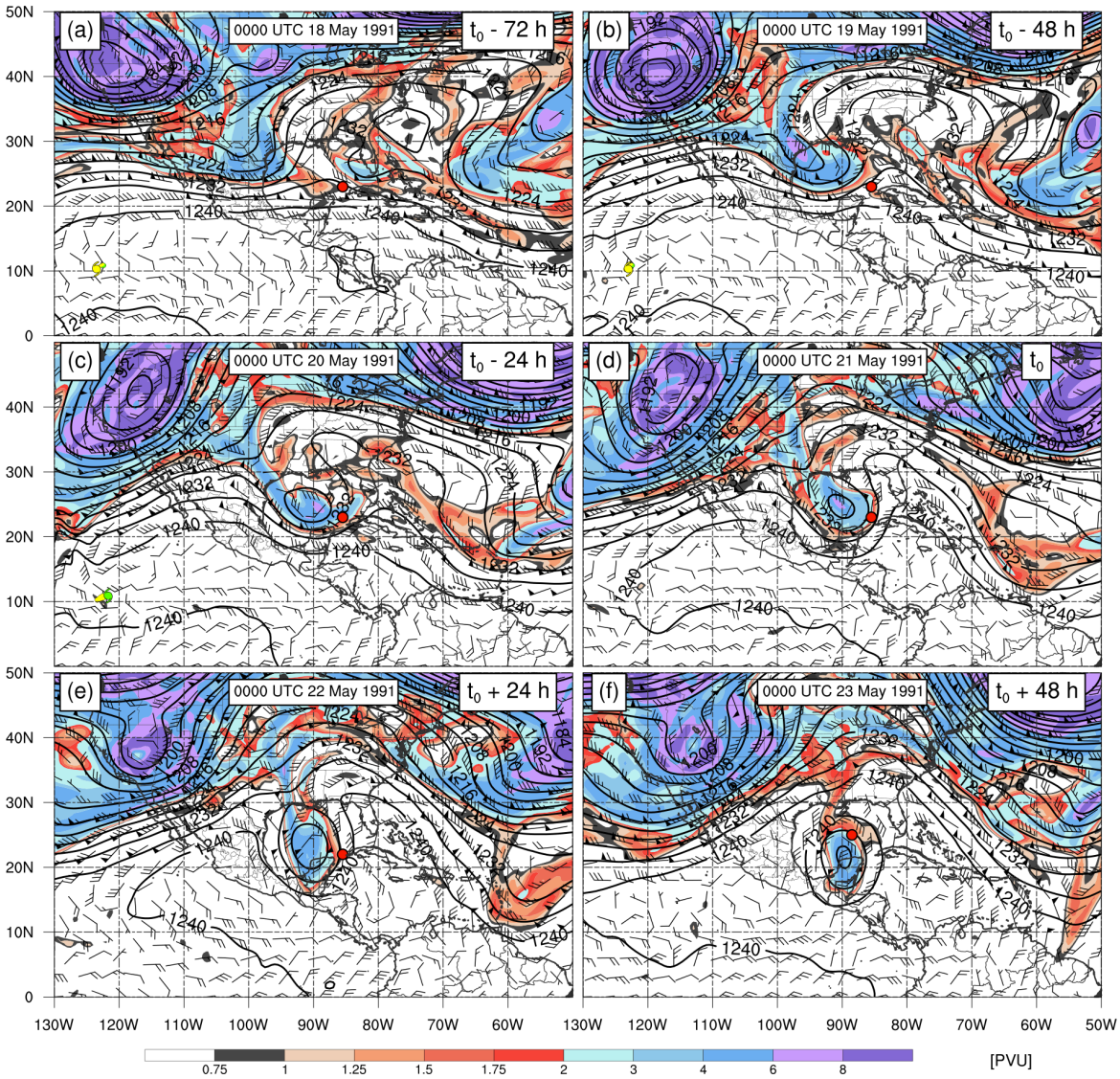

Fig. 3.49. As in Fig 3.37 except for trough CAG case study.

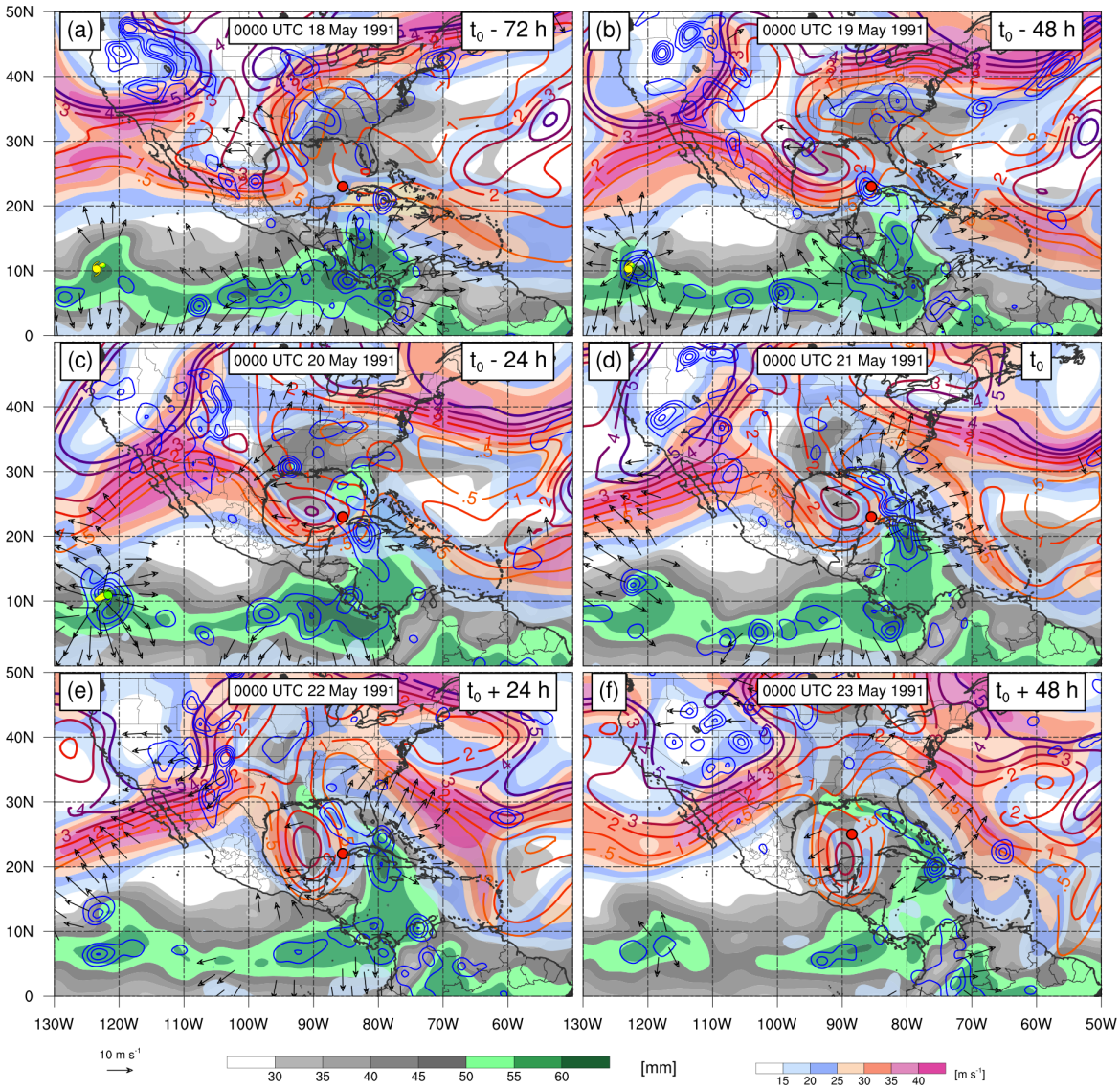

Fig. 3.50. As in Fig 3.38 except for trough CAG case study.

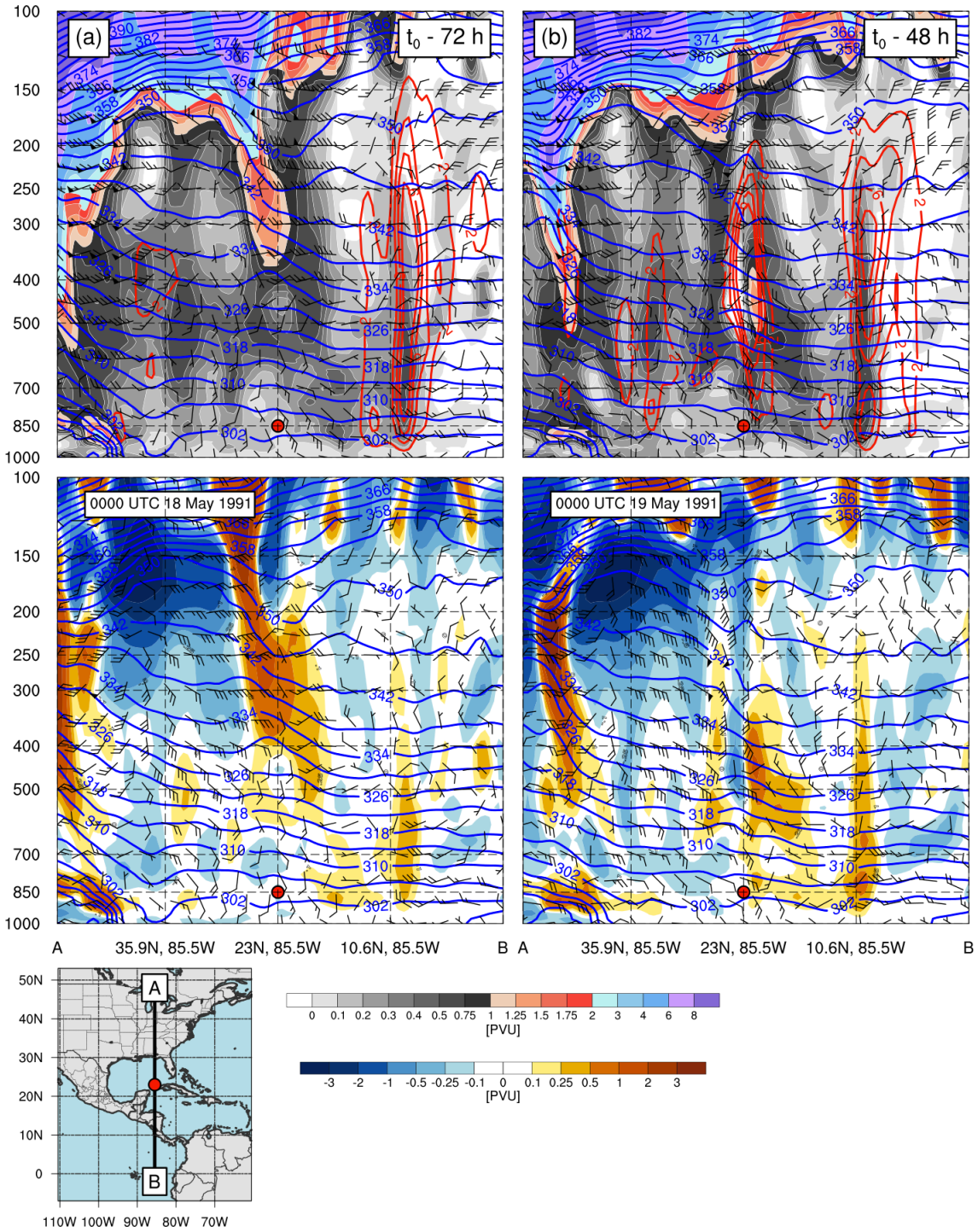

Fig. 3.51. As in Fig 3.39 except for trough CAG case study.

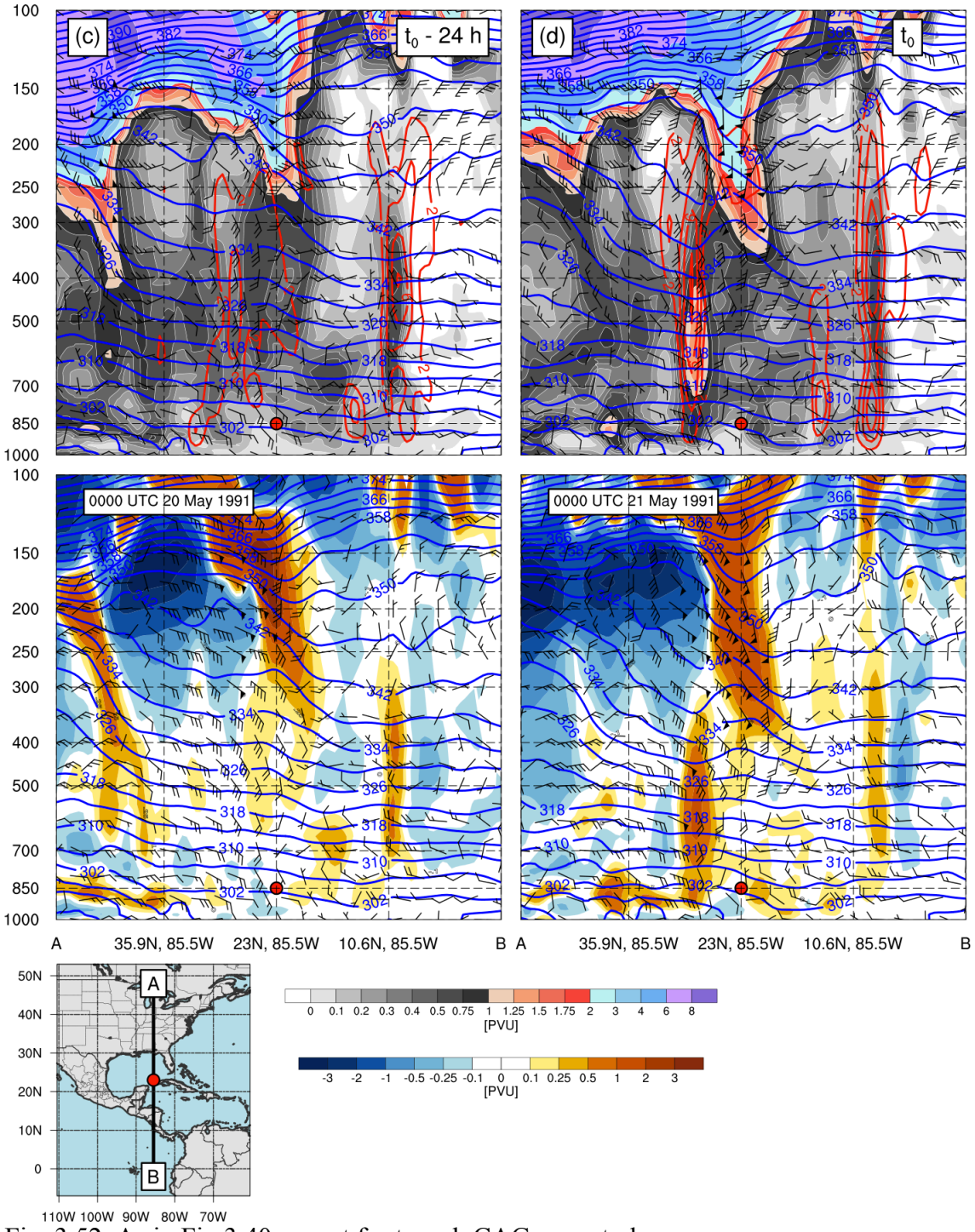

Fig. 3.52. As in Fig 3.40 except for trough CAG case study.

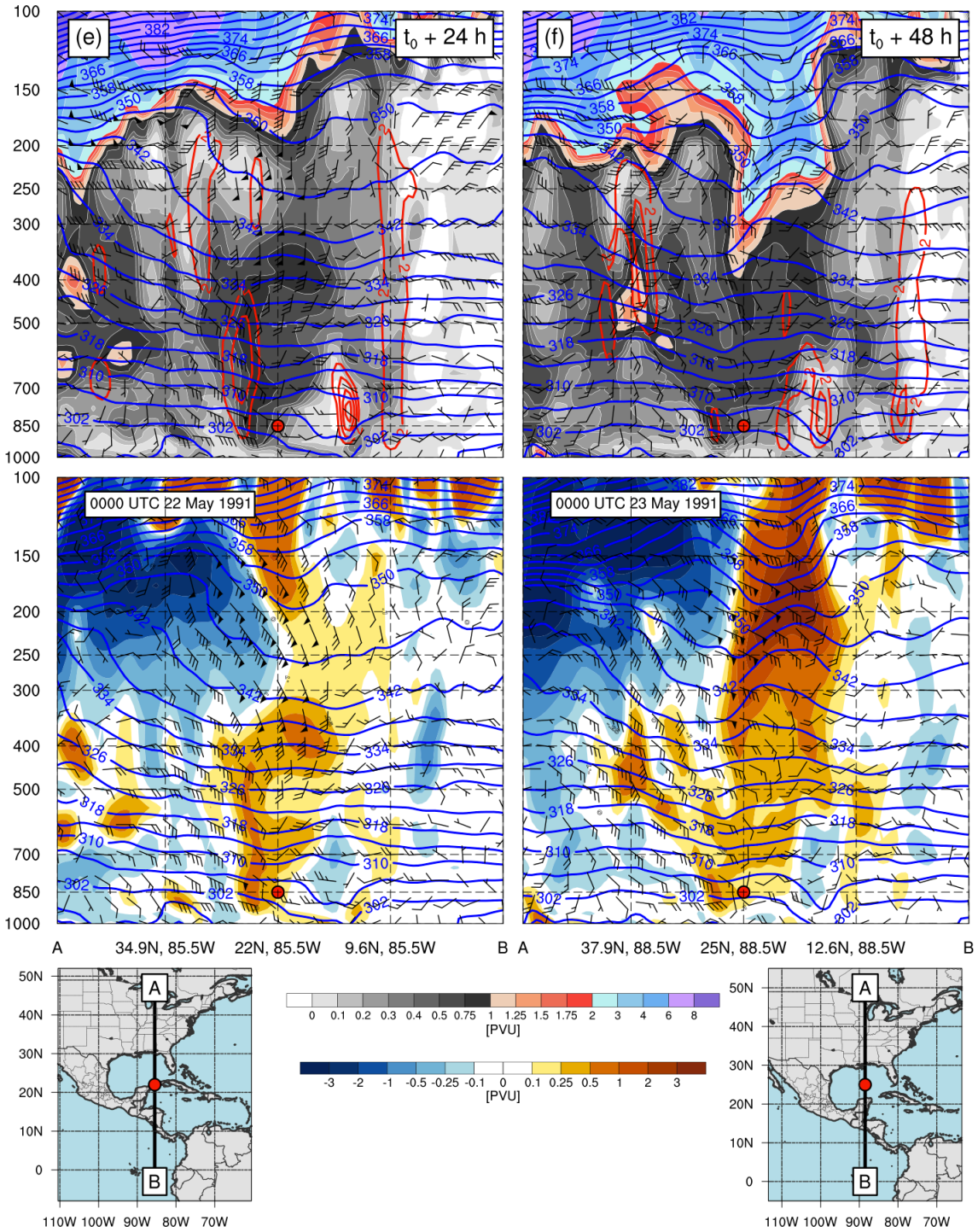

Fig. 3.53. As in Fig 3.41 except for trough CAG case study.

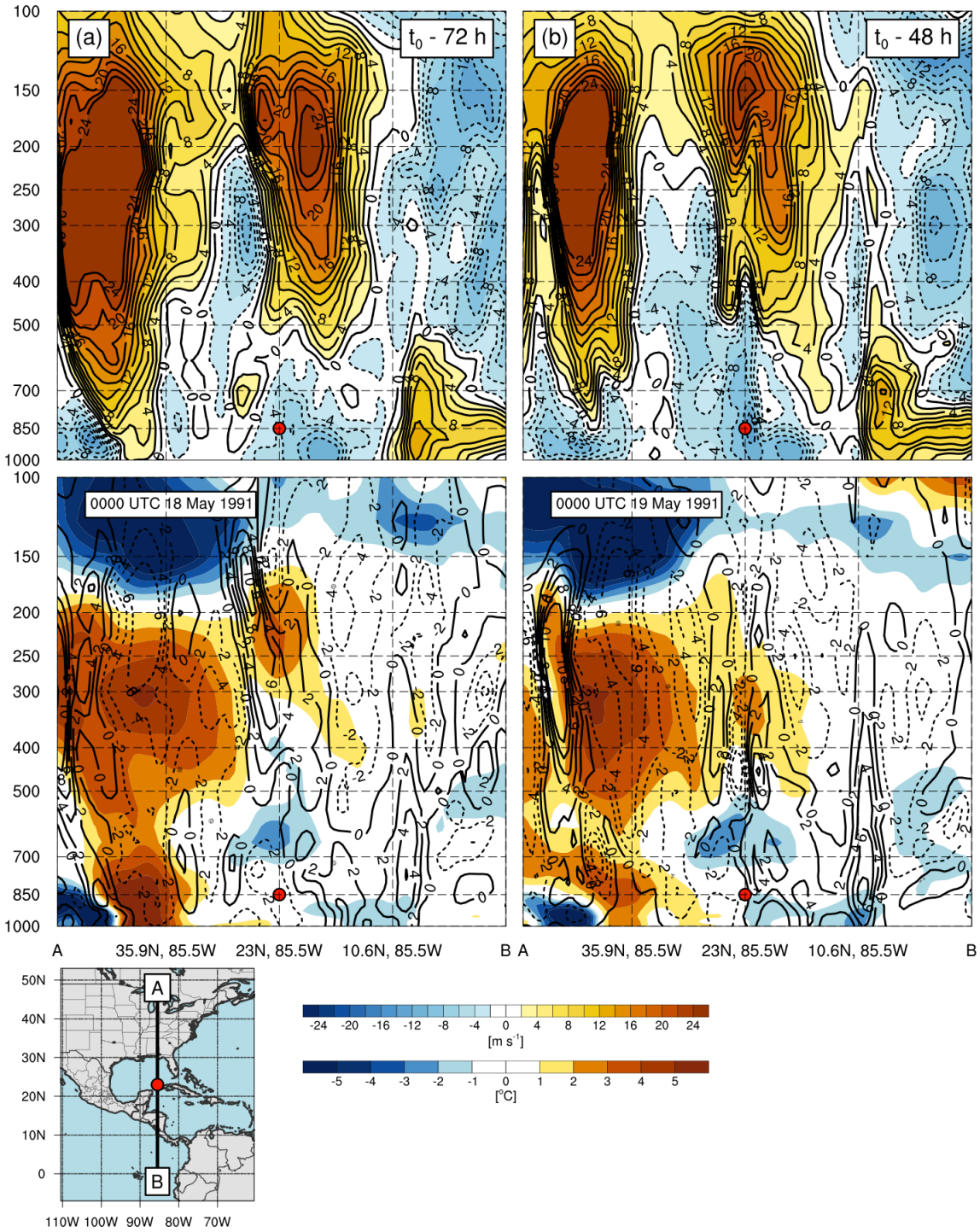

Fig. 3.54. As in Fig 3.42 except for trough CAG case study.

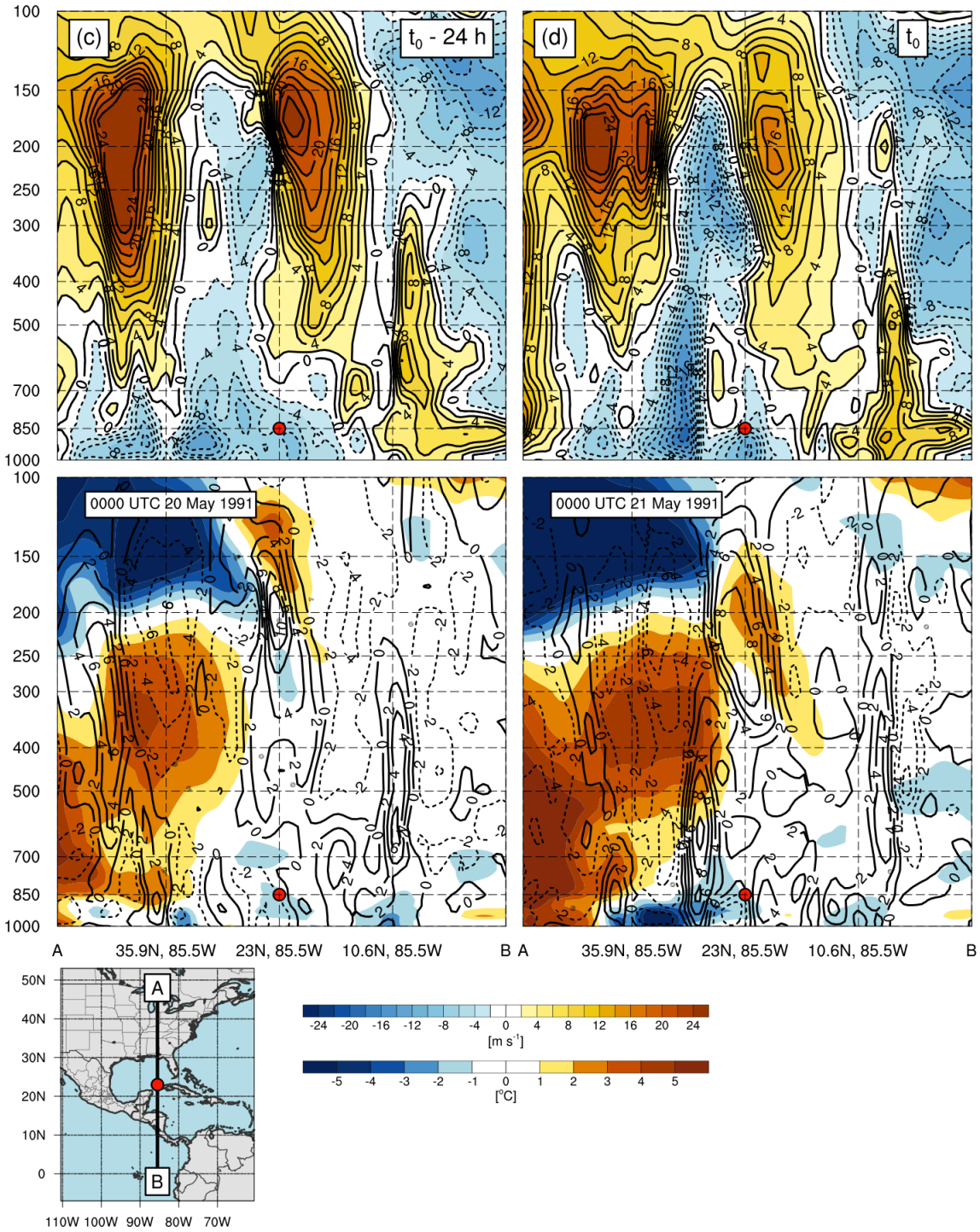

Fig. 3.55. As in Fig 3.43 except for trough CAG case study.

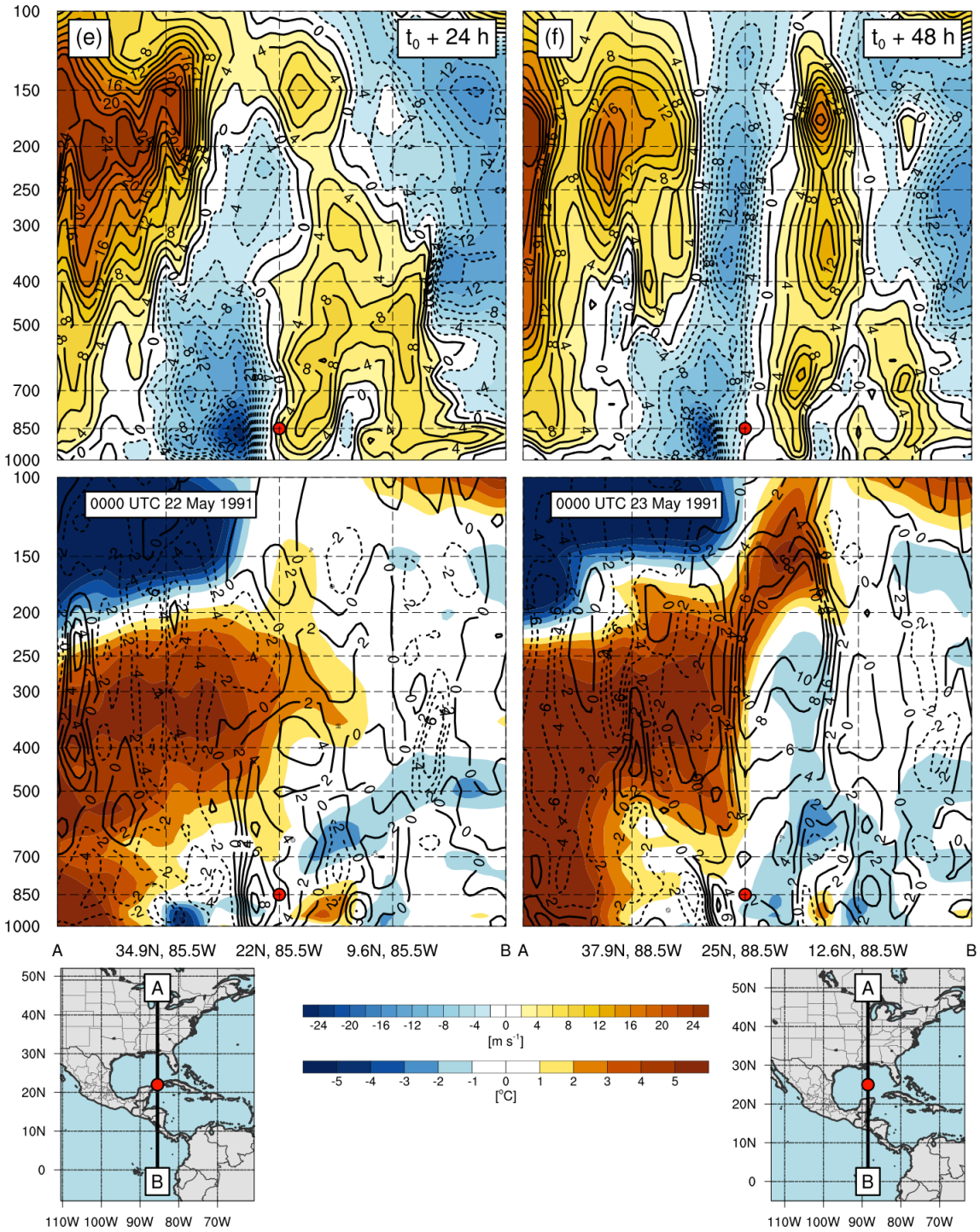

Fig. 3.56. As in Fig 3.44 except for trough CAG case study.

4. Discussion, Summary, and Suggestions for Future Work

4.1. Discussion and Summary

The May – Nov 1980 – 2010 CAG climatology is the first climatology developed to understand the underlining synoptic conditions that occur prior and during CAG formation, in addition to quantifying TCs occurrence within CAGs. The identification of CAGs was adapted and modified from the classification of MDs and MGs in other literature, with the resulting methodology using a sophisticated algorithm based on a series of objective tests tailored to CAG classification.

4.1.1 CAG Climatology

Between May – Nov 1980-2010, a mean seasonal frequency of ~1.4 CAG cases was identified, along with a mean lifespan of ~3 days and mean radius of maximum winds ~600 km from the CAG center. Most studies have noted a higher seasonal frequency of MDs and MGs in the IND and WPAC basins (Chen and Weng 1999, Yoon and Chen 2005, Beattie and Elsberry 2013, Wu et al. 2013, Boos et al. 2014, Hurley and Boos 2014) relative to CAGs over Central America. On average, CAGs tend to be smaller than previously identified MGs (Lander 1994, Crandall 2012), but are similar in size to MDs (Harr et al. 1996, Beattie and Elsberry 2013). CAGs also tend to have shorter lifespans compared to MDs and MGs in other basins (Lander 1994, Harr et al. 1996, Wu et al. 2013). Of these studies, only Hurley and Boos (2014) identified MDs in a similar but larger region from where CAGs are identified in the present study. In this region, Hurley and Boos (2014) noted little monthly variation in the frequency of MDs, which is

in contrast to the bimodal distribution of CAGs identified in this study (Fig. 3.2). The significant differences in annual frequency of these prior studies are likely due to 1) different classification methodologies, 2) different gridded datasets, and 3) regional differences in the synoptic environment and size between different basins.

The seasonal variation of CAG genesis in the climatology illustrated in Fig. 3.2 is an important topic of discussion. A possible link between the lack of CAG activity in mid-summer and a relative minimum in climatological precipitation over Central America during the same period (known as the mid-summer drought) was proposed in section 3.1. As discussed in section 1.2.2, a time-mean low-level cyclonic circulation occurs over Central America during active rainfall periods in Jun and Sept – Oct, while a time mean low-level anticyclonic circulation is observed during the mid-summer drought (Magana et al. 1999). In particular, the low-level circulation during heavy rainfall periods was attributed to off equatorward convective heating. CAGs are one possible source of this convective heating, since these circulations are associated with large convective regions in a moist environment over Central America. The development of convection in CAGs generates LHR, with the resulting heating profile increasing thicknesses that contribute to reduced low-level geopotential heights and increased low-level cyclonic flow over Central America, as observed by Magana et al. (1999). The relative lack of rainfall during the mid-summer drought period could be attributed to a lack of CAG occurrence that occurs during Jul – Aug, where the lack of convection fails to produce a time-mean low-level cyclone related to increased rainfall over Central America. Other studies have noted that synoptic monsoonal circulations contribute large fractions (> 40%) of the climatological mean precipitation in other regions (Romatschke and Houze

2011, Hurley and Boos 2014). In this respect, the mid-summer drought could be seen as a suppression of transient synoptic systems (such as CAGs) that contribute a significant portion to the climatological rainfall total outside of the mid-summer drought. This hypothesis was initially proposed by Small et al. (2007) and appears to be supported by the findings of this study.

However, the association of little CAG activity during the mid-summer drought does not explain the lack of CAG activity in Jul – Aug. One idea proposed by this study is related to the hypothesized importance of meridional gradients of zonal wind, as highlighted in both the tropical and trough CAG composites (Figs. 3.6 and 3.18). A meridional gradient reversal of low-level zonal wind satisfies the necessary condition for barotropic instability. Prior studies on MD development in the north IND basin concluded that barotropic instability is an important mechanism in combination with LHR from convection in the genesis of MDs (Krishnamurti et al. 1976, Shukla 1978, Nitta and Masuda 1981). The results of Aiyyer and Molinari (2008) also suggest barotropic instability played a role in the development of a CAG in Sep 1998. Thus, the lack of CAG activity in Jul – Aug could be attributed to the lack of a meridional gradient reversal in the low-level zonal wind, preventing barotropic instability. Fig. 3.3 qualitatively supports this hypothesis, depicting a reduction in the climatological zonal wind gradient reversal during Jul-Aug, corresponding to a substantial reduction in CAG activity during this period. These preliminary findings suggest that climatological flow plays a role in modulating CAG frequency, which in turn could impact the seasonal rainfall distribution over Central America.

4.1.2. CAG Types

As discussed in section 2.2.4, CAGs were tested for the existence of an upper-tropospheric trough (as defined as PV > 2 PVU on the 350 K isentropic surface). As discussed in section 3.2, the majority (~83%) of CAGs do not possess an upper-tropospheric trough. This suggests that trough CAGs are a relatively rare phenomenon with their frequency occurring less than once per TC season. The tropical and trough CAG categories were identified to compare MD-like and MG-like CAG occurrences. The following discussion will compare the two CAG composites and make comparisons to previous literature on MDs and MGs.

4.1.3. Composite Analysis

Tropical and trough CAGs possess a relatively similar 850-hPa geopotential height pattern that results in the generation of anomalous westerly flow in the EPAC and anomalous easterly flow in the ATL basin (Figs. 3.6a-c). The composite tropical CAG exhibits larger areas of statistical significant due to the higher number of cases (35 tropical CAGs vs. 7 trough CAGs). The CAG composite structure of anomalously low 850-hPa geopotential heights, associated with the cyclonic flow of the low-level CAG circulation, is consistent with the structure observed in MDs and MGs in prior literature (Boos et al. 2014, Crandall et al. 2014). However, the importance of anomalously high 850-hPa geopotential heights surrounding CAG events in the EPAC and ATL basins prior to CAG development has not been explored previously with MDs or MGs. The vast

majority of prior literature has emphasized streamline or streamfunction analysis (Yoon and Chen 2005, Boos et al. 2014). The existence of statistically significant positive 850-hPa geopotential height anomalies in the ATL basin along the southeastern US coastline prior and during CAG development is an important finding of this work.

There are notable differences in moisture between the two composite subsets. Tropical CAGs possess a symmetrical large area of enhanced PW (> 50 mm, > 1 σ) in a circular region within 5^{o} of the tropical CAG center (Figs. 3.9d-f) while trough CAGs exhibit an asymmetrical moisture distribution, where enhanced moisture is primarily eastward of the trough CAG center and negative PW anomalies develop west of the trough CAG center by t_0 + 48 h (Fig. 3.21f). The more symmetrical PW of the tropical CAG is roughly consistent with the enhanced deep tropospheric moisture straddling the center of a MD identified in Krishnamurti et al. (1975) (Fig. 1.2d). The moisture pattern in the trough CAG composite is similar to the MG moisture pattern described in Crandall (2012) and Crandall et al. (2014), which suggested that an upper-tropospheric low was primarily responsible for asymmetry in the moisture pattern (Fig. 1.11b), where large-scale descent was observed to the east of the MG center (Fig. 1.11d).

Tropical CAGs also exhibit a relative symmetrical ring of higher cyclonic relative vorticity along the periphery of the circulation maxima after genesis (Figs. 3.8e-f) while trough CAGs are less symmetrical and possess higher cyclonic relative vorticity in the eastern quadrant of the circulation (Figs. 3.19e-f). Curvature vorticity dominates in the more circular tropical CAG at t_0 + 48 h (Fig. 3.9), while shear and curvature vorticity contribute roughly evenly to the relative vorticity in the trough CAG composite at t_0 + 48

h (Fig. 3.20), a result unsurprising given the asymmetrical and elongated structure of the trough CAG composite.

At 200-hPa there are additional differences between the two CAG composite subsets. Broad upper-tropospheric anticyclonic flow is present over the tropical CAG composite at nearly all time lags. In contrast, the trough CAG composite has an equatorward displaced subtropical ridge, which is bisected by an upper-tropospheric trough that is apparent by t_0 along the subtropical waveguide (Fig. 3.22d). As discussed in section 1.2.1.2, the existence of upper-tropospheric troughing in MGs is a primary distinction in classification from MDs (Molinari and Vollaro 2012, Crandall 2012, Crandall et al. 2014). The trough CAG composite at 200-hPa possesses a qualitatively similar structure in comparison to these MG events .The tropical CAG composite, in contrast, depicts large scale anticyclonic flow and upper tropospheric ridging, corresponding to low PV air (< 0.5 PVU) at 200-hPa. These characteristics are primarily found in MD circulations (Mulky and Banerji 1960, Beattie and Elsberry 2013, Boos et al. 2014, Hurley and Boos 2014). These results suggest that the upper-tropospheric structure of tropical CAGs is qualitatively similar to MDs, while the upper-tropospheric structure of trough CAGs is qualitatively similar to MGs.

The vertical structure of the two subsets of CAGs also draws parallels to the differences expressed between MDs and MGs. Tropical CAGs achieve a PV maximum > 0.5 PVU in the middle troposphere (Figs. 3.14e-f), similar to MDs in other basins (Boos et al. 2014 and Hurley and Boos 2014, Figs. 1.4 and 1.7). PV actually decreases between the middle and upper troposphere in the tropical CAG composite with a relative minimum in PV in the upper-troposphere corresponding to an anticyclonic vorticity

maximum (Figs. 3.17e-f). This anticyclonic vorticity maximum in the upper-troposphere (200-hPa) is also observed in WPAC MD cases (Beattie and Elsberry 2013, Fig. 1.6). The zonal wind structure of tropical CAGs (Figs. 3.16e-f top panels) also possesses similarities to MDs in other studies (Hurley and Boos 2014 and Beattie and Elsberry 2013, Figs. 1.6 and 1.7). The mid to upper tropospheric warm core (between +1 – 2^{o}C, Figs. 3.16e-f) are also similar to the mid to upper tropospheric warm core of composite MDs identified in Hurley and Boos (2014) (Fig. 1.6). Based on these comparisons, the composite structure of tropical CAGs is qualitatively similar to the structure of MDs in previous literature.

The vertical structure of trough CAGs is different to tropical CAGs primarily due to the presence of the upper-tropospheric trough. Instead of PV being maximized in the middle troposphere, PV increases throughout the tropospheric column, reaching a maximum in both actual and positive anomaly in the upper-troposphere. This is due to the existence of the upper tropospheric trough which is superimposed over the low-level trough CAG center by t_0 + 48 h (Fig. 3.26f). The composite trough CAG PV profile bares a close resemblance to the PV profile of a MG identified by Molinari and Vollaro (2012) (Fig. 1.10) in which the largest value of PV is found in the upper troposphere, which is likely attributed to an upper-level trough in proximity to this particular MG. Despite the fact that an upper-tropospheric trough is present in the composite trough CAG structure, a warm core is also present in the mid to upper troposphere, qualitatively similar to the tropical CAG composite. However, the low sample size of trough CAG cases in this composite (N = 7) limits the generalization we can make about this subset.

The synoptic evolution of composite tropical and trough CAG occurrence is summarized in Figs. 4.1 and 4.2. Tropical CAGs (Fig. 4.1) are qualitatively similar to MDs identified in the WPAC and north IND basins, where gradients in anomalous low-level geopotential height generate low-level flow that evolves into a large cyclonic circulation. Like MDs, tropical CAGs posses an upper-level anticyclone, where low vertical wind shear is favorable for tropical CAGs to evolve into TCs. Trough CAGs (Fig. 4.2) are qualitatively similar to MGs identified in the WPAC basin, in which upper-tropospheric trough interaction provides a large contribution to the overall low-level circulation, either indirectly via large-scale ascent upstream of the upper-tropospheric trough or directly via penetration of the upper-tropospheric trough into the lower-troposphere.

4.1.4. CAGs and Tropical Cyclones

TCs exist in ~52% of all CAG occurrences, and are more common in tropical CAGs (~57%) versus trough CAGs (~29%). However, TCs form in only ~33% of all CAGs. This latter value is similar to Beattie and Elsberry (2013), who found that ~39% of MDs went on to produce at least one TC in 2009. In contrast, Wu et al. (2013) found a much higher yield (~84%) of MGs that produce at least one TC. In addition, TCs appear to favor the eastern quadrant of the CAG circulation, ~500 km away from the CAG center (Fig. 3.30). Wu et al. (2013) also noted that most TCs that developed in MG cases favored the eastern semicircle, where lower vertical wind shear is present. Some CAGs can evolve into a TC in the latter stages of their lifecycle as cyclonic vorticity axis-

symmetrizes and intensifies over the circulation center. This evolution is similar to WPAC MDs, which tend to produce large TCs though a similar evolution (Harr et al. 1996, Lander 2004).

4.1.5. CAGs and the Madden Julian Oscillation

As discussed in section 3.6, the MJO in RMM phases 8,1, and 2 is associated with > 75% of all CAG genesis occurrences. These RMM phases roughly correspond to the active phase of the MJO over the western hemisphere. One characteristic of these MJO phases is the presence of anomalous zonal 850-hPa westerly flow across the EPAC along 10^{o}N, a feature consistent with the CAG composite at genesis (Fig 3.32). The importance of an active MJO leading to the formation of large-scale low-level cyclonic circulations has been discussed in case studies of both MDs (Boos et al. 2014), and MGs (Molinari et al. 2007, Molinari and Vollaro 2012, Crandall 2012). These results also provide support that an active MJO is associated with more CAG development relative to inactive phases of the MJO. In the EPAC, Aiyyer and Molinari (2008) showed the importance of barotropic instability associated with the active MJO that coincides with the formation of a CAG in Sep 1998. In their explanation, the MJO provides a favorable environment for the amplification of weak disturbances in which eddies grow at the expense of the mean flow. Therefore, it is possible that the active MJO in these CAG genesis cases is providing a similar favorable influence, where a zonal low-level flow over Central America evolves into a large cyclonic circulation, with meridional perturbations in the original low-level flow. The evolution of the synoptic environment from one that is primarily represented by shear vorticity to one dominated by curvature vorticity is also

suggestive of these barotropic energy conversions from the mean state to eddies (Figs. 3.8 and 3.20) resulting from barotropic instability. However, additional work is needed to compute the energy budget of CAGs to support these qualitative similarities in the synoptic pattern and the implied energy conversions taking place in the composite CAG. A few CAG cases still develop in the inactive MJO phases over Central America (Fig. 3.31), indicating the MJO is not the only factor in CAG formation.

4.1.6. Case Studies

In general, the tropical CAG case study selected (t_0 at 0000 UTC 24 Sep 2010) depicts similar characteristics to the tropical CAG composite. There are some minor differences in the tropical CAG case study, where positive 850-hPa geopotential height anomalies over the EPAC were less expansive while negative geopotential height anomalies over Central America were more expansive and covered a large portion of the EPAC (Figs. 3.33a-d). The large negative geopotential height anomalies (< -3.00 σ) in the west ATL basin at t_0 – 72 h are primarily associated with recurving TC Igor (Fig. 3.33a). It is also notable that one 850-hPa cyclonic vorticity maxima embedded in the tropical CAG is associated with TC Matthew (Figs. 3.34e-f), which is rotating cyclonically around the larger circulation of the CAG.

The trough CAG case study selected (t_0 at 0000 UTC 18 Sep 1991) depicts more substantial differences compared to the trough CAG composite. For example, at t_0 – 24 h, a distinct 850-hPa cyclonic relative vorticity maximum is located in the GoM, resulting in a maximum of 500-1000 km radial mean 850-hPa circulation in this region (Fig. 3.46c). This circulation maximum merges with another circulation maximum observed over

Central America, leading to trough CAG genesis in the case study (Fig. 3.46d). This evolution is different from the composite trough CAG evolution, which only depicts one circulation maximum developing in the northwest Caribbean (Figs. 3.18c-d). These differences can be traced to the upper-troposphere, as the trough CAG case study contains a potent (> 4.0 PVU) 200-hPa cutoff cyclone that has drifted southeastward into the GoM (Figs. 3.49a-f). The intensity of the cutoff cyclone likely results in the vertical penetration of cyclonic flow into the lower troposphere, contributing to the 850-hPa circulation maximum in the GoM (Fig. 3.46c). This evolution is different from the trough CAG composite, which depicts a weaker, positively tilted upper-tropospheric trough (Figs. 3.22a-f).

4.1.7. Applications of Research to Operational Forecasting

The CAG cases identified in the climatology highlight the propensity for large-scale low-level cyclonic circulations to develop and slowly move across Central America. Given that CAGs are associated with anomalously high precipitable water and large regions of ascent and cyclonic vorticity, CAGs can result in catastrophic rainfall over Central America. CAGs are frequently associated with TCs, which can result in further rainfall and additional societal impact. Thus, being able to recognize key synoptic features that occur prior to CAG formation would be of use to the forecasting community in providing early warning of CAG occurrence and associated impacts. The antecedent synoptic environment leading to CAG formation is summarized for both tropical and

trough CAG occurrence in Figs. 4.1-4.2. These common synoptic characteristics provide a way for forecasters to use pattern recognition in forecasting CAG occurrence.

The unique methodology applied to the identification of CAGs over Central America is easily customizable and adaptable to use in a real-time forecasting environment. While specifically developed and used for the CFSR dataset in this study, the CAG methodology employed here can be easily ported to other reanalysis and real-time gridded models such as the GFS, GFS-reforecast, ECMWF, and ERA-interim for testing in a forecasting environment. The use of this methodology on identification of other large-scale cyclonic circulations (e.g. MDs and MGs) in other basins (WPAC, North IND) in real-time would also likely be of use, given the recent ambiguity in the identification of such entities in these basins without a clear set of identification guidelines (see the JTWC's classification of TC Nakri [2014] in the WPAC).

4.2. Suggestions for Future Work

The CAG climatology as presented is unique to climatologies composed of large-scale low-level cyclonic circulations in other basins because of the use of Stokes theorem in associating large but disorganized filaments of vorticity to comprise one large circulation. The other steps developed in the CAG identification algorithm also show utility in removing both TC circulations and non-closed circulations that may possibly affect prior climatologies of MDs and MGs. With this in mind, an expanded climatology, adapting the CAG algorithm to other basins may provide unique insight beyond what previous research has unearthed. In particular, few studies have investigated the

differences between MDs and MGs in the WPAC basin, with some MG climatologies likely capturing MDs circulations in addition to MGs (Chen et al. 200, Wu et al. 2013). The current study provides a simple way to partition MD cases from MG cases via upper-level PV, and could mitigate the uncertainty associated with cross contamination of MDs and MGs. The author speculates that a redone climatology of MDs and MGs in the WPAC using the adapted CAG algorithm would reveal similar composite characteristics to tropical and trough CAGs, although perhaps with different seasonal frequency and distribution given the lack of a mid-summer drought over the open WPAC basin.

While the current CAG climatology is extensive and covers many basic aspects related to CAGs, there remain a number of additional areas of research that would likely provide additional insight into the structure and impact of CAGs. For example, the importance of the high terrain of Central America and how it impacts the development and maintenance of CAGs has largely been unexplored. While terrain is only coarsely depicted in the 0.5^{o} CFSR dataset, further numerical simulations using the weather research and forecast (WRF) model run at higher resolution would possibly reveal important characteristics of CAGs over Central America such as 1) flow channeling through low elevation mountain passes that focuses convergence and convective development in a moist unstable environment, 2) flow forced over steep terrain, contributing to vortex stretching in the lee which could impact the cyclonic vorticity composition of a CAG, and 3) rough topography of Central America acting as a sink of kinetic energy due to friction, resulting in the spin down of low-level flow over time. Another possible use of WRF modeling for CAGs is the ability to modify the topography directly in the model, allowing the test how CAGs may change with adjusted terrain.

Finally, while not encompassing the full 1980-2010 CAG climatology, gyre-relative composites of Tropical Rainfall Measuring Mission (TRMM) data would be especially useful in deducing the CAG contribution of rainfall over Central America during a typical season. Because the largest societal impact associated with CAGs is their ability to produce catastrophic rainfall, it would seem useful to provide a limited 1998-2010 satellite derived rainfall climatology of CAGs, as well as deducing the distribution of stratiform versus convective precipitation that occur in CAG events. The author hypothesizes that CAG rainfall provides a non-negligible percentage of the seasonal precipitation over Central America, and that the elimination of CAG precipitation events would lead to a significant reduction of the annual precipitation total over Central America. The use of stratiform and convective precipitation partitioning in TRMM could also be useful in prescribing a more accurate convective heating profile of CAGs rather than using convective heating profiles of global model such as the CFSR which are prescribed by cumulus parameterization.

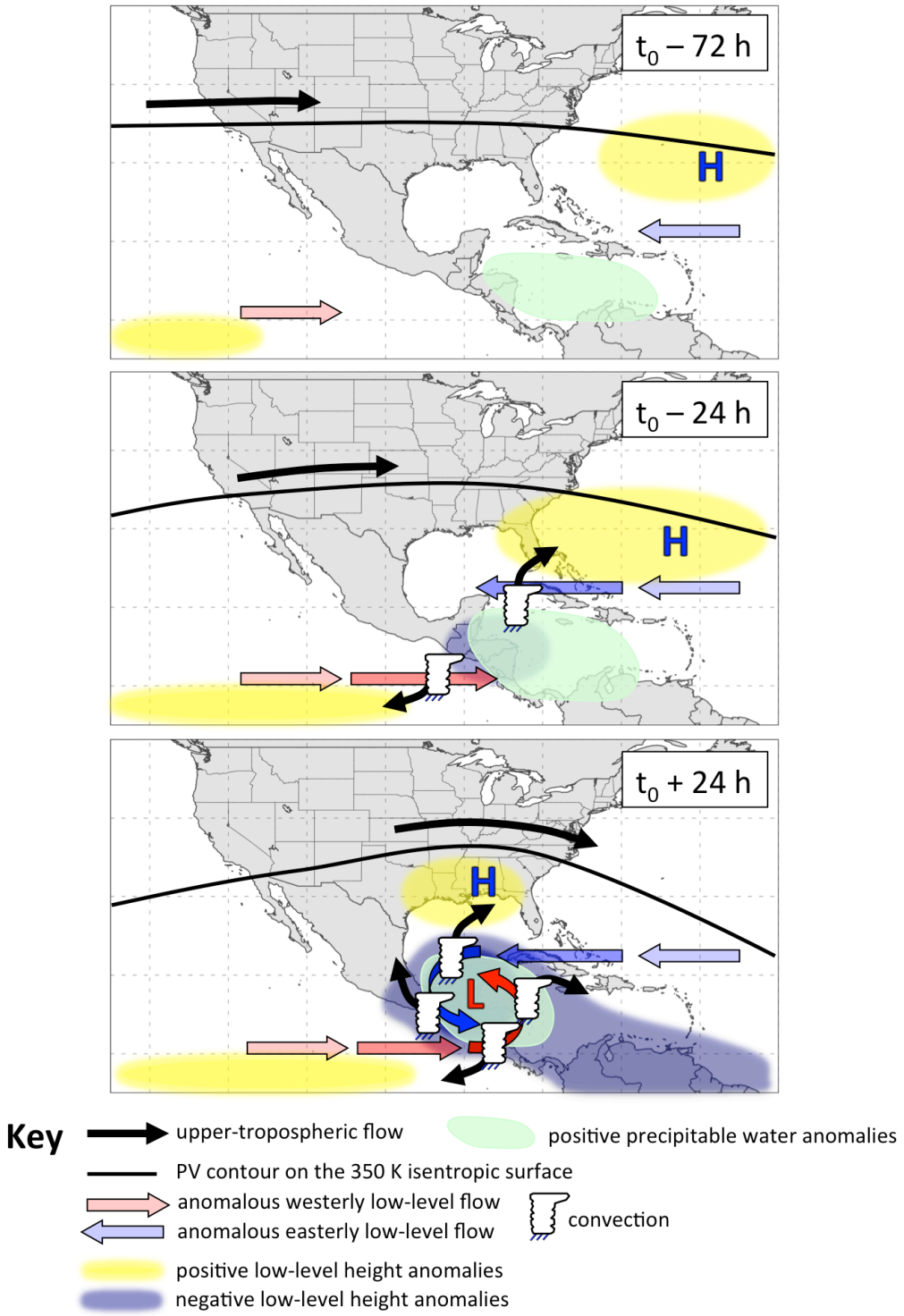

Fig. 4.1. Conceptual model of the relevant synoptic features associated with tropical CAG formation at (a) t_0 – 72 h, (b) t_0 – 24 h, and (c) t_0 + 24 h. Features shown according to key; others symbols are conventional.

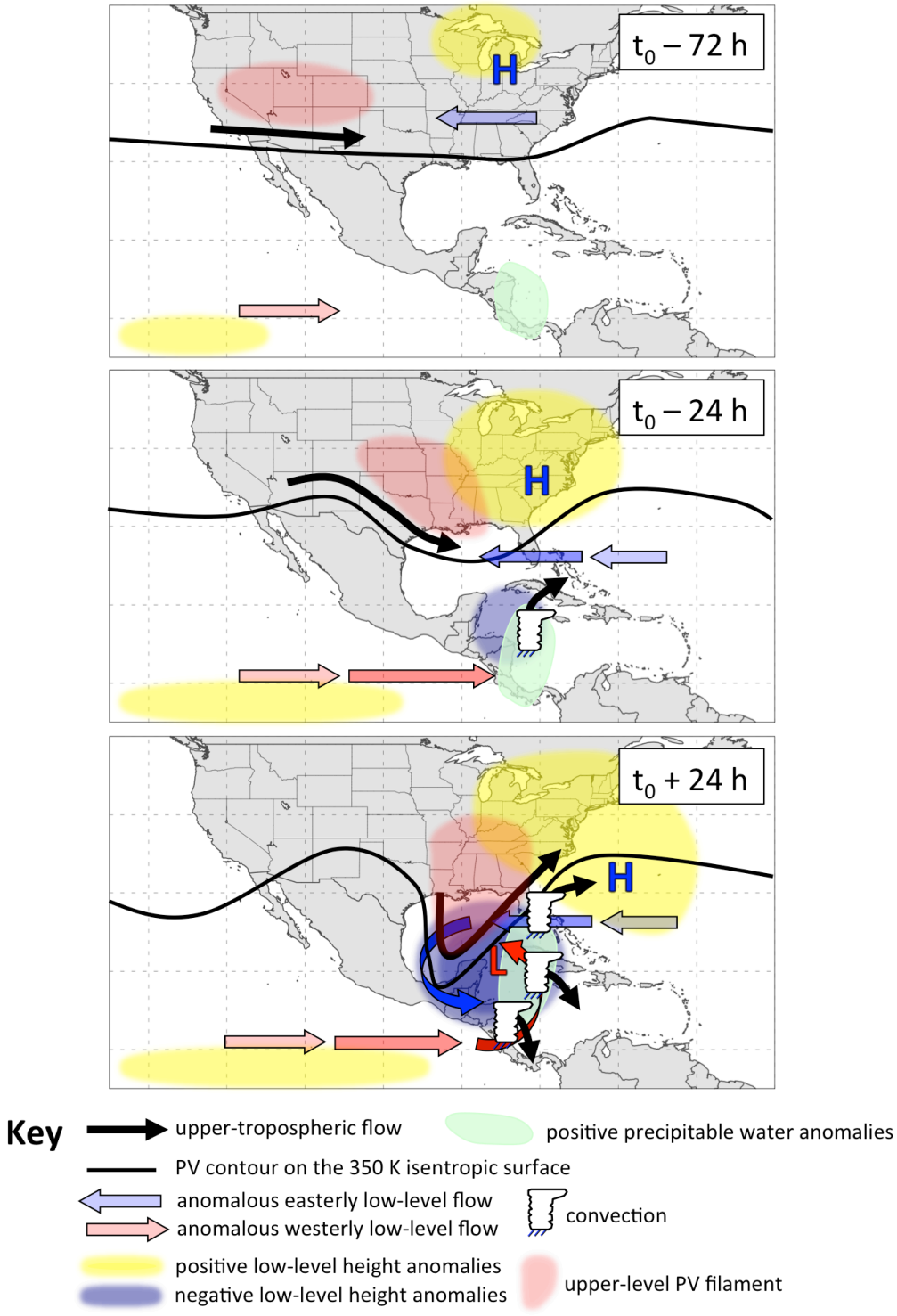

Fig. 4.2. Conceptual model of the relevant synoptic features associated with trough CAG formation at (a) t_0 – 72 h, (b) t_0 – 24 h, and (c) t_0 + 24 h. Features shown according to key; others symbols are conventional.

REFERENCES

Aiyyer, A., and J. Molinari, 2008: MJO and Tropical Cyclogenesis in the Gulf of Mexico and Eastern Pacific: Case Study and Idealized Numerical Modeling. *J. Atmos. Sci.*, **65**, 2691–2704.

Aldinger, W. T., and W. Stapler, 1998: *1998 Annual Tropical Cyclone Report*. J.T.W. Center, E., U.S. Navel Pacific Meteorology and Oceanography Center.

Baray, J.-L., G. Clain, M. Plu, E. Feld, and P. Caroff, 2010: Occurrence of Monsoon Depressions in the Southwest Indian Ocean: Synoptic Descriptions and Stratosphere to Troposphere Exchange Investigations. *J. Geophys. Res.*, **115**, D17108.

Beattie, J. C., and R. L. Elsberry, 2013: Horizontal structure of monsoon depressions in the western North Pacific at formation time. *Geophys. Res. Lett.*, **40**, 983–987.

Blake, E. S., 2011: Tropical Cyclone Report: Tropical Storm Nicole, 28-29 September 2010. National Hurricane Center Rep., 15 pp. [Available online at http://www.nhc.noaa.gov/data/tcr/AL162010_Nicole.pdf.]

Boos, W. R., J. V Hurley, and V. S. Murthy, 2014: Adiabatic westward drift of Indian monsoon depressions. *Q. J. R. Meteorol. Soc.*, In press. [Available online at http://people.earth.yale.edu/sites/default/files/files/Boos/depressprop_rev1_singlespace.pdf.]

Brennan, M. J., 2010: Tropical Cyclone Report: Tropical Storm Matthew, 23-26 September 2010. National Hurricane Center Rep., 15 pp. [Available online at http://www.nhc.noaa.gov/data/tcr/AL152010_Matthew.pdf.]

Carr, F. H., 1977: Mid-Tropospheric Cyclones of the Summer Monsoon. *Pure Appl. Geophys.*, **115**, 1383–1412.

Carr, L. E., and R. L. Elsberry, 1995: Monsoonal Interactions Leading to Sudden Tropical Cyclone Track Changes. *Mon. Weather Rev.*, **123**, 265–290.

Chen, T.-C., J.-H. Yoon, and S.-Y. Wang, 2005: Westward propagation of the Indian monsoon. *Tellus*, **57**, 758–769.

——, and S.-P. Weng, 1999: Interannual and Intraseasonal Variations in Monsoon Depressions and Their Westward-Propagating Predecessors. *Mon. Weather Rev.*, **127**, 1005–1020.

——, S. Y. Wang, M.-C. Yen, and W. A. Gallus Jr., 2004: Role of the Monsoon Gyre in the Interannual Variation of Tropical Cyclone Formation over the Western North Pacific. *Wea. Forecasting*, **19**, 776–785.

——, ——, ——, and A. J. Clark, 2008: Are Tropical Cyclones Less Effectively Formed by Easterly Waves in the Western North Pacific than in the North Atlantic? *Mon. Weather Rev.*, **136**, 4527–4540.

Coen, E., 1973: El Folklore Costarricense Relativo al Clima. *Rev. Univ. Costa Rica*, **35**, 135–145.

Crandall, B. A., 2012: An Analysis of the Formation and Evolution of the 1989 Western North Pacific Subtropical Gyre. M.S. thesis, Dept. of Atmospheric and Environmental Science, State University of New York, Albany, 80 pp.

——, B., J. Molinari, and D. Vollaro, 2014: Forecasting Challenges Associated with Tropical Cyclones within Subtropical Gyres. *Weather Forecast.*, **29**, 99–114.

Das, P. K., 1952: Monsoon Depressions in the Bay of Bengal. *Indian J. Metoeology Geophys.*, **3**, 225–229.

Davidson N, Holland G. 1987. A diagnostic analysis of two intense monsoon depressions over Australia. *Mon. Weather Rev.* **115**(2): 380–392.

Dee, D. P., and Coauthors, 2011: The ERA-Interim Reanalysis: Configuration and performance of the data assimilation sys- tem. *Quart. J. Roy. Meteor. Soc.*, 137, 553–597.

Douglas, M. W., 1992: Structure and Dynamics of Two Monsoon Depressions. Part I: Observed Structure. *Mon. Weather Rev.*, **120**, 1524–1547.

Eliot, J., 1890: *Hand Book of Cyclonic Storms in the Bay of Bengal for the use of Sailors*.

Fernandez, W., and J. A. Barrantes, 1996: The Central American temporal: A long-lived tropical rain-producing system. *Top. Meteorol. Y Oceanogr.*, **3**, 73–88.

Godbole, R. V, 1977: The composite structure of the monsoon depression. *Tellus*, **29**, 25–40.

Gibson, J. K., P. Kallberg, S. Uppala, A. Hernandez, A. Nomura, and E. Serrano, 1997: ERA description. ECMWF Re-Analysis Project Report Series, Vol. 1, 89 pp.

Gill, A. E., 1980: Some simple solutions for heat-induced tropical circulation. *Q. J. R. Meteorol. Soc.*, **106**, 447–462.

Guinn, T. A., and W. H. Schubert, 1993: Hurricane spiral bands. *J. Atmos. Sci.*, **50**, 3380–3403.

Harr, P. A., R. L. Elsberry, and J. C. L. Chan, 1996: Transformation of a Large Monsoon Depression to a Tropical Storm during TCM-93. *Mon. Weather Rev.*, **124**, 2625–2643.

Hastenrath, S., 1967: Rainfall distribution and regime in Central America. *Arch. Meteor. Geophys. Bioklimatol. Ser. B*, **15**, 201–241.

Holland, G. J., 1995: Scale Interaction in the Western Pacific Monsoon. *Meteorol. Atmos. Phys.*, **56**, 57–79.

Hurley, J. V., and W. R. Boos, 2014: A Global Climatology of Monsoon Low Pressure Systems. *Q. J. R. Meteorol. Soc.*, In press. [Available online at http://people.earth.yale.edu/sites/default/files/files/Boos/HurleyBoos2014_rev08072014.pdf]

IMD, 2003: *Cyclone Manual*. India Meteorological Department.

Kalnay, E., et al., 1996: The NCEP/NCAR 40-year reanalysis project, *Bull. Am. Meteorol. Soc*., **77**, 437-471, 1996

Knapp, K. R., and Coauthors, 2011: Globally Gridded Satellite Observations for Climate Studies. *Bull. Am. Meteorol. Soc.*, **92**, 893–907.

——, M. C. Kruk, D. H. Levinson, H. J. Diamond, and C. J. Neumann, 2010: The International Best Track Archive for Climate Stewardship (IBTrACS). *Bull. Am. Meteorol. Soc.*, **91**, 363–376.

Krishnamurti, T. N., M. Kanamitsu, R. Godbole, C.-B. Chang, F. Carr, and J. H. Chow, 1975: Study of a Monsoon Depression (I) Synoptic Structure. *J. Meteorol. Soc. Japan*, **53**, 227–240.

——, M. Kanamitsu, R. Godbole, C.-B. Chang, F. Carr, and J. H. Chow, 1976: Study of a Monsoon Depression (II) Dynamical Structure. *J. Meteorol. Soc. Japan*, **54**, 208–225.

Lander, M. A., 1994: Description of a Monsoon Gyre and Its Effects on the Tropical Cyclones in the Western North Pacific during August 1991. *Weather Forecast.*, **9**, 640–654.

Lessmann, H., 1964. Synoptic and climatologic views on the rainfall in Central America, especially in El Salvador. *Proc. Symp. On Tropical Meteorology*, Wellington, New Zealand, New Zealand Meteorological Service, pp. 295-305.

Magaña, V., J. a Amador, and S. Medina, 1999: The Midsummer Drought over Mexico and Central America. *J. Clim.*, **12**, 1577–1588.

Molinari, J., and D. Vollaro, 2012: A Subtropical Cyclonic Gyre Associated with Interactions of the MJO and the Midlatitude Jet. *Mon. Weather Rev.*, **140**, 343–357.

——, K. Lombardo, and D. Vollaro, 2007: Tropical Cyclogenesis within an Equatorial Rossby Wave Packet. *J. Atmos. Sci.*, **64**, 1301–1317.

Montgomery, M. T., and Coauthors, 2012: The Pre-Depression Investigation of Cloud-Systems in the Tropics (PREDICT) Experiment: Scientific Basis, New Analysis Tools, and Some First Results. *Bull. Am. Meteorol. Soc.*, **93**, 153–172.

Moore, R. W., O. Martius, and T. Spengler, 2010: The Modulation of the Subtropical and Extratropical Atmosphere in the Pacific Basin in Response to the Madden–Julian Oscillation. *Mon. Weather Rev.*, **138**, 2761–2779.

Mosino, A. P., and E. Garcia, 1966: Evaluacion de la sequıa intraestival en la Republica Mexicana. *Proc. Conf. Reg. Latinoamericana Union Geogr. Int.*, **3**, 500–516.

Mulky, G. R., and A. K. Banerji, 1960: The Mean Upper-Wind Circulation Around Monsoon Depressions In India. *J. Meteorol.*, **17**, 8–14.

Nitta, T., and K. Masuda, 1981: Observational Over the Study of a Monsoon Depression Developed Over the Bay of Bengal during Summer MONEX. *J. Meteorol. Soc. Japan*, **59**, 672–682.

Pena, M., and M. W. Douglas, 2002: Characteristics of Wet and Dry Spells over the Pacific Side of Central America during the Rainy Season. *Mon. Weather Rev.*, **130**, 3054–3073.

Piddington, H., 1876: Sailor's Horn-Book for the Law of Storms. 6 ed. Williams and Norgate.

Rao K, Rajamani S. 1970. Diagnostic study of a monsoon depression by geostrophic baroclinic model. *Indian J. Meteor. Geophys* 21: 187–194.

Ritchie, E. a, and G. J. Holland, 1999: Large-Scale Patterns Associated with Tropical Cyclogenesis in the Western Pacific. *Mon. Weather Rev.*, **127**, 2027–2043.

Romatschke, U., and R. a. Houze, 2011: Characteristics of Precipitating Convective Systems in the South Asian Monsoon. *J. Hydrometeorol.*, **12**, 3–26.

Saha, K., and C.-P. Chang, 1983: The Baroclinic Processes of Monsoon Depressions. *Mon. Weather Rev.*, **111**, 1506–1514.

Saha, S., and Coauthors, 2010: The NCEP Climate Forecast System Reanalysis. *Bull. Am. Meteorol. Soc.*, **91**, 1015–1057.

Shukla, J., 1978: CISK-Barotropic-Baroclinic Instablity and the Growth of Monsoon Depressions. *J. Atmos. Sci.*, **35**, 495–508.

Schultz, D. M., W. E. Bracken, and L. F. Bosart, 1998: Planetary- and Synoptic-Scale Signatures Associated with Central American Cold Surges. *Mon. Weather Rev.*, **126**, 5–27.

Small, R. J. O., S. P. De Szoeke, and S.-P. Xie, 2007: The Central American Midsummer Drought: Regional Aspects and Large-Scale Forcing*. *J. Clim.*, **20**, 4853–4873.

Thorncroft, C. D., B. J. Hoskins, and M. E. McIntyre, 1993: Two paradigms of baroclinic-wave life-cycle behaviour. *Q. J. R. Meteorol. Soc.*, **119**, 17–55.

Wang. Y., Holland. G. J., Leslie L. M., 1993: Some baroclinic aspects of tropical cyclone motion. In: Lighthill. J., Emanuel, K., Holland, G. J,. Zheng, Z. (eds.) *Tropical Cyclone Disasters*. 280-285.

Waugh, D. W., and L. M. Polvani, 2000: Climatology of Intrusions Into the Tropical Upper Troposphere. *Geophys. Res. Lett.*, **27**, 3857–3860.

Wheeler, M. C., and H. H. Hendon, 2004: An All-Season Real-Time Multivariate MJO Index: Development of an Index for Monitoring and Prediction. *Mon. Weather Rev.*, **132**, 1917–1932.

Wu, L., H. Zong, and J. Liang, 2013: Observational Analysis of Tropical Cyclone Formation Associated with Monsoon Gyres. *J. Atmos. Sci.*, **70**, 1023–1034.

Yoon, J.-H., and T.-C. Chen, 2005: Water vapor budget of the Indian monsoon depression. *Tellus*, **57**, 770–782.